RP TU Rheinland-Pfälzische Technische Universität Kaiserslautern Landau

Dissecting the molecular mechanisms by which intersectins shape neurotransmission

vom Fachbereich Biologie

der Rheinland-Pfälzischen Technischen Universität Kaiserslautern-Landau zur

Verleihung des akademischen Grades Dr. rer. nat. genehmigte

Dissertation

von

Alexandra Hilse, M.Sc., geb. in Bad Kreuznach

Mündliche Prüfung: 24.11.2025

Dekan:	Prof. Dr. Stefan Kins
Promotionskommissionsvorsitzender:	Prof. Dr. Jan Pielage
Berichterstattende:	Prof. Dr. Tanja Maritzen
	Prof. Dr. Stefan Kins

D 386

Eidesstattliche Erklärung

Hiermit erkläre ich wahrheitsgemäß, dass ich die hier vorliegende Dissertation selbstständig, ohne unzulässige Hilfe Dritter verfasst und keine anderen als die angegebenen Quellen und Hilfsmittel verwendet habe. Die aus anderen Quellen übernommenen Daten und Konzepte sind unter Angabe der Quelle gekennzeichnet.

Zur Erstellung der vorliegenden Arbeit habe ich keine entgeltliche Hilfe von Vermittlungs- und Beratungsdiensten in Anspruch genommen.

Diese Arbeit, und auch keine Teile hiervon, wurden weder im In- noch im Ausland bereits als Prüfungsarbeit für eine wissenschaftliche Prüfung eingereicht und ich habe mich zuvor noch keiner Doktorprüfung unterzogen. Ich erkläre, dass ich weder die gleiche noch eine andere Abhandlung bei einem anderen Fachbereich oder einer anderen Universität als Dissertation eingereicht habe.

Die Bestimmungen der Promotionsordnung des Fachbereiches Biologie der Rheinland-Pfälzischen Technischen Universität Kaiserslautern-Landau sind mir bekannt. Im Besonderen weiß ich, dass ich vor Vollzug der Promotion zur Führung des Doktortitels nicht berechtigt bin.

_____

Alexandra Hilse

Kaiserslautern, 15.08.2025

Darlegung des Eigenanteils

Alexandra Hilse
Dissecting the molecular mechanisms by which intersectins shape neurotransmission

Die Klonierung des Kv1.2 N-Terminus und die Pull-Down Assays mit den ITSN1-S Domänen in Maushirn-Lysat wurden von Linda Tscheschel im Rahmen ihrer von mir betreuten Masterarbeit durchgeführt (Figure 15A, Figure 16B). Die Pull-Downs mit FMRP-GST und FXR1-GST sowie die entsprechenden Transfektionen (Figure 25), und 3 von 4 Pull-Down Assays mit CTTN-GST (Figure 18) wurden von Alina Strietter im Rahmen ihrer von mir betreuten Bachelorarbeit durchgeführt und von mir eigenständig ausgewertet. Von den Pull-Down Experimenten mit den Kv1.2 Domänen und Kvβ2 (Figure 16D) wurden 1 von 2 Wiederholungen mit Michelle Kölsch und Katharina Schmitt im Rahmen ihres von mir betreuten Vertiefungpraktikums durchgeführt. Die Immunfluoreszenz der 6 Monate alten NMJs wurde in Zusammenarbeit mit Sean Partick Hartung und Phillip Baumann im Rahmen ihres von mir betreuten Vertiefungpraktikums aufgenommen und von mir ausgewertet (Figure 10). Mit ihnen wurde auch das Hämatoxylin und Eosin (HE) Staining des Trizeps von 6 und 2 Monaten alten Mäusen durchgeführt und ausgewertet (Figure 13, Figure 14). Das HE Staining der Tibialis Anterior 2 Monate alter Tiere wurde mit Sarah Link und Celina Nauerz im Rahmen ihres von mir betreuten Vertiefungpraktikums durchgeführt (Figure 12) und von mir ausgewertet. Das MS IP Datenset wurde von Marielle Eichhorn Grüning am Leibniz-Forschungsinstitut für Molekulare Pharmakologie in der Arbeitsgruppe von Volker Haucke in Berlin in Zusammenarbeit mit der Gruppe von Dr. Eberhard Krause generiert und von mir mit DAVID und STRING ausgewertet (Figure 23).

Alexandra Hilse	Prof. Dr. Tanja Maritzen
Kaiserslautern, den 15.08.2025	Kaiserslautern, den

Darlegung aller Benutzten Hilfsmittel und Hilfestellungen

Alexandra Hilse
Dissecting the molecular mechanisms by which intersectins shape neurotransmission

Zur Erstellung der Arbeit wurde das Microsoft Office 365 Software Paket genutzt. Das Literaturverzeichnis und die Literaturverweise wurden mit Zotero erstellt. Die statistischen Analysen und Auswertungen wurden mit Graph Pad Prism durchgeführt. Die Abbildungen wurden mit der Corel Technical Suite 2020 erstellt. Die Analyse des massenspektrometrischen Datensets wurde mit DAVID durchgeführt. Interaktionsnetzwerke wurden mit Hilfe von STRING dargestellt. Mikroskopische Aufnahmen wurden mit NIS Elements aufgenommen und mit Fiji, Cell profiler oder Cellpose analysiert. Western Blots wurden mit der Licor Acquisition Software aufgenommen und mit Image Studio ausgewertet. Eine detailiertere Auflistung der verwendeten Programme findet sich im Kapitel zu den Materialien.

Die Arbeit wurde von Anna Stoelting, UC Leuvain, und von Sophie Wölbert Korrektur gelesen. Deepl und ChatGPT wurden für Übersetzungen und zum Optimieren von Formulierungen verwendet.

_____

Alexandra Hilse

Kaiserslautern, den 15.08.2025

Summary

Recent studies have linked the scaffold protein intersectin 1 (ITSN1) to autism-spectrum disorders (ASD) in humans as well as mice. Mice lacking ITSN1 and its close relative ITSN2 display repetitive behavior and hyperactivity, likely based on altered cortico-striatal neurotransmission. In part, this phenotype might be due to reduced levels of the presynaptic potassium channels Kv1.1 and Kv1.2 and their subunit Kvβ2. Therefore, this study examined different molecular mechanisms which could affect Kv channel levels. Since the functions of scaffolding proteins like ITSNs are primarily defined by their binding partners, a direct interaction between ITSNs and Kv1.2 or Kvβ2 was hypothesized but could not be detected. Instead, an interaction between ITSN1 and Cortactin (CTTN), a known interactor of Kv1.2, could be identified, suggesting indirect stabilization. Another tested pathway involves the regulation of actin dynamics since ITSNs are known activators of Cdc42. However, no evidence supporting a presynaptic actin reduction was obtained. A third explanation draws on another autism mouse model, JAKMIP1 KO mice, with a strikingly similar behavioral phenotype. There, misregulation of mRNA translation, involving FMRP-associated RNP complexes, has been linked to ASD-like behavior. Intriguingly, we found ITSN1 to be potentially linked to translational regulation and FMRP-associated RNP granules via interactions with components of FMRP-positive granules like DDX5, PABP and FXR1, and a partial colocalization with FMRP itself. This supports a previously underappreciated potential role for ITSNs in translational regulation and mRNA stability, suggesting that they might contribute to synaptic dysfunction through multiple, converging pathways.

With increasing age ITSN1/2-deficient mice exhibit a progressive decline of motor coordination. Surprisingly, ITSN dKO mice exhibited normal neuromuscular junction morphology and largely unaltered age-dependent myofiber degeneration. Interestingly, this may underline the importance of ITSNs interaction with RNP components, especially DDX5 or SAM68, since functional impairments in these proteins might account for the impaired motor coordination phenotype, as in Fragile X-associated ataxia syndrome (FXTAS).

Together, these findings identify ITSN1 as a multifunctional regulator of synaptic function, not only through protein scaffolding but possibly through translational regulation relevant for ASD.

Zusammenfassung

Aktuelle Studien an Mäusen und Menschen haben das Gerüstprotein Intersectin1 (ITSN1) mit Autismus Spektrum Erkrankungen (ASDs) in Verbindung gebracht. Mäuse, denen ITSN1 und sein naher Verwandter ITSN2 fehlen, zeigen repetitives Verhalten und Hyperaktivität, was wahrscheinlich auf veränderter cortico-striataler Neurotransmission beruht. Dieser Phänotyp könnte zum Teil auf verminderte Level der präsynaptischen Kaliumkanäle Kv1.1 und Kv1.2 sowie ihrer Untereinheit Kvβ2 in ITSN dKO Mäusen zurückzuführen sein. Daher wurden in dieser Studie molekulare Mechanismen untersucht, die das Kv-Kanal-Vorkommen beeinflussen könnten. Da sich Gerüstproteine wie ITSN1 vor allem durch ihre Interaktionspartner definieren, wurde eine direkte Interaktion zwischen ITSN1 und Kv1.2 oder Kvβ2 als wahrscheinlich angenommen, welche letztlich nicht bestätigt werden konnte. Stattdessen wurde eine Interaktion zwischen ITSN1 und Cortactin (CTTN), einem Interaktor von Kv1.2, entdeckt, was auf eine indirekte Stabilisierung der Kv-Kanäle durch ITSN1 hinweist. Ein anderer möglicher Mechanismus basiert auf einer schlechteren Verankerung der Kv-Kanäle im Aktin Zytoskelett, welches durch ITSN1 über Cdc42 reguliert wird. Jedoch konnte keine Aktin Reduktion an der Präsynapse festgestellt werden. Eine dritte Hypothese war inspiriert durch ein anderes ASD-Mausmodell, sogenannten JAKMIP1 KO Mäuse. Diese zeigen ein sehr ähnliches repetitives Verhalten. Dies wird auf die Misregulation der mRNA Translation, unter anderem durch Veränderungen in FMRP-assoziierte RNP Komplexen, zurückgeführt. Interessanterweise kann ITSN1 auch mit der Translationsregulation und FMRP-assoziierten RNP Komplexen in Verbindung gebracht werden, da es mit Komponenten jener Komplexe, wie DDX5, PABP und FXR1 interagiert und zum Teil mit FMRP kolokalisiert. Dies untermauert eine potenzielle und unterschätze Rolle von ITSN1 in Bezug auf die Translationsregulation und eventuell auch mRNA-Stabilität. Alles in allem ist es wahrscheinlich, dass der Verlust der Intersectine über mehrere konvergierende Mechanismen zur synaptischen Dysfunktion beiträgt.

Mit zunehmendem Alter zeigen ITSN1/2 defiziente Mäuse eine progressive Verschlechterung der motorischen Koordination. Unerwarteterweise zeigen ITSN dKO Mäuse aber eine normale Morphologie der neuromuskulären Endplatte und keine verfrühte Myofibrillendegeneration. Dies könnte jedoch die Bedeutung der Interaktion von ITSN1 mit

RNP-Komponenten unterstreichen, da eine eingeschränkte Funktion von DDX5 und SAM68 mit gestörter motorischer Koordination beim Fragiles-X-assoziiertes Ataxie-Syndrom in Verbindung gebracht wurde.

Zusammenfassend deuten diese Ergebnisse auf Intersectine als multifunktionalen Regulatoren für synaptische Funktionen hin, nicht nur durch Proteingerüstbildung, sondern möglicherweise auch durch einen für ASD relevanten Beitrag zur Translationsregulation.

Contents

1 Introduction

1.1 Molecular mechanisms supporting synaptic transmission and plasticity

Neurons are the central units of our nervous system, involved in receiving, processing, and transmitting information throughout the body and within our brain (Kandel et al., 2013). Consequently, efficient communication between neurons is fundamental. Their most common communication site is the chemical synapse, where a signal originating from a presynaptic terminal is transferred by neurotransmitters via the synaptic cleft to the postsynapse of another neuron. This process is called neuro- or synaptic transmission and enables the fast passage of information (Kandel et al., 2013). Neurotransmission can be modified based on activity dependent mechanisms, to strengthen or weaken the transmission, which is called synaptic plasticity (Diering & Huganir, 2018).

The synapse is structurally and functionally adjusted to fit these demands. Repeated or high frequency activity of the presynapse requires a continuous replenishment of the synaptic vesicles containing neurotransmitters (Jäpel et al., 2020). Therefore, synaptic vesicle exocytosis and recycling are highly regulated processes. Neurotransmitters are actively transported into the synaptic vesicles, which set up the reserve pool. Those vesicles dock at the active zone and undergo ATP-dependent priming, enabling their fusion with the membrane upon action potential-triggered Ca^{2+} influx, thereby releasing neurotransmitters. For subsequent synaptic vesicle replenishment, vesicle retrieval can occur via clathrin-mediated endocytosis (CME) or clathrin-independent endocytosis. Either way, the vesicle membrane and synaptic vesicle proteins get recycled directly or via an endosomal sorting step (Siegelbaum et al., 2013). The spatial concentration of this process on the active zone facilitates fast transmission due to the closeness of Ca^{2+} channels. Important components of the active zone are proteins like bassoon, guiding synaptic vesicles to the active zone (Altrock et al., 2003; Hallermann et al., 2010) along with Rab3-interacting molecules, short RIMs. RIMs are involved in vesicle docking and priming (Deng et al., 2011), as well as in recruiting Ca^{2+} channels to the active zone (Kaeser et al., 2011).

As presynaptic active zone proteins like bassoon and RIM provide the structural and functional basis supporting fast neurotransmission, this is mirrored at the postsynapse by the proteins making up the postsynaptic density (PSD). A mesh of several scaffolding proteins

including PSD-95 (Cho et al., 1992), shank proteins and homer link glutamate receptors, such as α-amino-3-hydroxy-5-methyl-4-isoxazole propionic acid receptors (AMPARs) and N-methyl-D-aspartate receptors (NMDARs) (D. Cheng et al., 2006; Moon et al., 1994), to the actin cytoskeleton (Hirokawa, 1989) and organize downstream signaling (W. Feng & Zhang, 2009).

To supply the synapse with the plethora of pre- and postsynaptic proteins required for synaptic transmission and to allow for activity-dependent regulation, protein transport from the soma to the synaptic compartment is not sufficient. Therefore, the synapse is additionally equipped with its own translational machinery, including ribosomes (Steward & Levy, 1982) with their ribosomal RNA (Hafner et al., 2019). Several of the proteins regulating synaptic translation might even be locally transcribed, as the mRNAs of several eukaryotic translation initiation factors (eIFs) were identified at the synapse (Cajigas et al., 2012). Notably, approximately 2500 different mRNAs have been identified in the dendrites and axons of hippocampal neurons. These encode proteins with synaptic functions (Cajigas et al., 2012), though which and how many transcripts are present seems to depend on the type of synapse (Hafner et al., 2019). Presynaptic terminals are enriched in mRNAs which regulate neurotransmitter release such as Snap25, RIM proteins, bassoon or synapsin (Batista et al., 2017; Hafner et al., 2019), and transcripts encoding voltage-gated ion channels like Kv1.1, Kv1.2 and Kvβ2, cytoskeleton components such as β-actin, PSD scaffolds like PSD95 and homer were identified as well in the synaptic neuropil (Cajigas et al., 2012). While the full functional impact of local translation for many of these proteins remains unclear, the loss of Snap25 mRNA and its local translation have been shown to impair vesicle release and synaptic transmission (Batista et al., 2017).

Local translation is highly regulated by ribonucleoprotein (RNP) granules, which are macromolecular complexes, containing (poly-A+) mRNAs as well as mRNA binding proteins (Berg et al., 2015; Y. Feng et al., 1997; Knowles et al., 1996). One key regulator is the Fragile X mental retardation protein (FMRP) encoded by the gene FMR1. This RNA binding protein associates with synaptic ribosomes and RNP granules (Figure 1). There, it stalls the translation of several mRNAs, including many implicated in autism spectrum disorder (ASD) (Darnell et al., 2011; El Fatimy et al., 2016; Y. Feng et al., 1997). This translational regulation is based on FMRPs C-terminal binding domain which associates with ribosomes (D'Souza et al., 2022). Phosphorylation of this domain modulates the regulation of translation and the size of FMRP-

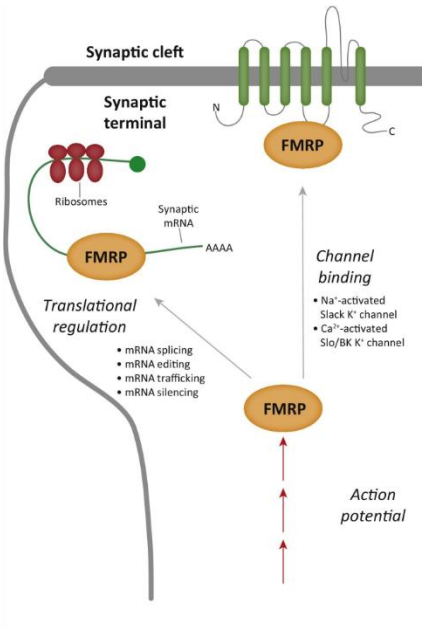

Figure 1: FMRP and its synaptic functions (Modified from Davis & Broadie, 2017).

FMRP is a multifunctional protein involved in regulation of RNA metabolism at the synapse. Additionally, it can interact with different proteins, e.g. ion channels, and thereby regulate protein function.

positive granules (D'Souza et al., 2022). In addition, FMRP itself seems important to enable the transport of FMRP-positive granules along microtubules (D'Souza et al., 2022; H. Wang et al., 2008).

Many different proteins have been associated with FMRP-positive granules. Among them are the two FMRP homologs FXR1 and FXR2 (Kanai et al., 2004; Y. Zhang et al., 1995) and other RNA-binding proteins like staufen and Purα (Kanai et al., 2004; Villacé et al., 2004), translation initiation factors like eIFs and poly(A)-binding protein (PABP) (Kanai et al., 2004; Villacé et al., 2004) and RNA-helicases including DEAD-box proteins (DDX) (Kanai et al., 2004). In line with their association with the microtubule cytoskeleton, motor proteins like kinesin or myosin heavy hain were identified in FMRP/staufen granules (Villacé et al., 2004), and regulators of the actin cytoskeleton, including Rac1, Cdc42 and CYFIP1 and 2 (Pasciuto & Bagni, 2014; Villacé et al., 2004), could be identified as well. Loss of translational regulation by FMRP-positive granules highly impacts mice. The loss of FMRP results in hyperactivity (Pietropaolo et al., 2011; Spencer et al., 2005) and repetitive behaviors such as increased levels of self-grooming (Pietropaolo et al., 2011) or marble burying (Veeraragavan et al., 2012). Along with behavioral alterations, neurons exhibit an increased spine density, though those spines mostly remain immature (Galvez & Greenough, 2005), and altered neurotransmission. More specifically, presynaptic terminals exhibit an increased excitability (Yang et al., 2018) and a reduced AMPAR to NMDAR ratio at the postsynapse (Pilpel et al., 2009).

However, local translation does not only depend on the ribosome-mediated translation of axonal and synaptic proteins, but the subsequent processing of these proteins is also necessary for protein function. Therefore, components of the co- and post-translational machinery, like the endoplasmic reticulum (ER) and Golgi outposts, can be found in dendrites and axons supporting functional folding and membrane integration of locally transcribed transmembrane proteins (Gardiol et al., 1999; Merianda et al., 2009). As Golgi cisternae are not

present throughout basal and apical dendrites, a Golgi satellite system enables postsynaptic local glycosylation (Mikhaylova et al., 2016). Thus, a microsecretory system, comprising ER, ER-Golgi intermediate compartment and Golgi satellites allows local control of transmembrane protein synthesis and processing at the postsynapse. In addition, a variety of glycosylation profiles were identified in neuronal surface membrane proteins, which suggests an alternative Golgi-independent secretory pathway (Hanus et al., 2016). However, for the presynapse information on the mechanisms behind local translation of transmembrane proteins is still scarce.

As synaptic transmission needs to be adaptable to enable learning and memory formation, there are pre- and postsynaptic pathways in place to adjust synaptic strength in a process referred to as synaptic plasticity. At the presynapse, the release of neurotransmitters can be modified, e.g. by changes in Ca^{2+} influx, or the quantity of neurotransmitters released (Siegelbaum et al., 2013). Meanwhile at the postsynapse, changes in the composition of AMPARs and NMDARs as well as the total amount of receptors at the membrane enable long-term potentiation and depression. In general, long-term potentiation refers to an increase in postsynaptic strength and is accompanied by the insertion of additional receptors into the postsynaptic membrane, while a decrease in the size of the postsynaptic response is referred to as depression and is induced by the endocytic removal of receptors (Siegelbaum et al., 2013). However, there is more to this process, as also the actin cytoskeleton is remodeled upon potentiation and depression, e.g. to adapt the spine size (K.-I. Okamoto et al., 2004). Another key component for plasticity is the already mentioned local translation, as long lasting forms of plasticity need protein synthesis (Kang & Schuman, 1996). This has been observed in long-term depression (Huber et al., 2000), as well as potentiation (Kang & Schuman, 1996; Vickers et al., 2005).

1.1.1 Molecular and cellular mechanisms underlying neurotransmission at the neuromuscular junction

At the neuromuscular junction (NMJ), the terminal of a motor neuron forms a highly specialized synapse with a skeletal muscle fiber. Typically, each skeletal muscle fiber is innervated by a single NMJ. This is a notable feature considering the length of the innervated muscle fiber can vary from less than 1 cm to more than 20 cm (Desaki & Uehara, 1981;

Rodríguez Cruz et al., 2020). Still, the NMJ retains the basic structure of a classical chemical synapse with a presynaptic terminal, synaptic cleft, and postsynaptic muscle membrane.

The presynaptic terminals hold synaptic vesicles loaded with the neurotransmitter acetylcholine (ACh), which is released into the synaptic cleft upon excitation by an action potential. Like in synapses of the central nervous system, to sustain neurotransmission, the synaptic vesicle pool has to be constantly replenished and recycled, as described in the previous chapter (Kandel & Siegelbaum, 2013; Rodríguez Cruz et al., 2020). The synaptic cleft is filled with synaptic basal lamina, a specialized extracellular matrix composed of laminins and collagens (Sanes, 2003). This matrix includes the enzyme acetylcholinesterase, terminating synaptic transmission by hydrolyzing ACh (Ohno et al., 1998). The postsynaptic membrane is highly organized, featuring numerous junctional folds formed by deep membrane invaginations. Clusters of acetylcholine receptors (AChRs) are located at the crest of these folds, aligned with the presynaptic active zones and open upon ACh binding. This causes postsynaptic depolarization travelling towards the base of the junctional folds, where voltage-gated Na^+ channels initiate the action potential in an "all-or-non" response. (Kandel & Siegelbaum, 2013; Rodríguez Cruz et al., 2020).

The postsynaptic AChR clusters need to be properly anchored to the subsynaptic cytoskeleton, which is supported by the scaffolding protein rapsyn (Burden et al., 1983; Gautam et al., 1996; Walker et al., 1984). Cytoskeletal anchoring and rearrangement are important processes at the NMJ. Already during NMJ development, neuronal agrin, a proteoglycan, induces a signal transduction pathway via the muscle-specific kinase MuSK, reorganizing the actin cytoskeleton and promoting AChR clustering. This pathway involves small Rho GTPases like Rac and Cdc42 (Nizhynska et al., 2007).

Neuromuscular transmission is a highly organized process, and its impairment is associated with various diseases, including congenital myasthenic syndrome (Rodríguez Cruz et al., 2018), spinal muscular atrophy (Kariya et al., 2008), and Duchenne muscular dystrophy (DMD) (Pratt et al., 2015).

1.2 Intersectin proteins: structure, expression and functional diversity

1.2.1 Domain architecture, expression patterns, and localization of intersectins

Scaffolding proteins are important for cellular signaling at the pre- and at the postsynapse as they provide interaction platforms, bringing together proteins in complexes and acting as signal processing hubs (Zeke et al., 2009). Intersectins (ITSN) are a great example for scaffolds, as their multidomain structure highlights their diverse functions. Mammals have two ITSN genes, ITSN1 and ITSN2, which share a high sequence homology (Pucharcos et al., 2000). Composed of 8-11 domains, they form a platform for a multitude of interactions, while their prevalence in different isoforms results in a high variability in function (Gerth et al., 2019). There are two main isoforms described, the short isoform ITSN-S, and the long isoform ITSN-L (Guipponi et al., 1998; Pucharcos et al., 2001), which are common for both ITSN proteins, ITSN1 and ITSN2 (Guipponi et al., 1998; Pucharcos et al., 2001). At its N-terminus ITSNs contain two Eps15 homology (EH) domains, providing an interaction site for numerous endocytic proteins, like epsin 1 & 2 and stonin2 by binding the asparagine-proline-phenylalanine (NPF) motifs of these proteins (Martina et al., 2001; Santolini et al., 1999; Yamabhai et al., 1998). The adjacent coiled coil (CC) domain harbors the binding site for the interaction with Eps15 and Eps15R, crucial interactions for CME (Henne et al., 2010; Koh et al., 2007; Sengar et al., 1999), as well as with itself (Wong et al., 2012). This domain is followed by five Src homology 3 (SH3) domains (SH3A-E) mediating the majority of interactions by binding PxxP motifs (Kurochkina & Guha, 2012; Tsyba et al., 2011) in diverse proteins, among them dynamin1 & 2, N-WASP and PI3K-C2β (Das et al., 2007; Hussain et al., 2001; Sengar et al., 1999; Yamabhai et al., 1998). In addition, ITSN-L contains a Dbl family guanine nucleotide exchange factor (GEF) activity, mediated by the Dbl homology (DH) domain and a pleckstrin homology (PH) domain, of which the DH domain is sufficient to catalyze exchange of GDP to GTP, thereby activating Cdc42 GTPases (Hussain et al., 2001). Activated Cdc42 then regulates neuronal Wiskott-Aldrich syndrome protein (N-WASP), with ITSN-L providing interaction surfaces for bringing them together, exemplary for its scaffolding nature (Humphries et al., 2014; Hussain et al., 2001). At the end of the GEF domain, ITSN-L contains a C-terminal C2 domain, usually promoting Ca^{2+} dependent lipid or membrane interactions, however, its function in the ITSNs is still unclear (Corbalan-Garcia & Gómez-Fernández, 2014; Guipponi et al., 1998).

The domain structure of ITSN-S is highly conserved, as proteins with similar domain structures were found in mammals, flies, and nematodes (Figure 2). The ortholog to ITSN in *Drosophila melanogaster*, Dap160, consists of two EH domains, a CC domain and four out of the five SH3 domains observed in vertebrates (Roos & Kelly, 1998), while the ortholog in *Caenorhabditis elegans* includes all five SH3 domains (Rose et al., 2007).

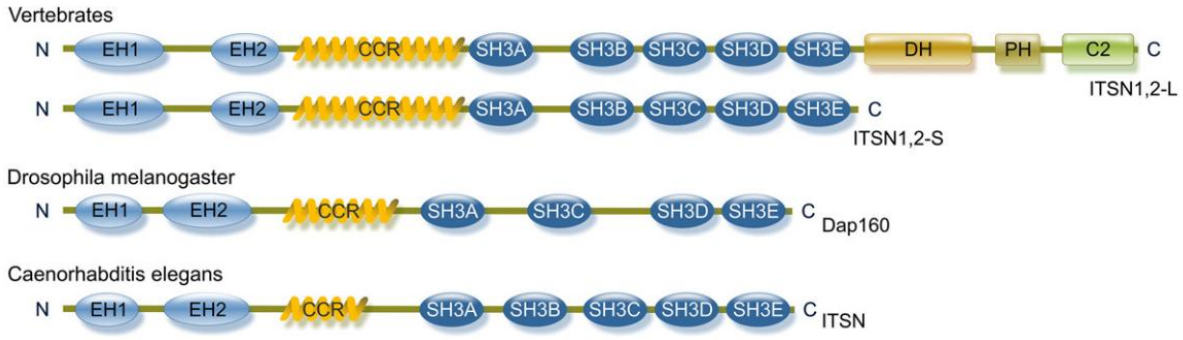

Figure 2: ITSN domain structure. The domain structure of ITSN-S is highly conserved from nematodes to mammals. (Taken from Tsyba et al., 2011).

The ITSN-S isoform, corresponding to Dap160 in D. melanogaster, contains 2 EH-domains, a CC region and only 4 SH3 domains (SH3A, C-E), while the vertebrate-specific long isoform contains the SH2B domain and possibly DH, PH and C2 domains.

While ITSN2-L is expressed widely in human tissues (Pucharcos et al., 2000), the ITSN1-L isoform is primarily expressed in neurons (Guipponi et al., 1998). In neurons, ITSNs appear to play a role both during development and in mature neurons, as demonstrated in *C. elegans*. (Rose et al., 2007). They have been shown to be expressed in the central and peripheral nervous system, as well as at the *D. melanogaster* neuromuscular junction (NMJ), while little is known for the mouse NMJ (Hussain et al., 1999; Koh et al., 2007; Roos & Kelly, 1998). Within neurons, both ITSN1-S and ITSN2-S, have been shown to localize at clathrin-coated pits, at the synaptic vesicle pool as well as with membrane-enclosed organelles like the Golgi and its vesicles (Hussain et al., 1999; Predescu et al., 2003; Pucharcos et al., 2000). Especially high levels of ITSN1 were identified at the pre- and post-synapse by immunogold-labeling (Pechstein et al., 2010), and localization of ITSN1 to the pre- and post-synapse could be verified biochemically as also with STED microscopy (Vollweiter et al., 2023).

1.2.2 Molecular functions of intersectins

ITSNs were initially known for their role in endocytosis. Endocytosis is a process by which cells can regulate nutrient uptake and transmembrane receptor levels at the membrane. CME

is the most common type of endocytosis, as it is responsible for about 95% of endocytic flux (Bitsikas et al., 2014). The CME process can be divided into four steps: initiation, stabilization and growth, maturation and scission, and uncoating. The precise mechanism of CME initiation and the exact timing of ITSN recruitment is still under debate. However, ITSNs are involved in nearly every step of the process (Figure 3). Recent models proposes that the early endocytic proteins Eps15 and FCHo1 form weak, liquid-like condensates to initiate the assembly of endocytic structures (Day et al., 2021). This initial condensate recruits downstream endocytic proteins which could lead to a second condensate involved in membrane curvature (Witkowska & Haucke, 2021). A study by Jin et al. in 2024 recently proposed that ITSN1 does not function as initiating protein in the Eps15 and FCHo complex, as previously proposed by Henne et al., 2010. Instead, ITSN1 is recruited in the subsequent stabilization and growth of the endocytic assembly, as upon ITSN knockdown more CME initiation events were observed,

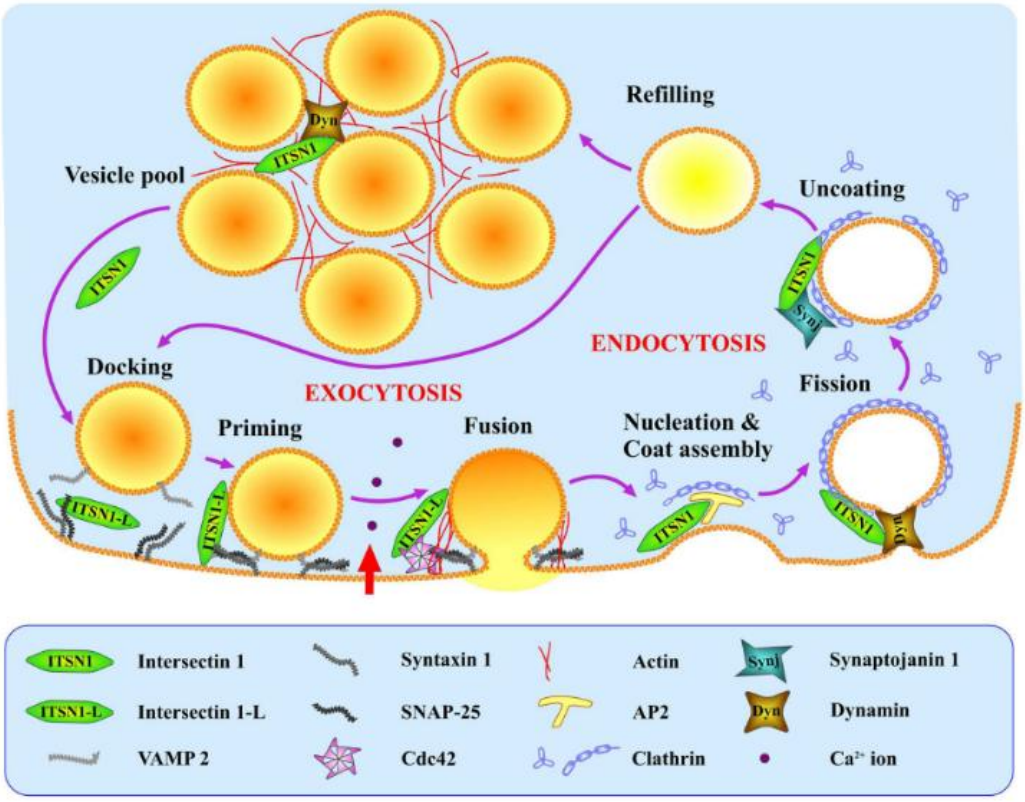

Figure 3: ITSNs are important regulators for synaptic vesicle recycling, exo- and endocytosis. (Adapted form Gubar et al., 2013).

They participate in neurotransmitter release guiding synaptic vesicle docking, priming and membrane fusion. But also, for recycling of synaptic vesicles, ITSNs facilitate endocytic processes like initiation, stabilization and growth, also called nucleation & coat assembly in the figure, and maturation and scission, simplified as fission in the figure, and uncoating. Additionally, they remain with the synaptic vesicle cluster or pool.

while Eps15 depletion decreased CME initiation events (Jin et al., 2024). Still, ITSNs cluster FCHo and together with Eps15 recruit the cargo adaptor AP2 and clathrin, which coats the vesicles, to the growing endocytic sites (Pechstein et al., 2010). At the next step of CME, during maturation, ITSNs relocate to the neck of forming versicles where they interact with the GTPase dynamin, which needs interactions with several SH3 containing proteins for proper scission of clathrin-coated versicles from the plasma membrane (Pechstein et al., 2010; Rosendale et al., 2019). By binding the phosphatidylinositol phosphatase synaptojanin 1, ITSNs support the $PI(4,5)P_2$ hydrolysis and thus the uncoating of clathrin-coated pits (Cremona et al., 1999; Koh et al., 2004; Pechstein et al., 2010).

While endocytosis ensures the regulated internalization of membrane components and signaling molecules, exocytosis complements this process by facilitating the delivery of vesicular cargo to the plasma membrane. In this process ITSN1 contributes by interacting with Snap25, a component of the SNARE complex (Figure 3), which is needed for synaptic vesicle exocytosis (M. Okamoto et al., 1999). Specifically the ITSN1-L isoform might be important in this process, as it has been shown that ITSN1-mediated activation of Cdc24 stimulates actin remodeling at docking sites for vesicles facilitating exocytosis (Malacombe et al., 2006). Hence, ITSNs have been proposed as adaptors, linking exo- and endocytosis (Gubar et al., 2013). The interplay between endocytosis and exocytosis is critical, especially for synaptic function, as synaptic vesicles must be retrieved and replenished to sustain neurotransmission. Here, ITSNs are also suspected to regulate the synaptic vesicle replenishment from reserve pools by regulating synapsin localization in relation to the active zone (Gerth et al., 2017; Sakaba et al., 2013). Additionally ITSNs facilitates clearance of the synaptic release site by association with synaptobrevin and the post-exocytic SNARE complex (Jäpel et al., 2020).

These functions are not restricted to synapses of the central nervous system, but apply also to the NMJ, at least in *D. melanogaster* where ITSNs function at the NMJs was investigated. As shown in two independent Dap160 loss of function or null mutant strains, Dap160 interacts with the *D. melanogaster* Eps15 organizing synaptic vesicle endocytosis (Koh et al., 2007), and stabilizing endocytic proteins like dynamin, synaptojanin and AP180 at the NMJ (Koh et al., 2004; Marie et al., 2004). Loss of Dap160 results in a decrease of synaptic vesicles, the accumulation of endocytic intermediates at the active and periactive zone along with impaired endocytosis (Koh et al., 2004), and defects in synaptic vesicle recycling (Marie et al., 2004). As

in the central nervous system, Dap160 interacts with synapsin, to archive efficient synaptic vesicle clustering for the reserve pool at the NMJ (Winther et al., 2015).

In addition to its role in endocytosis and synaptic vesicle regulation, ITSNs are known for their role in actin polymerization (Figure 4). The actin cytoskeleton is important for maintaining cell shape and providing structural support, whilst enabling dynamic processes, such as cell movement and endocytosis (Pollard & Cooper, 2009). With its GEF domain, ITSN-L interacts with the Rho GTPase Cdc42, as well as with the Cdc42 effector N-WASP (Hussain et al., 2001). Hussain et al. propose a model, where N-WASP binds ITSN prior to Cdc42 binding, as N-WASP enhances the DH domain functionality of ITSN to catalyze GDP to GTP exchange on GDP-bound Cdc42, thereby regulating its own activation. N-WASP then promotes Arp2/3-dependent actin polymerization and branching. The GEF activity of ITSNs can be modulated. For example, binding of numb, another endocytic adapter protein, enhanced the GEF activity of ITSN toward Cdc42 (Nishimura et al., 2006). This mode of action was further investigated by Gryaznova et al., 2015 leading to the identification of an additional regulation by WASP interacting protein (WIP), which has been shown to interact with ITSN1 and ITSN2 *in vivo* and *in vitro* via ITSNs SH3A, C, E domains and N-WASP (Gryaznova et al., 2015). Binding of WIP promotes N-WASP association with ITSN although they interact with ITSN via the same

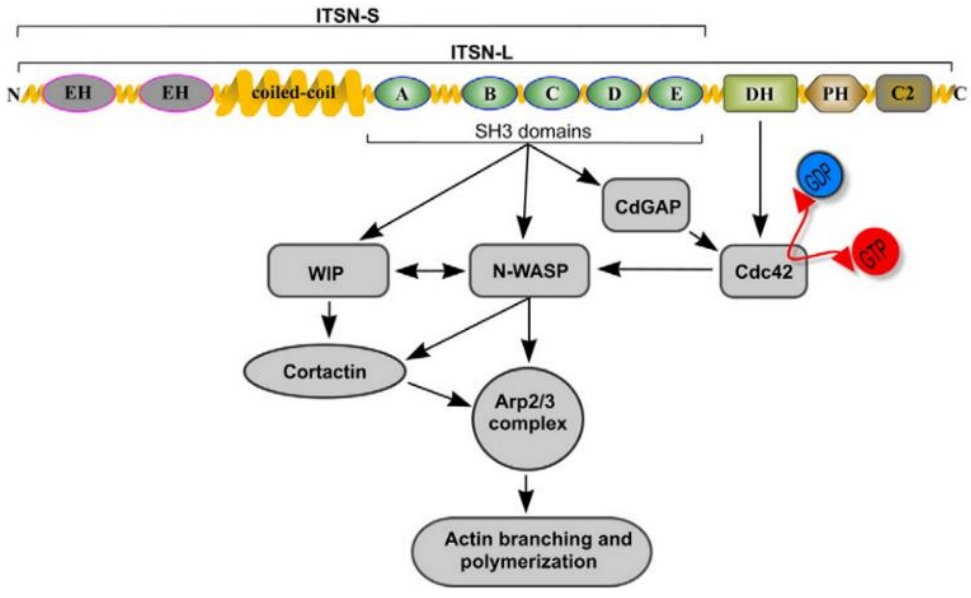

Figure 4: Model of ITSN-dependent actin polymerization via N-WASP and Cdc42. (Adapted from Gryaznova et al. 2015).

ITSNs promote actin polymerization by coordinating the activity of WIP, N-WASP and Cdc42 through distinct interaction domains. These proteins cooperatively regulate the activation of the Arp2/3 complex resulting in actin polymerization and branching.

domains (Gryaznova et al., 2018). While WIP is not necessary for N-WASP-mediated actin polymerization (Gryaznova et al., 2015), WIP overexpression resulted in an increased association between ITSN1 and actin, highlighting its importance in regulating this pathway (Gryaznova et al., 2018). Aside from influencing ITSN, WIP enhances cortactin (CTTN)-mediated Arp2/3 activation for actin polymerization (Kinley et al., 2003), suggesting an alternative way for WIPs to influence actin polymerization. Interestingly, ITSN1, WIP and CTTN have been reported to colocalize in U87-MG glioblastoma cells (Gryaznova et al., 2015), suggesting crosstalk between the two modes of actin regulation.

ITSN1-dependent actin polymerization via Cdc42 and N-WASP appears to be a conserved mechanism, as ITSN2-L regulates Cdc42 activity and downstream actin dynamics in *Xenopus laevis* development (Novokhatska et al., 2011). Similarly, in *D. melanogaster* Dap160 regulates actin polymerization along with nervous wreck via Cdc42 to promote WASp (*D. melanogaster* ortholog of WASP) mediated actin polymerization (Rodal et al., 2008).

On one hand ITSN-regulated actin polymerization appears to be important for dendritic spine development, as loss of ITSNs as well as their overexpression were shown to result in altered dendritic spine morphology (Nishimura et al., 2006; Thomas et al., 2009; Vollweiter et al., 2023). On the other hand, the ITSN-WIP complex reportedly localizes to invadopodia of MDA-MB.231 cells as well as to clathrin-coated pits (Gryaznova et al., 2015).

Apart from the previously mentioned subcellular localizations of ITSN1, ITSN1-S has been found in the nucleus, imported by importin α, likely due to a bipartite nuclear localization signal (NLS) in the SH3D domain (Alvisi et al., 2018) and/or a bipartite NLS within the EH domains (H. Zhang et al., 2021). In a yeast two-hybrid screen in 2012 Wong et al. already identified several interactions of ITSNs with different nuclear proteins, ranging from RNA-binding proteins to transcription factors. However, recent publications provide better insights into ITSNs nuclear functions. For example, ITSN1 was shown to interact with the nuclear protein SAM68, an mRNA-binding protein which can accumulate in so-called SAM68 nuclear bodies in the nucleus. The interaction with ITSN1 affects its solubility and thereby regulates SAM68 function. Interestingly, an interaction of ITSN1 with mRNA via its SH3D domain was identified, suggesting ITSN1 may recruit mRNA to regulate their splicing via SAM68 (Pankivskyi et al., 2021). In addition, ITSN1-S has been found to interact with DNA helicase II

(NDHII), also called ATP-dependent RNA helicase A. This protein has several functions, ranging from DNA replication to post-transcriptional RNA regulation, RNA-mediated gene silencing and mRNA translation. It suppresses DNA replication and DNA synthesis in cancer cells (H. Zhang et al., 2021).

Moreover, ITSNs perform a multitude of additional functions: they are involved in the PI3K-C2β-Akt pathway for cell survival, Ras activation and RTK ubiquitylation. ITSNs are implicated in a variety of disorders, including cancer (C. Xie et al., 2019), Alzheimer's and Parkinson´s disease (Hunter et al., 2011; Skuladottir et al., 2024), Down syndrome (Hunter et al., 2011; Pucharcós et al., 1999), and neuropsychiatric diseases (Wong et al., 2012; Zhou et al., 2022).

1.3 The ITSN double-knockout mouse model

1.3.1 – what is known for young to adolescent mice

Protein function is often studied by the knockout or knockdown of proteins with subsequent search for alterations to the condition where the protein was still present. When knocking down only ITSN1, the impact of this single knockdown resulted in slowed down endo- and exocytosis (Yu et al. 2008). Though investigating the calyx of Held, this expected impact on endocytosis could not be detected (Sakaba et al., 2013). This suggested compensatory mechanisms, e.g. due to redundant functions of ITSN2. Therefore, a double-knockout (dKO)

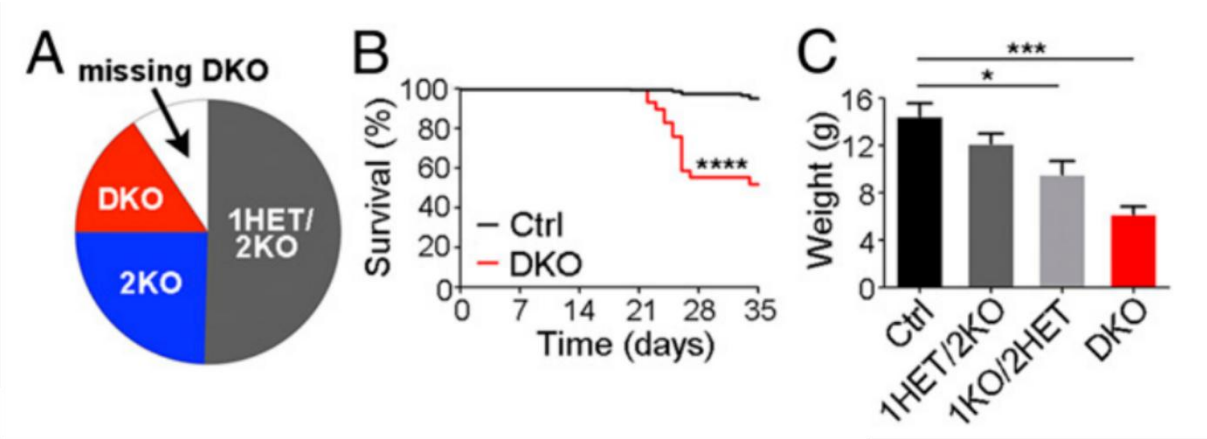

Figure 5: ITSN dKO mice have compromised viability. (Adapted from Gerth et al. 2017).

A) The genotypic distribution of offspring from ITSN1$^{+/-}$ / ITSN2$^{-/-}$ breedings revealed a non-mendelian distribution. B) Decreased post-natal viability of ITSN dKO mice (red) in comparison to ITSN2 KO control mice (black). C) Weight reduction of ITSN dKO and ITSN1$^{-/-}$ / ITSN2$^{+/-}$ mice.

generated by crossing ITSN2 KO with ITSN1 KO mice and breeding the resulting ITSN1$^{+/-}$ / ITSN2$^{-/-}$ as described in Gerth et al., 2017. Here, ITSN2 KO mice are used as control condition, as they show neither behavioral alterations nor changes in body weight or anatomy and endocytic protein levels remained also unaffected in the ITSN2 KO (Gerth et al., 2017).

In contrast to ITSN2 KO and ITSN1 KO mice which are born in mendelian ratio from heterozygous crossings, some ITSN dKO mice die prenatally, resulting in non-mendelian distributions (Figure 5A). Even postnatally, their viability is compromised as dKO mouse survival within the first month of life is reduced (Figure 5B). Additionally, a reduction in weight could already be observed in ITSN1$^{-/-}$ /ITSN2$^{+/-}$ mice, which is even more pronounced in ITSN dKO mice (Figure 5C) (Gerth et al., 2017). Behavioral observations of adult mice of at least 2 months age revealed some unexpected behavioral features. Most striking is a high number of corner jumps, a jackhammer like jumping in the corner of the home cage (Figure 5A). Furthermore, ITSN dKO mice exhibit hyperactive behavior characterized by stereotypic running-like behavior at the cage wall, and an increased locomotion speed (Figure 5B) alongside increased distance travelled and abrupt movement direction changes (Vollweiter et al., 2023). Since other behaviors like wall rearing (Figure 5C) or grooming remained unaltered, only specific motor routines seem to be obsessively repeated (Vollweiter et al., 2023). This behavior is reminiscent of ASD-like behavior, and similar repetitive behavior has been observed in other ASD related mouse models (Berg et al., 2015; Blundell et al., 2010). Indeed, mutations in ITSNs have been linked to autism in humans in several independent studies, identifying it as potential risk gene (Bruel et al., 2022; Liaqat et al., 2024; Zhou et al., 2022). As repetitive behaviors are associated with cortico-striatal imbalance (Langen et al., 2011), volumetric analysis of dKO brain volumes indeed revealed a relative reduction in striatal volume, with a slight increase in cortical volume (Figure 5D), taken the overall reduced brain volume into account (Vollweiter et al., 2023).

Therefore, striatal medium spiny neurons were further analyzed. They were found to be less branched in ITSN dKO mice, exhibiting less intersections as well as reduced spine density (Figure 5E). In line with that, cortico-striatal transmission was found to be impaired as discharging of medium spiny neurons is reduced (Vollweiter et al., 2023). Also, spontaneous excitatory currents are increased in frequency, suggesting an impaired postsynaptic function

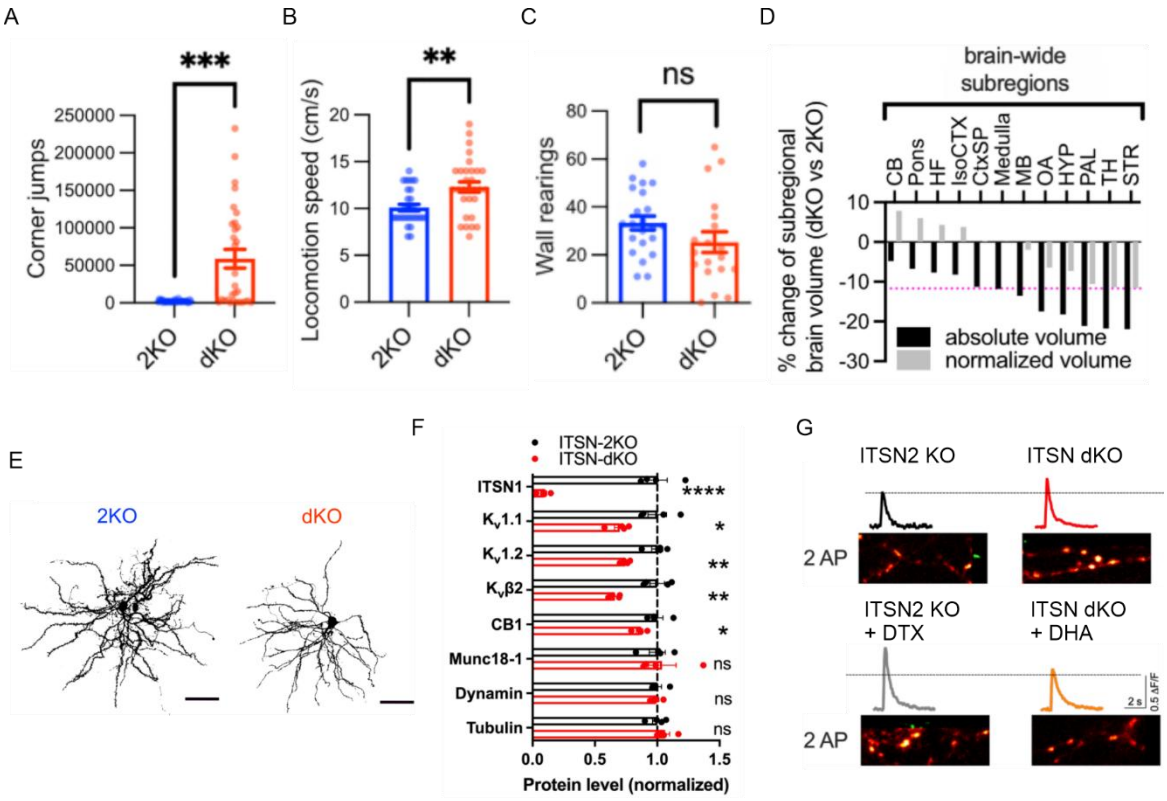

Figure 6: ITSN dKO mice exhibit repetitive behavior with structural alterations in the striatum. Adapted from (Vollweiter, 2021; Vollweiter et al., 2023).

Behavioral tracking for 24 h revealed that A) ITSN dKO mice exhibit excessive repetitive jumping in the corner of their cages. B) ITSN dKO mice exhibit increased locomotion speed, but no alterations in number of wall rearing (C). D) Volumetric analysis reveals structural alterations in the basal ganglia, especially the striatum. E) Medium spiny neurons in the striatum show reduced complexity and a decrease in spine density. F) Several presynaptic proteins, like Kv1.1, 1.2 and Kvβ2, are reduced in the synaptic membrane fraction. G) Loss of both ITSNs results in increased presynaptic Ca^{2+} levels, which can be mimicked by pharmacological manipulation of Kv1 channels.

(Vollweiter et al., 2023). And indeed, a reduced NMDA/AMPA current ratio hinted at alterations in postsynaptic receptor prevalence, which was verified biochemically. The NMDA receptor subunits NR2A and NR2B, as well as the postsynaptic scaffold PSD95 and actin, were found to be reduced, while NR1 and the AMPA receptor subunits GluA1 and GluA2 remained unaltered (Vollweiter, 2021). As ITSN1 interacts with NR2A and PSD, it was assumed that ITSNs stabilizes NMDA receptors and PSD95 at the postsynapse, likely by promoting local actin polymerization (Vollweiter et al., 2023).

In addition, presynaptic protein levels were determined, revealing decreased levels of voltage-gated potassium channel (Kv) subunits in the ITSN dKO brain (Figure 5F). Loss of Kv channels should be mirrored in prolonged Ca^{2+} influx, as repolarization slows down, and indeed, Ca^{2+} imaging of ITSN2 KO and ITSN dKO synapses revealed increased Ca^{2+} signals at the synapse. The reduction of Kv channels could be pinpointed as likely cause, as pharmacological

manipulation of Kv channels in ITSN2 KO mice with α-DTX, a Kv1 channel blocker (Harvey, 2001), increased Ca^{2+} influx to levels comparable to those in ITSN dKO mice. Conversely, treatment of ITSN dKO neurons with docosahexaenoic acid (DHA), an allosteric agonist of Kv1.2 (Yang et al., 2018), rescued their Ca^{2+} influx (Figure 5F). Taken together, ITSN dKO mice exhibit a hyperexcitable presynapse due to prolonged repolarization, while the postsynapse is hypoexcitable, caused by a reduction in NMDA receptors, which could be the reason for the repetitive behavior (Figure 7) (Vollweiter, 2021).

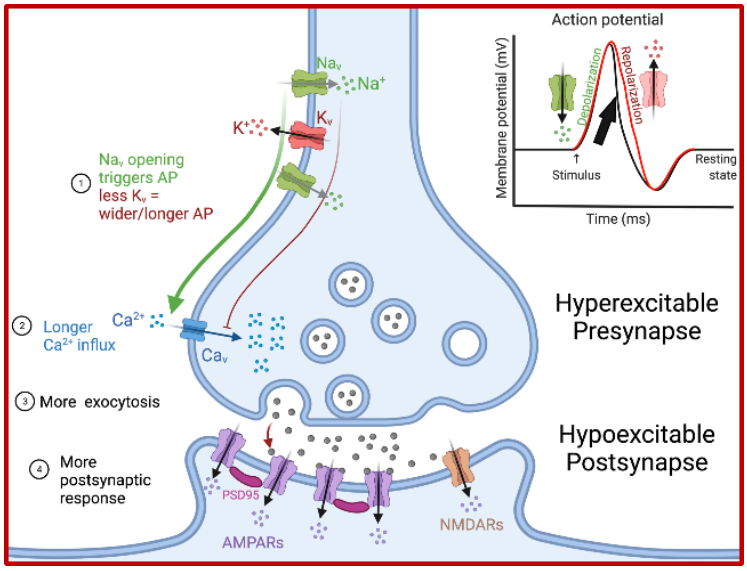

Figure 7: Proposed model of synaptic changes at the ITSN dKO synapse. (Unpublished figure created with Biorender by Tanja Maritzen)

The reduction in Kv channels results in a prolonged repolarization phase, allowing a longer Ca^{2+} influx at the ITSN dKO synapse. The increased Ca^{2+}-influx results in increased neurotransmitter exocytosis. However, as the NMDA receptors are decreased at the postsynapse, the postsynaptic response is weaker than it should be.

1.3.2 – what is known for middle aged mice

Since the stereotypic autism-related behavior was most prominent in mice around 2-months-old, it was also analyzed in older mice aged 6 months to 1 year. Surprisingly, the repetitive jumping decreased with age, and is less common, if present at all, in dKO mice older than 4 months (Figure 8A). While 2-months-old dKO mice moved at a higher speed than control mice (Figure 6B), 1 year old dKO mice exhibited a decrease in locomotion speed (Figure 8B), losing their characteristic, autism-related behavior. Unexpectedly, other behaviors which were not altered in 2-months-old mice, were now changed for 1 year old ITSN dKO mice. While ITSN2 KO mice show normal levels of wall rearing, ITSN dKO mice barely exhibit this behavior (Figure 8C) (unpublished data from Tanja Maritzen). Wall rearing requires mice to

bear weight on their hind limbs, but ITSN dKO mice appeared to avoid this weight shift. Along with their slower movement this shift in behavior may indicate hind limb impairments. The repeated and excessive jumping behavior observed in young mice could have caused permanent muscle tissue damage. In line, ITSN dKO mouse performance on a balance rod decreased progressively with age, hinting at gradually impaired motor coordination (Figure 8D). Additionally, ITSN dKO mice spent progressively more time exhibiting hind limb clasping with age (Figure 8E). Usually, this behavior is related to motor deficits and neurological dysfunction, including cortico-striato-pallido reticular pathways (Lalonde & Strazielle, 2011). As no electrophysiological recordings of these pathways or histological analyses of muscle tissues were performed up to this point, the cause for this phenotype is unknown. Possible explanations include impaired neurotransmission within the striatum, as

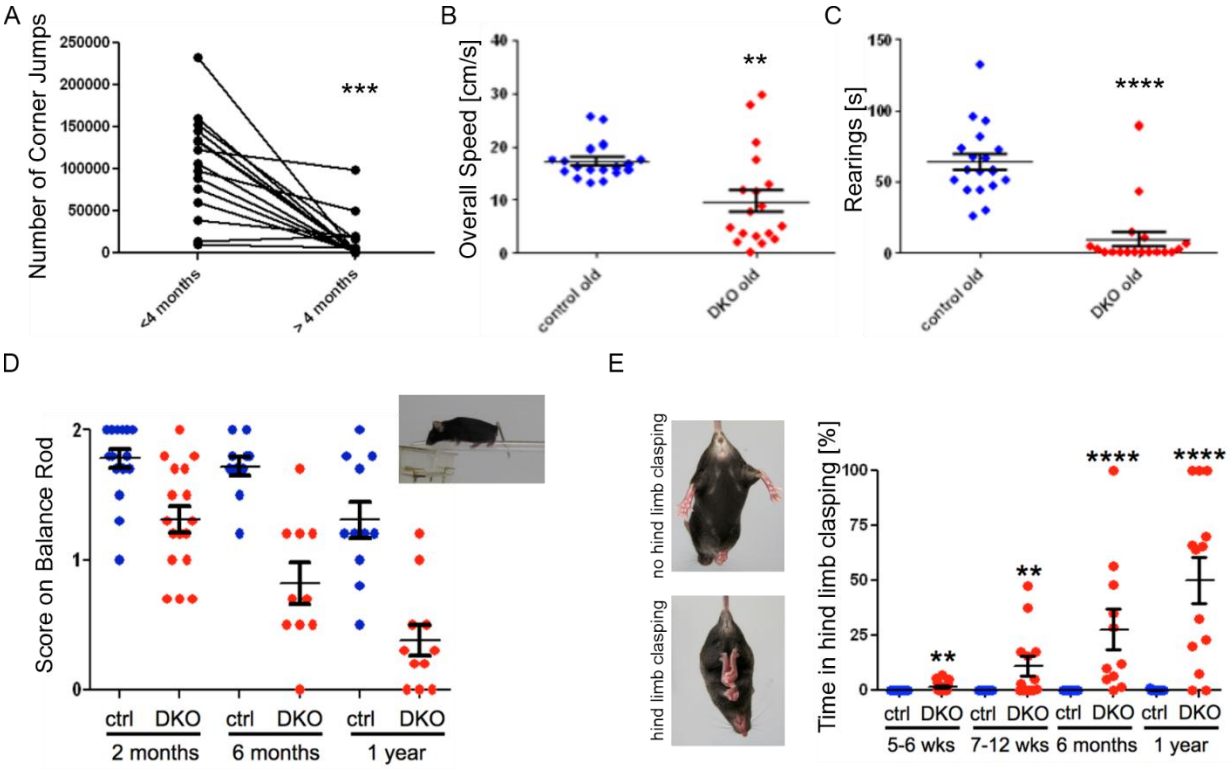

Figure 8: Decreased activity and progressive motor deficits in up to 1 year old ITSN dKO mice (unpublished data from Tanja Maritzen).

*A) Number of corner jumps decreases for mice older than 4 months. Wilcoxon matched-pairs signed rank test. B) The overall movement speed for 1 year old dKO mice is significantly reduced. Mann Whitney test. C) Number of rearings decreased significantly for 1 year old dKO mice. Mann Whitney test. D) Examination of balance in ITSN dKO mice reveals decrease in balancing abilities which decrease further with age. E) Left: example images of hind limb clasping in mice. Right: amount of time spent in hind limb clasping increases with age. Mann Whitney test. (A-E) Data points represent individual animals. (B-E) Data is given as mean +/- SEM. **p<0.01, ***p<0.001, ****p<0.0001.*

observed in 2-months-old mice, impaired neurotransmission to the muscle at the NMJ, or damage to the muscle tissue based on the excessive jackhammer-like jumping or as a consequence of differently induced muscular degeneration. Interestingly, it could recently be shown that ITSN1s play a role in internalization of active β1 integrin, while defect β1 integrin localization is associated with myopathies based on its role in myotube fusion and contractile machinery (Samsó et al., 2022). Nevertheless, up to now the cause of those progressive motor and coordination deficiencies in aging ITSN dKO mice remains unknown.

1.4 Aim of this study

The aim of this thesis is to better understand the molecular role of ITSNs in maintaining synaptic function and motor behavior by analyzing the effects of ITSN loss of function in ITSN dKO mice and identifying novel protein interactions that may contribute to its function.

More specifically, the goal of this thesis is divided into several parts.

The first objective is to get further insight into the potential defects underlying the progressive decrease in motor coordination with increasing age for the ITSN dKO mice. As shown by Vollweiter et al. (2023), ITSN dKO mice at the age of 2-months exhibit alterations of the basal ganglia, especially of the striatum, in regard to brain volume as well as cortico-striatal transmission which likely causes obsessive-compulsive disorder (OCD) and ASD like behavior. However, it is unclear whether the progressive decrease in motor coordination is a consequence of these alterations or if it might be based on changes in the muscular innervation or caused by progressive muscle degeneration. Therefore, one aim of this thesis is to investigate potential structural alterations in the synaptic connection between innervating nerves and muscles as well as muscle histology as possible causes for progressive motor coordination deficits.

My second objective focusses on alteration in presynaptic protein expression. It is yet to be clarified how the loss of ITSNs results in reduced levels of several presynaptic proteins, especially the voltage-dependent potassium channel Kv1.2. While the roles of ITSNs in endocytosis and synaptic vesicle recycling are well described, how can the loss of an endocytic adaptor results in a reduction of protein levels at the synapse? Rather one would expect cargo proteins to be stranded at the plasma membrane and therefore to display increased levels.

A number of mechanisms could be responsible for the observed decrease in protein levels. In the context of this thesis, I want to probe the following three hypotheses that have been proposed to explain this observation:

I) The scaffolding hypothesis: ITSNs are large scaffolds with a multitude of interaction partners. Therefore, they might directly or indirectly interact with the affected proteins. Indeed, it has been previously established for the postsynaptic NMDA receptor which also displays reduced levels in ITSN dKO mice that ITSN1 interacts with NMDA receptor subunits (Nishimura et al., 2006; Vollweiter et al., 2023). Thus, this study will investigate a potential interaction between the ITSNs and the presynaptic proteins Kv1.2 and its accessory subunit Kvβ2 since an interaction with ITSNs might stabilize the protein and protect it from degradation.

II) The actin hypothesis: ITSNs are interactors of actin-binding proteins and regulators of actin polymerization and, therefore, could either indirectly anchor proteins to the actin cytoskeleton or trigger the necessary presynaptic actin polymerization to supply actin for anchorage via other proteins. As the loss of ITSNs has been shown to reduce the actin prevalence at the synaptic membrane (Vollweiter, 2021), one might hypothesize that these proteins might lack stable anchorage and, consequently, be reduced. Therefore, I will investigate how far the presynaptic actin cytoskeleton might be altered in absence of ITSNs and if ITSNs interact with actin binders that are known to link Kv1.2 to the actin cytoskeleton.

III) The translation hypothesis: The translation of several of the reduced proteins is proposed to be regulated by FMRP (Darnell et al., 2011). Therefore, ITSNs might be part of the FMRP-dependent translation regulation. This idea is supported by the fact that mice deficient for JAKMIP1, a component of FMRP-positive mRNA granules, show a similar behavioral phenotype (Berg et al., 2015). In addition, ITSN1 has been shown to directly bind to mRNA (Pankivskyi et al., 2021). Thus, ITSNs might even have an impact on mRNA stability, that is independent of FMRP. To investigate a potential involvement of ITSNs in translational regulation, I will probe for interactions between ITSNs and components of the machinery associated with neuronal RNA granules and translational regulation.

2 Results

2.1 Decreased motor-coordination in ITSN dKO mice is neither based on alterations in NMJ morphology nor on muscle degeneration

2.1.1 The NMJ does not differ between ITSN2 KO and ITSN dKO mice

In the ITSN dKO mouse line, a variety of behavioral irregularities have been observed, from the repetitive jumping in up to 4-months-old animals, to a decreased activity in 1 year old animals. This decreased activity is accompanied by decreased motor coordination, such as impaired ability to balance on a rod. While the stereotypic and hyperactive behavior in younger animals is reminiscent of ASD and OCD, the decreased motor-coordination is not as straightforward to align with these diseases. Instead, the behavior seems more similar to muscular and neurodegenerative diseases (Lalonde & Strazielle, 2007; Prigogine et al., 2024).

In line with my first objective, I investigated if the impaired motor activity is based on the already known neuroanatomical changes, as observed for striatal medium spiny neurons, or whether it might have a different origin, such as an impaired innervation of the muscles. Therefore, I took a closer look at the connection between the central nervous system and the muscle, the NMJ. As morphological NMJ parameters like the presynaptic terminal area are proportional to quantal content (Harris & Ribchester, 1979; Jones et al., 2017), changes in the NMJ morphology can hint towards alterations in neuromuscular transmission. Since the motor coordination worsens with increasing age, the NMJ was examined in 2-months-old mice and 6-months-old mice. For this analysis, the NMJs of the triangularis sterni have been chosen due to several advantages: 1) their easy accessibility, (Kerschensteiner et al., 2008) 2) the thin and flat muscle morphology elucidating further processing or cutting for staining (McArdle et al., 1981) and 3) the lack of other sensory innervation (Duron et al., 1978; Kerschensteiner et al., 2008).

The triangularis sterni was isolated and stained with antibodies for synaptophysin, a synaptic vesicle protein used as a marker for presynaptic terminals, and bungarotoxin-AF594, a neurotoxin fused with AlexaFluor594, targeting nicotinic AChRs and thereby labeling postsynaptic structures (Figure 9A). A preliminary examination of ITSN2 KO and dKO NMJs did not show obvious alterations. However, to ensure no subtle changes were missed, a more

in-depth characterization of NMJs, such as colocalization of pre- and postsynaptic markers, pre- and post-synaptic area, endplate area, which refers to the convex hull area of the

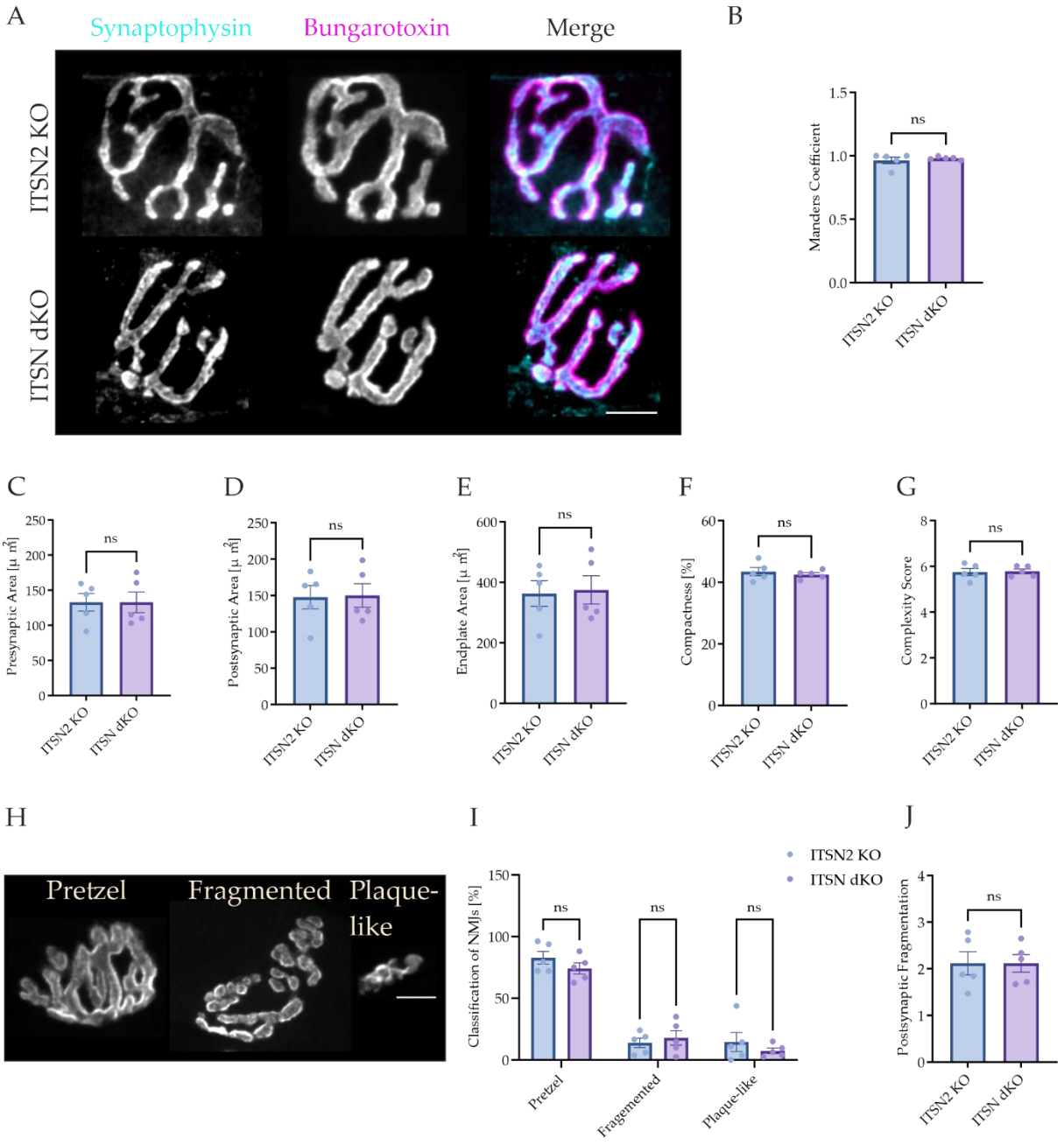

Figure 9: Same NMJ morphology for 2-months-old ITSN2 KO and ITSN dKO mice.

*A) Representative z-projections of NMJs from the triangularis sterni muscle of ~p60 ITSN2 KO and ITSN dKO mice. Presynaptic structures were stained with synaptophysin (pink) and postsynaptic terminals with bungarotoxin (red). Scale bar 10 µm. B) Colocalization of synaptophysin staining with bungarotoxin with the Manders Coefficient. C-G) Quantification of NMJ characteristics as C) presynaptic area, D) postsynaptic area, E) endplate area, F) compactness and G) complexity score. H) representative z-projections of pretzel, fragmented and plaque-like postsynaptic structures. Z-stacks projections were adjusted individually due to differences in slice number. Scale bar 10 µm. I) Quantification of morphological classification of ITNS2 KO and ITSN dKO NMJs. J) Quantification of the postsynaptic fragmentation. All plots shown as mean with SEM, single datapoints represent singe experiments. Statistical analysis for B-G, J) is a two-tailed, unpaired t-test was performed, while for I) a 2-way ANOVA was performed. ns p≥0.05, *p < 0.05, **p < 0.01, ***p < 0.001, N=5*

postsynaptic area were conducted. Additionally, more sophisticated measurements of morphology, including compactness and complexity, were determined. First, to probe the accurate alignment of pre- and postsynaptic structures, a prerequisite for proper signal transmission, the Mander's Coefficient for the overlap of presynapse with postsynapse was calculated. This resulted in a value of roughly 1 for the Ctrl and dKO NMJs, indicating a nearly complete overlap for both conditions (Figure 9B). Similarly, the apposition, another measure for the overlap of pre- and postsynaptic area, reached a value of ~0.9 for both conditions (Figure S 1A, B) confirming the overlap. In addition, the quantification of NMJ morphological features showed no significant differences in pre- or post-synaptic area (Figure 9C, D) or endplate area (Figure 9E) between the two genotypes. For both genotypes, the presynapse with a mean area of 132.8 μm^2 for ITSN2 KO (132.8 ± 12.59 μm^2) and dKO (132.8 ± 14.69 μm^2) is slightly smaller than the postsynaptic area with 147.7 ± 16.06 μm^2 for ITSN2 KO and 150 ± 16.21 μm^2 for ITSN dKO, as shown in Figure 9A and B. Furthermore, the compactness, a measure of how much of the endplate is covered with AChRs, or complexity, the logarithm of the product of number of branches, endpoints, and length of postsynaptic skeleton, (Jones et al., 2017) was not different for the dKO (Figure 9F, G; mean values for those measurements are shown in Figure S 1C, D, E). Next, the NMJ morphology was classified into pretzel-like, fragmented and plaque-like morphology (Figure 9H), but again, no significant differences could be found between ITSN 2 KO and dKO (Figure 9I). Although NMJ fragmentation only being one parameter for NMJ classification, it has been shown to be one of the main parameters determining NMJ morphology (Jones et al., 2017). Therefore, further examination was conducted, but again, without observing any significant changes in fragmentation (Figure 9J).

As the motor coordination deteriorates with age in the ITSN dKO mice, the 2-months time point may not yet be sufficiently advanced to discern age-dependent effects. Consequently, 6-months-old mice were included in the analysis, where coordination deficits are more pronounced. Due to the low number of aged ITSN2 KO and ITSN dKO littermates, $ITSN1^{+/-}$ / $ITSN2^{-/-}$ (ITSN1 het/ITSN2 KO) animals were used as an alternative control group in this dataset. Their behavior is consistent with the ITSN2 KO, without signs of autism- or OCD-like tendencies or motor impairment. Upon initial observation, the 6-months-old NMJs appeared similar to the 2-months-old stage (Figure 9A, Figure 10A), with the typical branching and pretzel-like arms, although the NMJ compactness increased from ~42% for both ITSN2 KO

(43.43 ± 1.33%) and dKO (42.49 ± 0.62%) to ~ 58% for both (ITSN1 het / ITSN2 KO 58.39 ± 0.81%; ITSN dKO 59.14 ± 0.18%) with age (Figure 9F, Figure 10F). Also, the overlap of

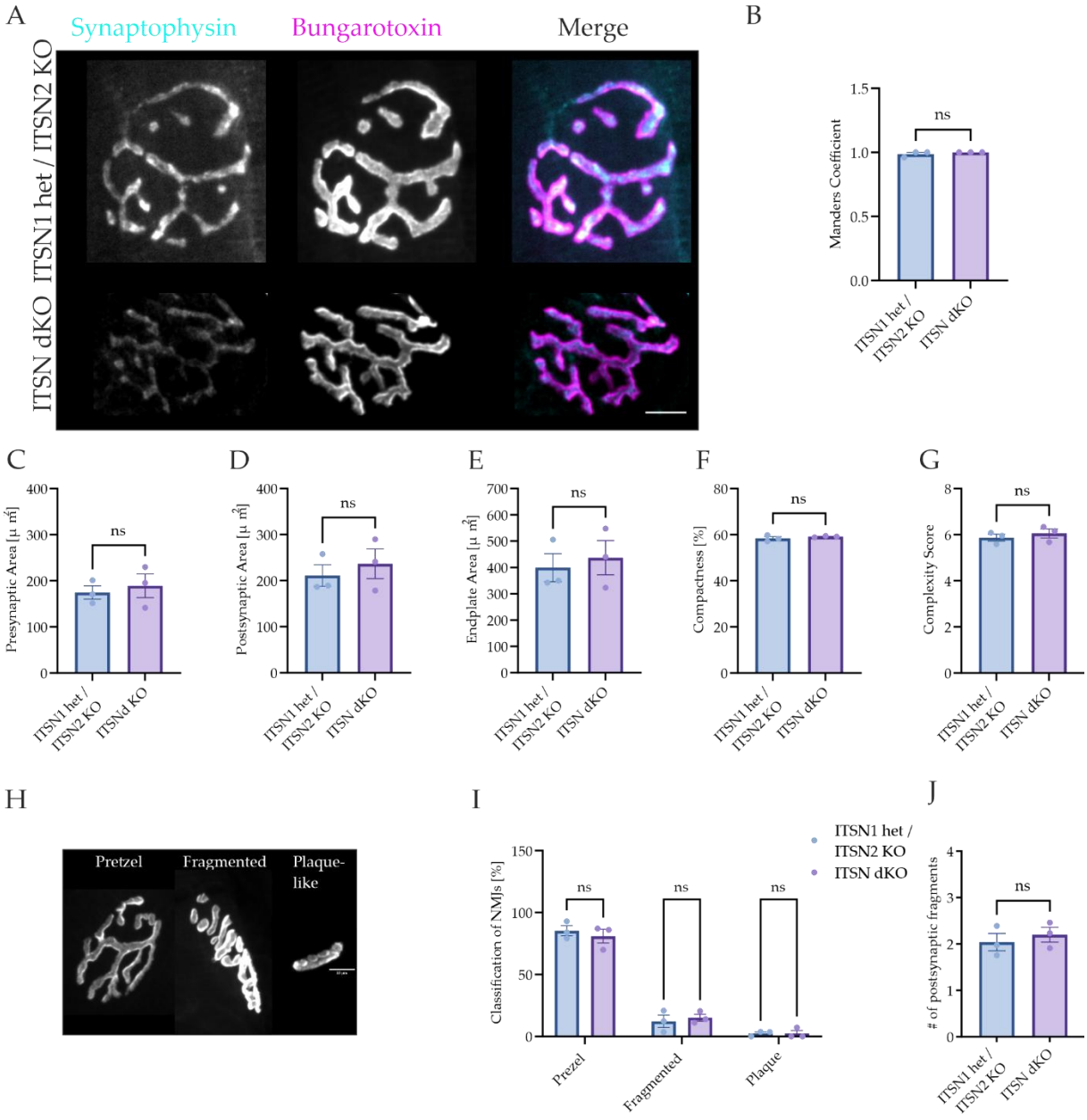

Figure 10: NMJ morphology in 6-months-old ITSN dKO mice remains unchanged.

*A) Representative z-projections of NMJs from the triangularis sterni muscle of 6-months-old ITSN1 het / ITSN2 KO and ITSN dKO mice. Presynaptic structures were labelled with synaptophysin (pink) and postsynaptic terminals with bungarotoxin (red). Scale bar 10 µm. B) Colocalization of synaptophysin staining with bungarotoxin estimated as Manders Coefficient. C-G) Quantification of NMJ characteristics as C) presynaptic area, D) postsynaptic area, E) endplate area, F) compactness and G) complexity score. H) representative z-projections of pretzel, fragmented and plaque-like postsynaptic structures. Scale bar 10 µm. I) Quantification of morphological classification of ITSN1 het / ITSN2 KO and ITSN dKO NMJs. J) Quantification of the postsynaptic fragmentation. All plots shown as mean with SEM, single datapoints represent singe experiments. Statistical analysis for B-G, J) is a two-tailed, unpaired t-test. For I) a 2-way ANOVA was performed. ns p≥0.05, *p < 0.05, **p < 0.01, ***p < 0.001, N=3*

the pre- and postsynaptic sites are not visibly or quantitatively different, as the Mander´s Coefficient remained the same for both conditions (Figure 10B). The presynaptic and postsynaptic area, as well as the endplate area, are slightly increased for control and ITSN dKO NMJs at 6-months of age (Figure 10C, D,E) compared to the 2-months of age (Figure 9C, D, E), while they do not differ significantly between ITSN1 het / ITSN2 KO and ITSN dKO (Figure 10C, D, E). Taking pre- and postsynaptic colocalization, and size (Figure 10B, C, D, E), apposition (Figure S 1G) NMJ branching and other morphological features (Figure S 1H, I, J) into account, there were no significant differences between controls and ITSN dKO. NMJ compactness and complexity remained unchanged (Figure 10F, G). In line with those unaltered morphological parameters, the classification into pretzel-like, fragmented or plaque-like NMJs stayed at roughly the same levels for both conditions (Figure 10H, I) and the postsynaptic fragmentation was similar for ITSN1 het / ITSN2 KO controls and ITSN dKO (Figure 10J). Since the proportion of pretzel-shaped NMJs remains stable at ~80% across both time points for all conditions, there is no indication of premature degradation or degeneration of ITSN dKO NMJs based on NMJ classification. Therefore, the observed motor coordination deficits are unlikely to result from early NMJ degeneration.

2.1.2 2-months-old jumping ITSN dKO but not 6-months-old dKO mice have a smaller myofiber area in the Triceps brachii and Tibialis anterior

Since the innervation appears intact, I next examined the muscle tissue, as impaired motor coordination could also result from progressive skeletal muscle weakness, degeneration, or loss of muscle mass. This pathology is characteristic for muscular dystrophy and myopathies (Tubridy et al., 2001). However, muscular dystrophies and myopathies are distinct disease entities. Muscular dystrophies are characterized by a degenerative pattern involving necrosis, fibrosis, and regeneration, which is typically absent in myopathies (Tubridy et al., 2001). DMD is a well-studied form of muscular dystrophy, commonly studied with the *mdx*-mouse, which is lacking full-length dystrophin (Bulfield et al., 1984; Dubuisson et al., 2022).

As a first indicator of muscle dystrophy or loss, the muscle weight is evaluated, relative to the total body weight. These relative values are necessary as ITSN dKO mice are slightly lighter in weight than ITSN2 KO littermates at 2- and 6-months-age (Figure S 3), confirming the observation for 21-36 day old mice by Gerth et al., 2017. Again, two different timepoints, 2-

months-age and 6-months-age, were chosen as the motor coordination deficits increase with age. Usually, the most severely affected muscle should be studied to asses myopathies (Terry & Wells, 2016), which favors examining muscles of the hindlimbs, like the Tibialis anterior (TA), in our mouse model. To account for possible artifacts in the TA due to hindlimb overuse during repetitive jumping, the Triceps brachii (TB) was included as a forelimb control muscle. Additionally, a slow-twitch muscle (soleus, mostly type I fibers) and a fast-twitch muscle (extensor digitorum longus (EDL), predominantly type II) were included for the 6-months-old mice to assess whether type I or type II fibers are differentially affected.

The dissected muscles appeared similar in size (Figure 11A) for the 2-months-old ITSN2 KO and ITSN dKO, which was evident after quantification (Figure 11B). This observation holds true even when taking the sex into account (Figure S 2B, C). Even the 6-months-old dKO mice muscles do not differ in weight for the TB, TA, or EDL. But the soleus is significantly increased in weight for the dKO (Figure 11C) with 0.035±0.003% to 0.024±0.003% of total Body Weight for the 2KO. This increase in weight is unexpected as a loss of muscle tissue appeared more likely.

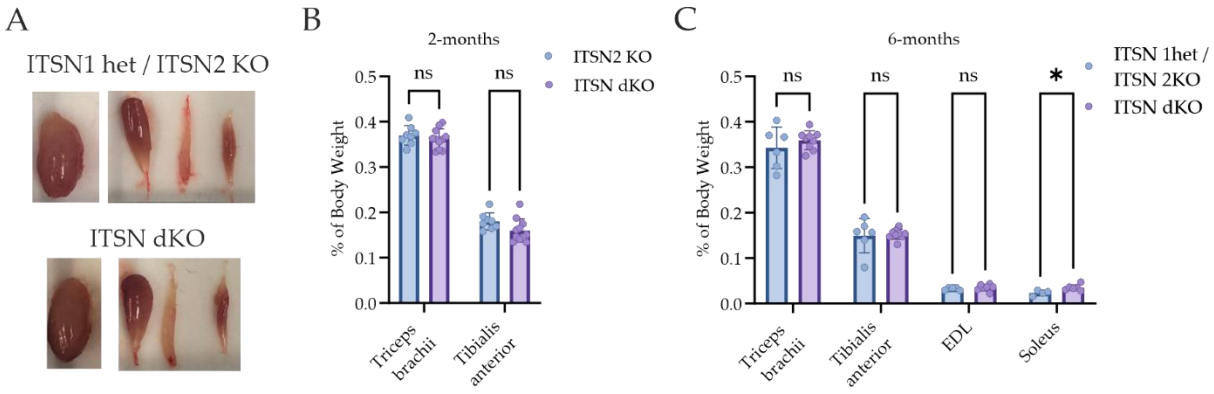

Figure 11: Muscle weights for TB and TA do not differ between ITSN2 KO and ITSN dKO for 2-months-old or 6-months-old mice.

*A) Representative images of dissected muscles of 2-months-old mice. Order from left to right: TB, TA, EDL, soleus. B) Quantification of muscle weight relative to total body weight for TB and TA of 2-months-old mice. C) Quantification of muscle weight relative to total body weight for TB, TA, EDL and Solus of 6-months-old mice. Two-sided, unpaired t-tests, ns p≥0.05, *p < 0.05, N(ITSN2 KO, 2-months) =8, N(ITSN dKO, 2-months) =11, N(ITSN2 KO, 6-months) =4-6, N(ITSN dKO, 6-months) =6-9.*

Given the absence of any evident muscle dystrophy in the weight quantification, the subsequent analysis focused on the myofiber morphology. For this, histopathological evaluations with freshly frozen sections are the gold standard, especially to study muscular

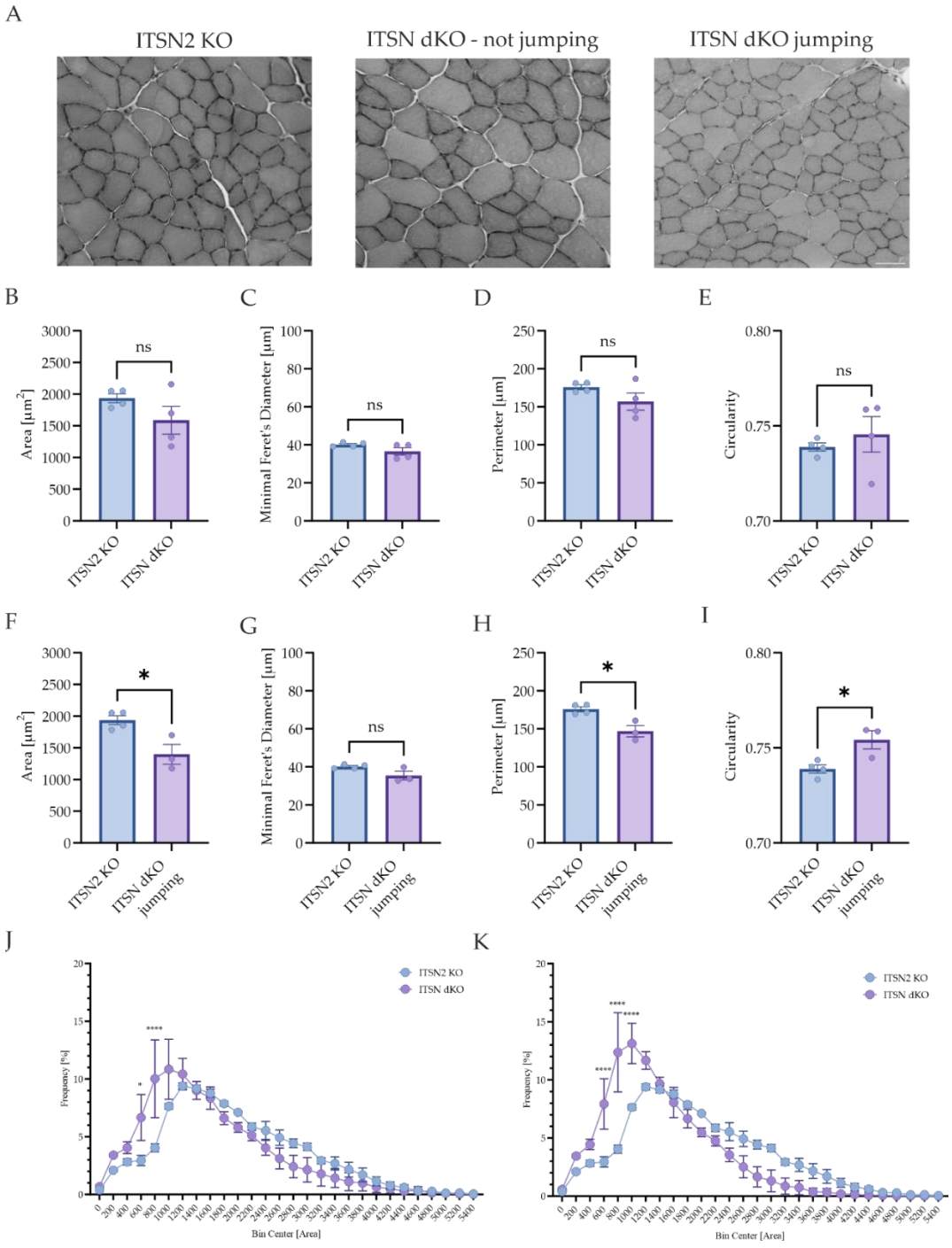

Figure 12: Histological evaluation of the TA reveals changes for 2-months-old ITSN dKO mice exhibiting the "jumping" phenotype.

A) Representative images of TA myofibers analyzed for ITSN2 KO and ITSN dKO mice. For the dKO, two different examples are shown to illustrate the differences between non-jumping and jumping dKO mice. Scale bar, 50 µm. B-E) Quantification of myofiber parameters such as B) Area, C) Minimal Feret's Diameter, D) Perimeter, and E) Circularity of 2 months old ITSN2 KO and ITSN dKO mice. F-I) Quantification of myofiber parameters of ITSN2 KO mice compared to only the "jumping" ITSN dKO mice from the cohort of dKO mice analyzed in B-E). The analyzed parameters are: F) Area, G) Minimal Feret's Diameter, H) Perimeter, and I) Circularity. J) Frequency distribution of TA myofiber area for ITSN2 KO and ITSN dKO. K) Frequency distribution of TA myofiber area for ITSN2 KO and "jumping" ITSN dKO. Statistical analysis for B-I) was performed by two-tailed, unpaired t-tests. for J-K) a Mixed-effects analysis with a Bonferroni's multiple comparison test, $\alpha=0.05$, ns $p \geq 0.05$, *$p < 0.05$, **$p < 0.01$, ***$p < 0.001$, ****$p<0.0001$, *N(ITSN2 KO, ITSN dKO all) =4, N(ITSN dKO only jumping) =3.*

dystrophy or other neuromuscular disorders (Terry & Wells, 2016) with classical histochemical dyes like hematoxylin and eosin (HE) being extensively applied in myofiber research (Dubuisson et al., 2022). HE stains can uncover substantial information about the myofiber, such as the myofiber area and its size distribution, perimeter, and circularity. Because the area is highly susceptible to small errors from sections not cut perfectly perpendicular to the fiber length, the minimal Feret's diameter, the shortest distance between two parallel tangents of an object, provides a more stable measurement, allowing for more reliable estimates (Briguet et al., 2004). Hematoxylin stains the nuclei, enabling identification of increased muscle degeneration and regeneration, since muscle regeneration is characterized by central nuclei. Eosin stains the myofiber, or the cell body of other cell types, and thus reveals information about fiber integrity, or inflammation and necrosis (Dubuisson et al., 2022; Terry & Wells, 2016).

The TA is a commonly evaluated muscle (Terry & Wells, 2016) and was stained with HE. The tissue appears healthy, without any signs for inflammation or necrotic fibers. Also regenerating fibers, marked by central nuclei, as they appear at 7-weeks of age for the *mdx*-mouse model for DMD (Briguet et al., 2004), were sparsely observed for both conditions (Figure 12A). A quantitative analysis of the myofibers including area, minimal Feret's diameter, perimeter, and circularity of the TA did not reveal significant differences between ITSN dKO and ITSN2 KO mice (Figure 12B-E). Closer analysis of the area distribution revealed a shift towards smaller myofibers, even with significantly smaller myofibers in the range of 600-800 μm^2, which were not represented when looking at the means (Figure 12J). Though for the mean dKO, areas there is an apparent variability. Upon closer observation, it might be linked to the phenotypical variation of the ITSN dKO mice which can be divided in "jumping" and "non-jumping" mice, depending on a short behavioral observation. Three out of four dKO mice were classified as "jumping" and their values for area, minimal Feret's diameter and perimeter are lower than for the one "non- jumping" mouse in the analyzed cohort. This must be interpreted cautiously, as the analysis of a single non-jumping mouse does not provide sufficient data for generalization. Still, comparing only the "jumping" ITSN dKO subgroup with the ITSN2 KO mice reveals that the area, perimeter as well as the circularity differ significantly between ITSN2 KO and jumping ITSN dKO mice (Figure 12F, H, I). The frequency distribution of the area shows an enhanced reduction in area for jumping ITSN dKO

compared to all ITSN dKO mice based on a significant increase in number of 600-800 μm² fibers (Mixed-effects analysis with a Bonferroni's multiple comparison test) while fibers in the range of 2600-4000 μm² are reduced, though not significantly (Figure 12K).

As the reduction in the area can only be detected in jumping animals, these findings might be an artefact based on repetitive behavior. To investigate whether the results are different in a muscle that should not be affected by excessive use caused by the repetitive behavior the TB muscles of 2-months-old ITSN2 KO and ITSN dKO mice were stained with HE. Again, the tissue appeared healthy, without signs of inflammation, necrotic fibers or regenerating fibers (Figure 13A). A quantitative analysis of the myofibers revealed no substantial differences in the area, minimal Feret's diameter, perimeter, or circularity (Figure 13B-E). When taking a closer look at the relative frequency distribution of the area, the differences between ITSN2 KO and ITSN dKO were even more striking than for the TA. The ITSN dKO seemed to have smaller myofibers, especially for bins spanning 600-1000 μm², where a significant difference was detected (Mixed-effects analysis with a Bonferroni's multiple comparison test, α=0.05) (Figure 13J). But like the TA myofibers, the dKO mean values varied and seemed to segregate based on the behavioral phenotype of the mice. As before, when excluding the "non-jumping" dKO mouse from the dataset, a significant decrease in myofiber area, minimal Feret's diameter and perimeter, but not circularity (Figure 13F, H-I) was seen. Surprisingly, the extent of myofiber reduction is stronger in the TB myofibers which were reduced by 39,3%, while the TA myofiber area was only reduced by 27.7%. Taking a closer look at the frequency distribution of the area comparing ITSN2 KO with "jumping" ITSN dKO mice, the smaller myofibers are based on significantly more small fibers in the bins spanning 600-1400 μm² together with a significant decrease in relatively large fibers of 2800-3600 μm² (Figure 13K). This was unexpected, as the TB is not involved in the excessive repetitive behavior. However, the loss of ITSN1 seems to affect this muscle even stronger than the TA, hinting at "jumping" ITSN dKO being more affected by the ITSN1 loss than "non-jumping" animals.

As the motor coordination deficits of ITSN dKO mice were shown to increase with age, I decided to investigate also muscles of 6-months-old dKO mice. If the phenotype observed in 2-months-old dKO mice is indeed the cause of motor impairment, it would be expected to be more pronounced in the muscles of older dKO animals. Therefore, 6-months-old ITSN dKO

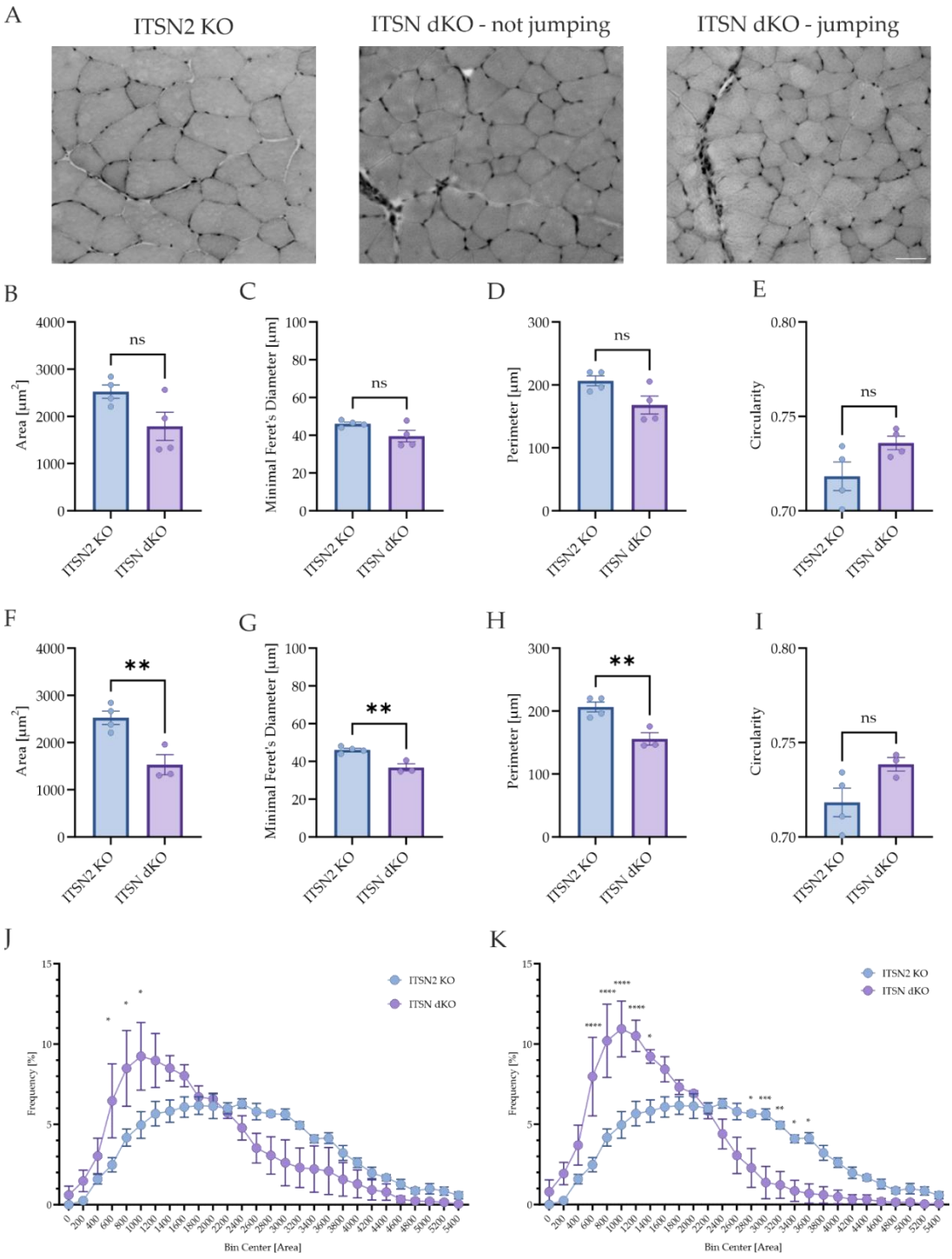

Figure 13: Histological evaluation of TB reveals morphological changes for 2-months-old ITSN dKO mice exhibiting the "jumping" behavioral phenotype.

*A) Representative images of TB myofibers analyzed for ITSN2 KO and ITSN dKO. Scale bar, 50 µm. B-E) Quantification of myofiber parameters such as B) Area, C) Minimal Feret's Diameter, D) Perimeter, and E) Circularity of 2 months old ITSN2 KO and ITSN dKO mice. F-I) Quantification of myofiber parameters of ITSN2 KO mice compared to only the "jumping" ITSN dKO mice from the cohort of dKO mice analyzed in B-E). The analyzed parameters area: F) Area, G) Minimal Feret's Diameter, H) Perimeter, and I) Circularity. J) Frequency distribution of myofiber area for ITSN2 KO and ITSN dKO. K) Frequency distribution of myofiber area for ITSN2 KO and "jumping" ITSN dKO. Statistical analysis for B-I) was performed by two-tailed, unpaired t-tests, for J-K) a Mixed-effects analysis with a Bonferroni's multiple comparison test, α=0.05, ,ns p≥0.05, *p < 0.05, **p < 0.01, ***p < 0.001, ****p<0.0001, N(ITSN2 KO, ITSN dKO all) =4, N(ITSN dKO only jumping) =3.*

mice were assessed for their myofiber area. In line with the previously described decrease in jumping behavior, none of the ITSN dKO exhibited this behavior during a short behavioral observation period prior to the experiment. As for the investigation of 6-months-old NMJs, due to a lack of 6-months-old ITSN2 KO mice, ITSN1 het / ITSN2 KO animals were considered as the control condition, as they lack the behavioral phenotype of ITSN dKO mice. Comparing the HE stains between the control and ITSN dKO mice, some of the dKO myofibers appear a little more structured, as the myofiber is stained less evenly than the ITSN1 het / ITSN2 KO (Figure 14A), similar to myofibers with fragmented sarcoplasm. Usually, this is accompanied by highly irregular sizes of the myofibers, and nuclei spread throughout the myofiber. This was, for instance, observed in 3-months-old *mdx*-mice (Dubuisson et al., 2022), but is not the case for the dKO myofibers. In general, some more centrally located nuclei can be identified. However, their prevalence is consistent across the ITSN1 het / ITSN2 KO and the ITSN dKO mice and sparse compared to *mdx*-mice (Dubuisson et al., 2022). Surprisingly, the quantification of the mean area, minimal Feret's diameter, perimeter and circularity reveals similar values for all parameters for the dKO and the control condition (Figure 14C-F). As the ITSN dKO motor coordination declined with increasing age, an effect represented in the myofibers was expected. Even the frequency distribution of the area that was shifted to smaller areas of 600-100 μm^2 for the 2-months-old dKO mice (Figure 13J), appears unaltered in the 6-months-old dKO mice compared to the age-matched ITSN1 het / ITSN2 KO control (Figure 14B).

In summary, based on the muscle weight at 2- or 6-months age and the overall myofiber morphology, no muscle dystrophy could be identified in the TA or TB of either 2-months- or 6 months-old ITSN dKO mice. However, 2-months-old jumping ITSN dKO mice have smaller myofibers area in the TB and TA muscle. Intriguingly, although located in the hindlimbs and therefore being used during the repetitive jumping, the phenotype for the TA myofibers, is not stronger than in the TB. Unexpectedly, this phenotype is lost in the 6-months-old dKO mice, thus making it unlikely to be the cause for the declining motor coordination.

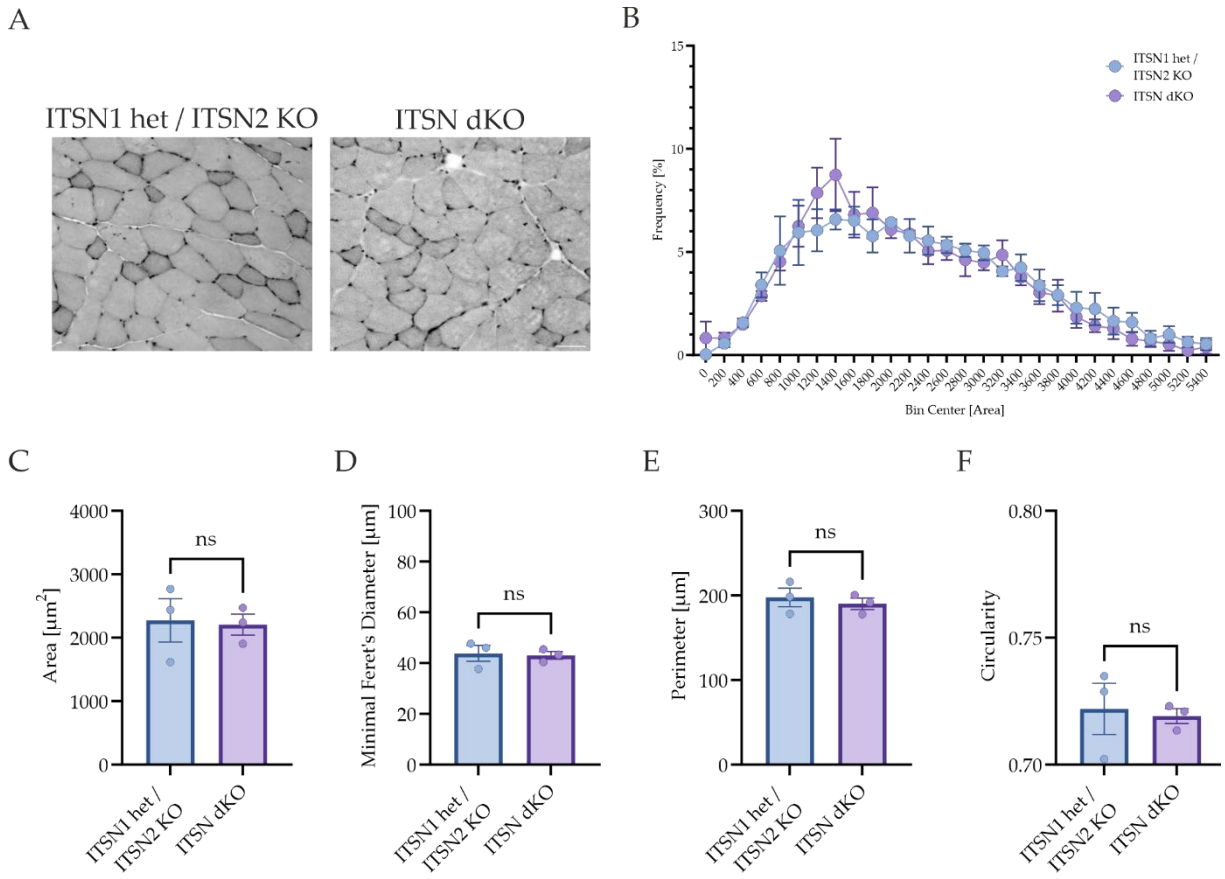

Figure 14: TB myofiber area of 6-months-old ITSN dKO and ITSN1 het / ITSN2 KO do not differ anymore.

A) represnetative Images of TB myofibers for 6-months-old ITSN1 het / ITSN2 KO and ITSN dK mice. Scale bar 50 µm. B) Frequency distribution of 6-months-old ITSN1 het / ITSN2 KO and ITSN dKO mice. Quantification of myofiber parameters such as C) Area, D) Minimal Feret's Diameter, E) Perimeter, and F) Circularity of ITSN1 het / ITSN2 KO and ITSN dKO mice of 6-months-age Statistical analysis for C-F, is a two-tailed, unpaired t-test, for B a Mixed-effects analysis with a Bonferroni's multiple comparison test, α=0.05, ns p≥0.05. N(ITSN1 het / ITSN2 KO, ITSN dKO) =3

2.2 Possible mechanisms by which ITSNs could regulate Kv-Channel prevalence at the presynaptic membrane

Previous studies of ITSN dKO mice showed a variety of alterations, ranging from altered survival, weight, neuronal morphology and transmission to decreased membrane levels of synaptic proteins (Gerth et al., 2017; Vollweiter, 2021; Vollweiter et al., 2023). Aiming to find the reason for the reduced protein levels, I addressed three hypotheses regarding a potential underlying cause of the observed protein levels reduction, the scaffolding hypothesis, the actin hypothesis and the translation hypothesis. For the postsynaptic neurotransmitter receptor NMDAR and the postsynaptic scaffold PSD95 it has been established that they interact with ITSNs (Vollweiter et al., 2023), suggesting that ITSNs help stabilize these postsynaptic proteins by scaffolding them. Therefore, I will focus on the presynaptic proteins, especially Kv1.2 and its accessory subunit Kvβ2, as they are severely affected by the dKO, with their loss functionally supported by Ca^{2+}-imaging and pharmacological modulation (Vollweiter, 2021).

2.2.1 ITSN1 does not stabilize Kv1.2 or Kvb2 by direct binding

To probe for the scaffolding hypothesis, which suggests that ITSN1 might stabilize Kv1.2 via scaffolding similar to the situation of NMDARs, I will start with investigating protein–protein interactions.

Among various methods available to study protein–protein interactions, the pull-down assay offers a distinct advantage. It allows overexpression of one protein or domain to ensure sufficient bait availability while maintaining near-physiological levels of endogenous interaction partners, particularly when using lysates such as those from brain tissue. However, full-length ITSN1 fused to a GST tag cannot be efficiently produced in *E. coli.* Therefore, smaller parts comprising individual interaction domains were generated, which has the added advantage of enabling an investigation of domain-specific interactions.

Because the SH3 domains of ITSN1 are known to act as its main interaction hubs, they were considered as likely candidates for binding Kv1.2 or Kvβ2. Although analysis of the protein sequence (obtained from the UniProt database; Kv1.2: P63141, Kvb2: P62482), with the SH3-domain motif miner MoDPeptInt (Kundu et al., 2014) did not identify an ITSN1 specific binding site, they contain several core PxxP motifs (Figure 16C) (Kurochkina & Guha, 2012). Those motifs were sufficient for SH3-mediated interaction of CTTN with Kv1.3 (Hajdu et al.,

2015). However, a pull-down with mouse brain lysate did not reveal any interaction between Kv1.2 or Kvβ2 and the ITSN1 SH3 domains (Figure 15A). Only an interaction with the known interaction partner dynamin, which interacts with the SH3 A, C and E domains and was used here as positive control, was successfully detected (Figure 15A). Since the reduced Kv1.2 levels could only be detected at the synaptic membrane and not in a total mouse brain lysate, a synapse-specific interaction remained a possibility. To address this, a pull-down was performed with a crude synaptosome lysate. The N-terminal EH and CC domains of ITSN1

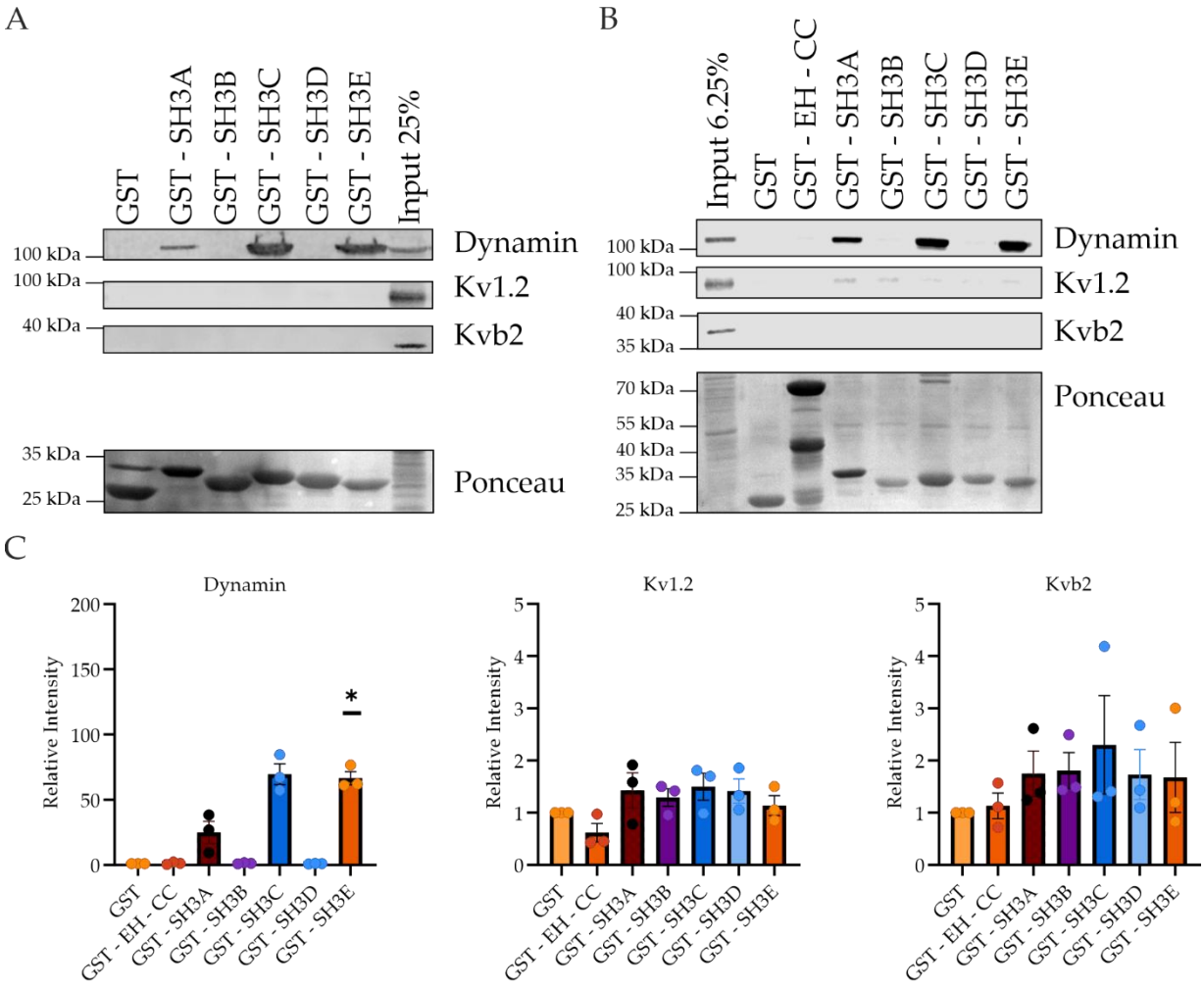

Figure 15: No interaction between ITSN1 and Kv1.2 or Kvb2 based on pull-down experiments.

*A) Pull-down of GST-fused ITSN1 SH3 domains with mouse brain lysate. Eluates were analyzed by immunoblotting and probed for dynamin as positive control and Kv1.2 and Kvb2 as proteins of interest. Ponceau staining confirms similar amounts of bait-constructs. 50 µg were loaded for the input. B Pull-down of GST-fused ITSN1 SH3 domains with crude synaptosome lysates. Eluates were analyzed by immunoblotting and probed for dynamin as positive control and Kv1.2 and Kvb2 as proteins of interest. Ponceau staining confirms similar amounts of bait-constructs. 25 µg brain lysate were loaded for the input. C) Quantification of signal intensities of putative interactors normalized to their background signal using GST as bait for pull-down experiments with synaptosome lysates. From left to right: dynamin, Kv1.2, Kvb2. Statistical significance was evaluated by several one-sample t-tests, with a Bonferroni correction for multiple testing. *p < 0.05, N(A: Dynamin, Kvb2) =3, N(A: Kv1.2) =2, N(B) =3.*

were included this time to avoid overlooking a possible interaction. Still, no robust interaction was detected, although faint bands were observed at the SH3 domains (Figure 15B). To obtain reliable data, the pull-downs were repeated and quantitatively analyzed. This analysis confirmed the absence of specific binding to Kv1.2 or Kvβ2 (Figure 15C).

While splitting ITSN1 into domains is experimentally practical, it may disrupt its native tertiary structure, potentially compromising interaction fidelity. To surpass this shortcoming, a co-immunoprecipitation (Co-IP) was used as an alternative. In this approach, a primary antibody against the bait protein captures endogenous protein complexes. Still, immunoprecipitations with Kv1.2-specific antibodies did not detect an interaction between ITSN1 and Kv1.2 in the crude synaptosome lysate, although Kvβ2, used as positive control being a known interactor of Kv1.2, was successfully co-precipitated (Figure 16A). Given the technical challenges often encountered with transmembrane proteins like Kv1.2 in precipitation-based assays, constructs containing the sequence of the cytosolic N- or C-terminus of Kv1.2 or full-length Kvβ2 fused to the GST sequence were generated for use in pull-down assays (Figure 16B). Nevertheless, no interaction between ITSN1 and any of the GST-fusion constructs could be detected in the crude synaptosome lysate. Still, the positive controls confirmed the general functionality of the assays. The Kv1.2 N-terminus, which contains the binding site for Kvβ2, served as a positive control and successfully precipitated Kvβ2 in the GST-Kv1.2-N pull-down. Interestingly, for the Kv1.2-C terminus, which should not bind to Kvβ2, a faint band was detected. It is weaker than for the N-terminus and likely reflects indirect binding of Kvβ2 via endogenous Kv-channel complexes, based on the C-terminal interaction with other Kv-channels (Zhao et al., 2009). For the GST-Kvβ2 construct, Kv1.2 served as positive control. Unexpectedly, Kv1.2 was also detected in the GST-control, though the signal of the Kv1.2 band for the GST-Kvβ2 sample was clearly stronger confirming its specificity. ITSN1 could be detected on the GST-control, but not for the GST-Kvβ2 pull-down, suggesting that its presence was likely unspecific (Figure 16D).

In summary, no direct interaction between ITSN1 and Kv1.2 or Kvβ2 could be detected using either pull-downs assays or co-immunoprecipitations. This was unexpected, given the previous data by Dennis Vollweiter and the fact that both Kv subunits contain SH3 binding motifs and ITSN possesses 5 SH3 domains.

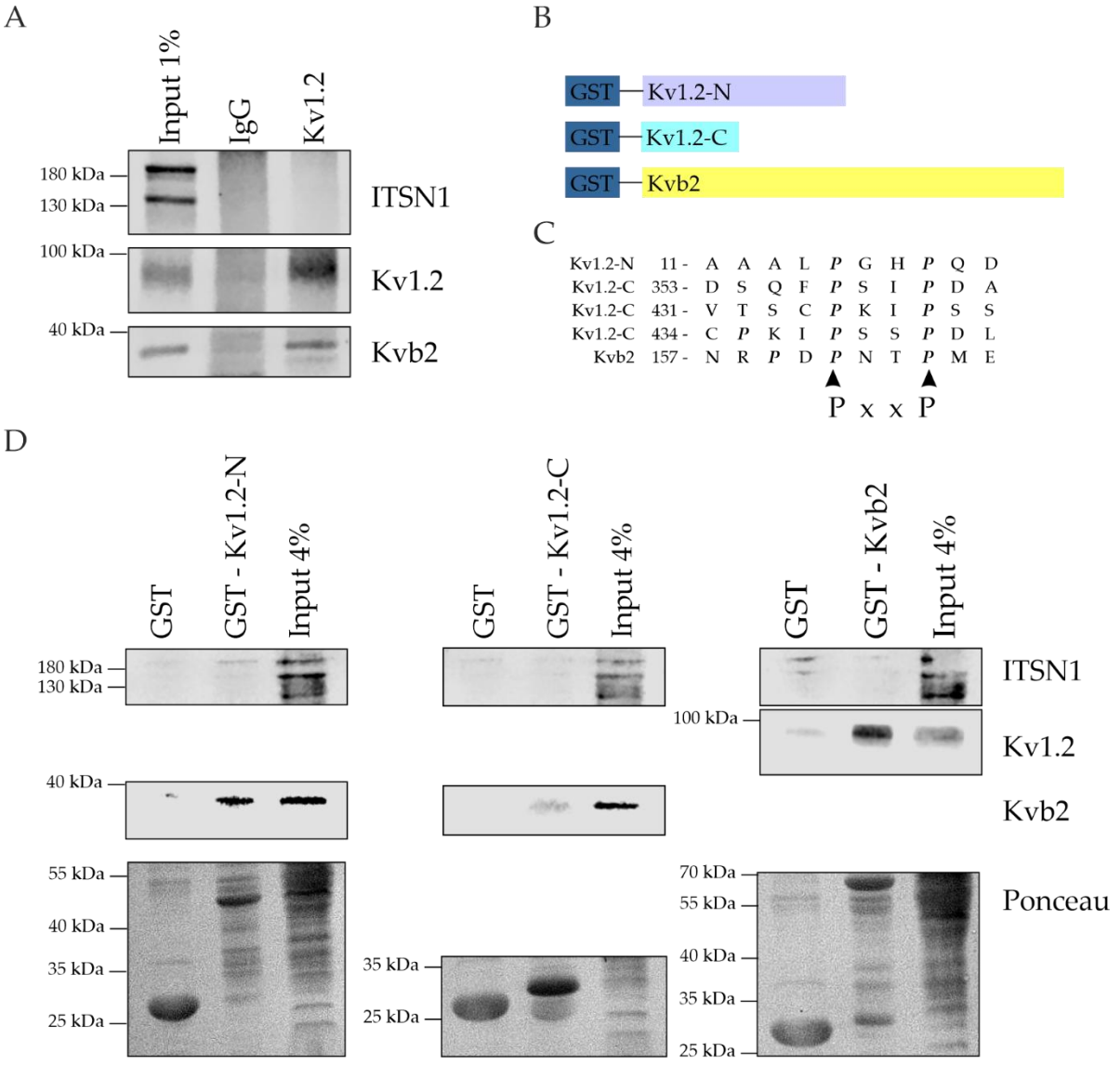

Figure 16: Kv1.2 or Kvβ2 do not bind to ITSN1.

A) Co-immunoprecipitation with Kv1.2 does not precipitate with ITSN1 but itself and its known binding partner Kvb2 in a crude synaptosome fraction. N =2. B) Cloned Kv1.2 and Kvb2 GST fusion constructs. For Kv1.2 the cytoplasmic domains, the N-terminus and the C-terminus fused with a N-terminal GST-tag. Full-length Kvb2 fused to a N-terminal GST-tag D) Pull-down approach of the different Kv1.2 and Kvb2 fusion constructs show no interaction with ITSN1 in mouse brain lysate. N=2.

2.2.2 *ITSNs might stabilize Kv1.2 and Kvb2 indirectly via CTTN*

The absence of a detectable interaction between ITSN1 and Kv1.2 or Kvβ2, as revealed by pull-down and co-immunoprecipitation experiments, suggests that ITSNs might stabilize Kv channels through an indirect mechanism. A potential mediator is CTTN, an actin-binding protein involved in actin polymerization and rearrangement, which is known to bind Kv1.2 and to regulate its currents and surface localization by influencing its endocytosis based on experiments in HEK293 cells (Hattan et al., 2002; Williams et al., 2007).

CTTN modulates actin dynamics through the Arp2/3 complex. Notably, ITSNs have been demonstrated to regulate Arp2/3 activity via WIP and N-WASP as well (Gryaznova et al., 2015), thereby supporting the possibility of a shared signaling axis. In addition, CTTN and ITSN1 have many shared interaction partners such as dynamin, WIP and N-WASP (Cosen-Binker & Kapus, 2006; Gryaznova et al., 2018; Tsyba et al., 2011) so that it seems likely that they might be part of the same complex. These parallels suggest that ITSNs may influence Kv1.2 localization and stability indirectly by being part of a CTTN-containing complex. This ITSN1-CTTN-Kv1.2 complex could stabilize Kv1.2 and Kvb2 just by scaffolding or might anchor Kv1.2 to the actin cytoskeleton. Based on this, three main questions arise: a) can we replicate the interaction of Kv1.2 and Kvb2 with CTTN, b) does ITSN1 bind CTTN, and c) is this complex linked to the actin cytoskeleton.

First, to replicate the results by Hattan et al., 2002 and Williams et al., 2007 regarding an interaction of Kv1.2 and CTTN in HEK cells in another cell culture model, I transfected HeLa cells with constructs encoding Kv1.2-GFP, untagged Kvβ2 and CTTN-mCherry. Kv1.2 is co-transfected with Kvβ2 to increase Kv1.2 surface expression (Yee et al., 2022). Additionally, I visualized the F-actin cytoskeleton with phalloidin to probe for a possible link to the actin cytoskeleton. When transfecting cells with Kv1.2-GFP and Kvβ2, different expression patterns of Kv1.2 were observed. Kv1.2 either clustered to puncta-like structures, and/or was highly expressed in a cellular compartment close to the nucleus (Figure 17A, Kv1.2 & Kvβ2). This is likely the endoplasmic reticulum (ER) or Golgi apparatus, as Kv-channels are produced and assembled in the ER from which they are transported to the Golgi. There they are further modified (Nagaya & Papazian, 1997) before transport to the plasma membrane. My research is focused on the study of Kv-channels located on the surface. To this end, I have directed my attention toward the analysis of puncta-like structures, as they appear to be surface-based Kv-channels. Still, the levels of Kv-puncta vary, probably based on either missing co-transfection with Kvβ2 or low expression levels of Kvβ2. Either way, Kv1.2-puncta were not observed to overlap with the F-actin cytoskeleton (Figure 17A, merge). The transfection of HeLa cells with CTTN-mCherry revealed cytosolic localization and puncta (Figure 17B, CTTN). A high proportion of CTTN puncta exhibited overlap with actin puncta (Figure 17B, merge), suggesting that the CTTN localization observed upon overexpression is reliable, given its

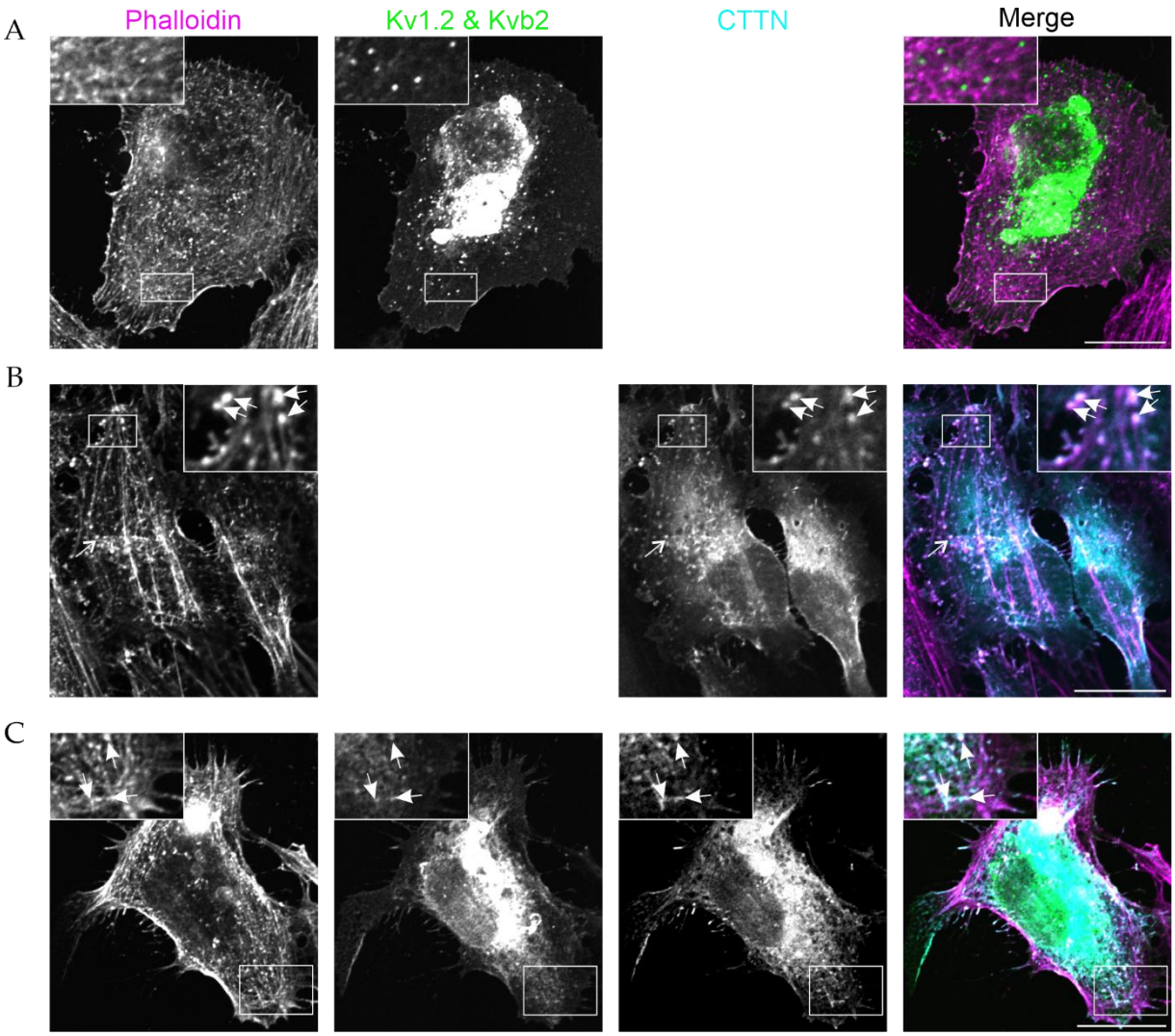

Figure 17: Co-transfection of CTTN, Kv1.2 and Kvβ2 shows partial localization of CTTN and Kv1.2 to actin puncta in HeLa cells.

A) HeLa cells transfected with Kv1.2-GFP and Kvβ2 and probed with the F-actin marker phalloidin showed no overlay of Kv1.2 with F-actin. Scale bar, 20 µm B) HeLa cells transfected with CTTN-mCherry and stained with phalloidin showed colocalization of cortactin and actin (white arrows in zoomed images). Scale bar, 20 µm. C) Triple transfection of HeLa cells with CTTN-mCherry, Kv1.2-GFP and Kvβ2 and stained with phalloidin showed that Kv1.2-GFP is partially present at CTTN-positive actin puncta (white arrows in zoomed images). Scale bar 20 µm. Representative images were adjusted individually due to differences in expression levels.

established role as an actin-binding protein. A triple transfection with CTTN-mCherry, Kv1.2-GFP and Kvβ2 was performed but proved difficult, as cells transfected with all three constructs were in poor health. Cells in better condition either seemed to lack Kvb2, as Kv1.2 was not present in puncta, or lacked at least one of the transfected constructs. Still, as representative image, a relatively healthy appearing cell with seemingly low Kvβ2 expression was chosen, as the health of the cell could influence the localization pattern (Figure 17C). Interestingly, with the co-transfection of Kv1.2, Kvb2 and CTTN, CTTN located to the cellular compartments,

where Kv1.2 was observed. However, some CTTN puncta could be observed which colocalized with actin (Figure 17C, merge). A small fraction of those puncta overlapped with Kv1.2, too (Figure 17C, merge arrow). Despite its minimal colocalization with CTTN at the cell surface, the presence of CTTN at the same cellular compartments as Kv1.2 suggests that the interaction of Kv1.2 with CTTN, as demonstrated by Hattan et al. in HEK cells, can be replicated in Hela cells. Additionally, this complex of CTTN and KV1.2 appears to be linked to actin puncta.

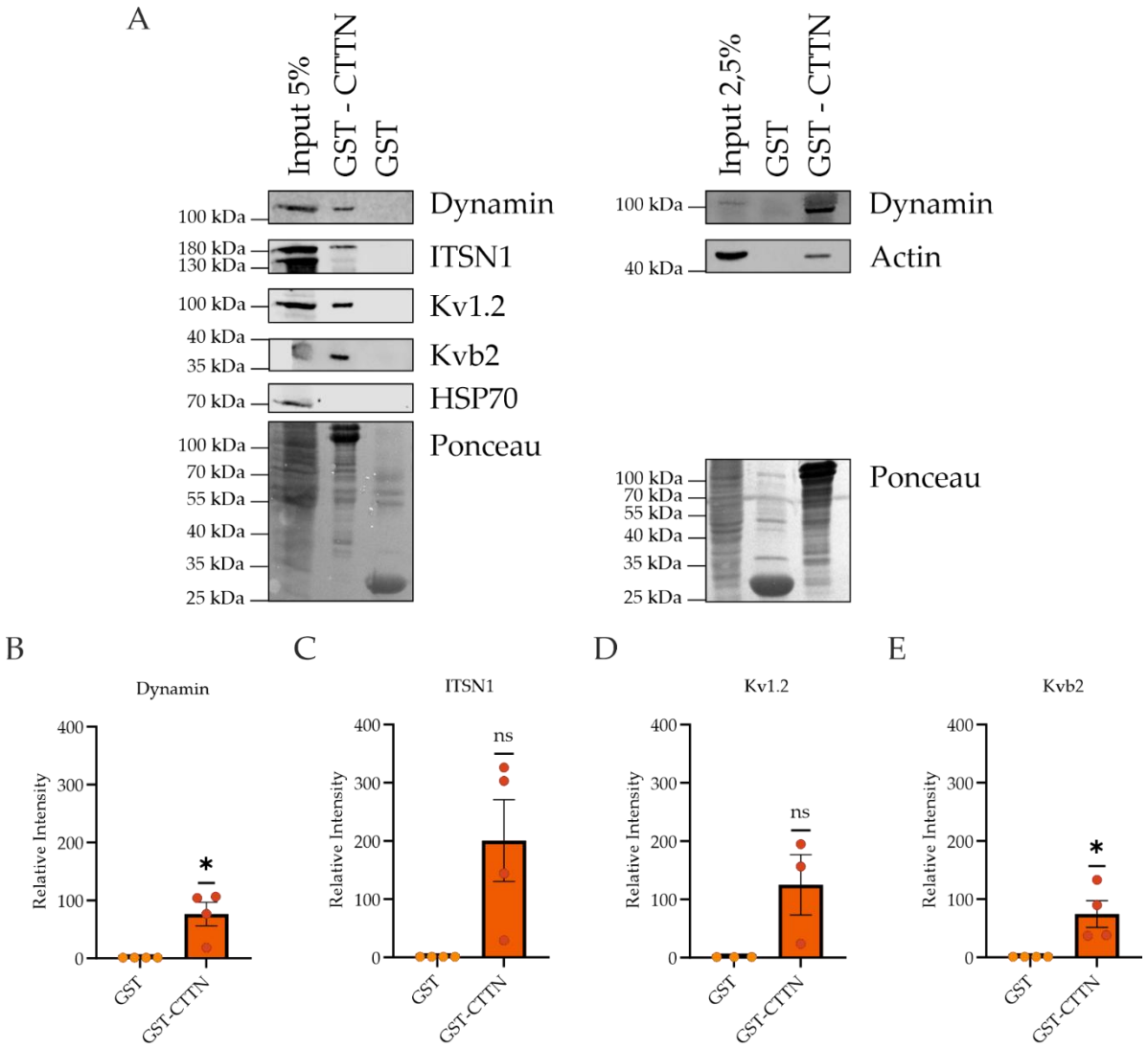

Figure 18: GST-CTTN interacts with ITSN1, Kv1.2, Kvβ2 and actin from mouse brain lysate.

*A) Pull-down experiments using GST-CTTN and mouse brain lysate. Eluates were probed by immunoblotting for the indicated proteins. Dynamin as a known interactor of CTTN served as positive control, and HSP70 as negative control. Ponceau staining confirms similar amounts of bait-constructs. B-E) Quantification of the binding extent of the protein indicated on the y-axis to GST-CTTN relative to its background binding to GST which was set to 1. Statistical analysis was performed with a one sample t-test comparing the results to a hypothetical value of 1. ns= p > 0.05 *=p < 0.05, N(Dynamin, ITSN1, Kvβ2)=4, N(Kv1.2, HSP70)=3, N(Actin) =1.*

Next, the question of whether ITSN1 and CTTN interact was addressed. At the same time, the interaction of Kv1.2, Kvb2 and CTTN was probed in mouse neuronal tissue. For this, a GST-fusion construct of CTTN, GST-CTTN, was generated, and a pull-down assay was performed with brain lysate. As expected, the known CTTN interactor dynamin was successfully co-precipitated, along with Kv1.2 and Kvβ2 (Figure 18A, left). Surprisingly, upon quantification, only the interaction between CTTN and Kvβ2 reached statistical significance (Figure 18E), likely due to the greater variability of the relative Kv1.2 signal intensities across replicates (Figure 18 D). Notably, ITSN1 was also successfully co-precipitated with GST-CTTN (Figure 18A, left) in four independent experiments. However, based on the one-sample t-test this interaction did not reach significance, likely due to the high variability of relative ITSN1 intensities, as for Kv1.2 (Figure 18C, D). Interestingly, the band for the neuronal long isoform of ITSN1 at ~180 kDa appeared to be co-precipitated more strongly than the shorter isoforms in 3 out of 4 experiments (Figure 18A), even though most interaction domains are shared between both isoforms. Additionally, the known interaction between CTTN and actin was confirmed (Figure 18A, right), supporting the observed colocalization between CTTN and actin puncta (Figure 17B). However, this result does not prove that Kv subunits are physically linked to the actin cytoskeleton via CTTN and/or ITSN1, as these proteins may reside in distinct protein complexes.

To determine whether the interaction of ITSN and CTTN occurs at actin puncta, where the CTTN-Kv1.2 interaction is observed, a double transfection combined with a co-staining of the actin cytoskeleton was performed in Hela cells (Figure 19). ITSN1 and CTTN show some cytosolic colocalization, which might be caused by protein overexpression, as ITSN1 typically appears more punctuated due to its association with clathrin-coated pits or reticular adhesions. However, at some actin puncta (Figure 19, zoom in), a colocalization of all three proteins can be detected (Figure 19, white arrows), suggesting an interaction of ITSN1 and CTTN at the same subcellular structures where CTTN binds Kv1.2.

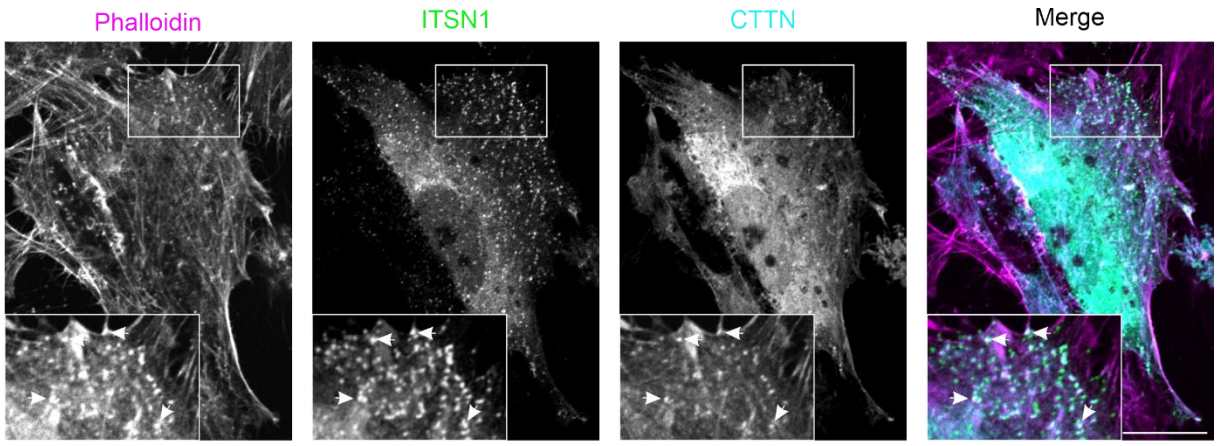

Figure 19: Co-transfection of HeLa cells with ITSN-GFP and CTTN-mCherry reveals colocalization at actin puncta.

Confocal images of HeLa cells transfected with ITSN-GFP and CTTN-mCherry and probed for F-actin with phalloidin. The boxed in area at the top is shown enlarged at the lower left corner of the image. White arrows point towards colocalization sites. Scale bar, 20 µm.

Investigating a potential indirect ITSN-dependent stabilization mechanism of Kv-subunits revealed CTTN as a promising mediator since CTTN binds Kv1.2 and Kvb2 as well as ITSN1. This interaction can be located to actin puncta, suggesting that Kv-subunits may be stabilized through anchorage to the actin cytoskeleton via a CTTN-ITSN complex.

2.2.3 Synaptic actin alterations in ITSN dKO mice

Actin plays an essential role in the structural and functional organization of pre- and postsynaptic compartments. At the presynapse it is involved in synaptic vesicle endo- and exocytosis, by regulating and maintaining the synaptic vesicle pool, and by influencing vesicle mobilization, docking and priming (Cingolani & Goda, 2008; Sankaranarayanan et al., 2003). At the postsynapse, especially in dendritic spines, actin functions as a dynamic cytoskeletal scaffold critical for spine morphology, receptor anchoring, and thereby synaptic strength modulation in an activity-dependent manner (Hotulainen & Hoogenraad, 2010; Matus, 1999).

Actin polymerization is assumed to be impaired in ITSN dKO mice and thereby disrupting receptor anchorage, potentially contributing to the observed reduction of NMDA receptor subunit levels (Vollweiter et al., 2023). Aside from its role in regulating the synaptic vesicle pool and its dynamics at the presynapse, actin likely anchors Kv1.2 and/or Kvβ2 via CTTN at the plasma membrane (Williams et al., 2007). With a lack of actin, the base of the anchorage might be missing, resulting in lower protein levels at the membrane. Therefore, the precise localization of the actin loss observed in the LP1 fraction of ITSN dKO mice, as well as a

determination of the amount of polymerized actin, could give further insights into the probability of the actin hypothesis.

Actin polymerization can be indirectly biochemically assessed by differentiating between globular (G-) actin, the monomeric form, and filamentous (F-) actin, the polymerized form. The F/G-actin ratio provides insight into the balance between polymerization and depolymerization, potentially indicating altered actin dynamics under different conditions. For the ITSN dKO mice as compared to ITSN2 KOs mice, this ratio remained unchanged at forebrain synapses as band intensities for G- and F- actin were comparable, as confirmed by the quantification (Figure 20A, F). This was unexpected, as the long isoform of ITSNs can

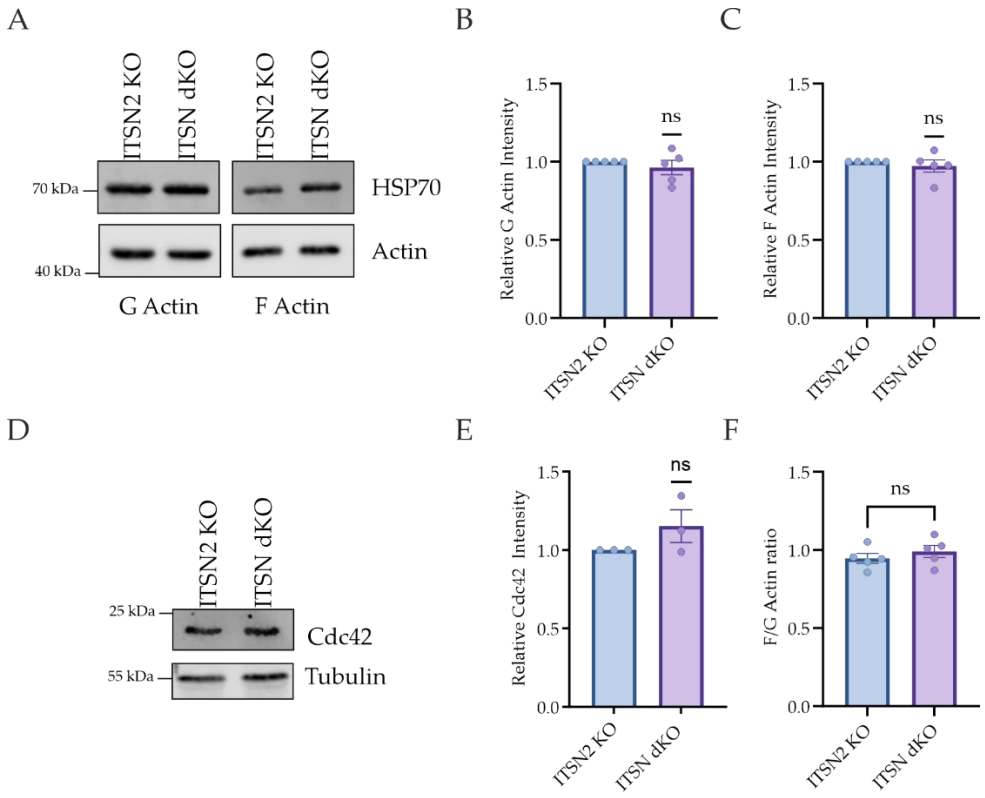

Figure 20: Unaltered F- to G-actin ratios at the synapses of ITSN dKO mice.

A) Representative Western blots of G- and F-actin fractions from ITSN2 KO and ITSN dKO synaptosomes probed for actin and HSP70. B) Relative G-actin intensities in synaptosomes revealed no change in G-actin levels between ITSN2 KO and ITSN dKO mice. C) Relative F-actin intensities in synaptosomes revealed no change in F-actin levels between ITSN2 KO and ITSN dKO mice. D) Representative Western blots from ITSN2 KO and ITSN dKO synaptosomes probed for Cdc42 and tubulin. E) Relative Cdc42 intensities in synaptosomes revealed no change in Cdc42 levels between ITSN2 KO and ITSN dKO mice. F) F-/G-actin ratio of normalized F- and G-actin intensities normalized to HSP70 do not differ between ITSN2 KO and ITSN dKO. Statistical analysis was performed with a two-sided, unpaired t-test. Ns= p>0.05 For B-C, E-F) a one sample t-test was performed comparing the results to a hypothetical value of 1. N(F- and G-actin)=5. N(Cdc42)= 3.

regulate Cdc42- and N-WASP-dependent actin polymerization (Humphries et al., 2014; Hussain et al., 2001), therefore, a decreased F/G-actin ratio was anticipated. A closer examination of the G- and F- actin levels of 2KO and dKO synaptosomes revealed comparable actin levels for G- (Figure 20B) or the F-actin (Figure 20C) between the ITSN2 KO and ITSN dKO, explaining the unaltered F/G-actin ratio. As ITSNs influence actin polymerization via Cdc42 (Hussain et al., 2001), its prevalence at the synapse might have an influence on actin levels, but no significant change was observed (Figure 20D, E). This contradicts the finding of reduced overall actin levels observed by Vollweiter et al. 2023. However, the previous loss of actin was observed specifically in the synaptic membrane fraction, whereas crude synaptosomes were used for this assay.

The unaltered G- and F- actin levels observed in the synaptosomes raised the question whether the method was appropriate to detect subtle actin changes. So, as an additional method to evaluate the synaptosome actin content in ITSN2 KO and dKO mice, striatal synaptosomes, which are substantially impacted by the loss of ITSNs as shown in striatal volume loss, morphological deficits and altered synaptic transmission by Vollweiter 2021, were purified and sorted by FACS. This approach ensured selective analysis of individual, intact synaptosomes (Figure S 4) stained with the presynaptic marker bassoon and the actin dye phalloidin. Single synaptosomes were identified with the SynaptosomesMacro, which normalized, blurred and filtered the image, plotting the retrieved maxima for the user for review. Afterwards, the macro measured bassoon and actin intensities, and background corrected intensities plotted against each other, in a scatter plot with Graphpad Prism (Figure 21A, C). This revealed distinct synaptosome populations, with varying levels of actin and bassoon as can be seen in the scatter plots and exemplary immunofluorescent images. The distribution of ITSN dKO synaptosomes seemed to indicate more synaptosomes with a high-phalloidin and high-bassoon content (Figure 21C) than the ITSN2 KO synaptosomes (Figure 21A). To explore this further, synaptosomes were grouped into four populations based on marker intensity and quantified. If actin levels were reduced in dKO synaptosomes, an increase in the low- phalloidin populations would be expected. However, the comparison did not reveal any significant differences in any defined population (Figure 21B), even though there were trends in the categories that were high or low in both markers. However, these trends rather pointed to having higher actin levels in the ITSN dKO, contrary to expectations.

To complement this categorial analysis, the median phalloidin intensities of the entire ITSN dKO synaptosome population was calculated and normalized to the median of the ITSN2 KO control. Here, as the data is not normally distributed, the median has been chosen as for non-normal distributed data, as it is more robust than the mean. Again, no significant difference could be detected. However, the variability between individual experiments was very high, suggesting that additional replicates would be necessary to be able to detect small differences and draw a reliable conclusion (Figure 21 D). I probed for Kv1.1, Kv1.2 and Kvβ instead of actin as well, with similar results.

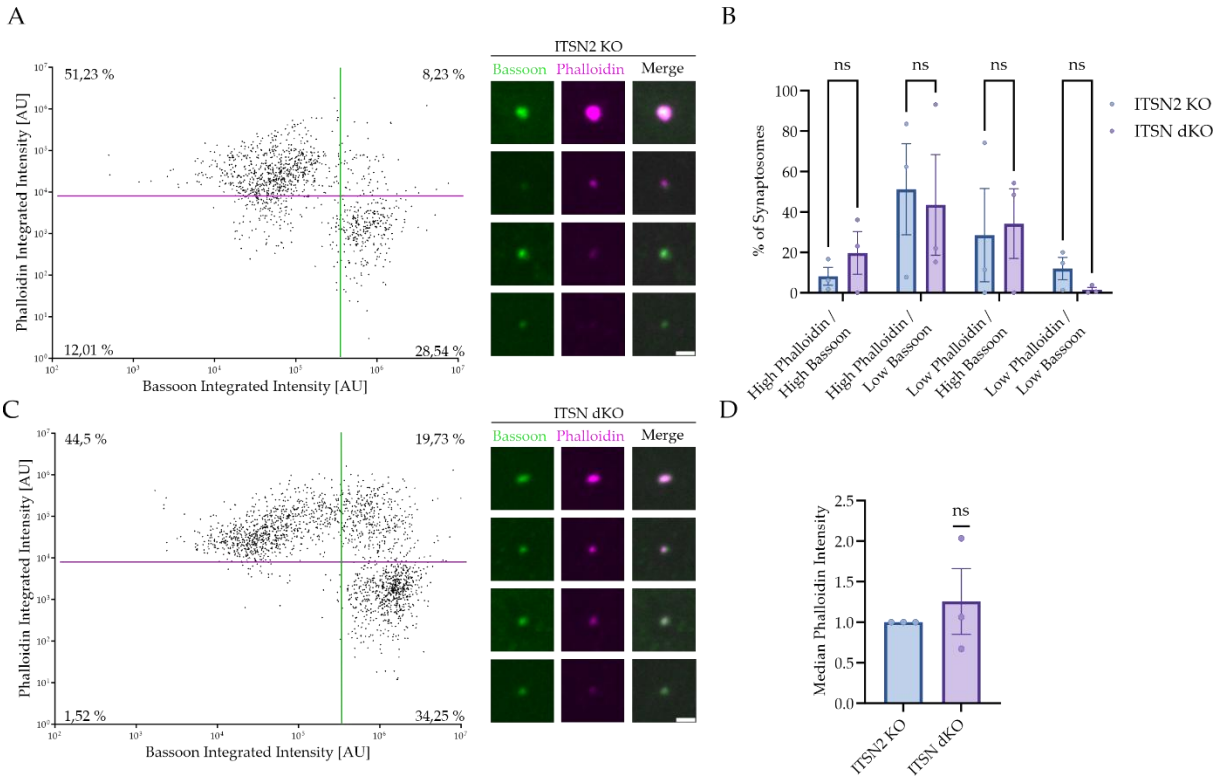

Figure 21: Immunofluorescence analysis showed unaltered actin levels of ITSN dKO synaptosomes.

A,C) Left: Scatter plot population analysis of the fluorescence intensities of phalloidin, a probe for the actin cytoskeleton, and bassoon, a presynaptic marker, on FACS-sorted synaptosomes from ITSN2 KO and ITSN dKO brains revealed different subpopulations. The set thresholds are given by lines in the representative colors, and the percentage of synaptosomes in the respective population is indicated in the corners. Right: Representative confocal images of ITSN2 KO and ITSN dKO synaptosomes immobilized on coverslips and probed for bassoon and phalloidin. Scale bar 2 µm. B) The quantification of the percentages of the different populations (e.g. high phalloidin / high bassoon, high phalloidin, low bassoon,..) relative to the total number of synaptosomes showed no significant difference between ITSN2 KO and ITSN dKO samples. D) Quantification of the normalized median integrated intensity of phalloidin for ITSN2 KO and ITSN dKO synaptosomes revealed unaltered actin levels for ITSN dKO synaptosomes. The statistical analysis for B) was performed by multiple two-sided, unpaired t-tests, and for D) by a one sample t-test comparing the results to a hypothetical value of 1. Ns =p>0.05. N=3.

Although the actin reduction could only be found in the LP1 fraction and not in crude synaptosomes, the spatial specificity of a possible actin reduction remains unknown. To address this, a trypsin cleavage assay was chosen. Here, synaptosomes are incubated with the protease trypsin, which will cleave off postsynaptic density components including postsynaptic neurotransmitter receptors, like GluA1 (Figure 22A, B) since they are not protected by a membrane, so that only presynaptic proteins like Snap25 remain, which are enclosed within the sealed presynaptic compartment and therefore not accessible by the protease (Figure 22A, B). Consequently, actin remaining after trypsin digest can be assumed to be presynaptic. Surprisingly, the presynaptic actin fraction of the ITSN dKO was not reduced as expected, but significantly increased to 1.5x the level of the ITSN2 KO (Figure 22B, C), while other presynaptic proteins like Snap25 remained at the same level.

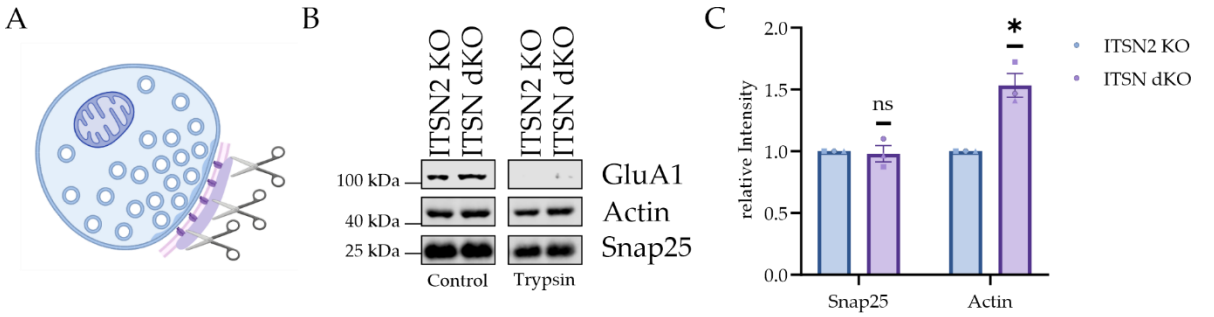

Figure 22: ITSN dKO mice show increased actin levels at the presynapse.

*A) Schematic representation of the trypsin digest of synaptosomes. Synaptosomes represent resealed presynaptic terminals. Since the postsynaptic terminal does not reseal, its proteins are exposed to the protease trypsin (indicated by scissors), in contrast to the protected presynaptic proteins. Schematic created with Biorender.com B) Representative Western blot of the undigested and trypsin digested synaptosomes. GluA1, a postsynaptic protein, was nearly completely digested, while Snap25, a presynaptic protein, was maintained. After tryptic digest, only presynaptic actin should remain intact. C) Quantification of relative signal intensities for Snap25 and actin on digested synaptosomes. Values were normalized to the results for the ITSN2 KO. While Snap25 levels are unaltered, presynaptic actin levels are increased in ITSN dKO mice. Statistical significance was tested by a one sample t-test comparing the results to a hypothetical value of 1. ns= p>0.05, *p<0.05. N=3.*

Taken together, at the level of crude synaptosomes, the additional loss of ITSN1 in the ITSN2 KO background does not seem to decrease actin polymerization or overall actin amount, as judged by biochemical and microscopical approaches. Thus, the reduced actin levels previously observed in the synaptic membrane fraction could not be reproduced in this context. Surprisingly, the biochemical estimation of presynaptic total actin levels even revealed the opposite phenotype, an increase in actin. On the one hand, this suggests that the previously found reduction in actin may be restricted to the subpool of membrane-attached F-actin and therefore not visible in approaches which analyze also the presumably larger

synaptic cytosolic actin pool. On the other hand, the finding of a higher overall presynaptic actin pool in the ITSN dKO hints at more complex alterations in actin regulation than anticipated from the loss of a positive actin regulator, possibly due to compensatory effects.

2.2.4 ITSNs could play a role in translation or mRNA stability

Apart from stabilizing Kv1.2 and Kvβ2 by direct or indirect scaffolding or by influencing the actin cytoskeleton, ITSNs could have an impact on the prevalence of the Kv-channel subunits either by influencing their mRNA stability or by influencing translational regulation. The translation of several of the proteins reduced at the ITSN dKO synapse, like Kv1.2, is supposed to be regulated by FMRP (Darnell et al., 2011). Interestingly, knockout mice of components of FMRP-positive granules such as Jakmip1 exhibit similar repetitive behaviors and reduced synaptic levels of PSD95 as ITSN dKO mice (Berg et al., 2015). The idea of ITSNs playing a role in translational regulation is supported by ITSN1 being able to bind mRNA (Pankivskyi et al., 2021).

To investigate ITSN1s potential involvement in translational regulation, I first analyzed its interactome. For this purpose, I used two mass spectrometry (MS) datasets (MS707 and MS713) derived from ITSN1 Co-IPs using mouse hippocampal lysate. These datasets were generated by Marielle Eichhorn Grüning in 2014 at the Leibniz-Forschungsinstitut für Molekulare Pharmakologie (FMP) in the group of Prof. Volker Haucke in collaboration with the group of Dr. Eberhard Krause who provided mass spectrometric analysis of the samples. Proteins identified in both datasets were considered robust interactors and subjected to subsequent analysis. Using DAVID (Huang et al., 2009; Sherman et al., 2022), I performed an enrichment analysis based on a comparison to the *Mus musculus* background dataset provided by DAVID and functional annotation clustering based on Gene Ontology (GO) categories, including biological processes, cellular components, and molecular functions (top hits can be found in Table S 1,Table S 2,

Table S 3). Nine proteins could not be mapped in DAVID and were excluded, leaving 136 out of 145 for analysis. The remaining annotations were grouped into 11 enriched functional annotation clusters (Figure 23A, B). Within those clusters, the terminology with the highest statistical power was defined as Top Term, though this term does not always fully represent

A

Cluster	Top Term	Enrichment Score	Representative GO-Annotation terms
1	GO:0005852~eukaryotic translation initiation factor 3 complex	6.65	GO:0001732~formation of cytoplasmic translation initiation complex, GO:0033290~eukaryotic 48S preinitiation complex, GO:0016282~eukaryotic 43S preinitiation complex
2	GO:0005686~U2 snRNP	6.49	GO:0000398~mRNA splicing, via spliceosome, GO:0005681~spliceosomal complex
3	GO:0140662~ATP-dependent protein folding chaperone	6.19	GO:0050821~protein stabilization, GO:0006457~protein folding, GO:0042026~protein refolding
4	GO:0008104~protein localization	4.54	GO:0005940~septin ring, GO:0060090~molecular adaptor activity, GO:0003924~GTPase activity
5	GO:0031209~SCAR complex	3.45	GO:2000601~positive regulation of Arp2/3 complex-mediated actin nucleation, GO:0016601~Rac protein signal transduction, GO:0031267~small GTPase binding
6	GO:0006338~chromatin remodeling	2.91	GO:0006338~chromatin remodeling, GO:0004677~DNA-dependent protein kinase activity, GO:0004674~protein serine/threonine kinase activity
7	GO:0019904~protein domain specific binding	2.37	GO:0045184~establishment of protein localization, GO:0006605~protein targeting
8	GO:0006606~protein import into nucleus	2.16	GO:0006913~nucleocytoplasmic transport, GO:0005635~nuclear envelope
9	GO:0022627~cytosolic small ribosomal subunit	1.97	GO:0022626~cytosolic ribosome, GO:0006412~translation, GO:0002181~cytoplasmic translation
10	GO:0005956~protein kinase CK2 complex	1.81	GO:0031519~PcG protein complex, GO:0016055~Wnt signaling pathway, GO:0000785~chromatin
11	GO:0098884~postsynaptic neurotransmitter receptor internalization	1.81	GO:0012505~endomembrane system, GO:0016192~vesicle-mediated transport, GO:0006886~intracellular protein transport

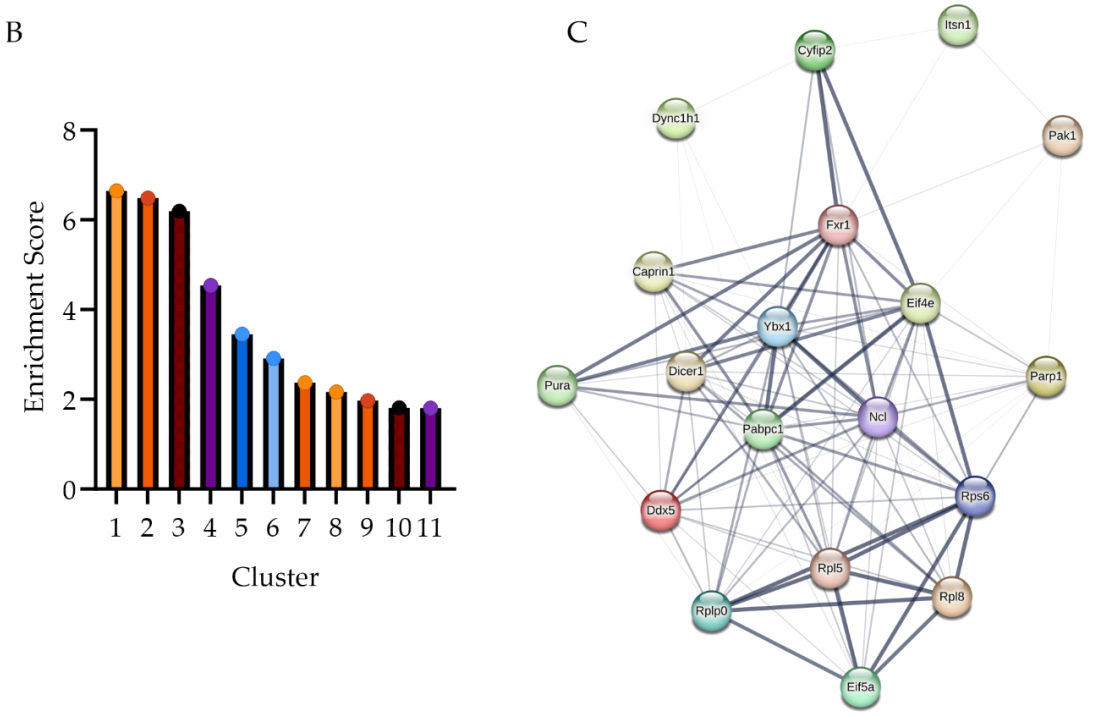

Figure 23: Enrichment Analysis of ITSN1 MS-IP datasets reveals enrichment in translation and translation regulation related gene ontology terms.

A) Functional annotation clusters analyzed with DAVID. 11 clusters were grouped, and the top term defined as the GO-term with the highest statistically enrichment based on Benjamini-corrected p-values. To provide a better insight into the clusters, 2-3 additional GO-terms of the biological processes, molecular functions and cellular compartments were given. Clusters 5 and 11 fit the known ITSN1 functions of actin cytoskeleton rearrangement and endocytic vesicle formation, as well as cluster 8 as ITSN1 has been shown to enter the nucleus. Several clusters (1,2,9) are related to mRNA processing or translation. B) Visualization of the enrichment scores for the clusters identified by DAVID functional annotation clustering. C) For the MS713 dataset, known FMRP-interactors were identified and visualized with STRING. Edge (connection between nodes) line thickness indicates strength of data support for association. FMRP interactors form a network to which ITSN1 might be connected, although the data supporting this is not as strong as for within the network. N(MS-IP) =2.

the functions clustered. Therefore, two to three additional representative terms were included for broader context. These clusters reflect some known ITSN1 functions, including (synaptic vesicle) endocytosis (cluster 11) (Hussain et al., 1999), nucleocytoplasmic trafficking (cluster 8) (Alvisi et al., 2018) and regulation of the Arp2/3-dependent actin polymerization via its GEF activity (cluster 4, 5) (Hussain et al., 2001). Cluster 6, enriched for terms related to histone kinase activity and protein phosphorylation, likely reflects ITSN1's scaffolding role in assembling kinases and their substrates and its involvement in the PI3K-AKT pathway (Das et al., 2007). Interestingly, several clusters were related to RNA metabolism, including mRNA processing/splicing (cluster 2) and translation (clusters 1 and 9), particularly, translation initiation (cluster 1) and cytosolic ribosomes (cluster 9). Cluster 1 had the highest enrichment score (6.65), followed by cluster 2 (6.49), indicating a strong link between ITSN1 and translational regulation. (Figure 23A, B).

Given that the MS Co-IP screens support a role for ITSN1 in mRNA stability and translation regulation and that several proteins related to FMRP are present in the MS707 and MS713 dataset, I evaluated the abundance of selected proteins (for which antibodies were available in our group) in the synaptosome fraction of ITSN2 KO and ITSN dKO mice. Among the candidates analyzed were Ago2, Jakmip1, CYFIP2, eIF-4E, PABP and DDX5. Although Jakmip1 was not identified in the MS Co-IP dataset, it was included due to its phenotypic relevance. As mentioned before, the Jakmip1 KO mice exhibit repetitive jumping and reduced PSD95 levels (Berg et al., 2015), similar to the ITSN dKO mice. Ago2, a protein involved in transcriptional regulation, was included, too. Unfortunately, reliable antibodies for FMRP and FXR1 were not available, thus, these proteins could not be included. Initial visual inspection of synaptosome western blots revealed no apparent difference in protein abundance of the tested candidates between genotypes (Figure 24A). Quantification of relative protein levels confirmed unaltered protein levels for Ago2, Jakmip1, CYFIP2, eIF-4E, PABP or DDX5 in the dKO compared to controls (Figure 24B).

Although the loss of ITSNs does not alter the protein levels of selected FMRP-interaction partners, ITSNs might still associate with FMRP-positive RNP granules or interact with FMRP or its homologue FXR1 outside of those granules. To probe for a potential interaction in the absence of reliable FMRP or FXR1 specific antibodies, GST-fusion constructs of FMRP and

FXR1 were generated and used in pull-down approaches using mouse brain lysate (Figure 25A). Unexpectedly, CYFIP2 and eIF-4E, both known interactors of FMRP, which were probed

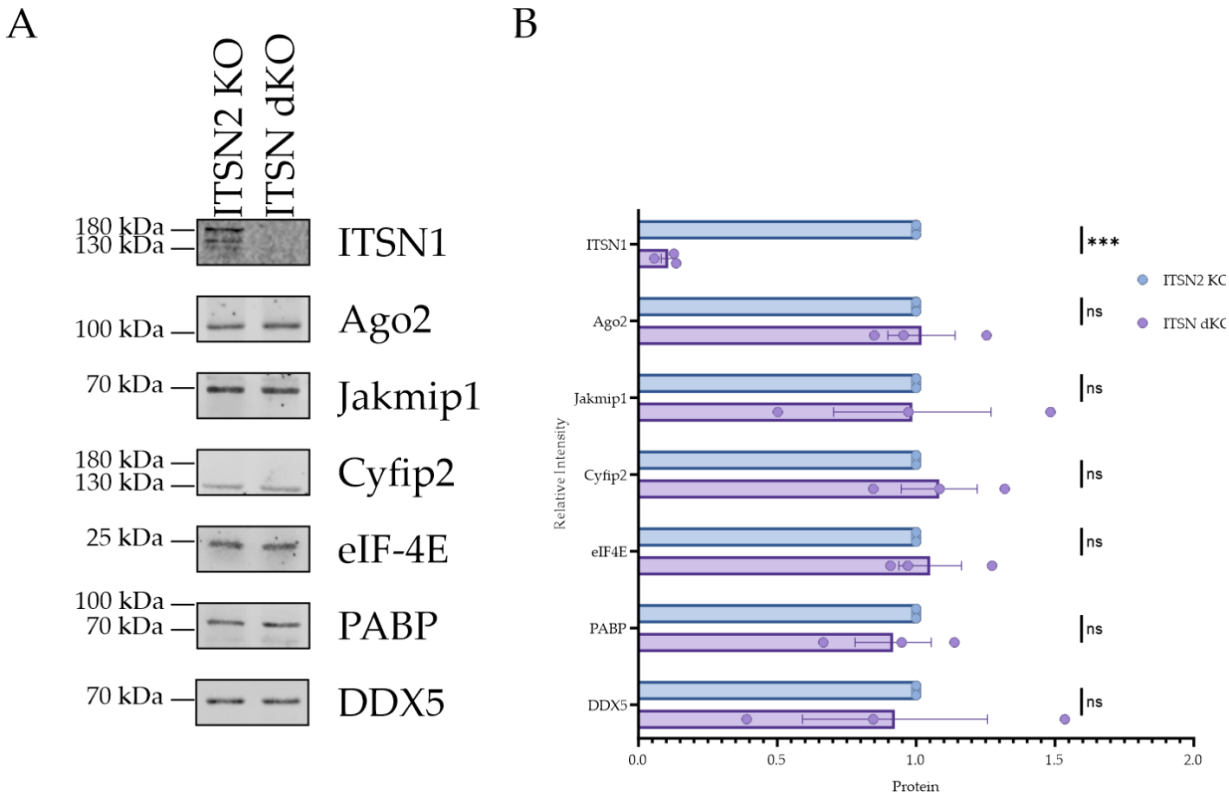

Figure 24: Levels of potential interactors based on MS Co-IP not reduced in ITSN dKO synaptosomes.

*A) Representative Western Blot images of synaptosomes from ITSN2 KO and ITSN dKO probed for several potential interactors that are related to transcriptional and translational regulation. B) Quantification of protein levels in ITSN dKO synaptosomes relative to ITSN2 KO control values for ITSN1, Ago2, Jakmip1, CYFIP2, eIF-4E, PABP and DDX5 does not reveal a reduction. Statistical significance was evaluated by one sample t-test comparing the results to a hypothetical value of 1. ns = $p > 0.05$, *** $p < 0.001$. N=3.*

as positive controls, were not detected in the eluates. This absence is likely due to the phosphorylation-dependent nature of their interaction with FMRP, as CYFIP1, which likely behaves similarly to CYFIP2, and eIF-4E are known to dissociate upon FMRP dephosphorylation (Napoli et al., 2008; Narayanan et al., 2007). Since the GST-FMRP construct was expressed in *E. coli* without posttranslational modifications, it may not have been in the correct phosphorylation state to support these interactions. Hsp70 was used as a negative control. Both fusion proteins appeared to be functional, as both successfully precipitated Kvβ2 (Figure 25A, B). However, that interaction also depends on the phosphorylation state of the Kv1.2 C-terminus (Yang et al., 2018), which is unknown in the used brain lysate, which might explain the lack of detectable interaction. Intriguingly, probing for ITSN1 revealed co-precipitation with GST-FXR1 but not with GST-FMRP (Figure 25A), which points to a very

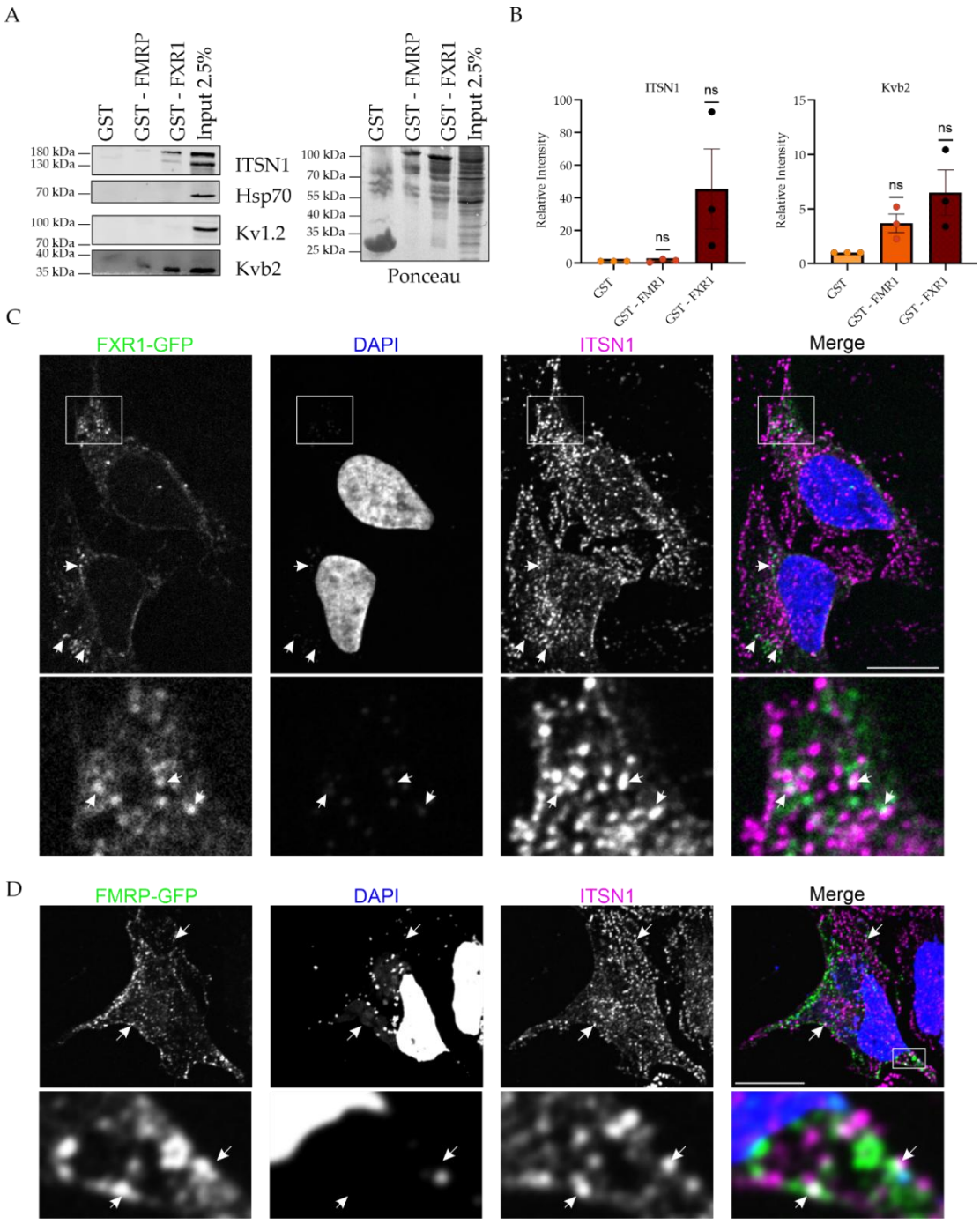

Figure 25: Interaction between ITSN1 and FXR1 detected via pull-down approach and supported by immunofluorescence.

A) Pull-down of GST-fused FMRP and FXR1 using mouse brain lysate (left). Eluates were analyzed by immunoblotting and probed for Hsp70 as negative control and ITSN1, Kv1.2 and Kvβ2 as proteins of interest. Ponceau staining confirmed similar amounts of bait-constructs at ~100 kDa. Samples in the GST-FMRP lane ran unevenly causing the uneven staining for Kvβ2 (right). 50 µg were loaded for the input. N(ITSN1, Kvβ2, Hsp70) =3. N(Kv1.2) =1. B) Quantification of ITSN1 and Kvβ2 intensities normalized to their background signal when using GST as bait. Statistical analysis was performed with several one sample t-tests comparing the results to a hypothetical value of 1, but no condition reached significance ($p > 0.05$), therefore no post hoc test has been performed. C) HeLa cells transfected with FXR1-GFP and probed with ITSN1-specific antibodies and DAPI shows overlap between ITSN1 and FMRP-GFP at distinct locations (white arrows). Zoom in (white box) focused on an area of overlap. D) HeLa cells transfected with FMRP-GFP and probed with ITSN1-specific antibodies and DAPI reveals overlap between ITSN1 and FMRP-GFP at a few locations (white arrows). Zoom in (white box) focused on an area of overlap. Scale bar 20 µm.

selective binding mode. Even though FXR1 but not FMRP was found in the MS713 dataset, this was surprising, as FMRP is considered as neuron-specific family member, while FXR1 is expressed more ubiquitously (Majumder et al., 2020). Interestingly, as observed with GST-CTTN, the ITSN1-L band at ~180 kDa appeared more prominent in 2 out of 3 experiments. However, quantification revealed that the interaction does not reach statistical significance yet with the used sample size (Figure 25B). To further validate this interaction by a complementary approach, HeLa cells were transfected with FMRP-GFP or FXR1-GFP respectively and immunostained with an ITSN1 specific antibody followed by a fluorescently labelled secondary antibody and the DNA-marker DAPI. Colocalization of FXR1-GFP and ITSN1 was observed in a small subset of FXR1-GFP puncta. These puncta were also positive for DNA, likely the transfected DNA, as can be observed more clearly in the zoom-in (Figure 25C). Similarly, FMRP-GFP also showed partial colocalization with ITSN1 in cytosolic puncta (Figure 25D). As ITSN1 did not precipitate with FMRP-GST, the colocalization of ITSN1 with FMRP-GFP was not anticipated but could be explained by endogenous FXR1 or another ITSN1 interactor recruiting ITSN1 to FMRP-GFP puncta. Taken together, these findings suggest that ITSN1 may be associated with FMRP-positive granules, although this association appears to be more FXR1-dependent than directly mediated by FMRP.

To broaden the analysis of ITSN1s involvement in translation and mRNA splicing by probing for interactions with the translational machinery, I decided to look closer at DDX5 and PABP. Although these proteins are interacting with FMRP (Pasciuto & Bagni, 2014), they fulfil also a multitude of functions independently of FMRP. DDX5 is highly involved in RNA metabolism, in steps like mRNA processing, splicing and ribosome biogenesis (Dardenne et al., 2014; Xing et al., 2019). PABP facilitates translation initiation as well as termination, recycling of ribosomes and mRNA stability (Ivanov et al., 2016; Mangus et al., 2003). These functions are reminiscent of the clusters from the enrichment analysis of the ITSN1 MS Co-IP (Figure 23A) and DDX5 and PABP show up in the MS Co-IP datasets as potential interactors (PABP in MS707 and MS713, DDX5 only in MS713). To confirm the MS Co-IP results, I performed ITSN1 Co-IPs using crude synaptosome fractions with subsequent immunoblotting for DDX5 and PABP, along with AP2, a known ITSN1 interactor as positive control, and syntaxin as negative control (Figure 26A). Excitingly, AP2, DDX5 and PABP were successfully detected in the eluates with only a faint background band in the unspecific IgG control (Figure 26A) while

syntaxin was not detected. For AP2 the enrichment in the ITSN1 IP reached statistical significance, while for DDX5 and PABP it did not. This is likely due to the fact that their levels

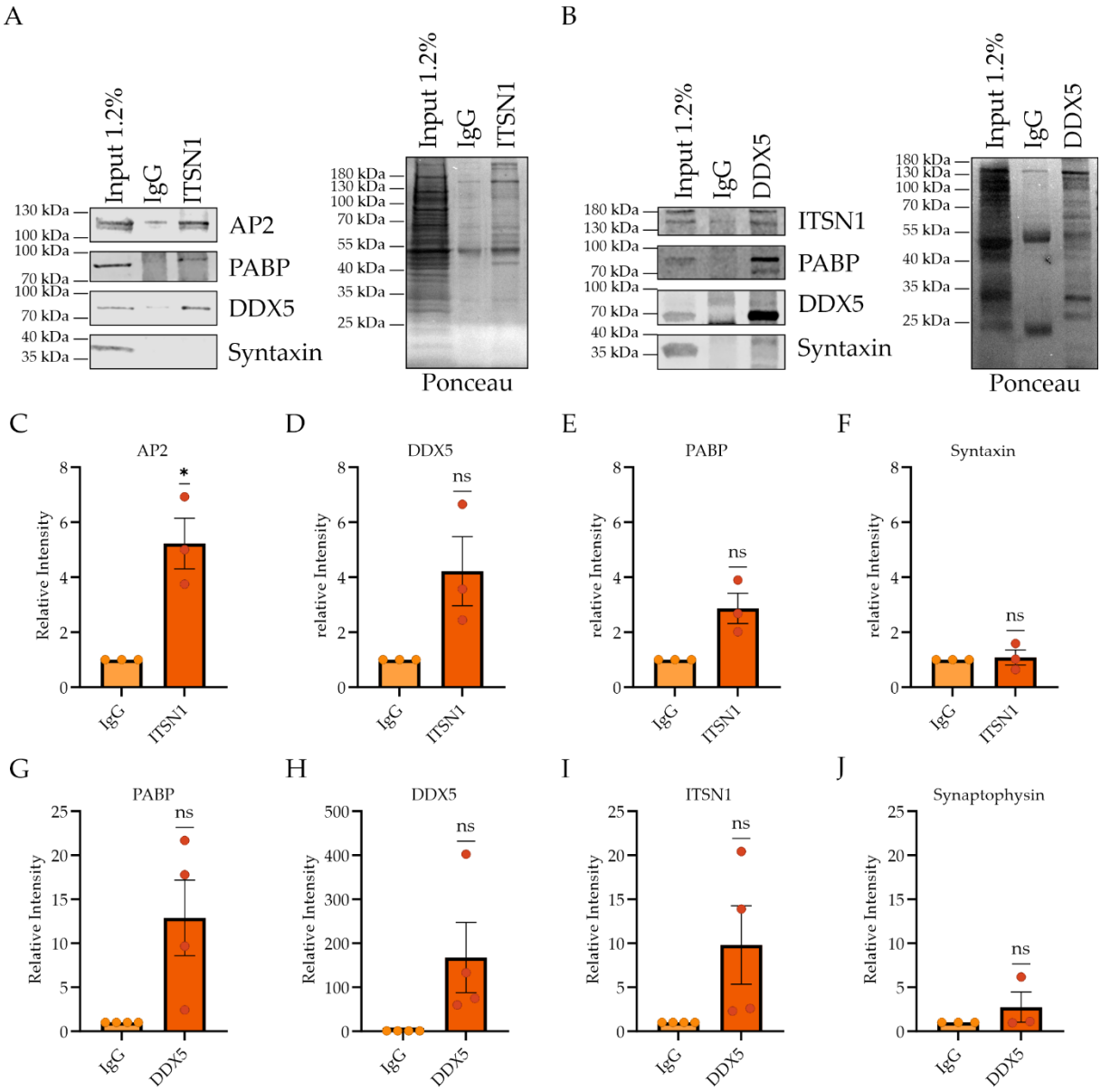

Figure 26: DDX5 and PABP immunoprecipitated with ITSN1 in crude synaptosome fraction.

A) *Co-IP with ITSN1 as bait co-precipitated DDX5, PABP and its known binding partner AP2 from a crude synaptosome fraction (left). The negative control syntaxin was not co-precipitated. Ponceau staining confirmed similar amounts of antibody used of the IgG control and ITSN1. B) Co-IP with DDX5 as bait co-precipitated ITSN1 and its known binding partner PABP, while the negative controls syntaxin (n=1) or synaptophysin(n=3) did not co-precipitate (left). Ponceau staining does not clearly show equal amounts of primary antibodies, as they are overshadowed by precipitated proteins for the DDX5 IP. C-F) Quantification of signal intensities of known (AP2) and putative interactors (DDX5, PABP) normalized to their background signal when using the unspecific IgG antibody as bait. G-J) Quantification of signal intensities of known (PABP) and putative interactors (ITSN1), of the self IP (DDX5) and of negative controls (only synaptophysin, syntaxin not included) normalized to their background signal when using the unspecific IgG antibody as bait. Statistical significance was evaluated by one sample t-test comparing the results to a hypothetical value of 1. ns = $p > 0.05$, * $p < 0.05$. N(ITSN1 Co-IP) =3. N(DDX5 Co-IP) =4.*

were a bit lower than for AP2 and that the variation between experiments was large even though all experiments showed the enrichment (Figure 26C,D,E,F). This interaction between ITSN1 and DDX5 was further confirmed by a reverse IP with DDX5 as bait (Figure 26B) where ITSN1 was successfully detected with roughly equal levels of its shorter isoform at ~130 kDa and longer isoform at ~180 kDa (Figure 26H). Additionally, I probed for PABP, as known interactor of DDX5, which indeed successfully precipitated with DDX5 (Figure 26B) although it did not reach statistical significance (Figure 26G). As negative controls I also tested either syntaxin or synaptophysin, which did not co-precipitate (Figure 26B, J). Additionally, probing for DDX5 showed that the self-IP efficiently worked revealing high protein levels of precipitated DDX5 (Figure 26B, H).

Next, to gain further insight into the interaction of ITSN1 with DDX5 and PABP, pull-down experiments were performed with the different ITSN1 domains fused to GST and mouse brain lysate. Probing for the established ITSN interactor dynamin confirmed a functional pull-down by reproducing dynamin´s known interactions with the ITSN1 SH3A, C and E domains (Figure 27A) although its enrichment does not reach statistical significance (Figure 27B). Surprisingly, the interaction with PABP that was found in the Co-IP could not be detected for any of the probed domains of ITSN1-S (Figure 27A, B). Therefore, it might require other ITSN domains or depend on ITSN1 phosphorylation. Still, for DDX5 the interaction with ITSN1 was confirmed and the SH3D of ITSN1 identified as interaction site. Although other domains, like the SH3B or EH-CC domains, exhibit a slight enrichment in DDX5, it is strongest for the SH3D domain (Figure 27A, B). This effect is not based on uneven loading of the protein domains, as similar amounts were loaded (Figure 27A Ponceau). Additionally, in HeLa cells transfected with ITSN1-GFP and probed for DDX5, ITSN1-GFP and DDX5 overlap at a few locations (Figure 27C arrows). It must be noted that DDX5 was mainly observed in the nucleus but could be found at low concentrations in the cytoplasm in some, but not all cells. DDX5 can become more cytoplasmic in G2/M phase of the cell cycle or based on post-translational modification (Choi & Lee, 2012) and has previously been detected in cytoplasmic granules, upon transfection in HeLa cells (Geißler et al., 2013). Taken together, ITSN1 interacts with DDX5 via its SH3D domain, and might interact with PABP, although no interaction domain could be specified here, suggesting an indirect interaction, maybe via DDX5 or FMRP positive granules.

Summarizing, several novel ITSN1 interaction partners were identified, such as FXR1 and DDX5. As those proteins are part of FMRP positive granules and ITSNs partially localizes with FMRP, ITSNs might be part of FMRP positive granules or impact mRNA stability or translation.

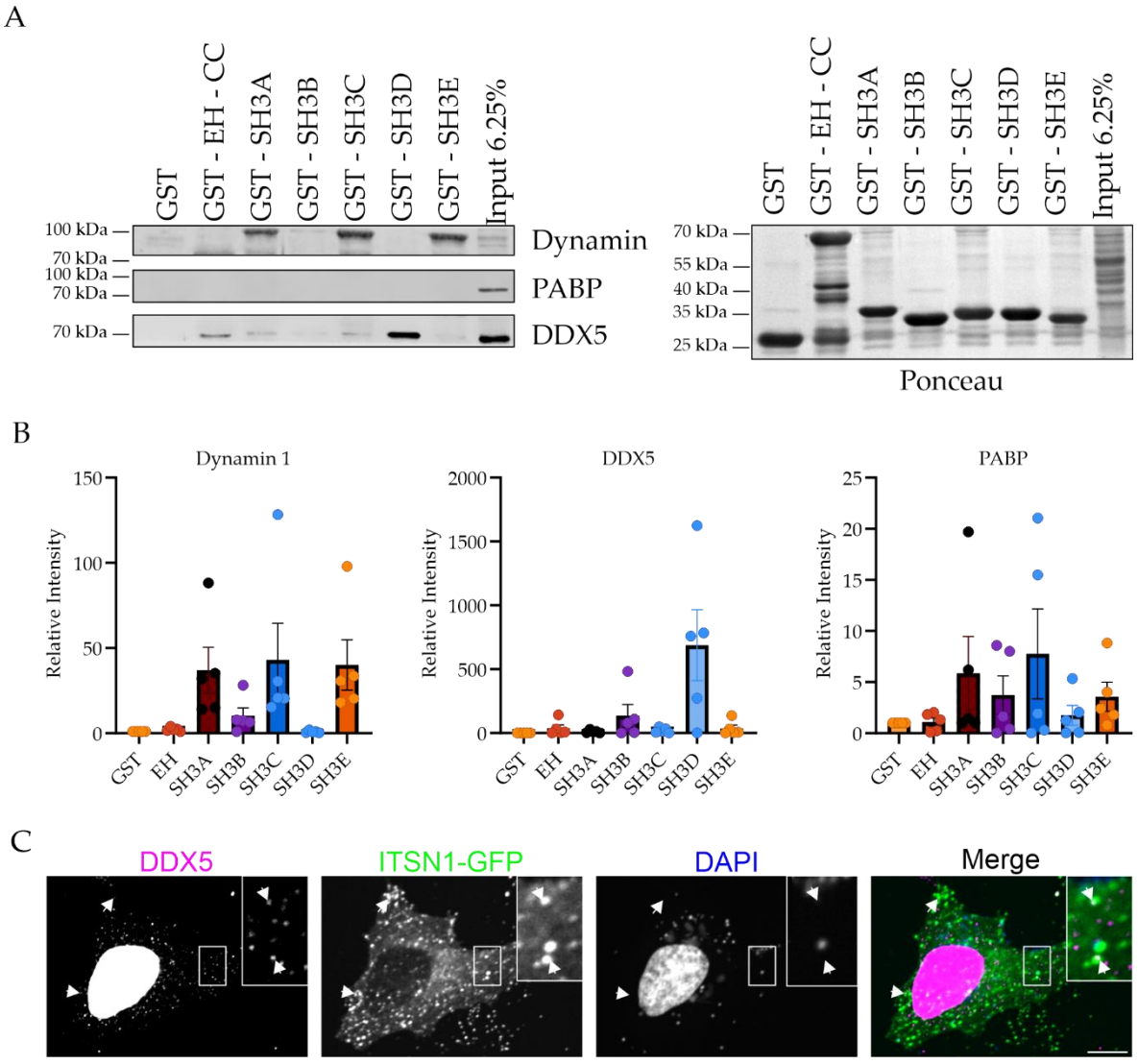

Figure 27: GST-SH3D domain of ITSN1 interacts with DDX5, and colocalizes in the nucleus and cytoplasm.

A) Pull-down of GST-fused ITSN1 domains with mouse brain lysate (left). Eluates were analyzed by immunoblotting and probed for dynamin as positive control and PABP and DDX5 as proteins of interest. Ponceau staining confirms similar amounts of bait-constructs (right). 50 µg were loaded for the input. B) Quantification of signal intensities of putative interactors normalized to their background signal when using GST as bait. From left to right: dynamin, DDX5 and PABP. Statistical analysis was performed for all three proteins with several one sample t-tests comparing the results to a hypothetical value of 1, but no condition reached significance ($p > 0.05$), therefore no post hoc test has been performed. C) HeLa cells transfected with ITSN1-GFP and probed with DDX5-specific antibodies and DAPI. DDX5 is mainly present in the nucleus, marked by DAPI, where it overlaps with some nuclear ITSN1-GFP. But some cytosolic DDX5 puncta can also be detected of which a few colocalize with ITSN1-GFP (white arrows). Zoom in (white box) focused on an area of overlap. Scale bar 10 µm.

2.3 Inducible deletion of ITSN2 on an ITSN1 knockout background does not recapitulate previously reported synaptic protein loss

Aside from my goals to gain further insight into the synaptic function of ITSNs, I tested another model as a possible replacement for the constitutional dKO mice. Those mice suffer from health deficits, such as seizures causing premature death. To reduce animal suffering, a partially inducible dKO mouse line was generated. In this model, the *ITSN2* gene is flanked by loxP sites, and the gene for an inducible Cre recombinase gene is included. Upon Tamoxifen administration, Cre expression is induced, resulting in excision at the loxP sides and thereby knock out ITSN2 while ITSN 1 is constitutively deleted. Using primary neurons of this mouse model in culture, I can easily induce the dKO.

As this was a newly generated mouse line, I first confirmed the efficient knockout by immunoblotting of cell lysates of primary cortico-hippocampal neurons. As expected, the loss of ITSN1 was confirmed, by comparing to a WT brain lysate (Figure 28A). Also, Tamoxifen treatment successfully induced *ITSN2* knockout (Figure 28B). Notably, the antibody appears to produce an unspecific band at ~180 kDa, the same weight as the long isoform, which remained unchanged after induction. Still, this band is considered unspecific, as it can be detected in the whole brain lysate of constitutive ITSN dKO mice as well (Figure S 5). Therefore, only the reduction of the 130 kDa ITSN2 variant was quantified, revealing a significant reduction to 8.98±4.56% of the ITSN1 control (Figure 28C), confirming the inducibility of the dKO.

Next, to determine if this model is an appropriate replacement and accurately reproduces the phenotypes observed comparing ITSN2 KO and ITSN dKO synaptosome membrane fractions obtained from brain, synaptosomes were purified from cortico-hippocampal neurons. Since it was not possible to purify the synaptosome membrane fraction, used by Vollweiter 2021, with the more limited material coming from cultured neurons as compared to brain, protein levels were tested in synaptosome lysates instead. For this, a subset of proteins previously investigated by Vollweiter 2021 along with additional endocytic proteins were analyzed by immunoblotting, using tubulin as an unaffected reference for normalization (Figure 28D). Surprisingly, none of the expected proteins, neither NR2A, Kv1.2, Kvβ2 nor actin showed a significant reduction. Still, actin displayed a minimal reduction to 91.9 ± 4.57% while for

Vollweiter in 2021 only 80.2 ± 1.5% remained. Additionally, levels of endocytic proteins like AP2, Munc18 and Snap25 were slightly decreased (AP2 80.1 ± 5.0%, Munc18 85.1 ± 18.7%, Snap25 78.9 ± 12.1%), however, these changes did not reach statistical significance (Figure 28E). On the one hand, this discrepancy in results can be based on the different samples used, as I worked with synaptosomes, which already did not show the same actin phenotype as the membrane fraction used in Vollweiter, 2021. On the other hand, this can be due to the different

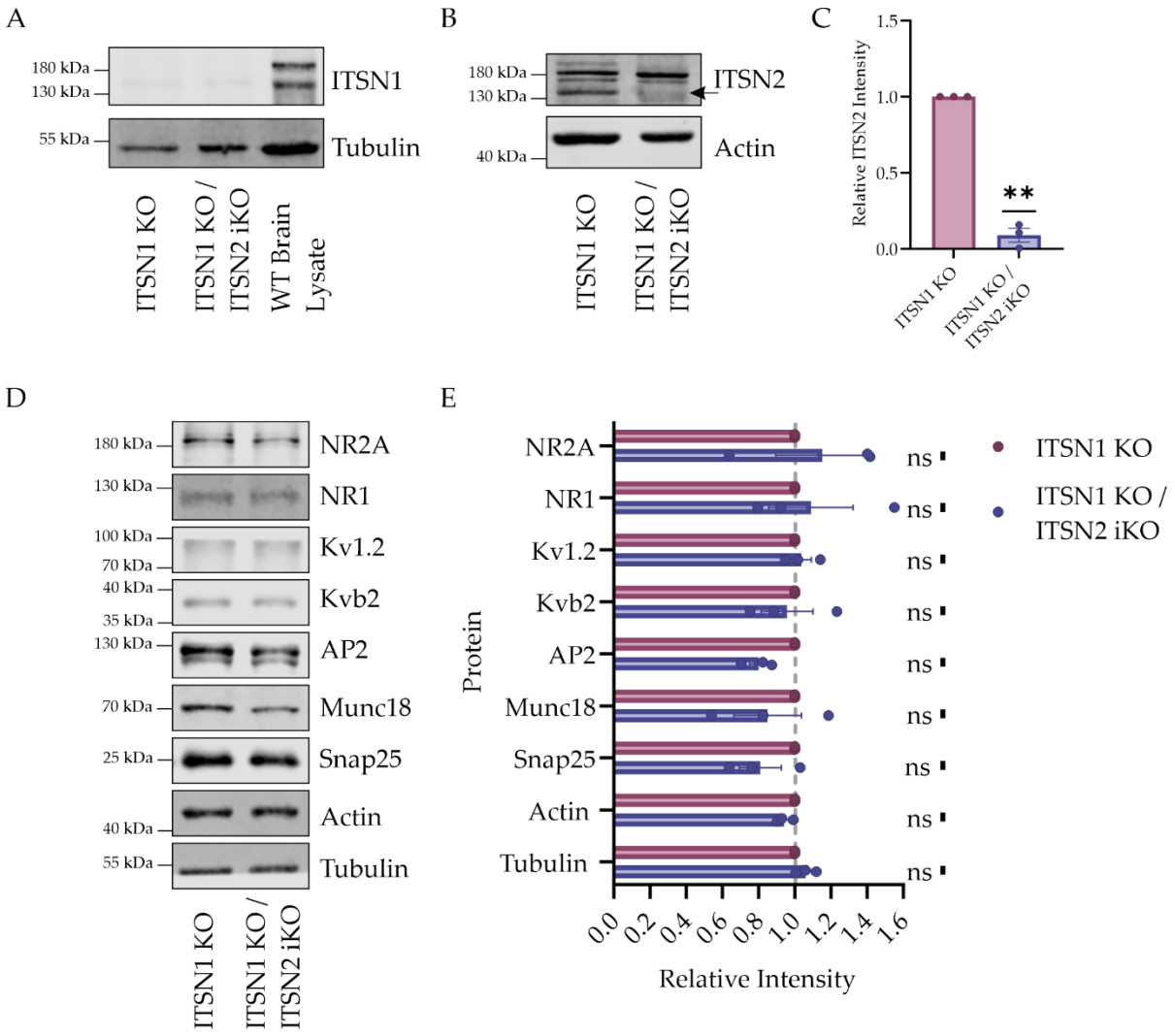

Figure 28: No alterations in synaptosome levels of tested proteins in an induced dKO compared to the ITSN1 KO in cultured cortico-hippocampal neurons.

*A) Representative Western blot probed for ITSN1 and tubulin showed successful knock-out of ITSN1 in ITSN1 KO and ITSN1 KO / ITSN2 iKO primary neurons. B) ITSN2 KO (black arrow) was successfully induced by Tamoxifen addition to neuronal cell cultures. C) Quantification of ITSN2 loss showed significant reduction of ITSN2 levels to ~9% of Ctrl condition. D) Representative Western blots of synaptosome lysates obtained from primary cortico-hippocampal neurons of ITSN1 KO and ITSN1 KO / ITSN2 iKO mice and probed for several proteins, which were previously investigated in Vollweiter 2021. E) The quantification of the relative protein intensities in synaptosomes from ITSN1 KO and the induced dKO neuronal cultures did not reproduce the decrease in protein levels observed by Vollweiter 2021 for synaptic membranes from ITSN dKO vs ITSN2 KO forebrains. For C) and E) a one sample t-test was performed comparing the results to a hypothetical value of 1. ns = $p > 0.05$, ** = $p < 0.01$. N=3.*

control condition used in this study compared to Vollweiter, 2021, which utilized an ITSN2 KO as control, whereas here, an ITSN1 KO was used. Since ITSN1 is predominantly expressed in neurons (Guipponi et al., 1998), its absence may have a more pronounced effect than the loss of ITSN2 alone. Consequently, the combination of an ITSN1 KO on top of an ITSN2 KO might result in a stronger phenotype than a KO of ITSN2 on top of ITSN1 loss.

Therefore, we adjusted the breeding scheme to generate ITSN1 het / ITSN2 WT mice as littermate control animals. These mice have a higher birth probability than the ITSN1 WT / ITSN2 WT genotype, while still enabling me to compare to a near-wild-type condition, where the effect of the ITSN1 loss should be stronger. As expected with this control, a reduction of several protein levels was detected (Figure 29A, B), among them NR2A (71.8 ± 2.4%), Kv1.2 (88.0 ± 16.9%), Kvb2 (85.7% ± 27.8%) and actin (82.3 ± 6.7%), which were reduced in the constitutive dKO. Interestingly, the actin loss reached a similar level as in Vollweiter 2021 with 80.2 ± 1.5%, while NR2A, Kv1.2 and Kvb2 were not as strongly reduced (NR2A 61.2 ± 1.8%, Kv1.2 74.4 ± 1.8% and Kvb2 66.0 ± 2.2% in Vollweiter 2021). Other proteins, which were not reduced in previous experiments, such as NR1 and Munc18, might be reduced

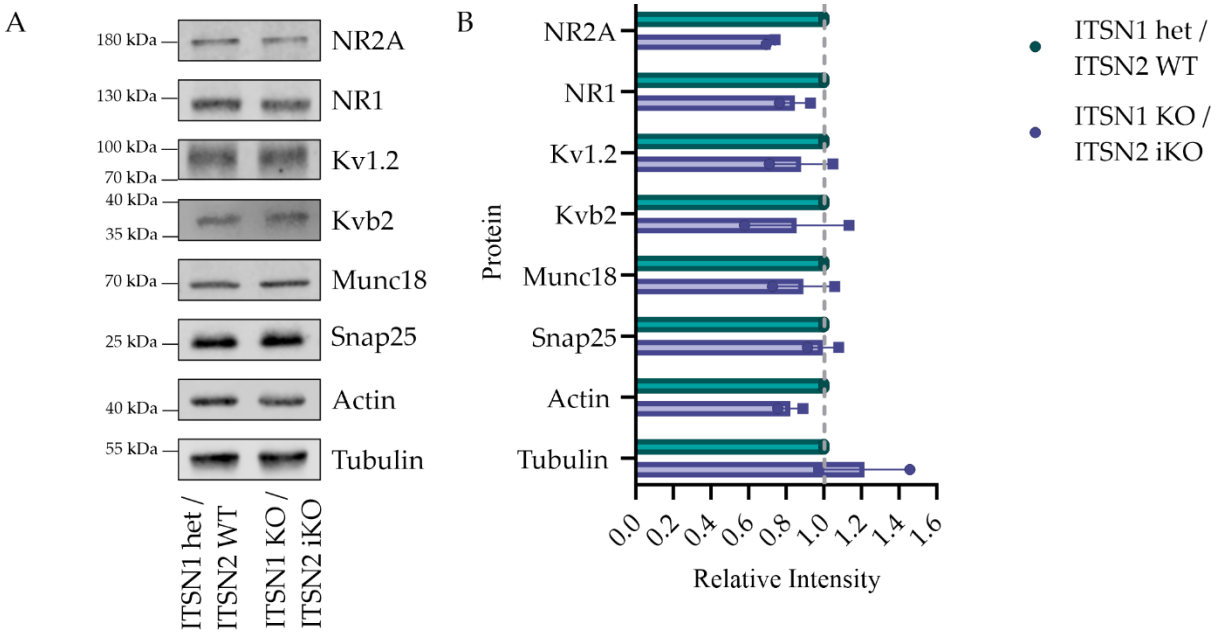

Figure 29: Some synaptosome protein levels might be reduced in neuronal cultures of the induced dKO when comparing it to ITSN1 het / ITSN2 WT neuron cultures.

A) Representative Western blots of synaptosome lysates obtained from primary cortico-hippocampal neurons of ITSN1 het / ITSN2 WT and the induced dKO mice and probed for several proteins, which were previously investigated in (Vollweiter, 2021). B) The quantification of the relative protein intensities in synaptosomes hints at a possible reduction of NR2A, NR1, Kv1.2, Kvβ2, Munc18 and actin. No statistical test performed due to the low sample size. These results must be interpreted with care as N=2.

here (NR1 84.7 ± 8.2%, Munc18 89.3 ± 16.5%). However, these results must be interpreted with caution, as only two experiments were performed and the protein levels for the Kv-channel subunits and Munc18 show a high variability. More experiments are necessary to confirm this trend. Consequently, the genetic background of the control condition appears to play an important role when comparing synaptic protein levels. While the comparison of the induced dKO to an ITSN1 KO does not yield the same results as the comparison of the constitutive dKO to the ITSN2 KO, the comparison between ITSN1 het / ITSN2 iKO and the induced dKO in primary neurons might be an appropriate alternative. Still, further experiments are necessary, especially to determine if endocytic proteins might be reduced in addition to the NMDA receptor subunits and Kv-channel subunits.

3 Discussion

3.1 Motor impairments of aging ITSN dKO mice: neuromuscular implications and neurological causes

To move in an organized and coordinated matter, muscles need to function and be innervated. Additionally, upstream movement coordination is essential, e.g. normal function of the basal ganglia and cerebellum, which are movement regulating (Graybiel, 1998; Grillner et al., 2013). Degeneration of the muscle, defective innervation or impairments of the upstream CNS neurons can all result in motor dysfunction (Dubuisson et al., 2022).

For 2-months old ITSN dKO mice, we observed hyperactive and repetitive, i.e. ASD- and OCD-like, behaviors which are most likely linked to altered neurotransmission in the basal ganglia, more precisely the striatum (Vollweiter, 2021). However, after 4-months of age, these behaviors reduce, e.g. the repetitive jumping decreases; and by 1 year of age, the mice exhibit neither repetitive jumping nor hyperactivity. Instead, they attenuated movement compared to ITSN2 KO littermates and avoid wall rearing. Though this change is uncommon for ASD, as in humans, motor control improves with age (Fournier et al., 2010), it is reminiscent of muscular- or neurodegenerative diseases, like spinal muscular atrophy (Kariya et al., 2008) and DMD (Pratt et al., 2015). As the underlying pathologies for these diseases are detectable at the NMJ or the muscles, I decided to take a closer look at the ITSN dKO NMJ and two muscles, the TA and TB.

3.1.1 NMJ integrity despite motor symptoms in ITSN dKO mice

My morphological analysis of ITSN2 KO and ITSN dKO NMJs at 2-months and 6-months of age did not reveal differences between genotypes. For both ages and genotypes, the NMJ pre- and postsynapse overlaps nearly completely, whereas a mislocalization could have hinted at defects in development, maturation or degeneration. The area of the pre- and postsynapse remains similar between genotypes at a given age but increase in size from 2-months to 6-months of age. This was observed in other studies as well (Augustin, 2023; Pratt et al., 2015), and is likely related to increases in muscle fiber size. As the NMJ size is coupled to the muscle fiber size (R. Balice-Gordon et al., 1990), it is suspected that the presynaptic terminal adjusts to the growth of the postsynaptic terminal (R. J. Balice-Gordon & Lichtman, 1990). This growth

is mainly brought by the expansion or widening of the existing presynaptic terminal and postsynaptic receptor region, as the convex hull of the postsynaptic area or endplate area remains the same (R. J. Balice-Gordon & Lichtman, 1990). This growth pattern explains why the complexity, a factor of branches, endpoints and branch length, of the NMJ remains the same between 2- and 6-months of age, while the compactness, the ratio between postsynaptic AChR area and endplate area, increases. The postsynaptic area increases while the endplate area remains similar (Figure 9D, E, Figure 10D, E). Morphological classifications into plaque-like, pretzel-shaped or fragmented give insight into NMJ development. However, ITSN dKO mice do not show any delay in development at 2- or 6-months of age, as would have been identifiable by a higher number of plaque-like ITSN dKO NMJs, nor do they display premature signs of aging which could be reflected by an increase in fragmented NMJs (Figure 9I, Figure 10I). The average number of NMJ fragments is similar for both ages (Figure 9J, Figure 10J), and neither fragmentation pattern nor classification change much between 2-months and 6-months of age. Taken together, none of these morphological or NMJ classification parameters differ between ITSN2 KO and ITSN dKO mice, neither at 2-months of age nor at 6-months of age. This was unexpected, as at the striatal synapses exhibited clear morphological and functional alterations (Vollweiter et al., 2023). Although many processes at the NMJ regarding synaptic vesicle turnover are similar (see chapter 1.1.1), apparently those regulating NMJ morphology are regulated differently, likely in a cell-type specific manner. Especially for the 6-months of age, a morphological alteration was expected. At this timepoint the ITSN dKO do not exhibit repetitive jumping anymore but display impaired motor coordination and balance. As this was hypothesized to be potentially caused by dystrophic muscles, an increase in presynaptic or postsynaptic area and altered branching represented in the complexity score, was expected (Harris & Ribchester, 1979; Pratt et al., 2013, 2015). Also, muscular atrophy, observed in the neuromuscular disease spinal muscular atrophy, could have been identified at an early stage as it shows an impact on the NMJ, by smaller and more immature NMJs or denervation (Valsecchi et al., 2015). However, at later stages, this phenotype can get lost, while alterations in neuromuscular circuits persist (Ling et al., 2010). Therefore, an investigation of neurotransmission at the ITSN dKO NMJ could still be of interest. However, to distinguish between impaired neurotransmission secondary to neurodegeneration and impaired neurotransmission caused directly by ITSN1 loss, might prove complicated.

While there is no publication so far investigating ITSN loss at the NMJ in mammals, in *D. melanogaster* NMJs loss of Dap160 results in more and smaller synaptic boutons, so called "satellite boutons", thought to be caused by some developmental defects (Marie et al., 2004). Additionally, they present with mild endocytic deficits (Koh et al., 2004) and NMJs that are unable to sustain high-frequency neurotransmitter release (Marie et al., 2004) suggesting alterations in neurotransmission. However, the presynaptic quantal size is increased *D. melanogaster* (Marie et al., 2004), which is supposed to be proportional to the presynaptic area in mice (Jones et al., 2017). Although the presynaptic area was not significantly increased, for 6-months old ITSN dKO mice, the presynaptic area, the postsynaptic area, and the endplate area are slightly bigger than for the ITSN2 KO mice(Figure 9C, Figure 10C). This subtle increase is reminiscent of changes seen upon muscular dystrophy, as observed for *mdx*-mice at a higher age and/or upon advanced disease progression (Dubuisson et al., 2022; Harris & Ribchester, 1979; Pratt et al., 2013, 2015). Therefore, electrophysiological recordings at young and advanced ages might provide further insight into a possible ITSN-based NMJ phenotype. Additionally, studies with membrane-dyes, visualizing synaptic vesicle recycling, could complement electrophysiological findings. To assess denervation, stainings of the innervation, e.g. with β3-tubulin, would provide the possibility to compare its prevalence at NMJs. In general, it might be useful to include 1 year old mice in the analysis, as they showed the strongest motor coordination impairments. Along with this, the ITSN1 het / ITSN2 KO mice might not have been an accurate control, as their balance and motor coordination were not estimated with progressive age, so ITSN2 KO mice or even WT should be considered as potential as controls.

3.1.2 Progressive motor deficits in absence of morphological alterations

Though the NMJ appears unaffected by ITSN loss, alterations in the muscle might be an alternative cause. Indeed, ITSNs themselves play a role in regulating integrin β1 surface levels of cultured myoblasts, important for proper muscle fiber function (Samsó et al., 2022).

A loss of muscle tissue can be identified by measuring the general size of the muscle but also by a morphological analysis of the muscle tissue itself, as muscle degeneration is often accompanied by a visible inflammation within the tissue, and changes in muscle fibers due to degeneration and regeneration processes (Dubuisson et al., 2022). However, alterations in

muscle weight can be complex and hard to predict. For example, in *mdx*-mice, a common mouse model for DMD, the specific changes depend on the genetic background. E.g. *mdx*-mice on a C57BL/10 background exhibit an increase in muscular weight. Contrary, *mdx*-mice on a DAB/2-J background show a decrease (Hammers et al., 2020). Nonetheless, typically, muscle atrophy and dystrophy are associated with a decrease in muscle weight. For the TA of 2-months-old ITSN dKO mice, I observed a slight reduction in muscle weight, although not statistically significant. Interestingly, when analyzing the myofibers of these muscles, it appears that the ones of those dKO mice, which exhibited the repetitive, jackhammer-like jumping, showed subtle differences from the myofibers of those mice which did not show the jumping phenotype or belonged to the ITSN2 KO control group. Indeed, even statistically, when comparing only the jumping ITSN dKO mice to the ITSN2 KO controls, there is a significant reduction in size, as visible in the myofiber area and perimeter (Figure 12F, H, K, Figure 13F, H, K). Additionally, the TA myofibers become rounder (Figure 12I). Since the animals were of different sex, this effect does not seem to depend on sex. Although no statistical significance was reached, the mean of all analyzed ITSN dKO and ITSN 2KO mice depicted a similar trend. Yet, when looking at the frequency distribution of the area, the shift towards smaller myofibers is evident here, as well (Figure 12J, Figure 13J). Thus, the ITSN dKO myofibers exhibit characteristics reminiscent of muscular atrophy, but lack dystrophy characteristics, such as tissue necrosis, fibrosis, or muscle degeneration and regeneration, as would be visible by central nuclei and a high variability in myofiber diameter (Tubridy et al., 2001) (Figure 12A, Figure 13A). This phenotype presentation could be caused by neuromuscular degeneration or excessive repetitive behavior. Surprisingly, when examining the TB of 6-months-old dKO mice, the muscular atrophy is lost. The muscle weight of TA and TB remain at similar levels and the trend towards a reduction in myofiber area is not observed anymore. Additionally, even in the frequency distribution the area distribution between ITSN2 KO and the ITSN dKO mice, appears similar at this age. Thus, no progressive myopathy which could account for the progressive decline of motor coordination could be identified.

3.1.2.1 Possible causes for muscular atrophy

Still, as muscular atrophy was observable at younger age in mice prominently exhibiting excessive jackhammer-like jumping. It is likely that this behavior caused the observed phenotype. Exercise is usually beneficial to prevent muscle weakness, and wasting, and

promotes muscle growth, even in *mdx*-mice (Mattina et al., 2025; Tauer et al., 2021). While there are studies showing that unilateral resistance training prevents muscle atrophy of contralateral muscles and induces some transcriptomic changes (Carr et al., 2025; Shirai et al., 2025), little is known about the effect on other muscles in the body. As training reportedly changes the composition of myosin heavy chains, shifting it from 2b fibers to type 1, 2a and 2d/x (Allen et al., 2001; Demirel et al., 1999), the myosin heavy chain composition might be similarly altered in ITSN dKO mice. This might explain the increase in soleus weight at 6-months-old(Figure 11C), as the soleus is mostly composed of type 1 and 2a fibers (Demirel et al., 1999). Additional soleus samples at 2-months-old were collected and show a similar trend, but more samples are needed (Figure S 2D). Also, rats performing high-intensity exercises with insufficient recovery time show muscle atrophy along with a change in myofiber type composition (De Souza et al., 2011). Additionally, bouts of fast velocity movements or muscle contractions seem to favor muscle atrophy in the rat gastrocnemius, another muscle in the hindlimb (Ochi et al., 2015). This was reflected in a reduced muscle weight, as well as a reduced myofiber area, caused by increase protein breakdown by FoxO proteins and myostatin along with impaired protein synthesis (Ochi et al., 2015). Therefore, it seems likely that the observed changes in muscle weight and myofiber area are caused by the excessive repetitive behavior of 2-months-old ITSN dKO mice and that the muscle might recover again, once the excessive jumping stops with higher age. However, a larger cohort of mice would need to be analyzed before being sure that the excessive jumping and the alterations in muscle morphology stringently correlate.

In contrast to the increased protein breakdown upon fast velocity movements (Ochi et al., 2015), impaired autophagy as caused by loss of endophilin A or Atg5, a process for protein degradation and recycling, also results in hind limb clasping and decreasing motor coordination (Hara et al., 2006; Murdoch et al., 2016). This is particularly interesting, as ITSNs interact with several autophagy-related proteins like endophilin A (Pechstein et al., 2015) and beclin-1 (Wong et al., 2012).

3.1.2.2 Striatal implications in movement coordination

Although ITSN dKO mice show some characteristics of muscular atrophy at 2-months of age, they are not present anymore in the 6-months-old dKO mice. Therefore, muscle defects are unlikely to account for the progressive motor coordination decline. In addition, the lack of

changes in NMJ morphology does not argue for impaired neuro-muscular transmission, even though this was not yet measured directly. This leads to the conclusion that the motor impairments probably arise neurologically, i.e. by a progressive decline of neuronal functionality or viability.

In ITSN dKO mice, alterations in basal ganglia volumes and the morphology of striatal medium spiny neurons are accompanied by abnormal neurotransmission in these brain regions (Vollweiter, 2021). These alterations are presumed to result in the repetitive behavior as striatal dysfunction is associated with this kind of behavior (Kohls et al., 2014; Langen et al., 2011). This raises the question whether progressive changes in the striatum might also underlie the observed decline in motor coordination. The basal ganglia are critical for formation and execution of motor skills (Graybiel, 1998; Grillner et al., 2013) with striatal signaling implicated in action selection (Markowitz et al., 2018; Redgrave et al., 1999) and movement intensity regulation (Dudman & Krakauer, 2016). In line, lesions of the dorsolateral striatum disrupt the formation of naturalistic behavioral sequences (Markowitz et al., 2018). In Parkinsons Disease, which is defined by a gradual decline in motor control and the ability to initiate movement, dopamine depletion in the dorsolateral striatum is necessary to result in gross movement deficits but might not be sufficient as a singular cause (González-Rodríguez et al., 2021). However, it has been shown several times that striatal dopaminergic signaling is important for pathway balance (Kovaleski et al., 2020; Kravitz et al., 2010). Therefore, alterations in striatal neurotransmission and circuits could result in movement deficits and impaired action selection. Whether dopamine depletion occurs in the striatum of ITSN dKO mice is unknown so far. Subsequently it could be speculated that this depletion would result in the transition of repetitive behavior to movement deficits.

3.1.2.3 Linking ITSN1 deficiency to cerebellar dysfunction and ataxia-like phenotypes

Although motor symptoms, such as impaired fine and gross motor skills, impaired balance, and muscle weakness are considered features of ASD by now (da Silva et al., 2025; Fournier et al., 2010), progressive motor decline is not typical for ASD. However, impaired motor coordination and learning in ASD mice has been linked to a dysfunction in cerebellar plasticity (Palmen et al., 2004; Piochon et al., 2014; Tsai et al., 2012). Heterozygous and homozygous loss of tuberous sclerosis complex in the cerebellum can also be linked to repetitive, autistic-like behaviors (Tsai et al., 2012). In addition, in mice and patients with Fragile X syndrome (FXS),

a genetic ASD case caused by the absence of functional FMRP (Y. Chen et al., 2022), cerebellar deficits are thought to contribute to motor and motor learning deficits (Y. Chen et al., 2022; Koekkoek et al., 2005). Structural abnormalities are reported in many cases of FXS, often including a reduction of the medial vermis, a part of the cerebellum (Greco et al., 2011; Guerreiro et al., 1998; Mostofsky et al., 1998; Wilson et al., 2009) which is associated with posture and locomotion (Coffman et al., 2011). Although the relative volume of the cerebellum is increased in ITSN dKO mice (Vollweiter, 2021), instead of decreased like in FXS, alterations in cerebellar motor control may manifest as motor coordination difficulties. A prominent disease associated with cerebellar dysfunction and impaired motor coordination is ataxia, which often affects gaze, gait and balance (Mariotti et al., 2005). It presents mostly as a chronic and progressive disease, commonly with an early-onset in infancy or adolescence or as late-onset in adult age. Nevertheless, there are also forms which present as acute, recurrent diseases called episodic or paroxysmal ataxia (Harding, 1983). The ataxia manifestations are reminiscent of middle-aged ITSN dKO mice. Especially, as different mouse models for ataxia show a reduction in movement or locomotion speed, as well as impaired balance in a rotarod test (Glynn et al., 2005; Orengo et al., 2022). Intriguingly, ataxia is associated with Kv1.1 (Herson et al., 2003) and Kv1.2, as in humans several cases of *KCNA2* (the gene encoding Kv1.2) mutations were diagnosed with ataxia (Masnada et al., 2017). Similarly, Pingu mice, which have a point mutation in *KCNA2*, exhibit an ataxic phenotype, thought to be caused by altered Purkinje cell output (G. Xie et al., 2010). These mice also present with reduced levels of Kv1 channels (G. Xie et al., 2010), similar to the reduction of Kv1.1 and Kv1.2 in ITSN dKO mice (Vollweiter, 2021).

Alterations in cerebellar structures are assumed to be key drivers in fragile X-associated tremor/ataxia syndrome (FXTAS), a late onset neurodegenerative disease with decreased levels of FMRP (Jacquemont et al., 2003) with differential progression of motor skill dysfunction, including progressive gait ataxia (Faruq et al., 2014; P. J. Hagerman & Hagerman, 2015; R. J. Hagerman et al., 2007). One mechanism hypothesized to result in FXTAS is sequestration of the protein SAM68, an ITSN1 interactor (Pankivskyi et al., 2021), by its binding to CGG repeats on FMR1-RNA (Sellier et al., 2010, 2013). SAM68 is recruited to expanded CGG repeats along with the proteins hnRNP-G and MBNL1 forming large RNA-protein aggregates and thereby losing its splicing regulatory function (Sellier et al., 2010). This

recruitment is dependent on DGCR8 and its interaction partner drosha, two proteins involved in miRNA processing (Sellier et al., 2013). Now, there are two different mechanisms by which ITSN loss could favor FXTAS. Firstly, ITSN1 regulates SAM68 localization by influencing its solubility (Pankivskyi et al., 2021). Therefore, loss of ITSN1 could reduce the amount of soluble SAM68 and subsequently result in increased levels of sequestered SAM68. This could result in altered splicing and reduced levels of mature miRNA based on reduced levels of SAM68 availability and loss of DGCR8/drosha activity. Interestingly, SAM68 deficient mice also present motor coordination defects, especially for beam walking, similar to the ITSN dKO mice (Lukong & Richard, 2008). As FXTAS is late-onset (Hall et al., 2014; Jacquemont et al., 2003), this could explain why these phenomena where not yet present in the 2-months-old dKO mice. Another mechanism is possible as well. FXTAS is based on a permutation of the *FMR1* gene with 55-199 CGG repeats (Hall et al., 2014) resulting in increased FMR1 mRNA levels (Jacquemont et al., 2003). This specific mutation is unlikely to occur in the ITSN dKO mice, but other mechanisms may result in increased FMR1 mRNA levels as well. FMRP regulates its own translation, by binding its own transcript (Ashley et al., 1993; Sung et al., 2000). Since ITSNs may be involved in regulating translation (in an FMRP-dependent or independent manner, which will be discussed in chapter 3.2.3.2), the increased FMR1 mRNA levels could be caused by different FMRP-granule target mRNAs upon ITSN1 loss. Thus, FMR1 mRNA could accumulate progressively and result in the aggravating FXTAS-like symptoms.

3.1.2.4 Experimental approaches elucidating the pathophysiology of motor impairment in ITSN dKO mice.

On one hand, it might be interesting to further assess the extent of the motor impairments in aging ITSN dKO mice, even after the age of 6-months. Additional analyses, e.g. of the gait, or grip force measurements, and motor learning tasks, like delay eyeblink conditioning, could help to narrow down possible causes, as the latter are often associated with cerebellar dysfunction and ataxia (Mariotti et al., 2005; Piochon et al., 2014). Also, in relation to the hypothesized activity-dependent atrophy, determination of atrophy-related molecules like FoxO1, FoxO3 and myostatin via western blotting might confirm the hypothesis as well as staining of the muscle tissue for different myofiber types.

On the other hand, to gain insight into the possible mechanism responsible for declining motor coordination, further experiments are necessary. Especially investigation of striatal neuron morphology and viability, as well as neurotransmission in the ageing ITSN dKO mice, seems promising. Here, immunohistochemical staining of brain sections for dopaminergic markers like tyrosine hydroxylase and electrophysiological recordings of medium spiny neurons, as already performed for younger mice by Vollweiter, 2021, could be of interest, since repetitive behavior is thought to arise from cortico-striatal imbalance. This imbalance could worsen with age, e.g. resulting in dopaminergic depletion based on so far unknown mechanisms, facilitating motor decline. Additionally, protein levels of tyrosine hydroxylase and other proteins involved in dopaminergic protein in the striatum could be monitored at different ages. In relation to other possible pathways, a closer examination of other brain regions involved in motor control, like the cerebellum, should be conducted. Here, especially Purkinje cells and their plasticity could be of interest, as they are already known to be involved in movement deficits in ASD (Piochon et al., 2014; Tsai et al., 2012). Also, as Kv1.1 and Kv1.2 levels were already found to be reduced in ITSN dKO mice forebrains, it could be beneficial to quantify Kv1.2 and Kv1.1 levels in the cerebellum of ITSN dKO, as reduced levels of these proteins might favor ataxic behavior. Furthermore, instead of reduced Kv1-channel levels, a slow accumulation of FMR1 mRNA based on altered translational regulation or a SAM68 dysfunction upon ITSN loss might cause FXTAS, accounting for the delayed ataxia onset. To unravel a potential crosstalk of ITSN loss with the FXTAS pathomechanism causing the ataxia-like phenotype, it would be important to investigate on one hand FMR1 mRNA and FMRP levels and on the other hand SAM68 localization and function in the ITSN dKO mice.

To summarize, as neither the examination of the NMJ nor of the TA or TB muscle uncovered characteristics of neuro-muscular degeneration, the observed progressive motor decline is more likely to be caused by progressive impairments of the central nervous system. While changes in the striatum, cerebellum, autophagy or FXTAS-related alterations are possible causes, further research is needed.

3.2 Mechanisms by which ITSNs regulate Kv-channel prevalence

Kv-channels, like Kv1.2, are important for regulating neurotransmission and presynaptic excitability, located at the transition from axon to synaptic terminal (Dodson et al., 2003; W.

Shen et al., 2003). Kv1.2 loss, loss-of-function or gain-of-function mutations are associated with seizures and epilepsy (Brew et al., 2007; D'Adamo et al., 2020) and altered Kv-channel prevalence results in changes in neurotransmission (Vollweiter, 2021). In ITSN dKO mice, the prevalence of several Kv1 family subunits, like Kv1.1 and Kv1.2, as well as the regulatory β-subunit Kvβ2, is decreased. This comes along with functional implications, such as an increase in neurotransmitter releases based on a prolonged action potential repolarization and increased Ca^{2+} signal at the presynapse (Vollweiter, 2021). However, up to now it is unclear how loss of ITSN1 results in decreased Kv-subunit levels.

3.2.1 Indirect scaffolding of ITSNs might stabilize Kv-subunits

The scaffolding hypothesis proposed ITSNs scaffolding function as a possible mechanism by which ITSNs could stabilize Kv1 channels at the synapse. ITSNs and Kv1 channel subunits might directly or indirectly interact, akin to ITSN1´s interaction with postsynaptic NMDARs (Vollweiter et al., 2023) that appears to stabilize NMDARs at synaptic membranes. While Dennis Vollweiter, a previous scientist in our lab, had initially observed an interaction of ITSN1 with Kv1.2 and Kvβ2 in the context of a Co-IP (unpublished data), this interaction could not be replicated. Neither pull-down approaches with GST-tagged ITSN1-S domains or the cytosolic domains of Kv1.2 and Kvβ2 nor the more physiological approach of co-immunoprecipitation confirmed the interaction (Figure 15, Figure 16). This was unexpected as Kv1.2 and Kvβ2 contain the core SH3 binding motif PxxP, which was sufficient for other Kv1-channels to mediate an SH3-dependent interaction (Hajdu et al., 2015).

However, ITSNs might stabilize Kv1 channels indirectly. A promising candidate for providing a link between ITSNs and Kv1.2 channels is the actin-binding protein CTTN. It shares a signaling axis with ITSNs in actin polymerization and is regulating Kv1.2 surface expression and endocytosis in HEK293 cells (Hattan et al., 2002; Williams et al., 2007). The interaction of CTTN and Kv1.2 was confirmed in mouse brain lysate and extended to the regulatory subunit Kvβ2 (Figure 18). Additionally, CTTN forms a complex with ITSN1-L and actin (Figure 18). This hints at an indirect link between ITSNs and Kv-channels. In addition, colocalization studies revealed CTTN and Kv1.2 to be present at actin puncta (Figure 17), similar to ITSN1 and CTTN as many CTTN and ITSN1-positive puncta are also positive for actin (Figure 19). As ITSN interacts with CTTN at the same subcellular structures as Kv1.2, these Kv channels

might be anchored to the actin cytoskeleton via a CTTN-ITSN complex. This indirect link to Kv1.2 and Kvβ2 might explain, why Vollweiter might initially have detected an interaction in a co-immunoprecipitation, which could not be replicated.

3.2.1.1 Differential CTTN binding motifs may explain Kv1.1 and 1.2 reduction in ITSN dKO mice

While the functional aspect of CTTN and Kv channel interaction seems conserved, the domains for an interaction between CTTN and Kv-channels are diverse. CTTN is known to anchor several Kv1 channel subtypes to the actin cytoskeleton or regulate their surface expression, e.g. for Kv1.2 (Hattan et al., 2002; Williams et al., 2007), Kv1.3 (Hajdu et al., 2015) and Kv1.5 (L. Cheng et al., 2011), as well as others channel family subunits like Kv10.1 (Herrmann et al., 2012). However, the interaction sites employed by CTTN vary for different Kv-channel subtypes. For Kv1.2 an SH3 binding motif independent interaction was identified (Hattan et al., 2002), while Kv1.3 interacts with CTTN through an SH3 binding motif (Hajdu et al., 2015). For Kv1.5 the interaction has been identified by co-immunoprecipitation (L. Cheng et al., 2011), but the precise binding site is still unknown. This variability in the binding modes for the involved proteins might explain why specifically Kv1.1, Kv1.2 and Kvb2 were found to be decreased in ITSNdKO mice, as different scaffolds or complexes may support the different CTTN-Kv channel interactions. However, as no systematic evaluation of the levels of all the different Kv channel types has been performed in ITSN dKO mice, no final conclusion can be drawn.

3.2.1.2 Possible alternative interaction sites for CTTN and ITSN1

Clearly, this possible Kv1.2-CTTN-ITSN complex must be investigated further as a complex formation by CTTN and ITSN could involve additional components or might occur independent of Kv1.2 anchorage. For example, ITSN and CTTN share the protein WIP as common interactor (Gryaznova et al., 2015; Kinley et al., 2003), and CTTN, WIP and ITSN colocalize in glioblastoma cells (Gryaznova et al., 2015). This interaction might cause a co-precipitation of CTTN with ITSN independent of a complex linking Kv1.2 to the actin cytoskeleton. More precisely, WIP could link CTTN and ITSNs as the residues 318-450 of WIP mediate its interaction with ITSN1 (Gryaznova et al., 2015), while it binds CTTN via the residues 110-170 (Kinley et al., 2003). N-WASP might present another part of the complex, as it binds ITSNs and WIP. As the WIP residues 454-485 are responsible for the N-WASP

interaction (Peterson et al., 2007), ITSNs in tandem with WIP could provide a platform bringing CTTN and N-WASP together for their concerted Arp2/3 regulation (Lua & Low, 2005). As this possible link between ITSN and CTTN is related to the actin cytoskeleton and actin puncta are the common interaction site for CTTN and Kv1.2 as well, colocalization studies of all four components, CTTN, ITSN, Kv1.2 and actin, are needed to verify a Kv1.2-CTTN-ITSN complex.

While WIP could link CTTN and ITSN1, the CTTN sequence includes a proline rich region with core PxxP motifs (P**P**AS**P**SPQPIEDRP**P**SS**P**I) which could provide a binding site for ITSNs SH3 domains (based on Uniprot CTTN sequence, ID: Q60598). However, as mostly the ITSN1-L form precipitated, the interaction might rather be mediated by the domains specific for ITSN-L. Therefore, it would be interesting to probe for a direct interaction between CTTN and ITSN1.

Nevertheless, a complex of Kv1.2-CTTN-ITSN1 is possible, as up to now it is unknown whether there is another protein involved in linking Kv1.2 and CTTN to the actin cytoskeleton (Hattan et al., 2002; Williams et al., 2007). ITSN1 as part of this link might be of advantage as Kv1.2 phosphorylation results in CTTN dissociation as well as Kv1.2 endocytosis (Hattan et al., 2002; Nesti et al., 2004; Williams et al., 2007). Here, ITSNs could provide a bridge to endocytosis initiation as they are involved in early endocytic processes (Henne et al., 2010).

3.2.1.3 Further indirect scaffolding candidates

Aside from CTTN, FMRP also interacts with Kv1.2 (Yang et al., 2018) and Kvβ2 (Figure 25), possibly within a complex with FXR1, as FXR1 binds FMRP (Méndez-Albelo et al., 2024)and the intracellular channel subunit Kvβ2 (Figure 25). Since FXR1 binds ITSN1 as well (Figure 25), FXR1 and FMRP provide another indirect link or scaffold to Kv1.2 and Kvβ2. Functionally the dissociation of FMRP from Kv1.2 results in an increased synaptic vesicle release, and even in an increased Ca^{2+} transient in FMRP KO mice (Yang et al., 2018), similar to what has been observed for ITSN dKO mice (Vollweiter, 2021). For both models, this phenotype can be rescued by addition of a Kv1.2 activator (Vollweiter, 2021; Yang et al., 2018). Therefore, even if the implication of ITSNs in mRNA stability and/or translational regulation as discussed later (3.2.3.2) does not hold true, its interaction with FXR1 alone might indirectly influence Kv1 channel stability or activity.

Summarized, although not by a direct interaction, ITSNs may stabilize Kv1.2 and Kvβ2 indirectly by supporting CTTN anchorage of Kv1.2 to the actin cytoskeleton or by FXR1/FMRP interaction. However, those possible links need further investigation. Especially the link between CTTN and ITSN needs further investigation to unravel whether there is a direct link between CTTN and ITSN or if shared interactors promote complex formation, maybe even independent of Kv1.2. In the end, the loss of ITSNs could result in Kv-channel reduction indirectly either by FMRP/FXR1 interaction or via reduced CTTN anchorage to the actin cytoskeleton and/or by altering the actin cytoskeleton.

3.2.2 Complex actin regulation by ITSNs and Cdc42

The actin cytoskeleton is a crucial component of the synapse. It is important for neurotransmission, mobilization of the synaptic vesicle pool, and as scaffold stabilizing and anchoring transmembrane proteins at the pre- and postsynapse (Cingolani & Goda, 2008; Vollweiter et al., 2023). Therefore, it seemed likely that a reduction of actin as seen in ITSN dKO mice brains (Vollweiter, 2021) could reduce the anchorage of transmembrane channels like Kv1.2 at the presynapse. In this scenario, ITSNs themselves would not provide the scaffolding, but contribute to the stimulation of actin polymerization, thereby allowing actin to function as scaffold for the anchoring of presynaptic Kv channels.

3.2.2.1 Kv channels and their implications for the actin cytoskeleton

Indeed, actin polymerization is important in Kv-channel regulation, clustering, and anchorage. Conversely, Kv channels can also influence actin dynamics. Kv3.3 can regulate actin polymerization by recruiting Arp2/3 through Hax-1 and CTTN impacting its own inactivation dynamics (Y. Zhang et al., 2016). Similarly, actin depolymerization or capping can enhance channel activity as shown for mechanosensitive (J. Zhang et al., 2006) and for sodium channels (Shumilina et al., 2003). Actin disruption as well as stabilization alters Kv2.1 gating properties and clustering (Delgado-Ramírez & Rodríguez-Menchaca, 2019). Also, actin related proteins, like actinin2 and CTTN, are known to link Kv-channels to the actin cytoskeleton or even influence their mediated currents (Hattan et al., 2002; Maruoka et al., 2000; Williams et al., 2007; Y. Zhang et al., 2016). This anchorage is related to a local F-actin network and/or active actin polymerization (Hajdu et al., 2015; Y. Zhang et al., 2016) which might be reduced

in ITSN dKO mice as ITSN-based Cdc42 activation is lacking (Hussain et al., 2001). As direct actin association as well as indirect connections affect Kv-channel localization and stability, it was unexpected to find the rate of polymerized F-actin to available G-actin the same in ITSN2 KO and ITSN dKO mice (Figure 20A, F). More profoundly, I could not replicate the actin reduction previously observed by Vollweiter et al. in the synaptic membrane fraction at all, neither biochemically nor microscopically (Figure 20B, C, Figure 21, Figure 22). Similarly, a closer investigation of Cdc42 levels did not reveal any significant changes (Figure 20D, E). In contrast to the earlier results, my biochemical determination of presynaptic actin levels rather revealed the opposite effect, an increase in actin levels (Figure 22).

3.2.2.2 Methodological influences on actin detection

One factor that may contribute to this discrepancy is methodology. While Vollweiter, 2021, analyzed the synaptic membrane fraction, i.e. only the membranes of the pre- or postsynaptic compartments, I worked with synaptosomes. This includes the resealed presynapse with enclosed presynaptic proteins and synaptic vesicles, as well as the PSD and the proteins it anchors (Gray & Whittaker, 1962). ITSNs function in membrane-related processes like endo- and exocytosis (Gubar et al., 2013), and thus often localize in proximity to the cellular membrane. Supporting synaptic vesicle exocytosis, ITSNs interact with SNARE proteins like Snap25 (M. Okamoto et al., 1999) or synaptobrevin (Jäpel et al., 2020), which are both membrane-anchored (Gonzalo et al., 1999). During endocytosis, ITSNs localize to clathrin-coated pits, forming a membrane invagination to retrieve synaptic vesicle membranes post-fusion (Pechstein et al., 2010). In addition, outside of neurotransmission, ITSNs have been identified at αVβ5 positive adhesions, another membrane-associated structure (Lukas et al., 2024). So, as ITSNs often localize to the membrane, ITSN-stimulated actin polymerization should take place there, too. Indeed, the docking of secretory vesicles is supported by phosphatidylinositol-4,5-bisphosphat and Cdc42-dependent actin polymerization (Wen et al., 2011), which needs prior Cdc42 activation, likely by ITSN-L, as it localizes with Snap25 (Malacombe et al., 2006). Therefore, the membrane-associated actin might be more strongly affected by ITSN loss than the overall actin levels. Additionally, ITSN-L contains a C2 domain, which can promote Ca^{2+} dependent and independent lipid or membrane interaction (Corbalan-Garcia & Gómez-Fernández, 2014). Little is known about the function of ITSNs C2

domain specifically, but it shares a high similarity with synaptotagmins C2 domains (W. Zhang et al., 2013) which can bind to the phospholipid membrane (Dai et al., 2007). A similar

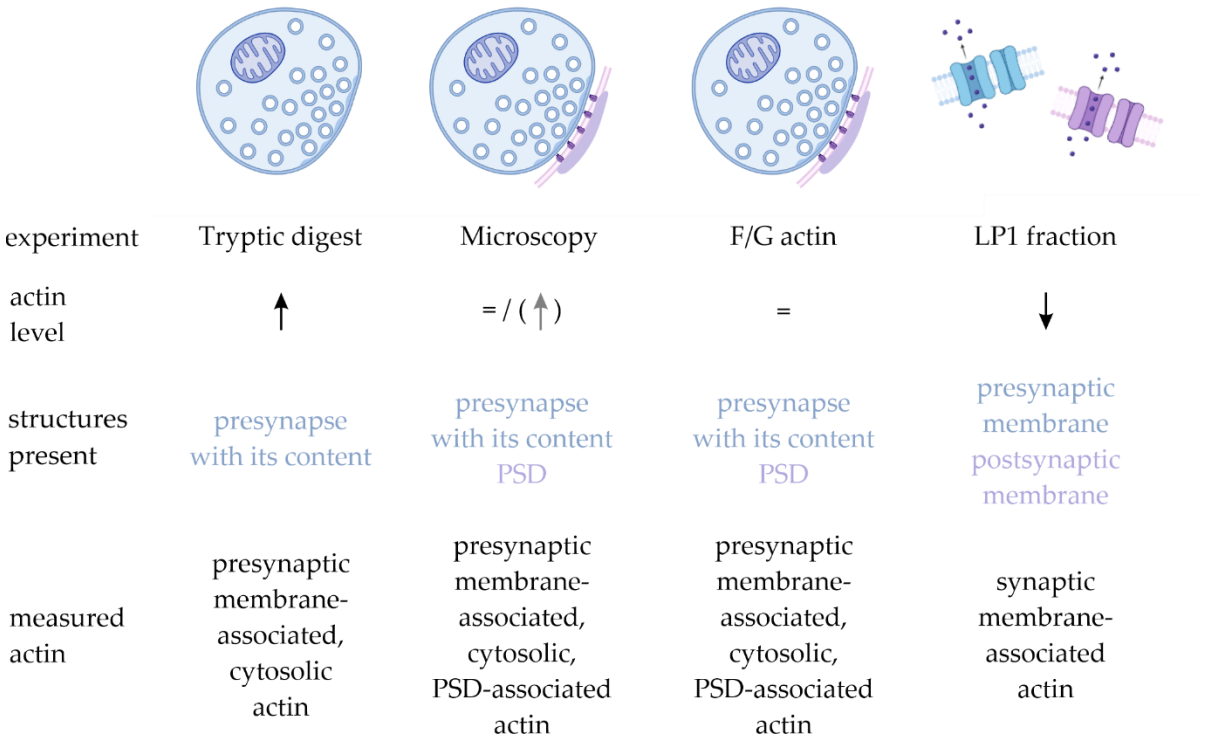

Figure 30: Actin levels of ITSN dKO synapses differ based on methodology.

Variation in experimental approaches resulted in different actin levels at ITSN dKO synapses. While investigating the presynaptic cytosolic and membrane-associated actin content, actin levels were elevated. For samples assessing cytosolic and membrane-associated actin for the presynapse and PSD structures, actin levels were comparable to the control condition. In contrast, for the pre- and postsynaptic membrane actin levels were decreased (Vollweiter, 2021). Schematics generated with Biorender.com.

function of the C2 domain in ITSN-L could link actin polymerization to the cellular membrane, and might be enhanced by a potential membrane association of its PH domain (Lemmon, 2003).

3.2.2.3 Possible compensatory mechanisms in Cdc42-dependent actin polymerization

Though this might explain why actin levels in synaptosomes remained unaltered, it does not account for the increase in actin observed at the presynapse upon postsynaptic digestion. Even in the microscopic evaluation of actin levels, a slight trend towards increased actin levels was revealed. These findings suggest compensatory effects, although their origin is unknown yet. One possibility is that alternative regulatory mechanisms come into play to restore membrane-associated actin in absence of the original pathways. Cdc42 dependent actin dynamics are involved in post-Golgi transport (Egorov & Polishchuk, 2019). Here, the loss/silencing of the

Cdc42 GEF, FGD1, resulted in an increase of Cdc42 downstream targets, especially PAK1 and IQGAP1, which might be targeted by FGD1 independent signaling pathways (Egorov & Polishchuk, 2019). For ITSN/Cdc42 mediated actin polymerization N-WASP is the main downstream target of Cdc42 (Hussain et al., 2001) and could be similarly upregulated, as Cdc42 levels themselves did not seem to be altered (Figure 20D, E). In addition, N-WASP needs to be activated, and there are some Cdc42 independent mechanisms for this. One possibility is via phosphorylation of N-WASP (Suetsugu et al., 2002) or by binding of SH3 domain containing adaptor proteins (Okrut et al., 2015). One such SH3 domain containing protein is CTTN (Kowalski et al., 2005). Interestingly, FGD1 interacts with CTTN (Hou et al., 2003), like ITSNs might (3.2.1), but N-WASP silencing did not mimic FGD1 loss (Egorov & Polishchuk, 2019). This suggests the absence of CTTN- or N-WASP-based compensatory mechanisms for FGD1/Cdc42 dependent polymerization but needs confirmation for ITSN/Cdc42 mediated actin polymerization.

Another possibility to maintain membrane-associated actin in absence of ITSNs could be by activating alternative actin regulatory pathways. These pathways would be independent of N-WASP as it is mainly activated by Cdc42 (Humphries et al., 2014; Hussain et al., 2001; J.-B. Wang et al., 2005). Cross-talk between Rho-GTPase family members, including Cdc42, Rac1, Rac2 and Rho, is common (Baptista & Westerberg, 2017; Diebold et al., 2004), however, the precise interplay between the family members seems to be dependent on cell type and localization (Baptista & Westerberg, 2017). Nevertheless, in dendritic cells, loss of WASP, an N-WASP homolog, induces a negative feedback loop through Cdc42 (Diebold et al., 2004), resulting in the activation of Rac1 and Rac2 (Baptista & Westerberg, 2017). Similar crosstalk based on lacking Cdc42 dependent N-WASP activation and downstream adaptations could increase actin polymerization in absence of ITSNs and thus result in increased presynaptic actin levels. Intriguingly, compensatory effects might not be dependent of signaling downstream of Cdc42, but ITSNs loss itself. ITSN1-S been shown to impair mSos1-Eps8 interaction needed for Rac1 activation, therefore ITSN1-S reduction resulted in increased cytoskeletal rearrangement and cell proliferation (Jeganathan et al., 2016). This provides a compensatory mechanism, directly dependent on ITSN-loss.

Both previously described mechanisms, the compensatory as well as the methodological effect, may apply in tandem, resulting in the different actin levels I detected. While I observed

the increase in presynaptic actin by postsynaptic digest as might be caused by compensatory effects, looking at synaptosome actin levels by microscopy and immunoblotting, this is not visible. This could be based on ITSNs providing a possible membrane link for actin. The postsynapse and especially the PSD is an actin-rich structure but is not expected to reseal upon synaptosome preparation (Hotulainen & Hoogenraad, 2010). Therefore, for the ITSN dKO samples, the PSD-associated actin might get washed away more easily during the synaptosome wash step, while it remains attached for the ITSN2 KO control synaptosomes. Even without a direct link of ITSNs to the membrane, ITSNs are thought to link the actin cytoskeleton to the PSD (Vollweiter et al., 2023), so the missing anchorage to the actin cytoskeleton could have a similar effect. This might result in an increase in total presynaptic but decrease in membrane-bound postsynaptic actin, which roughly evens out for the total synaptosome, as used for the F/G-actin ratio and microscopy approach. Furthermore, the extent of postsynaptic actin loss by washes and handling might differ between experiments and would result in a high variation in actin levels, as observed in the microscopic approach.

It is important to consider what these results mean for the actin hypothesis. The main idea of lacking anchorage for (transmembrane-) proteins remains possible. The level of membrane bound actin was found to be reduced in ITSNdKO mice (Vollweiter, 2021) which could be explained by defects in local actin polymerization and linkage to the plasma membrane. Possible compensatory mechanisms, acting at the presynapse, might result in higher presynaptic actin levels in the tryptic digest assay, though those additional actin filaments might be intra-synaptosomal rather than membrane-associated, as they could not be detected in the synaptic membrane fraction (Vollweiter, 2021). In general, the loss of ITSNs could result in reduced and/or altered localization of the actin cytoskeleton, therefore reducing proper protein anchorage. In favor, this mode of action was proposed to account for the postsynaptic loss of NMDAR subunits in ITSN dKO mice (Vollweiter et al., 2023). Here, ITSNs interact with PSD95 and NMDAR subunits (Nishimura et al., 2006; Vollweiter et al., 2023), similar to other actin-associated scaffolds related to repetitive behavior and ASD, such as Shank2 and 3 (Peça et al., 2011; Won et al., 2012). Actin is an important structural organizer of the PSD (Hotulainen & Hoogenraad, 2010) and ITSN-based actin polymerization was suggested to stabilize postsynaptic NMDAR (Vollweiter et al., 2023).

However, the results and proposed mechanisms are not straightforward and need further investigation. It would be beneficial to replicate the reduction of actin in the synaptic membrane fraction taking the same approach as Vollweiter, 2021, to verify his initial findings and to take a closer look at ITSNs membrane localization. Here, comparative studies with ITSNs lacking certain potentially membrane-associated domains like the C2 or PH domain might prove helpful. Therefore, Ca^{2+} imaging, as performed by Vollweiter, 2021, with rescue of ITNS loss by different ITSNsisoforms, e.g. without the DH and PH domain or lacking single domains of ITSN-L, would provide further insight. Another interesting experiment regarding Ca^{2+} imaging would be to specifically inhibit ITSN-dependent actin polymerization, as described in Friesland et al., 2013 to determine its contribution on the synaptic ITSN dKO phenotype. In addition, it would be crucial to measure Cdc42 activity in synaptosomes to judge whether this Rho GTPase indeed displays altered activity at the presynapse in absence of ITSNs as previously shown in other cellular contexts (Baptista & Westerberg, 2017). Additionally, to assess if or which compensatory pathways may be activated, a determination of the protein and activity levels of N-WASP, PAK1 and other Rho-GTPases and their activators like mSos1-Eps8 would be crucial.

3.2.3 ITSNs as potential modulators of FMRP-positive granules and mRNA stability

A third possibility for the reduction of several proteins at the dKO synapse could be caused by the involvement of ITSNs with mRNA stability and/or translational regulation. This idea was triggered by the fact that mice which are deficient of Jakmip1, a component of FMRP-positive granules, show a very similar repetitive jumping behavior (Berg et al., 2015). In line with this idea, the translation of several proteins, which were found decreased at the ITSN dKO synapse, like Kv1.2, Kvβ2, NR2A and actin, is regulated by FMRP (Darnell et al., 2011; Vollweiter, 2021). Additionally, it has been shown that ITSN1 can interact directly with mRNA and regulates the mRNA-binding protein SAM68 (Pankivskyi et al., 2021). Therefore, I probed for further ITSN1 interactors related to mRNA and translation.

3.2.3.1 Implications of ITSNs interaction with RNA-binding proteins like DDX5 and PABP

Initially, to narrow down possible interactions, I analyzed two MS datasets of an ITSN-IP using hippocampal neurons. Indeed, upon clustering of GO terms, the two clusters with the highest enrichment were related to translation initiation and mRNA splicing, accompanied by

cytosolic translation and ribosomes with a lower enrichment score (Figure 23A). For verification, a closer investigation of two proteins, PABP and DDX5, involved in translation initiation and mRNA metabolism, was performed. Interestingly, Co-IPs using synaptosome lysates revealed an interaction with ITSN1 for both proteins (Figure 26). For DDX5, I could identify the SH3D domain of ITSN1 as main interaction site, while PABP could not be co-precipitated with any of the domains present in ITSN1-S (Figure 27). This could hint at an indirect interaction between ITSN and PABP. Other possible explanations are the need for a phosphorylation or other post-translational modification of ITSN1 or an interaction with the ITSN-L specific domains, which were not included in the pull-down. An indirect interaction would be possible as well. If DDX5 could serve as link between PABP and ITSN1 remains unknown as whether ITSN1, DDX5 and PABP reside in one complex remains unclear. Interestingly, PABP was shown to interact with ITSN-interactor SAM68. They interact upon virus infection facilitating translation (H. Zhang et al., 2015). As SAM68 binds ITSN through an N-terminal proline rich motif (Pankivskyi et al., 2021), ITSNs could link PABP and SAM68. However, the interaction between SAM68 and PABP was only described upon viral infection (Rai et al., 2015; H. Zhang et al., 2015), therefore, this interaction seems unlikely to be part of a general cellular mechanism. Another possible link are FMRP-positive granules, which might provide a platform for a ITSN/DDX5/PABP complex, as else, DDX5 and PABP share limited interaction sites (Berg et al., 2015; Kanai et al., 2004; Villacé et al., 2004). Interestingly, DDX5 and PABP have recently been proposed as ASD risk genes, mostly based on their role in FMRP granules. They are key components regulating RNP granule transport and granule composition by their interaction network, as they interact with other proteins involved in ASD, like hnRNPH2 or DDX3 (S. Chen et al., 2020). But first, it is worthwhile to look at FMRP-independent interactions and effects.

Indirect RNA-mediated interactions between DDX5 and PABP are proposed to occur during nonsense-mediated mRNA decay (Geißler et al., 2013). However, apart from the interactions found here, no further indications that ITSNs are involved in this process are known up to now. In general, ITSNs might either interact with DDX5 and PABP in the context of their individual functional pathways or within RNP granules. Further experiments associating ITSNs with nonsense-mediated mRNA decay would be necessary. As this process is regulated by the protein Upf, a co-precipitation or co-localization of ITSNs with this protein would

render an involvement of ITSN in nonsense-mediated mRNA decay more likely. An even better experiment to clarify ITSNs involvement in this process would be to measure nonsense-mediated mRNA decay, e.g. with nonsense-mediated mRNA decay receptor assays, in cultured ITSN2 KO and ITSN dKO cells.

Still, ITSNs and DDX5 could interact outside of a complex including PABP. Surprisingly, it seems likely that ITSNs can either bind RNA or DDX5, as both interactions are mediated by the SH3D domain (Pankivskyi et al., 2021)(Figure 27). Although DDX5 can bind RNA on its own, in a sequence-independent manner (Xing et al., 2019), it would appear useful for an interactor to bind DDX5 and the RNA at the same time, stabilizing this complex on its target. This would support DDX5´s function as RNP chaperone, replacing and connecting RNA-binding proteins on RNA (Xing et al., 2019). Additionally, the notion of competitive binding contradicts a hypothesis by Pankivskyi et al. where mRNA acts as scaffold to initiate interaction between RNA-binding proteins and their chaperones, at least for this specific interaction. However, this suggests a role for ITSNs in a complex which stabilizes DDX5 and other RNA-binding proteins. This complex might include DDX5´s close interactor and paralog DDX17, or hnRNP H/F, further interactors of DDX5 (Dardenne et al., 2014) that were detected in the MS713 dataset as possible interactors of ITSN1. Nonetheless, the precise interaction site within DDX5 is unknown so far. The DDX5 sequence contains one classical PxxP motif (aa 206-209; sequence from Uniprot. ID: Q8BTS0) which could serve as an interaction site, though an analysis with a motif miner program does not confirm this as interaction site (Kundu et al., 2014). In addition, little to no other SH3 domain proteins are known to bind DDX5. Abl1, a tyrosine kinase, might be an SH3 domain containing interactor since DDX5 was identified in an Abl1-based affinity capture MS (So et al., 2015), though the interaction was not investigated further.

The exact role of ITSN1's interaction with DDX5 in cellular processes remains to be elucidated. ITSN1 interacts with NDHII (H. Zhang et al., 2021), a DNA and RNA helicase, to suppress DNA replication (H. Zhang et al., 2021). Though DDX5 is an RNA helicase as well, their functions are different as DDX5 is not involved in regulation of DNA replication. Although DDX5 and SAM68 both interact with the androgen receptor and are believed to act on the same splicing modules, even though with opposing effects (Seltzer et al., 2023), no closer interaction or dependency is described. Therefore, it appears unlikely that ITSNs might act as scaffold

linking them together. Interestingly, DDX5 and its paralog DDX17 are involved in miRNA biogenesis via their interaction with DGCR8 and drosha (Suzuki et al., 2009). These proteins are thought to be involved in FXTAS pathology together with ITSN1´s interactor SAM68 (Pankivskyi et al., 2021; Sellier et al., 2010, 2013). This provides another possibility of how ITSNs may contribute to FXTAS pathology, by regulating DGCR8 and drosha availability via DDX5.

Similarly, the functional effects of ITSN1´s interaction with PABP remain enigmatic. Although I could not precipitate PABP with the ITSN SH3 domains, it seemed like a likely SH3 domain interactor because according to the motif miner SH3PepInt (Kundu et al., 2014), PABP is predicted to contain a total of 4 SH3 binding motifs, of which the 2 N-terminal motifs should be able to bind the ITSN1 SH3 domains. The first SH3 motif spans aa 29-43 and is predicted to bind to the ITSN1 SH3A, C, D and E domain, and the second comprises aa 31-45 and would be a suitable ligand for the SH3D domain of ITSN1. As these interactions were predicted by MoDPeptInt, it seems likely that the interaction was not detectable in my experiments due to a lacking post-translational modification or required further determinants present in the full-length protein for high-affinity binding and/or correct spatial orientation of the protein. The SH3 motifs overlap with the first RNA recognition motif (RRM) of PABP, which together with its RRM 2 domain mediates the oligo(A) binding of PABP and is important for its interaction with eIF-4G for facilitating translation (Kühn & Pieler, 1996; Tarun et al., 1997). Therefore, direct binding with ITSNs might reduce translation initiation by preventing association with the poly(A) tail of mRNAs as well as by decreasing the eIF-4G interaction of PABP. But first of all, further experiments are necessary to confirm this proposed interaction, e.g. by a reverse IP or reverse PD with PABP-GST as bait, or by a direct binding assay. Next, the total levels of translation in cells with and without ITSNs should be compared e.g. by ribosome profiling or assays to monitor protein synthesis in cells, like SUnSET. However, this could prove difficult, as ITSNs might be involved in FMRP-dependent translation, which might confound the results.

3.2.3.2 Potential relevance of ITSN1´s interaction with FXR1 and its putative association with FMRP-positive granules

Since Vollweiter, 2021, noticed that the translation of many proteins present at reduced levels in the ITSN dKO is regulated by FMRP, I looked for FMRP and known interactors of FMRP

(based on Pasciuto & Bagni, 2014) in the ITSN interactome MS datasets. Though not many of them were present in both datasets, a total of 18 proteins were identified, which showed a strong network connectivity in STRING (Figure 23C). In addition to DDX5 and PABP, I could confirm ITSN1´s interaction with another member of this network, FXR1. This interaction is mostly mediated by the ITSN1-L isoform, while no interaction with FMRP itself could be detected experimentally or in the MS dataset. Intriguingly, both, FMRP and FXR1, belong to the Fragile X-related RNA-binding proteins (FXRs), along with a third family member FXR2. Their sequences share a high degree of homology, and the proteins are known to form hetero-multimers (Méndez-Albelo et al., 2024). While all of them associate with polyribosomes and messenger RNPs (mRNP), their precise effect on mRNA translation or synaptic plasticity can differ, depending on which FXR is within the RNP granule (Chyung et al., 2018; Cook et al., 2014). In the forebrain FXR-positive granules mostly consist of all three family members, FMRP, FXR1 and FXR2 (Chyung et al., 2018). This fits my observation of ITSN1 occasionally colocalizing with FMRP in HeLa cells (Figure 25D) and suggests recruitment of a subpool of ITSNs to FMRP-positive structures such as FMRP-positive granules.

Before exploring potential implications of an involvement of ITSNs in FMRP-positive granules, a closer look at FXR1 and its association with ITSNs is necessary. A direct comparison between FXR1 KO and ITSN dKO mice, especially behaviorally, is difficult as the constitutive loss of *FXR1* results in perinatal death (Mientjes et al., 2004). Therefore, most studies investigate postnatal or cell type-specific KO mouse models. Interestingly, a postnatal forebrain-specific KO of *FXR1* exhibited a reduced spine density, similar to the ITSN dKO mice (Cook et al., 2014). Also, parvalbumin-positive interneurons lacking FXR1 exhibited an increased half-width of the action potential and hyperactivity (M. Shen et al., 2021), reminiscent of ITSN dKO mice (Vollweiter, 2021). Though for FXR1 KO mice, the increase in half-width is related to a reduction in the protein level of a Ca^{2+}- channel, due to FXR1 regulating its translation. In the case of ITSN dKO mice, a similar phenotype of presynaptic hyperactivity is likely caused by reduced levels of Kv1.2 potassium channels. This might hint at different mRNA targets based on the composition of RNP granules as ITSN1 can bind mRNA and therefore might influence which RNA is captured in the granules. This would fit with the hypothesis that different neuronal RNA-binding proteins like ITSN1 or FXR1 might act in a cell type-specific manner and recruit different mRNAs for translational regulation

(Chyung et al., 2018; M. Shen et al., 2021). While the RNA-binding site within the ITSN1 SH3D domain is unknown up to now, for the protein Kin17 it has been shown that tandem SH3-like subdomains bind ribonucleotide homopolymers, like poly(A) or poly(U) (Pinon-Lataillade et al., 2004). If ITSNs SH3D domain binds the same mRNA motif, this would differ from FXR1 which recognizes AU-rich elements (Méndez-Albelo et al., 2024) supporting the notion that both recruit different mRNAs.

Intriguingly, the newly identified ITSN1 interactor FXR1 has recently been associated with actin regulation (X. Chen et al., 2024; St. Paul et al., 2023). It interacts with cytoskeleton-associated proteins, like Arp2, Rac1 and Cdc42 in muscle cells, together with other components of FMRP-positive granules, like CYFIP1 (St. Paul et al., 2023). Indeed, the loss of FXR1 results in decreased expression and activity of Cdc42 (St. Paul et al., 2023). The authors mostly discuss Rac1-dependent cytoskeletal modification through CYFIP1, while Cdc42 function remains unclear. The reduction of Cdc42 is based on reduced mRNA levels, while the cause for the reduced Cdc42 activity is unknown. Here, FXR1 might be able to recruit ITSN-L for Cdc42 activation. This FXR1-RNP complex is described in smooth muscle cells (St. Paul et al., 2023), but might be conserved in skeletal muscles. As loss of FXR1 results in reduced contractility (St. Paul et al., 2023), the ITSN1 interaction with FXR1 provides an alternative mechanisms potentially explaining impaired motor coordination in ITSN dKO mice. Further strengthening FXR1s association with actin, a newly identified FXR1 network is hypothesized to regulate actomyosin remodeling (X. Chen et al., 2024), which could include ITSN1.

FXR1 and FMRP both are thought to occur in the same FXR-positive RNP granules (Chyung et al., 2018) raising the questions if there are similarities between ITSN and FMRP KO mice. And indeed, FMR1 KO mice display a similar behavioral phenotype as ITSN dKO mice. FMR1 KO mice exhibit hyperactivity (Pietropaolo et al., 2011; Spencer et al., 2005) and repetitive behaviors like ITSN dKO mice (Pietropaolo et al., 2011; Veeraragavan et al., 2012). Nevertheless, there are clear differences regarding the specific repetitive behaviors executed since FMRP KO mice exhibit excessive self-grooming (Pietropaolo et al., 2011) and marble burying (Veeraragavan et al., 2012), while ITSN dKO mice display repetitive jumping and do not bury marbles (Vollweiter et al., 2023). Also while FMR1 KO mice exhibit an increase in immature spines (Galvez & Greenough, 2005), ITSN dKO show a decrease in spine density (Vollweiter et al., 2023). Nevertheless, the overlapping phenotypes of ITSN dKO, FMRP KO

and FXR1 KO mice support the idea of a shared signaling axis, likely based on ITSN and/or FXR1 modulating FMRP-dependent translation, although there may be FMRP-independent effects as well.

Determining the precise function of ITSNs in FMRP-dependent processes is difficult, especially with a presumed indirect involvement via DDX5, PABP and FXR1, or via NDHII and Cdc42, which were also identified in FMRP-positive transport granules (Kanai et al., 2004; Villacé et al., 2004). The function of FMRP can be divided into a nuclear function, translational regulation, transport of mRNA granules and local translation associated with cytoskeletal rearrangement at the synapse (Pasciuto & Bagni, 2014). However, these processes are intertwined, especially the general translation regulation, transportation of mRNA and local translation, as nearly all of them are based on mRNP granule formation and the translational machinery with overlapping interaction networks (Pasciuto & Bagni, 2014). As DDX5, PABP and FXR1 are involved in mRNP granules and/or translation (FXR1 in both, DDX5 in mRNP granules and PABP in translation) (Pasciuto & Bagni, 2014), it is difficult to postulate concrete roles for ITSNs. A differentiation between the processes is further complicated by different studies identifying diverse compositions of e.g. mRNP granules during transportation (Kanai et al., 2004; Villacé et al., 2004). Nevertheless, the ITSN dKO results in decreased protein levels, therefore the translation of the affected proteins should be reduced. As loss of FMRP is generally associated with an increase in protein synthesis (Méndez-Albelo et al., 2024), the reduced protein levels observed in the ITSN dKO would hint at an increase in FMRP dependent translational inhibition. Yet, in that case other proteins associated with FMRP-dependent translation regulation may be increased, which is not the case in ITSN dKO mice (Figure 24). Even though a contribution of ITSNs to functions involving FMRP-positive mRNP granules seems likely, this idea remains to be experimentally verified, similar to a possible role for ITSN in the regulation of translation initiation as described in a previous subchapter (3.2.3.1).

Furthermore, ITSNs′ scaffold nature favors its recruitment to protein complexes, based on liquid-liquid phase separation, causing droplet-like accumulations of proteins with multivalent interactions with low to medium binding affinities (Day et al., 2021). Interestingly, phase separation is hypothesized to support clathrin-coated vesicle formation (Day et al., 2021), a process known to involve ITSNs. Similarly, RNP granules are thought to assemble

based on phase separation influencing protein solubility, among others in proximity to the synaptic vesicle pool and in the periactive zone (Sasaki, 2020). There, ITSNs have been shown to interact with synapsin, (Gerth et al., 2017), which is able to condense into liquid droplets as well (Sasaki, 2020). The synapsin phase is thought to affect the formation and dispersion of the FMRP-positive RNP phase (Sasaki, 2020). Here, ITSNs could act as intermediates. As ITSNs could be part of both phases, they might act as sort of switch, promoting phase separation for one or the other population. This may be controlled by the intradomain switch which regulates ITSN1-synapsin interaction (Gerth et al., 2017). Other interactions of ITSNs, e.g. with SAM68, also affect protein solubility, thereby regulating protein function (Pankivskyi et al., 2021). Especially their interactions with SAM68 and the newly identified interactors here, as well as RNA itself, make ITSNs fitting components of RNPs and/or FMRP-positive granules (Pankivskyi et al., 2021).

Besides, RNPs or RNP granules are often associated with membranous structures, like the lysosome or endosome (Cioni et al., 2019; Liao et al., 2019). Locations associated with endocytosis and at which ITSNs have been found (Gryaznova et al., 2018). Similarly, mRNPs can be bound to transmembrane receptors and released upon receptor endocytosis to activate local protein translation (Koppers et al., 2019). ITSNs could link these processes by binding RNA as well as the endocytic machinery. These processes mostly involve FMRP, nevertheless, even without binding FMRP directly, ITSNs could connect these processes themselves or in tandem with FXR1, DDX5 or PABP.

3.2.3.3 How ITSNs may be involved in mRNA stability

While previous paragraphs discussed the possibility of ITSN-dependent translational regulation and ITSN-containing RNP granules as possible mechanisms to regulate Kv channel translation, ITSNs may not be involved in translation itself, but in mRNA stability. All three interaction partners identified in this study, DDX5, PABP and FXR1 are related to this process, though through different mechanisms. PABP can bind the poly(A)-tail of mRNAs which is thought to prevent access to exonucleases, enzymes degrading nucleic acids (Passmore & Coller, 2023). However, if ITSNs interact with PABPs through the identified SH3-binding sites, this likely would reduce PABP's association with mRNAs rather than resulting in a decrease of mRNA. Therefore, this would result in a stabilization of mRNAs in the ITSN dKO model, contradicting the observed phenotype. As DDX5 is highly involved in mRNA metabolism,

there are several possible pathways for mRNA stabilization. It has been shown to interact with the m6A methyltransferase METTL3, supporting m6A modification, a common modification supporting RNA stability. This modification occurs in the nucleus, where DDX5 and ITSN1 could interact, though this remains to be verified (Shi et al., 2024). In addition, the regulation of the previously mentioned nonsense-mediated mRNA decay by DDX5 and PABP impacts mRNA prevalence (Geißler et al., 2013). For FXR1, it has been shown to improve mRNA stability by direct interaction as well as by interacting with the pre-mRNA 3′ end processing cleavage factors (Méndez-Albelo et al., 2024). In neurons, FXR1 is known to stabilize Ca^{2+} channel mRNA (M. Shen et al., 2021) by interacting with microRNAs which can regulate mRNA stability themselves (Méndez-Albelo et al., 2024). As scaffolding protein, ITSNs might support FXR1´s association with cleavage factors or the nonsense-mediated mRNA decay machinery by facilitating complex assembly. Therefore, loss of ITSNs could result in a reduced mRNA stability, based on its FXR1 or DDX5 interaction, resulting in decreased protein levels at the pre- and postsynapse. Also, direct interaction of ITSNs with mRNA could impact RNA stability. However, these functions need further verification, e.g. by comparing mRNA stability in the ITSN2 KO and ITSN dKO cells.

Overall, the newly identified ITSN1 interactors DDX5, PABP and FXR1 suggest further functions of the ITSNs in translational regulation that go beyond previously described nuclear functions and mRNA interactions (Pankivskyi et al., 2021; Wong et al., 2012; H. Zhang et al., 2021). While further research is necessary to determine the precise functions and mechanisms, ITSNs may impact mRNA stability or translation via several pathways mediated by PABP, DDX5 and FXR1. As a subpool of ITSNs colocalize with FMRP and interacts with several proteins of FMRP-positive granules, ITSNs might be a negative regulator of FMRP-dependent translational inhibition. This would fit with the observed synaptic phenotype of ITSN dKO mice. However, a functional validation of this hypothesis is necessary.

3.3 Relative impact of ITSN1 versus ITSN2 loss

As the ITSN dKO mouse line exhibits health deficits like seizures and premature death, we hoped to reduce the breeding of this line by replacing upcoming cell culture-based experiments like Ca^{2+}-imaging with cells of an inducible ITSN dKO line. The mouse line available enabled us to induce the loss of ITSN2 on a constitutive ITSN1 KO background,

resulting in a comparison of ITSN dKO vs ITSN1 KO, while for previous experiments the constitutive ITSN dKO was compared to a ITSN2 KO background. In general, a comparison to a WT would be preferred, though with breeding schemes enabling this, the likelihood of matched ITSN dKO and ITSN WT would be extremely low. Even the current breeding for the constitutive dKO line yields only ~16% dKO and ~25% ITSN2 KO mice (Gerth et al., 2017), limiting the ability to obtain matched littermates for experiments.

Interestingly, a comparison between synaptic protein levels for the inducible dKO did not result in the same reduced protein levels as with the synaptic membrane fraction of the constitutive dKO (Figure 28). This might be caused by two different reasons, either discrepancies in the methodology used or the different genetic background of the control group. While the methodology might play a role to a certain degree, since discrepancies were also observed between synaptic actin and synaptic membrane associated actin (Figure 21) which was discussed in chapter 3.2.2, the genetic background could still account for the trend in protein reduction for endocytic proteins like Munc18, AP2 and Snap25. Those changes were not observed for endocytic protein levels of the constitutive dKO and ITSN2 KO (Gerth et al., 2017). As ITSN1-L is the predominant version of ITSNs in neurons (Tsyba et al., 2011), ITSN1 loss potentially has a stronger or different effect on cellular processes than ITSN2 loss. For a more comprehensive understanding of the background-dependent effects, the breeding scheme was adjusted and the induced dKO mice compared to ITSN1 het / ITSN2 WT mice. With the current breeding, the chances of an inducible dKO or a control are 25% each. A comparison to a ITSN WT would have been preferred but would have decreased the chances for the inducible KO and WT control within a litter even further. Though only two replicates with the adjusted breeding are available up to now, a trend for reduced protein levels of NR2A and actin is observable (Figure 29), similar to the results in the constitutive dKO. Similarly, Kv1.2 and Kvβ2 may be reduced, although for a definite conclusion, the experiment needs to be repeated several times as the measured protein levels vary largely. Analogously, protein levels for Munc18 may be reduced, though again, further experiments are needed. Therefore, the comparison of the induced dKO to a close to WT condition may more closely resemble the comparison between dKO and ITSN2 KO. This might indicate specific functions of ITSN1 vs ITSN2 and greater importance of one of the two within distinct processes in the brain. Indeed, although both proteins exhibit a very similar protein structure, it has been shown that ITSN2

can be differently phosphorylated (Novokhatska et al., 2013) which may result in the different functions in neurons. In line with this, only ITSN1 but not ITSN2 is linked to Down syndrome or Alzheimer's disease (Hunter et al., 2011), and only mutations in ITSN1 have been linked to neurodevelopmental disorders so far (Bruel et al., 2022).

In summary, the genetic background of the control group can influence experimental outcomes and therefore should be carefully considered while designing experiments. While a comparison of synaptic protein levels of ITSN dKO mice to ITSN1 KO mice versus to ITSN2 KO mice resulted in the detection of different alterations in protein levels, the comparison to a close to WT condition recollects both phenotypes. Therefore, the comparisons between ITSN2 KO and ITSN dKO, as performed for most experiments, rather give insight into ITSN1 specific function than ITSN2.

3.4 Conclusion

Several alterations were observed in ITSN dKO mice ranging from progressive motor decline (unpublished data from Tanja Maritzen) to reduced levels of synaptic proteins, including Kv-channels, reflected in prolonged Ca^{2+}-influx in ITSN dKO neurons (Vollweiter, 2021). Several mechanisms on how ITSN loss could result in this phenotype were discussed, raising the question which one is most likely.

For the progressive motor decline no morphological alterations have been found at the NMJ or of the myofiber appearance. This suggests progressive impairments of the central nervous system, likely the striatum or cerebellum, as likely causes. Still, autophagy and FXTAS-related alterations as well as impaired muscular contractility are possible explanations, as further experiments are needed to narrow down the source.

Regarding the synaptic protein levels, for the scaffolding hypothesis no direct interaction between ITSN1 and Kv1.2 or Kvβ2 could be identified. However, CTTN is a promising candidate for indirect stabilization, which might also support the hypothesis of an actin anchorage since CTTN is an actin-binding protein. As several other Kv channels are linked to the actin cytoskeleton or even regulate actin polymerization themselves (Delgado-Ramírez & Rodríguez-Menchaca, 2019; Hattan et al., 2002; Williams et al., 2007; Y. Zhang et al., 2016), reduced actin anchorage remains another possibility for reduced Kv1.2 channel subtypes at the synapse. Yet, as different alterations in actin levels were identified in different synaptic

compartments, a further verification of reduced membrane-associated actin at ITSN dKO synapses is necessary. However, while mechanisms like Kv channel stabilization by ITSNs via CTTN and/or via anchoring to the actin cytoskeleton could account for reduced protein levels of Kv channels in ITSN dKO mice, it remains unclear how they could account for the progressive phenotype of older ITSN dKO mice.

One of the proposed mechanisms appears especially attractive as it might account for the reduced protein levels as well as for the progressive motor deficits. This is an involvement of ITSNs with RNPs. The report of ITSNs´ interaction with SAM68 was the first description of ITSNs as RNP components or RNP effectors (Pankivskyi et al., 2021). Building on this, my discovery of the interaction of ITSNs with FXR1, DDX5 and PABP strongly links ITSNs to RNPs, especially to FMRP-positive RNP granules, as ITSNs partially colocalize with FMRP. Additionally, the dysfunction of FMRP-positive RNP granules observed in Jakmip1 KO mice (Berg et al., 2015) causes a phenotype which is strikingly similar to the one of ITSN dKO mice. Further phenotypic similarities between ITSN dKO and FMRP or FXR1 KO mice support the idea of their participation in shared pathways. In addition, ITSNs could provide a plausible link regulating RNP or FMRP-granule localization to endosomes, lysosomes or the periactive zone/ synaptic vesicle phase (Cioni et al., 2019; Liao et al., 2019; Sasaki, 2020), an idea which is supported by their RNA binding, endocytic and scaffolding functions. The transition from a regulatory role in mRNA stability, to RNP granule function or local translation is dynamic (Koppers et al., 2019; Pankivskyi et al., 2021) as these processes are closely linked. Therefore, it is hard to speculate what exactly ITSNs´ role(s) might be. Nevertheless, those processes could account for the reduced protein levels not only at the presynapse, possibly enhancing the postsynaptic phenotype as well. In parallel, without ITSNs SAM68 might be progressively sequestered along with loss of DGCR8 and drosha activity, decreasing their normal functions (Sellier et al., 2013). This could be enhanced further by an altered affinity of DDX5 for DGCR8 and drosha, resulting in decreased levels of FMRP and progressive ataxia-related symptoms like in FXTAS, including the decreased activity and impaired motor coordination of 1 year old ITSN dKO mice. Furthermore, FXR1 function has been linked to muscle contractility (St. Paul et al., 2023), which could be another mechanism through which ITSN loss could affect muscle function.

In summary, I propose the interactions with RNPs as possible cause for the presynaptic protein alterations. It could account for this phenotype either by providing a novel role for ITSN1 in translation and mRNA stability, or by stabilizing Kv channels through indirect scaffolding, as FXRs interact with Kv1.2 and Kvβ2. Intriguingly, RNP interactions, e.g. with FXR1 or SAM68, could account for the progressive motor decline as well.

4 Material

4.1 Chemicals & reagents

Commercially available chemicals, reagents, media and solutions used in this study can be found in Table 1.

Table 1: Chemicals and reagents used.

Chemical	Manufacturer
1,4-Dithiothreitol (DTT)	Carl Roth GmbH + Co. KG, Karlsruhe, Germany
1,4-Piperazine diethanesulfonic acid (PIPES)	Carl Roth GmbH + Co. KG, Karlsruhe, Germany
1-β-D-Arabinofuranosyl-cytosine-hydrochloride (Ara-C)	Sigma-Aldrich, St. Louis, MO, USA
4-(2-Hydroxyethyl)-piperazine-1-ethansulfic acid (Hepes)	Carl Roth GmbH + Co. KG, Karlsruhe, Germany
5xGC buffer	Thermo Fisher Scientific, Waltham, MA, USA
Acetic acid	Carl Roth GmbH + Co. KG, Karlsruhe, Germany
Acrylamide Mix 30%, ROTIPHORESE®	Carl Roth GmbH + Co. KG, Karlsruhe, Germany
Adenosine-5'-triphosphate disodium salt hydrate (ATP)	Sigma-Aldrich, St. Louis, MO, USA
Agarose	Biozym Scientific GmbH
Ammonium peroxodisulfate (APS)	Carl Roth GmbH + Co. KG, Karlsruhe, Germany
B27 supplement, 50x	Thermo Fisher Scientific, Waltham, MA, USA
Bovine Serum Albumin (BSA), Fraction V	Biomol, Hamburg, Germany
Bromophenol Blue sodium salt	Sigma-Aldrich, St. Louis, MO, USA
Buffer B	Bio & Sell, Feucht, Germany&Sell GmbH
c0mplete® Protease inhibitor tablet, Mini, EDTA-free	Roche, Basel, Switzerland
$CaCl_2$	Carl Roth GmbH + Co. KG, Karlsruhe, Germany
CHAPS, 98%, PUFFERAN®	Carl Roth GmbH + Co. KG, Karlsruhe, Germany
Chrom(III)-Potassiumsulfate-Dodecahydrate	Carl Roth GmbH + Co. KG, Karlsruhe, Germany
Coomassie® Brilliant G-250	Sigma-Aldrich, St. Louis, MO, USA
DAPI 98% (4',6-Diamidino-2-phenylindol)	Carl Roth GmbH + Co. KG, Karlsruhe, Germany
Desoxyribonuclease (DNase) I, from bovine pancreas, Type IV	Sigma-Aldrich, St. Louis, MO, USA
D-Glucose monohydrate	Carl Roth GmbH + Co. KG, Karlsruhe, Germany
Disodiumhydrogenphosphate-dihydrate 99% (Na_2HPO_4 x $2H_2O$)	Carl Roth GmbH + Co. KG, Karlsruhe, Germany
dNTPs	Bio & Sell, Feucht, Germany&Sell GmbH

Chemical	Manufacturer
Dulbecco's modified Eagle's medium (DMEM), high glucose	Sigma-Aldrich, St. Louis, MO, USA
Dulbecco's Phosphate Buffered Saline (DPBS)	Thermo Fisher Scientific, Waltham, MA, USA
Entellan ™	VWR International LLC, Radnor, PA, USA
Ethanol	Chemikalienausgabe RPTU, Kaiserslautern, Germany
Ethanol absolute	Carl Roth GmbH + Co. KG, Karlsruhe, Germany
Ethidium bromide, 1% solution	Carl Roth GmbH + Co. KG, Karlsruhe, Germany
Ethylene glycol bis-(2-aminoethyl ether) tetraacetic acid (EGTA)	Carl Roth GmbH + Co. KG, Karlsruhe, Germany
Ethylenediamine tetraacetic acid-Na_2-salt-$2H_2O$ (EDTA)	Serva, Heidelberg, Germany
FastDigest buffer, 10x	Thermo Fisher Scientific, Waltham, MA, USA
Fetal bovine serum (FBS)	Thermo Fisher Scientific, Waltham, MA, USA
Fetal bovine serum not inactivated	Thermo Fisher Scientific, Waltham, MA, USA
Ficoll® 400	Sigma-Aldrich, St. Louis, MO, USA
FM4-64 membrane dye	Interchime, Montlucon, France
Gelatin, from porcine skin gel strength 300, Type A	Sigma-Aldrich, St. Louis, MO, USA
GeneRuler™ DNA ladder mix	Thermo Fisher Scientific, Waltham, MA, USA
Glycerol	Sigma-Aldrich, St. Louis, MO, USA
Glycine	Carl Roth GmbH + Co. KG, Karlsruhe, Germany
Guanidine hydrochloride	Gift from AG Schroda
Hanks' Balanced Salt Solution (HBSS)	Thermo Fisher Scientific, Waltham, MA, USA
Hydrochloric acid (HCl), 37%	Carl Roth GmbH + Co. KG, Karlsruhe, Germany
IGEPAL® CA-630 NP40	Sigma-Aldrich, St. Louis, MO, USA
Immu-Mount TM	New Erie Scientific LLC; epredia , NH, USA
Insulin, human recombinant	Sigma-Aldrich, St. Louis, MO, USA
Isopentane (2-Methylbutane)	Sigma-Aldrich, St. Louis, MO, USA
Isopropyl-ß-D-thiogalactopyranosid (IPTG)	Carl Roth GmbH + Co. KG, Karlsruhe, Germany
JetPRIME® buffer	Polyplus, Illkirch, France
JetPRIME® transfection reagent	Polyplus, Illkirch, France
L-glutamine, GlutaMAX™-(100X)	Thermo Fisher Scientific, Waltham, MA, USA
LI-COR Intercept® blocking buffer	LI-COR Biosciences, Lincoln, NE, USA
Luria broth (LB)	Carl Roth GmbH + Co. KG, Karlsruhe, Germany
Magnesium chloride ($MgCl_2$)	Carl Roth GmbH + Co. KG, Karlsruhe, Germany
Magnesium sulfate heptahydrate ($MgSO_4$)	Carl Roth GmbH + Co. KG, Karlsruhe, Germany
$MgCl_2$ 25 mM	Bio & Sell, Feucht, Germany&Sell GmbH

Chemical	Manufacturer
Minium Essential Medium (MEM), with Earle's Salts, without L-Glutamine or Phenol red	Thermo Fisher Scientific, Waltham, MA, USA
N,N,N,N-Tetramethylethylendiamin (TEMED)	Carl Roth GmbH + Co. KG, Karlsruhe, Germany
Normal goat serum	Thermo Fisher Scientific, Waltham, MA, USA
Nuclease free water, DEPC treated, sterile, nuclease-fre	Carl Roth GmbH + Co. KG, Karlsruhe, Germany
OCT Embedding Matrix CellPath ready-to-use	Carl Roth GmbH + Co. KG, Karlsruhe, Germany
Orange Dye	Sigma-Aldrich, St. Louis, MO, USA
PageRuler™ Pre-stained protein ladder	Thermo Fisher Scientific, Waltham, MA, USA
Paraformaldehyde (PFA)	Carl Roth GmbH + Co. KG, Karlsruhe, Germany
Penicillin-Streptomycin (Pen/Strep), 10.000 U/ml	Thermo Fisher Scientific, Waltham, MA, USA
Phenylmethylsulfonylfluoride (PMSF)	Carl Roth GmbH + Co. KG, Karlsruhe, Germany
Phusion™ High-Fidelity DNA Polymerase	Thermo Fisher Scientific, Waltham, MA, USA
Pierce® Glutathione agarose beads	Thermo Fisher Scientific, Waltham, MA, USA
Pierce® Protein A/G magnetic beads	Thermo Fisher Scientific, Waltham, MA, USA
Poly-L-Lysine	Sigma-Aldrich, St. Louis, MO, USA
Ponceau S, for histology and electrophoreses	Carl Roth GmbH + Co. KG, Karlsruhe, Germany
Potassium chloride 99.5% (KCl)	Carl Roth GmbH + Co. KG, Karlsruhe, Germany
Potassium dihydrogen phosphate (KH_2PO_4)	VWR International LLC, Radnor, PA, USA
Protease inhibitor complex (PIC)	Sigma-Aldrich, St. Louis, MO, USA
Restriction enzymes, FastDigest	Thermo Fisher Scientific, Waltham, MA, USA
Sodium acetate	Sigma-Aldrich, St. Louis, MO, USA
Sodium bicarbonate $NaHCO_3$	Carl Roth GmbH + Co. KG, Karlsruhe, Germany
Sodium chloride 99.5% (NaCl)	Sigma-Aldrich, St. Louis, MO, USA
Sodium dihydrogen phosphate bihydrate (NaH_2PO_4)	Carl Roth GmbH + Co. KG, Karlsruhe, Germany
Sodium dodecyl sulfate (SDS)	Sigma-Aldrich, St. Louis, MO, USA
Sodium fluoride (NaF)	Sigma-Aldrich, St. Louis, MO, USA
Sucrose	Carl Roth GmbH + Co. KG, Karlsruhe, Germany
T4 Ligase	Thermo Fisher Scientific, Waltham, MA, USA
T4 ligase buffer, 10x	Thermo Fisher Scientific, Waltham, MA, USA
Taq Polymerase (5 U/µl)	Bio & Sell, Feucht, Germany&Sell GmbH
Transferrin, Holo, Bovine Plasma	Merck, Darmstadt, Germany
Tris	Carl Roth GmbH + Co. KG, Karlsruhe, Germany
Tris-hydrochloride (Tris-HCl)	Carl Roth GmbH + Co. KG, Karlsruhe, Germany

Chemical	Manufacturer
Triton X-100	Sigma-Aldrich, St. Louis, MO, USA
Trypan blue solution, 0.4%	Carl Roth GmbH + Co. KG, Karlsruhe, Germany
TrypLE™ Express, with Phenol Red	Thermo Fisher Scientific, Waltham, MA, USA
Trypsin, from bovine pancreas, Type XI, Lyophilized powder	Sigma-Aldrich, St. Louis, MO, USA
Tween®20	Sigma-Aldrich, St. Louis, MO, USA
Urea	Thermo Fisher Scientific, Waltham, MA, USA
Water, DEPC-treated	Carl Roth GmbH + Co. KG, Karlsruhe, Germany
Water, sterile	Carl Roth GmbH + Co. KG, Karlsruhe, Germany
Xylol	Chemikalienausgabe RPTU, Kaiserslautern, Germany
YT Medium, 2x	Carl Roth GmbH + Co. KG, Karlsruhe, Germany
β-Mercaptoethanol	Sigma-Aldrich, St. Louis, MO, USA

4.2 Buffers, solutions, media

Solutions prepared for this study are listed below. pH was adjusted with HCl or NaOH.

Table 2: Solutions used.

Solution	Composition
50% EtOH	400 ml EtOH 429.76 ml ddH_2O
70 % EtOH	400 ml EtOH 191 ml ddH_2O
90 % EtOH	400 ml EtOH 53 ml ddH_2O
Alkaline lysis buffer	25 mM NaOH 0.2 mM EDTA pH 12; stored at 4°C
Basic medium	5 g/l glucose 200 mg/l $NaHCO_3$ 100 mg/l Transferrin In MEM
Co-IP lysis buffer	50 mM Tris-HCl 100 mM NaCl 1% Triton-X Protease Inhibitor Tablet EDTA free
Coomassie destaining	10% acetic acid 20% Methanol
Coomassie staining	1 g/l Coomassie 10% Acetic acid 20% Methanol
Digestion solution	137 mM NaCl

Solution	Composition
	5mM KCl 7 mM Na_2PO_4 25 mM Hepes pH 7.2 filtered and stored at 4°C
Dissociation solution	12 mM $MgSO_4$ In HBSS Filtered and stored at 4°C
F Actin buffer	1.5 mM Guanidine Hydrochloride 1 mM Sodium acetate (CH3COONa) 1 mM $CaCl_2$ 1 mM ATP 20 mM Tris-HCl Adjusted to pH 7.5
FMR/FXR *E. coli* lysis buffer	25 mM Tris-HCl 300 mM KCl 1 mM EDTA 500 mM Urea 20% Glycerol 5% EtOH 0.5% NP40 1 mM PMSF
G Actin buffer	10 mM KH_2PO_4 100 mM NaF 50 mM Kcl 2 mM $MgCl_2$ 1 mM EGTA 0.2 mM DTT 0.5% TritonX 1 mM Sucrose Adjusted to pH 7
Gelatin-chorme alum solution	0.625 g gelatin 0.0625 g Chrom(III)-Potassiumsulfate-Dodecahydrate In 250 ml ddH2O, filtered
Growth medium	5% FBS not inactivated 1:400 GlutaMAX™ In basic medium Filtered and stored at 4°C
Laemmlie sample buffer	SDS Glycerol Tris-HCl Bromophenol Blue β-Mercaptoethanol
Lysis buffer	20 mM Hepes pH 7.4 50 mM KCl

Solution	Composition
	2 mM $MgCl_2$ 1% Triton X-100 1 mM PMSF c0mplete® Protease Inhibitor
Lysis buffer for transmembrane proteins	1% Chaps 100 mM KCl 2 mM $MgCl_2$ 20 mM Hepes 1 mM NaF c0mplete® Protease Inhibitor
Neutralization buffer	40 mM Tris-HCl 0.2 mM EDTA pH 5; stored at 4°C
PBS 1x	10 % PBS 10x In ddH_2O
PCR reaction mix for PCR based cloning	10 µl 5x GC buffer 20 µM dNTPs 0.5 µM forward primer 0,5 µM reverse primer 50 ng template DNA 0.02 U/µl Phusion™ Polymerase
PEM fixation buffer	80 mM PIPES 5 mM EGTA 2 mM $MgCl_2$ 4% PFA pH 6.8
Phosphate-buffered saline (PBS, pH 7.4) 10x	1.37 M NaCl 27 mM KCl 100 mM Na_2HPO_4 x $2H_2O$ 17.6 mM KH_2PO_4 In ddH_2O
Plating medium	10% FBS not inactivated 1% GlutaMAX™ 1:500 Insulin 1% Penicillin/streptomycin In basic medium Filtered and stored at 4°C
Poly-L-Lysin solution	5 ml Poly-L-Lysine 28 ml sterile H_2O
Ponceau stain	0.5% (w/V) Ponceau S 1% (V/V) Acetic Acid
Ripa lysis buffer, 2x	100 mM Tris-HCl (pH 7.4) 300 mM NaCl 2mM EDTA 0.2% SDS

Solution	Composition
	2% Triton-X 1% Sodium deoxycholate In ddH_2O
SDS Running buffer 10x	250 mM Tris 1.92 M Glycine 1% (w/V) SDS In ddH_2O
SDS Running buffer 1x	10% SDS Running buffer 10x In ddH_2O
Sodium phosphate buffer (PB, pH 7.4)	42.3 ml 1M NaH_2PO_4 57.7 ml 1M Na_2HPO_4 Add up to 1 l with ddH_2O
Sucrose buffer	0.32 M sucrose 5 mM Hepes pH 7.4
Supplemented DMEM	DMEM Pen/Strep 10% FBS
TAE buffer 50x	50 mM EDTA 2 M Tris 1 M acetic acid
TBS 1x	10 % TBS 10x In ddH_2O
TBST 1x	10 % TBS 10x 2 ml Tween® 20 In ddH_2O
Transfer buffer 10x	259 mM Tris 1.9 M glycine In ddH_2O
Transfer buffer 1x	10% Transfer Buffer 10% Methanol In ddH_2O
Triangularis sterni blocking solution	1% BSA 10% normal goat serum 0.5% Triton X-100 0.1 M sodium phosphate buffer
Tris-buffered saline (TBS) 10x	0.1 M Tris 0.7 M NaCl In ddH_2O
Washing solution I	20% FBS not inactivated 1% Penicillin/streptomycin In HBSS
Washing solution II	6.5 ml Penicillin/streptomycin In 500 ml HBSS

If not stated differently, 10x concentrated solutions were only used as stock solutions to prepare 1x concentrated solutions for use in experiments.

4.3 Kits

Table 3: Commercial Kits used for this study.

Kit	Producer
H&E quick dye kit	Carl Roth GmbH + Co. KG, Karlsruhe, Germany
Nucleobond plasmid midi kit	Machery-Nagel, Düren, Germany
Nucleospin gel and PCR cleanup kit	Machery-Nagel, Düren, Germany
Nucleospin plasmid mini kit	Machery-Nagel, Düren, Germany
Pierce ® BCA protein assay kit	Thermo Fisher Scientific, Waltham, MA, USA
Zymoclean™ Gel DNA recovery kit	Zymo Research, Irvine, Ca, USA

4.4 Consumables

Materials used to perform the experiments for this study can be found in Table 4.

Table 4: Consumables used.

Item	Model	Producer
Cell culture dishes	Standard, 60 + 100 mm	SARSTEDT, Nümbrecht, Germany
Cryotubes 2 ml	CryoPure	SARSTEDT, Nümbrecht, Germany
Gloves	StarGuard® protect	Starlab, Hamburg, Germany
Graduated glass pipettes	SILBERBRAND-ETERNA, 5 ml, 10 ml, 25 ml	Brand GmbH + Co. KG, Wertheim, Germany
Immersol™ 518 F	Microscopy immersion oil	Zeiss, Oberkochen, Germany
Kimtech precision wipes		Kimberly Clark, Irving, Texas, USA
Microscope cover glasses	Round, ø18 and 25 mm	Paul Marienfeld GmbH & Co.KG, Lauda-Königshofen, Germany
Microscopy cover glasses	24x60 mm	VWR International LLC, Radnor, PA, USA
Microscopy Slides	Ground 90° frosted	New Erie Scientific LLC; epredia, NH, USA
Needle	Sterican® G27	Braun, Melsungen, Germany
Nitrocellulose blotting membrane	Amersham©	Cytiva, Marlborough, MA, USA
Parafilm		Bemis Company Inc.; Sheboygan Falls, WI, USA

Item	Model	Producer
PCR Reaction tubes 0.2 ml	8er-SoftStripes	Biozym Scientific GmbH, Hessisch Oldendorf, Germany
Pipette Tips 10, 200, 1250 µl	SurPhob ◎	Biozym Scientific GmbH, Hessisch Oldendorf, Germany
Reaction tube 5 ml	Falcon©, Round-bottom, with or without cell strainer cap	Corning Inc, Corning, NY, USA
Reaction Tubes	DNA, DNA-, RNAse free 0.5 ml 1.5 ml 2 ml	Biozym Scientific GmbH, Hessisch Oldendorf, Germany
Reaction tubes 15 ml	Falcon© Sarstedt	Corning Inc, Corning, NY, USA SARSTEDT, Nümbrecht, Germany
Reaction tubes 50 ml	Falcon©	Corning Inc, Corning, NY, USA
Sorting chip	100 µm nozzle	Sony Biotechnology, San Jose, CA, USA
Syringe filters	0.2 µm	SARSTEDT, Nümbrecht, Germany
Syringes	1 ml 10 or 20 ml	Henke-Sass, Wolf GmbH, Tuttlingen, Germany
Weighting pans	8 ml, 100 ml, 330 ml	Carl Roth GmbH + Co. KG, Karlsruhe, Germany
Well plates	Costar® 12 + 6 well	Corning Inc, Corning, NY, USA
Whatman® Paper		Carl Roth GmbH + Co. KG, Karlsruhe, Germany

4.5 List of antibodies and fluorescent reagents

For IF, primary and secondary antibodies were diluted in blocking buffer. For immunoblotting, primary antibodies were diluted in 1:1 *LI-COR Intercept® Blocking Buffer* and TBST while secondary antibodies were diluted in TBST.

Table 5: List of used primary antibodies and fluorescent reagents. "m" stands for mouse and "rb" for rabbit.

Antigen/ reagent	Species	Dilution	ID	Provider	Used for
Ago2	m	1:500	ab57113	Abcam, Cambridge, UK	WB

Antigen/ reagent	Species	Dilution	ID	Provider	Used for
AP2	M	1:1000	610502	BD Transduction Laboratories, Franklin Lakes, NJ, USA	WB
Bungarotoxin-AlexaFluor 594		1:400		Kindly provided by AG Kins, ThermoFisher, Karlsruhe, Germany	IHC
CYFIP2	rb	1:500	PA5-50388	Thermo Fisher Scientific, Waltham, MA, USA	WB
DDX5	m	1:1000 3 µg	sc-166167	Santa Cruz Biotechnology, Dallas, TX, USA	WB IP
Dynamin 1	rb	1:100		D. Grabs/Camilli	WB **Figure 15**B
Dynamin 1,2,3	m	1:1000	115 002	Synaptic Systems, Göttingen, Germany	WB
eIF-4E	m	1:500	610270	BD Transduction Laboratories, Franklin Lakes, NJ, USA	WB
GluA1	m	1:1000	MAB2263	Merck, Darmstadt, Germany	WB
HSP70	m	1:2000	MA3006	Thermo Fisher Scientific, Waltham, MA, USA	WB
IgG Isotype control	m	3 µg	31903	Thermo Fischer Scientific	IP
ITSN1	m	1:200	SC-136242	Santa Cruz Biotechnology, Dallas, TX, USA	WB
ITSN1 1-440	rb	3 µg	Homemade	FMP Berlin in 2013	IP
ITSN1 SH3A-C	rb	1:600	Homemade	FMP Berlin ID: 7.8.20	WB Figure 26
Jakmip1	rb	1:2000	13846-1-AP	Proteintech, Rosemont, IL, USA	WB
Kv1.2	m	1:500 3 µg	75-008	NeuroMab, UC Davis, CA, USA	WB IP
Kvβ2	m	1:500	MABN652	Sigma-Aldrich, St. Louis, MO, USA	WB
Munc18	rb	1:1000	116002	Synaptic Systems, Göttingen, Germany	WB
PABP	rb	1:200	ab21060	Abcam, Cambridge, UK	WB

Antigen/ reagent	Species	Dilution	ID	Provider	Used for
Phalloidin STAR RED		1:100	STRED-0100-20UG	Abberior, Göttingen, Germany	IF
Snap25	m	1:250	111011	Synaptic Systems, Göttingen, Germany	WB
Synaptophysin	rb	1:400 1:500	Homemade	Reinhard Jahn	IHC WB
Syntaxin	m	1:500	110111	Synaptic Systems, Göttingen, Germany	WB
β-Actin	m	1:4000	A5441-2ML	Sigma-Aldrich, St. Louis, MO, USA	WB
β-Tubulin	rb	1:4000	302302	Synaptic Systems, Göttingen, Germany	WB

Table 6: List of used secondary antibodies.

Antigen	Species	Dilution	ID	Provider	Used for
IRDye© 680RD anti-mouse	goat	1:10000	926-68070	LI-COR Biosciences, Lincoln, NE, USA	WB
IRDye© 680RD anti-rabbit	goat	1:10000	926-68071	LI-COR Biosciences, Lincoln, NE, USA	WB
IRDye© 800CW anti-mouse	goat	1:10000	926-32210	LI-COR Biosciences, Lincoln, NE, USA	WB
IRDye© 800CW anti-rabbit	goat	1:10000	926-68071	LI-COR Biosciences, Lincoln, NE, USA	WB
α-guinea pig Alexa Fluor 488	goat	1:400	A21450	Thermo Fisher Scientific, Waltham, MA, USA	IF
α-mouse AlexaFluor 568	goat	1:400	A11001	Thermo Fisher Scientific, Waltham, MA, USA	IF
α-mouse AlexaFluor 647	goat	1:400	A21235	Thermo Fisher Scientific, Waltham, MA, USA	IF
α-rabbit AlexaFluor 647	goat	1:400	A31573	Thermo Fisher Scientific, Waltham, MA, USA	IHC

4.6 Plasmids

Table 7: Plasmids used for transfections.

Construct	Species	Backbone	Tag	Origin
CTTN-mCherry	Mouse	pmCherry-N1	mCherry	Gift by Scott A. Weed
FMRP-GFP	Mouse	pEGFP-C1	EGFP	Addgene #87929
FXR1-GFP	Mouse	pAAV	mEGFP	Addgene #112732

Construct	Species	Backbone	Tag	Origin
ITSN1 FL WT in pEGFP-C2	Human	pEGFP-C2	EGFP	Cloned by Marielle Gruenig, FMP Berlin
Kv1.2 WT pEGFP-C1	Rat	pEGFP-C1	EGFP	Gift by Anthony D. Morielli
Kvβ2	Mouse	pcDNA3		Gift by Anthony D. Morielli
pGex4T-1		pGex4T-1	GST	Gift by Volker Haucke

Oligonucleotides

Different oligonucleotides from Table 8 and Table 9 were utilized for genotyping and PCR based cloning.

Table 8: Primers used for genotyping of genetically modified mice.

Name	Used for	Sequence (5′-3′)
TM218	ITSN1, forward	gtagagctctaaactgcaccttag
TM219	ITSN1, forward	ctggtatgtatcgatcaccatcca
TM220	ITSN1, reverse	gtgacaacagtcaacacagcattg
TM227	ITSN2 WT, forward	gttaactgagtagatgactggaaagcc
TM227	ITSN2 KO, forward	gcccgtacttttttcctacagtcag
TM228	ITSN2 WT, reverse	gtaatagcccacatatttggccctc
TM230	ITSN2 KO, reverse	ggaatttgaaatttttgtcaagttagacag
TM63	Cre, forward	ccgggctgccacgaccaa
TM64	Cre, reverse	ggcgcggcaacaccatttttt

Genotyping primers were designed by Tanja Maritzen.

Table 9: Primers designed for PCR-based cloning.

Cloning	Sequence (5′-3′)
CTTN	forward: ataagaggatccaagatgtggaaagcttctgcagg reverse: ggcgacgcggccgcctactgccgcagctccacata
FMRP	forward: ataagagaattcgagatggagctggtggtggaag reverse: gccgacgtcgacttagggtactccattcaccagc
FXR1	forward: ataagaggatccaatagtgctggtggtgcgga reverse: gccgaccgaattcttatgaaacaccattcaggac
Kv1.2 C-Term	forward: agaattcttcaactacttctaccaccg reverse: agtcgactttcaatcagacatcagtta
Kv1.2 N-Term	forward: aaagaattcatcatgacagtggct reverse: tttctcgagttacctggccggccc
Kvβ2	forward: agaattcatgtatccggaatcaac reverse: agtcgacttaggatctatagtccttttgc

All primers purchased from Sigma-Aldrich, St. Louis, MO, USA

4.7 Mouse lines

Experiments were performed on male and female C57BL/6N wildtype (WT) mice, constitutive ITSN1/2 double knock-out (dKO) mice or CAG Cre-based inducible ITSN2 KO mice on an ITSN1 KO background (*mus musculus*). The constitutive ITSN dKO animals were generated by crossing ITSN1 het / ITSN2 KO mice. The generation of this mouse line is described in (Gerth et al., 2017). As ITSN2 KO mice did not show any impairments or alterations (Gerth et al., 2017), to adhere to the 3R guidelines and reduce the number of animals, the ITSN2 KO mice were used as control condition. For the inducible KO line ITSN1 $^{-/-}$ / ITSN2 $^{lox/lox}$ / CAG Cre $^{-}$ mice were bred with ITSN1 $^{-/-}$ / ITSN2 $^{lox/lox}$ / CAG Cre $^{+}$ mice, or ITSN1 $^{+/-}$ / ITSN2 $^{lox/lox}$ / CAG Cre $^{+}$ with ITSN1 $^{-/-}$ / ITSN2 $^{lox/lox}$ / CAG Cre $^{-}$ mice. Animals were bred in accordance with the German law for conducting animal experiments, with the constitutive KO under permit G21-2-072. Mice were kept in a light and dark cycle of 12 h with food and water *ad libitum* at the animal facility.

4.8 Devices & equipment

Devices and tools used in this study can be found in Table 10 and Table 11.

Table 10: Dissection tools.

Device	Model	Device
Fine forceps	Mirror Finish SS #13 13 cm length 0.3 x 0.15 mm tip Straight form	Fine Science Tools GmbH, Heidelberg, Germany
Fine forceps	Dumont #5 0.05 x 0.01 mm tip Straight form	Fine Science Tools GmbH, Heidelberg, Germany
Fine forceps	Dumont #7 0.07 x 0.03 mm tip Curved form	Fine Science Tools GmbH, Heidelberg, Germany
Hardened fine scissors	#09 Straight form 24 mm cutting edge 9 cm length	Fine Science Tools GmbH, Heidelberg, Germany
Scalpel blades	#10 30 mm cutting edge 0.4 mm thickness	Fine Science Tools GmbH, Heidelberg, Germany

Device	Model	Device
Scalpel handle	#3 12 cm length	Fine Science Tools GmbH, Heidelberg, Germany
Surgical scissors	Sharp blunt #18 57 mm cutting edge 18.5 cm length	Fine Science Tools GmbH, Heidelberg, Germany

Table 11: Used devices and their producer.

Device	Model	producer
Absorbance plate reader	SpectroStar® Nano	BMG Labtech, Ortenberg, Germany
Aspiration system	Vacusafe TM	Integra Bioscience, Zizers, Switzerland
Binocular	Stemi 508	Carl Zeiss Microscopy GmbH, Oberkochen, Germany
Blotting chamber	Criterion® Blotter	BIO-RAD, HERCULES, CA, USA
Bunsen burner	Labogaz® 206	Campingaz, Hattersheim, Germany
Cell sorter	SH800; LE-SH800SZFCPL	Sony Biotechnology, San Jose, CA, USA
CO_2 incubator	CB 170	Binder, Tuttlingen, Germany
Counting chamber	Neubauer Improved, 0.1 mm	Marienfeld Superior, Lauda-Königshofen, Germany
Cryotome	Leica CM3050 S	Leica Biosystems Nussloch GmbJ, Nussloch, Germany
Electrophoresis chamber for agarose gels	Mini-Sub® Cell GT Cell	BIO-RAD, HERCULES, CA, USA
Electrophoresis chamber for SDS-PAGE	Mini-PROTEAN® Tetra Cell	BIO-RAD, Hercules, CA, USA
Epifluorescence microscope	Eclipse Ti2-E	NIKON, Tokyo, Japan
Fluorescence microscope	Spinning Disk Confocal	NIKON, Tokyo, Japan
Freezer -20°C	GN5235 FNc 7227	Liebherr, Bulle, Switzerland Liebherr, Bulle, Switzerland
Freezer -80°C	CryoCube F740hi	Eppendorf, Hamburg, Germany
Fridge 4°C	K 3730 KW KSVV30A Unichromat 1500 "version 2011"	Liebherr, Bulle, Switzerland Bosch, München, Germany Foeth GmbH
Gel imaging system	E-BOX	Vilber, Marne-la-Vallée, France
Heat block	Thermal Shake*lite* ThermoMixer C	VWR International LLC, Radnor, PA, USA Eppendorf, Hamburg, Germany
Homogenizer	Hei-Torque Core	Heidolph Instruments, Schwabach, Germany

Device	Model	producer
IHC staining chambers	105 x 85 x 70 (mm)	Carl Roth GmbH + Co. KG, Karlsruhe, Germany
IHC staining cup	Semicircular Deepening Ø32 mm with lid 40 x 40 mm Pressed glass, Clear	Häberle LABORTECHNIK GmbH & Co.KG
IHC staining rack	85 x 60 x 45 (mm)	Carl Roth GmbH + Co. KG, Karlsruhe, Germany
Imaging system	Odysses® Fc Model 2800	LI-COR Biosciences, Lincoln, NE, USA
Inverted microscope	Axio Vert.A1	Zeiss, Oberkochen, Germany
Magnetic separation rack	MagJet	Thermo Fisher Scientific, Waltham, MA, USA
Magnetic stirrer	MR Hei-Mix L MR Hei-Tec	Heidolph Instruments, Schwabach, Germany
Microwave	MW7873	Severin, Sundern, Germany
Mini-centrifuge	MiniStar	VWR International LLC, Radnor, PA, USA
pH meter	FiveEasy	Mettler Toledo, Columbus, OH, USA
Pipette controller	accu-jet®pro	Brand GmBH + Co. KG, Anröchte, Germany
Pipettes (2, 20, 200, 1000 µl)	Transferpipette®S	Brand GmBH + Co. KG, Anröchte, Germany
Precision scale	Entris®II	Sartorius AG, Göttingen, Germany
Rotator for tubes	MultiMix	VWR International LLC, Radnor, PA, USA
Shaker	SHRK07AL2	OHAUS Europe GmbH, Nänikon, Swizerland
Sonifier	SFX 250, 5mm tip	Branson, Brookfield, CT, USA
Table-top centrifuge	MICRO STAR 17R MICRO STAR 17	VWR International LLC, Radnor, PA, USA
Table-top centrifuge	5804R 5910 Ri	Eppendorf, Hamburg, Germany
Thermocycler	peqSTAR 2x peq Start 2x Gradient	PEQLAB Biotechnologie GmbH, Erlangen, Germany
Thermocycler	peqSTAR 2x peqSTAR 2x Gradient	PEQLAB, Erlangen, Germany
Tube roller	RS-TR 05	Phoenix Instruments, Naperville, Il, USA
Vortex	VORTEX-GENIE®2	Scientific Industries, Inc. , Bohemia, NY, USA
Water bath	Hydro	LAUDA, Lauda-Königshofen, Germany

4.9 Software

Table 12: Software used to acquire, process, analyze and visualize the data.

Software	Model	Purchased/obtained from/website available under
Biorender		https://app.biorender.com/
BLAST	Nucleotide	https://blast.ncbi.nlm.nih.gov/Blast.cgi
Cellpose	2.0	https://www.cellpose.org/; Carsen Stringer & Marius Pachitariu
CellProfiler	4.2.6	Cimini Lab, Broad Institute of MIT and Harward, USA
CorelDraw 2020	Version 22.1.0.517	Software center RPTU / Corel corporation, Ottawa, Kanada
DAVID	V2025_1	https://davidbioinformatics.nih.gov/home.jsp
Fiji/ImageJ	Biovoxxel + normale version	NIH, Bethesda, MD, USA
GraphPad Prism	10.1.0	GraphPad Software, San Diego, CA, USA
Image Studio	Version 6.0	LI-COR Biosciences, Lincoln, NE, USA
Image Studio Lite	Version 5.2	LI-COR Biosciences, Lincoln, NE, USA
Licor Acquisition	1.2	LI-COR Biosciences, Lincoln, NE, USA
Microsoft Office	Version 2404	Microsoft Corporation, Redmond, USA
Multiple Primer Analyzer		https://www.thermofisher.com/de/de/home/brands/thermo-scientific/molecular-biology/molecular-biology-learning-center/molecular-biology-resource-library/thermo-scientific-web-tools/multiple-primer-analyzer.html
NIS Elements	5.30.06 (Build1567)	Nikon, Tokyo, Japan
SH3PepInt	5.0.12 SH3PepInt 1.0.0	MoDPepInt Server https://modpepint.informatik.uni-freiburg.de/SH3PepInt/Input.jsp
Snap gene viewer	5.0.7	GSL Biotech LLC, San Diego, CA, USA
STRING	Version 12.0	https://string-db.org/cgi/input?sessionId=bQE0VPAmJ8NT&input_page_show_search=off
Synaptosome macro	v1.0	https://github.com/fabricecordelieres/IJ-Toolset_SynaptosomesMacro/tree/master
T_m Calculator	For primers	https://www.thermofisher.com/de/de/home/brands/thermo-scientific/molecular-biology/molecular-biology-learning-center/molecular-biology-resource-library/thermo-scientific-web-tools/tm-calculator.html

Software	Model	Purchased/obtained from/website available under
Uniprot		https://www.uniprot.org/
Weight to Molar Quantity		https://www.bioline.com/media/calculator/01_07.html

5 Methods

5.1 Histology

5.1.1 Triangularis sterni preparation and staining

The preparation of the triangularis sterni muscle was slightly adjusted from the protocol from Kerschensteiner et al., 2008. Briefly, the mice were sacrificed by cervical dislocation. The fur was sprayed with 70% EtOH to avoid hairs sticking to the prepared tissue, and a midline incision was made. The skin on the thorax as well as the forelimbs was removed, and the connection between the pectoral muscle and its sternal insertion and the muscular connection from the scapula to the thorax was severed. The abdominal wall was opened from the xiphoid cartilage following the thorax borders at both sides towards the spinal cord. The diaphragm beneath the xiphoid cartilage was cut and carefully dissected off along the circumference of the thorax, avoiding damage to the triangularis sterni on the inside of the thorax. Incisions were made laterally on the thorax, approximately at the level of the axillae, and extended superiorly to allow the removal of the anterior part of the thorax, after removing the remaining connective tissue. The thorax was rinsed in 4°C PBS and fixed for 1 h at 4°C in 4% PFA in PBS. After fixation, the thorax was washed 3x in PBS and stored at 4°C until the triangularis sterni was dissected. To obtain the actual muscle, the ribs were cut off between the sternum and the mammary vessel and trimmed till the cartilage-bone transition. The remaining tissue piece corresponded to the triangularis sterni in shape, and the muscle itself was detached by carefully picking up one side and severing the underlying muscle using a needle as a dissection tool. The muscle was cleaned and either stored in PBS at 4°C or immediately immunohistochemically stained. Blocking and labelling with synaptophysin-specific antibodies and bungarotoxin-AF594 were performed in one step overnight (ON) at 4°C on a shaker. The following day, the muscle tissue was washed 3x for 5 min with PB on a shaker and incubated with secondary antibodies diluted in PB on a shaker for 1 h at RT. The secondary

antibodies were removed, and the tissue was washed 3x for 5 min with PB before mounting in Immumount. The used chemicals, solutions and equipment are listed in Table 1, Table 2, Table 12 and primary and secondary antibodies are listed in Table 5 and Table 6. Images were taken with a confocal microscope as z-stacks of 1 µm thickness containing several neuromuscular junctions (NMJs). The z-stacks were summed up (see Z-projections), single NMJs were selected, and single channels saved with Fiji (see Split channels). Subsequently, images were analyzed with a CellProfiler pipeline (see CellProfiler Pipeline for NMJ Analysis) to obtain the following parameters: presynaptic area, postsynaptic area, endplate area, which refers to the convex hull area of the postsynaptic area, postsynaptic branching and endpoints, total length of postsynaptic branches and Mander's Coefficient. Pre- and post-synaptic segmentation was reviewed and only correctly segmented NMJs included in the analysis. The apposition and NMJ classification into pretzel, fragmented and plaque-like was defined as in Weyer et al., 2011. The compactness and complexity score were calculated as defined by Jones et al. 2017 in Excel as follows:

$$Complexity = \log_{10}(number\ of\ branches * number\ of\ endpoints * total\ length\ of\ postsynaptic\ branches\ [pixel])$$

$$compactness = \left(\frac{postsynaptic\ area}{endplate\ area}\right) * \ 100$$

5.1.2 Limb-Muscle preparation

The mouse was sacrificed by cervical dislocation, and the fur sprayed with 70% EtOH. The skin of the limbs was removed. To receive the TB, the surrounding fascia was removed, and the forceps tips carefully inserted between the triceps and the surrounding muscle to loosen it up and allow space for the scissors to cut the muscle as close as possible toward the elbow. The muscle was mobilized and cut as close to the shoulder as possible. The muscle was cleaned and stored on wet Whatman paper until the end of the preparation. Next, the TA was dissected, starting again by removing the fascia. The tendon of the TA muscle is close to the EDL tendon, and one arm of the forceps were moved under the TA tendon and up toward the knee to loosen the TA muscle out of the tissue. Next, the tendon at the foot was cut and the muscle mobilized by pulling it up once, cutting as close to the knee as possible. For the underlying EDL, the same steps were conducted. The soleus is located on the posterior side of the hindlimbs beneath the gastrocnemius, therefore, the gastrocnemius tendon was cut and

pulled upwards to reveal the soleus underneath. The soleus was carefully separated from the gastrocnemius and cut as close as possible at the knee.

All muscles were weighed before snap-freezing in isopentane. The isopentane was cooled down by liquid nitrogen until it started crystalizing to ensure the correct temperature range. Then, the muscles were frozen for ~20 s in isopentane. Afterwards, they were transferred to liquid nitrogen until storage at -80°C.

5.1.3 Cryosections

5.1.3.1 Microscopy slide coating

Microscopy slides were cleaned with 70% EtOH and soaked in gelatin-chrome alum solution for 20 s. After drying for 1 h, the slides were soaked for another 20 s, and dried for 2h and stored dust-free.

5.1.3.2 Preparation of muscle cryo-sections

The muscles were cut with a Leica CM3050 S Cryotome into sections of 10 µm thickness. The muscles were thawed at -20°C for a minimum of 1 h prior to cutting at -25°C. If needed, the temperature was slightly adjusted, but kept in a range between -20°C and -25°C. Every 300 µm, a section was taken throughout the entire muscle. The sections were stored at -80°C until use.

5.1.4 HE staining and analysis

Sections were taken out of the -80°C freezer and thawed for 1 h at RT. Slides were stained by transferring them between baths of several solutions. Solutions and times of incubation can be found in Table 13, with the chemicals in Table 1 and Table 3. After the last incubation in Xylol II, slides were dried under the hood and mounted with Entellan™. Images of 2-3 areas/section from 2-3 matched sections per genotype were taken with the Eclipse Ti2-E and segmented with the Cellpose implementation for Fiji (Stringer et al., 2021) and area, feret diameter, perimeter and circularity measured (see Cellpose analysis for details).

Table 13: HE staining steps.

Incubation time	Solution
2 min	Tap water
10 min	Hematoxylin
3 min	Tap water

Incubation time	Solution
3 min	Tap water
2 min	Tap water
Total of 15 s dipping in and out of solution	70% EtOH / 1% HCl
1 min	Tap water
7 min	Tap water
4 min	Eosin
Dip in 1x	Tap water
40 s	50% EtOH
1 min	70% EtOH
2 min	90% EtOH
2 min	100% EtOH
2 min	100% EtOH
3 min	Xylol I
3 min	Xylol II

5.2 Molecular biology

5.2.1 Genotyping

Prior to working with the animals, their genotype was assessed. For this, tissue biopsies from the ears or tail (only for constitutive dKO mice) were taken by animal caretakers. Samples were either stored at -20°C or used immediately. To prepare the DNA, the tissue was lysed in 50 µl alkaline lysis buffer and boiled at 95°C for 30-60 min. Upon addition of an equal volume of neutralization buffer the sample was mixed thoroughly to inactivate the lysis.

Polymerase chain reaction (PCR) was used to amplify specific DNA fragments for ITSN1, ITSN2, or CAG Cre, to identify the different genotypes. The PCR reaction mix was made according to Table 14, and the cycling program was chosen according to Table 15.

Table 14: PCR reaction mix with respective amounts for one sample.

Compound	**ITSN1**	**ITSN2**	**CAG Cre**
Nuclease free water	10.7 µl	10.4 µl	7.4 µl
10x Orange Dye	2 µl	2 µl	1.5 µl
MgCl2 (25mM)	2 µl	2 µl	1.5 µl
Buffer B	2 µl	2 µl	1.5 µl
dNTPs (5 mM)	0.6 µl	0.6 µl	0.3 µl
Primer Mix (10 µM) including forward and reverse primer	1 µl	0.75 µl	0.5 µl
Taq Polymerase (5 U/µl)	0.5 µl	0.5 µl	0.5 µl
Genomic DNA	1.2 µl	1 µl	1.5 µl

Table 15: Thermocycling programs for ITSN1, ITSN2 and CAG Cre genotyping.

	ITSN1	ITSN2	CAG Cre
Denaturation	94°C for 3 min	94°C for 3 min	94°C for 2 min
Number of cycles	30x	30x	35x
Denaturation	94°C for 30 s	94°C for 30 s	94°C for 30 s
Annealing	55°C for 30 s	55°C for 30 s	55°C for 30 s
Elongation	72°C for 1 min	72°C for 30 s	72°C for 30 s
Final elongation	72°C for 5 min	72°C for 5 min	72°C for 2 min
	Stored at 8°C	Stored at 8°C	Stored at 8°C

PCR products were analyzed by gel electrophoresis on a 2% (w/v) agarose gel in 1x TAE buffer. To dissolve the agarose, the solution was heated in a microwave, and ethidium bromide added to a final concentration of 0.007%. The polymerized gels were immersed in an electrophoresis chamber with 1x TAE buffer, and the total PCR product loaded. Electrophoresis was run for 15 min at 150 V, and the gel was imaged under UV-light. The respective band sizes were interpreted as given in Table 16.

Table 16: DNA fragments and their size.

DNA fragment	Fragment size
Cre	400 bp
ITSN1 KO	544 bp
ITSN1 WT	666 bp
ITSN2 KO	331 bp
ITSN2 lox	425 bp
ITSN2 WT	235 bp

5.2.2 Generation of recombinant proteins by PCR based cloning.

To generate needed GST-fusion constructs, PCR-based cloning was performed to introduce the appropriate restriction sites to the inserts.

5.2.2.1 PCR for restriction site insertion

For each insert, primers were designed containing a leader sequence (very short or missing for Kv1.2 N-Term and C-Term cloning), the restriction site, additional base pairs to adjust the reading frame for the forward primer, and a hybridization sequence (Table 9). The primers were checked for primer dimerization with the Multiple Primer Analyzer (Table 12). The PCR reaction mix for PCR-based cloning can be found in Table 2 with primers in Table 9. For amplification of the insert, the default thermocycling program was used with the annealing temperature depending on the primers. To determine the annealing temperature, the T_m

calculator for the Phusion DNA polymerase was used (Table 12). If the PCR did not work with the default settings, a touchdown PCR was performed alternatively (Table 17). PCR products were analyzed by gel electrophoresis on a 1% agarose gel with Ethidium bromide added to a final concentration of 0.007%. The volume of the total PCR product was divided into two lanes and run at 120 V depending on the length of construct, but usually about 30 min. To purify the DNA construct, it was cut out of the gel and purified using the Nucleospin Gel and PCR Cleanup Kit or Zymoclean™ Gel DNA recovery kit, according to the manufacturer's instructions.

Table 17: Default and alternative thermocycling program for PCR-based cloning.

	Default	**Touch-down**
Denaturation	98°C for 30 sec	98°C for 30 sec
Number of cycles	30x	10x
Denaturation	98°C for 10 s	98°C for 10 s
Annealing	T_m for 30 s	T_m -0.5°C/cycle for 30 s
Elongation	72°C for 95 s	72°C for 95 s
		20x
		98°C for 10 s
		T_m-5 for 30s
		72°C for 95 s
Final elongation	72°C for 5 min	72°C for 5 min
	Stored at 8°C	Stored at 8°C

5.2.2.2 Restriction Digest

1 µg pGex4T-1 backbone as well as the insert produced by PCR in the previous step were digested with the corresponding restriction enzymes in 1x FastDigest buffer with 1 µl of each restriction enzyme (Table 18) at 37°C for 1 h. Additional controls to check on the function of the restriction enzymes were included and functionality of the digest tested by loading on a 0.75% agarose gel with 0.007% Ethidium bromide. Digested DNA was purified as described in the previous subchapter (5.2.2.1) and DNA concentration measured.

Table 18: Restriction enzymes used for cloning.

Cloning	**Restriction enzymes**
GST-CTTN	BamHI, NotI
GST-FMRP	EcoRI, SalI
GST-FXR1	BamHI, EcoRI
GST-Kv 1.2 N-Term	EcoRI; XhoI

Cloning	Restriction enzymes
GST-Kv1.2 C-Term	EcoRI, SalI
GST-Kvβ2	EcoRI, SalI

5.2.2.3 Ligation

The overhangs on the backbone and insert generated by the restriction enzymes in the digest were ligated in 1x T4 ligase buffer by a T4 ligase at 22°C for 1 h. T4 ligase was heat inactivated at 70°C for 10 min. Backbone and insert were added in a ratio of 1 to 4. Calculations for this were performed using the Weight to Molar Quantity calculator (Table 12)

5.2.2.4 Transformation, plasmid DNA isolation and sequencing

Competent Top10 or NEB stable *E. coli* cells were transformed with the newly generated fusion construct. For this, they were taken from -80°C and thawed on ice. The ligation product was added and left to incubate with the cells for 30 min on ice. In the meantime, LB plates supplemented with ampicillin were prewarmed at 37°C in an incubator. After incubation, the cells were heat shocked at 42°C for 50 s and put back on ice for 5 min. Subsequently, cells were supplemented with 250 µl LB medium and grown at 37°C for 30 min. *E. coli* were pelleted and resuspended in 50 µl LB medium with ampicillin, before plating on the prewarmed LB plates. Cells were grown ON at 37°C. To test if the cells contained the construct, a negative control was included for transformation, and a test digest was performed for 2-4 colonies. These colonies were grown in ~3-4 ml LB with antibiotic at 37°C ON with rotation at 180 rpm. The DNA was purified with the Nucleospin Plasmid Kit, according to the manufacturer's instructions and sent for sequencing by Eurofins Genomic (Ebersberg, Germany). The sample was prepared according to their instructions and sequenced by Sanger sequencing. Sequencing results were analyzed using nucleotideBLAST (Table 12).

If the sequencing confirmed successful cloning of the desired construct, BL21 cells were transformed for protein expression according to the same protocol and glycerol stocks for storage at -80°C generated. To do so, equal parts of cell suspension and 50% sterile glycerol were mixed and stored in 2 ml cryotubes at -80°C.

To harvest larger amounts of plasmid DNA for transfections, a preculture was prepared from the glycerol stocks and DNA purified with the Nucleobond Plasmid Midi Kit, according to the manufacturer's instructions.

5.3 Biochemistry

5.3.1 Overexpression of recombinant protein in E. coli

BL21 cells are a common *E. coli* strain used for overexpression of recombinant proteins. To express recombinant proteins, a preculture of 50 ml LB with a selection marker was grown ON at 37°C. The subsequent day, the preculture was added to 500 ml 2xYT medium with antibiotics and grown at 37°C till it reached OD_{600} 0.5 - 0.8. Upon reaching the appropriate OD_{600}, fusion protein expression was induced by adding IPTG to a final concentration of 1 mM in the cell medium. The time needed for proper protein expression depends on the fusion construct and can be read out of Table 19. Cells were centrifuged at 4500 g for 20 min. The supernatant was discarded, and for most cells, the pellet was resuspended on ice in 30 ml ice-cold PBS. Samples were divided in 2x 15 ml or 4x 7,5 ml in falcons and stored at -20°C till usage or used fresh. For GST-FMRP and GST-FXR1 expressing cells, the cell pellet was resuspended in 12 ml FMR/FXR *E. coli* Lysis Buffer, and affinity purification was performed immediately.

Table 19: Fusion constructs and their overexpression conditions.

Construct	Temperature	Time
GST	30°C	3 h
GST-EH-CC	30°C	3 h
GST-SH3A	30°C	3 h
GST-SH3B	30°C	3 h
GST-SH3C	30°C	3 h
GST-SH3E	30°C	3 h
GST-Kv1.2N	30°C	3 h
GST-Kv1.2C	30°C	3 h
GST-Kvβ2	30°C	3 h
GST-CTTN	37°C	4 h
GST-FXR1	20°C	3 h
GST-FMRP	20°C	3 h

5.3.2 Affinity-purification of recombinant GST-fusion protein

To purify the fusion proteins, the resuspended cell pellet was lysed by bringing the solution to 1 mM PMSF and adding a spatula tip of lysozyme. Immediate inverting prevented the lysozyme from clumping, and samples were incubated on rotation for 10 min at 4°C. Subsequently, the samples were sonified by pulses of 1 s on and 1 s off with an amplitude/power of 30% for 1.5 min. Triton X was added to a final concentration of 1% and

the sample incubated on ice for 10 min before it was centrifuged at 12000 rpm for 30 min. The resulting pellet contained cell debris and the supernatant the fusion protein, which was added to 67.5-250 µl pre-washed GST binding resin, depending on the observed binding efficiency. The suspension was incubated for 2-2,5 h at 4°C while rotating, only FMRP-GST and FXR1-GST were incubated ON at 4°C due to lower binding efficiency. Afterwards, the beads were washed 3x with ice-cold PBS and the protein amount on the beads determined with Bradford or BCA assay according to the manufacturer's instructions. Additionally, the purified beads were loaded on an SDS-PAGE gel and stained with Coomassie (for more details see 5.3.8), to ensure that protein had been purified and to adjust the protein measurement, as measurement of the bead-bound protein are prone to inaccuracies.

5.3.2.1 Affinity purification for GST-FXR1 and GST-FMRP

To purify the GST-FMRP and GST-FXR1 fusion proteins, a specialized protocol was adapted from (Khayachi et al., 2018). In brief, the resuspended cell pellet was lysed by adding a spatula tip of lysozyme. Immediate inverting prevented the lysozyme from clumping, and samples were incubated on rotation for 30 min at 4°C, followed by additional 30 min after adding SDS to a final concentration of 0.1% and $MgCl_2$ to a final concentration of 10 mM. Subsequently, the sample was sonified by pulses of 1 s on and 1 s off with an amplitude/power of 30% for 1.5 min. Cells were centrifugated for 15 min at 4°C at 10000 rcf and subsequent washes and purification with GST-beads were performed as described in the previous paragraph (5.3.2).

5.3.3 Preparation of mouse brain lysate for GST pull-down

Frozen mouse brain from a p60-65 mouse was lysed in 8 ml lysis buffer with 12 strokes at 900 rpm while cooled in ice-water and centrifuged for 30 min at 4°C with 15000g. Protein estimation of the supernatant was performed via Bradford or BCA assay according to the manufacturer's instructions and the lysate adjusted to 2 µg/µl.

5.3.4 Preparation of crude synaptosome fractions for GST-pull-downs or IPs

For investigations of an interaction between ITSNs and Kv channel subunits, a specialized lysis buffer for transmembrane proteins was used (Table 2: Solutions used.). The brain was homogenized in 8 ml sucrose buffer with 1 mM PMFS at 900 rpm with 12 strokes while cooled in ice-water and centrifuged at 4°C with 900 xg for 10 min. The supernatant (S1) was transferred to a new falcon and centrifugated for 15 min at 12.500 xg at 4°C. The pellet P2 was

washed once with sucrose buffer and centrifuged again for 15 min at 12.500 xg at 4°C. The supernatant S2 was discarded and the pellet P2' resuspended in 2 ml lysis buffer (Chaps 1%, KCl 100 mM, $MgCl_2$ 2mM, Hepes 20 mM, NaF 1mM, Complete Protease Inhibitor Tablet), and the protein concentration was measured with a Bradford or BCA assay according to the manufacturer's instructions.

5.3.5 GST pull-down assay

To precipitate possible interaction partners of the fusion construct, 100 µg of fusion construct bound to GST-beads were incubated with 2 mg mouse brain lysate or a crude synaptosome fraction on rotation at 4°C ON. After the incubation, the beads were washed 3x with lysis buffer without inhibitors but containing detergent and 2x with lysis buffer without inhibitors and detergent. The remaining liquid was removed, and the protein eluted from the beads by adding 80-100 µl 1x Laemmli sample buffer and boiling the sample for 5 min at 95°C. Afterwards, the sample was either stored at -20°C or immediately loaded onto a gel to separate the contained proteins. For ITSN1-fusion constructs and GST, 1/5 of the whole pull down eluate was loaded onto a gel, for CTTN ¼, and for FMRP- and FXR1-GST ½ of the eluates were loaded.

5.3.6 Immunoprecipitation

To investigate endogenous protein interactions, co-immunoprecipitations offer the advantage of isolating native protein complexes. For these experiments, 3 µg of a specific primary antibody and an unspecific IgG control antibody of the same species were each incubated with 5 mg of synaptosome protein for 1 h at 4°C while on rotation. Synaptosomes were purified as described previously (see chapter 5.3.4), but using Co-IP-Lysis buffer (Table 2). Then, 30 µl of Protein A/G magnetic beads were washed 2x for 5 min in TBST, added to the primary antibodies in the lysate and incubated for another 3 h at 4°C with rotation. The beads and attached immunoprecipitated proteins were collected by putting the sample on the magnetic rack. The supernatant was discarded, and the beads were washed 3x for 10 min at 4°C with lysis buffer without inhibitors. After the last wash, the beads were resuspended in 20 µl Laemmli buffer and boiled for 15 min at 95°C. The whole sample was loaded onto an SDS-PAGE gel.

5.3.7 SDS Polyacrylamide gel electrophoresis (SDS-PAGE)

SDS-PAGE is used to separate proteins based on their molecular weight. For this, the proteins are denatured by SDS and β-Mercaptoethanol and become negatively charged due to SDS binding.

5.3.7.1 Preparation of SDS-PAGE gels

SDS-PAGE gels were prepared either immediately before use or up to 1 week ahead of time. The glass plates were cleaned with 70% EtOH and placed in the casting frames. The separating gel was prepared either with 8%, 10% or 12% acrylamide (see Table 20) and poured between the glass plates. A thin layer of isopropanol was used to ensure an even edge of the gel. After polymerization of the separating gel, the isopropanol was removed and the stacking gel (Table 21) poured on top. A comb with either 10 or 15 pockets was inserted before polymerization of the stacking gel.

Table 20: Composition of the separating gel. Volumes are given for 2 gels.

Separating gel (15 ml for 2 gels)	**8%**	**10%**	**12%**
ddH_2O	7 ml	6 ml	5 ml
1.5 M Tris-HCl (pH 8.8) + 0.4% SDS	3.75 ml	3.75 ml	3.75 ml
30% acrylamide mix	4 ml	5 ml	6 ml
10% APS	150 µl	150 µl	150 µl
TEMED	15 µl	15 µl	15 µl

Table 21: Composition of the stacking gel. Volumes are given for 2 gels.

3.8% Stacking gel (5 ml for 2 gels)	**Volumes for 2 gels**
ddH_2O	3.25 ml
1 M Tris-HCl (pH 6.8)	1.25 ml
30% acrylamide mix	0.66 ml
10% APS	75 µl
TEMED	7.5 µl

5.3.7.2 SDS-PAGE

Samples were prepared in 1x Laemmli sample buffer and loaded onto a self-cast SDS-PAGE gel. For this, the gel was placed in the running chamber with SDS running buffer in the inner and outer chamber. If the samples were stored in the freezer before use, they were quickly

boiled for 5-10 min at 95°C. The gel ran at 80 V till the sample entered the separating gel. Then, the voltage was increased to 120 V, and the gel was run for about 90 min or till the sample reached the end of the gel.

5.3.8 Coomassie Staining

To stain the proteins contained in the gel, it was rinsed with ddH_2O and incubated with Coomassie Staining for 30-60 min. Subsequently, the gel was destained with Coomassie Destainer, till protein bands were clearly visible, most times ON at room temperature (RT).

5.3.9 Western Blotting

To analyze specific proteins, which were previously separated according to molecular weight by SDS-PAGE, the proteins were transferred onto a nitrocellulose membrane. For this, a wet transfer was performed. Here, the SDS-PAGE gel was placed in a transfer sandwich made of a sponge, two thin Whatman papers, the polyacrylamide gel, a membrane, two thin Whatman papers, and another sponge and placed in the transfer chamber, filled with transfer buffer, on ice. To transfer the proteins from the gel to the membrane, 110 V were applied for 60-90 min. After the transfer, the membrane was stained with the pan-protein stain PonceauS, to ensure the proteins were transferred onto the membrane. For this, the membrane was stained with Ponceau staining diluted 1:5 in ddH_2O for 5 min and rinsed once or twice with 1% acetic acid before imaging. If the membrane needed to be cut for the following immunolabelling, this was done before destaining the stained membrane with TBST. Then, the membrane was incubated in *LI-COR Intercept® Blocking Buffer* for at least 45 min to 1 h. To label specific proteins, the membrane was incubated with the corresponding primary antibodies 4°C ON on rotation (Table 5). On the subsequent day, the membrane was washed 3x with TBST for 5 min and incubated with secondary antibodies diluted 1:10.000 in TBST for 45 min while shaking at RT (Table 6). The membrane was washed 3x with TBST for 5 min and 2x with TBS for 5 min while shaking and imaged with the LI-COR Odysseus using the Licor Acquisition software.

5.3.10 F/G actin ratio

G- and F-actin can be separated based on their sedimentation behavior, to obtain insight into actin dynamics. For this, the cerebellum and brainstem of the brain were removed, and the forebrain homogenized in 8 ml sucrose buffer at 900 rpm with 12 strokes while cooled in ice-water. Nuclei and cell debris were removed by centrifugation at 900 xg for 10 min at 4°C. The

supernatant (S1) was centrifugated for 15 min at 12500 g at 4°C. The supernatant (S2) was removed and the pellet (P2) washed by resuspension in 8 ml sucrose buffer, followed by centrifugation at 12500 xg for 15 min at 4°C. The supernatant (S2') was removed and the pellet (P2') resuspended in 0.5 ml G-actin buffer. The sample was centrifugated at 15000 xg for 30 min at 4°C. The resulting supernatant was collected, as it contains the G-actin. The larger F-actin fractionates into the pellet, which was resuspended in 0.5 ml G-actin buffer and 0.5 ml F-actin buffer. The sample was incubated on ice for 1 h and inverted a few times every 15 min to depolymerize the F-actin to G-actin. After another centrifugation at 15000 xg for 30 min at 4°C, the supernatant now containing the former F-actin was collected. Laemmli buffer was added to both fractions and double the volume of F- actin compared to G-actin loaded for an SDS-PAGE and Western blot.

5.3.11 Trypsin Cleavage Assay

A frozen mouse brain was homogenized in 8 ml sucrose buffer with 12 strokes at 900 rpm while cooled with ice-cold water. The homogenate was transferred into a 15 ml tube and centrifuged at 900 xg for 10 min at 4°C. The supernatant S1 was transferred to a fresh tube and centrifuged with 10000 xg for 15 min at 4°C. The resulting pellet P2 was washed by resuspension with 8 ml sucrose buffer and centrifuged again with 15000 xg for 15 min at 4°C. The protein concentration was measured with a BCA assay, and equal amounts of protein were digested with different amounts of trypsin for 10 min at 30°C in a water bath. The samples were gently mixed during the incubation. After the incubation, synaptosomes were pelleted for 3 min at 8700 xg and resuspended in Laemmli buffer. All samples were analyzed to determine the trypsin concentration, at which most postsynaptic proteins are degraded but the presynapse still intact. Those samples were immunoblotted again and quantified.

5.3.12 Striatal synaptosome purification and immobilization

The synaptosome purification and immobilization was established by Paget-Blanc et al., 2022.

5.3.12.1 Preparation of Ficoll® gradients

To remove remaining axon parts and other debris from the crude synaptosome sample, it can be run over a sucrose gradient composed of an upper 7.5% and a lower 13% Ficoll® layer. Upon centrifugation the synaptosomes will form a layer at a different height than the

remaining debris. Therefore, Ficoll® solutions of 7.5% and 13% were prepared in sucrose buffer and layered on top of each other.

5.3.12.2 Poly-Lysin coating of coverslips

Coverslips were washed once with DPBS and incubated with Poly-L-Lysin solution for at least 1 h at RT while shaking. Poly-L-Lysin solution was removed, and the coverslips were washed 2x with DPBS. Coverslips were either used immediately or stored in DBPS at 4°C till needed.

5.3.12.3 Striatal synaptosome preparation

The mouse was sacrificed by cervical dislocation and decapitated. The head was quickly frozen in liquid nitrogen for 3 s and the brain removed from the skull. The brain was placed in ice-cold DPBS and transferred onto an ice-cold surface for the striatal dissection. The two hemispheres were separated, and the brainstem and midbrain removed along with the olfactory bulb and cerebellum. The striatum was identified by its fine radial white matter tracts and removed from the surrounding cortex with forceps. Leftover non-striatal tissue was removed and the striata placed in 100 µl ice-cold sucrose buffer with PIC. Striata were homogenized in 0.333 ml sucrose buffer with PIC per brain by 12 strokes with 900 rpm while cooled in ice-water. To collect as much homogenate as possible, the glass potter was rinsed in 0.25 ml ice-cold sucrose buffer with 3 manual strokes, before the Teflon pestle was rinsed with 0.25 ml ice-cold sucrose buffer. Both washes were added to the homogenate and mixed by inverting 3x. The homogenate was centrifugated at 1000 xg for 5 min at 4°C. The supernatant (S1) was transferred to a fresh reaction tube and centrifuged at 12500 xg for 8 min at 4°C. While the supernatant (S2) was thrown and the resulting pellet (P2, crude synaptosomes) was resuspended in 300 µl sucrose buffer containing PIC and layered on top of the previously described Ficoll® gradient in ultracentrifugation tubes. The sample was centrifuged with 20100 rpm for 36 min at 4°C in the table-top ultracentrifuge Optima MAX-XP with the MLS-50 swinging bucket rotor. The synaptosome layer between the Ficoll® layers was removed with a syringe. These purified synaptosomes were stored ON at 4°C in the dark.

5.3.12.4 Sorting for intact synaptosomes

The next day, synaptosomes were sorted using the FACS sorter Sony SH800. The sorting is based on the property of disrupted, collapsed, or aggregated synaptosomes to clump together resulting in a more intense membrane staining which can be detected with the lipophilic dye

FM4-64, used at 1 µg/ml, in the PerCP-Cy5.5 Channel. Device settings were as follows: 100 µm nozzle, sample cooled to 4°C and agitated at 300 rpm while sorting, 488 nm laser on, forward window extension 50, sort mode set to "semi-purity" comparable to Sort precision modes (yield=0, phase=16, precision=0) on other devices, FSC/SSC filter: 525/50 nm, PerCP filter: 720/60 nm. Samples were analyzed and sorted with a sort rate of 6000-9000 events/s and a flow rate of 8. To differentiate between individual intact synaptosomes or "singlets" and collapsed or aggregated synaptosomes, a control with increased amount of aggregated synaptosomes was generated by vortexing thoroughly before measurement. Synaptosome yield was ~85%, similar to amounts found in literature with a slightly higher amount of aggregates ~5-10% compared to literature (Paget-Blanc et al., 2022).

5.3.12.5 Synaptosome Immobilization

Immediately after sorting, ~ 500,000 synaptosomes per well were centrifuged onto a poly-L-lysine coated coverslip at 4347 rcf (4500 rpm) for 50 min at 4°C. Synaptosomes were fixed in freshly prepared PEM fixation buffer, to ensure cytoskeletal preservation, for 10 min at RT and washed 3x in PBS. Samples were sealed with Parafilm and stored at 4°C.

The staining of the immobilized synaptosomes was performed as described in 5.4.3.

5.3.12.6 Microscopy and Image processing

Immuno-stained synaptosomes were imaged with the spinning disk confocal microscope in 10 to 13 images as z-stacks with for total depth of 5 µm in 0. 5 µm steps per coverslip and analyzed with ImageJ using the Synaptosomes Macro by Fabrice Cordelieres (Table 12). The background corrected intensities were read out and negative values excluded. These integrated intensities were reviewed and the threshold for classification was to fit all experiments and set for Bassoon at $10^{5.4}$ and $10^{3.9}$. As data was not normally distributed, the median integrated intensity was chosen as more accurate representation.

5.4 Cell Culture

5.4.1 General mammalian cell culture

As cultured mammalian immortalized cell lines are simpler to obtain than primary cells, HeLa cells were used to look at colocalization. Cells were cultured in DMEM, supplemented with Pen/Strep and FBS, in a humidified incubator at 37°C with 5% CO_2 and handled under sterile

conditions. Cells were passaged twice a week, by washing with 1x DPBS and incubation with TrypLE™ Express at 37°C for a few minutes till the cells detached. Trypsin was inactivated by an equal volume of supplemented DMEM and transferred to a 15-ml tube. Cells were pelleted by centrifugation at 400 rcf for 5 min. The resulting cell pellet was resuspended in supplemented DMEM and plated at 1:4-1:12 dilutions into culture dishes. Medium and other reagents were incubated in a water bath at 37°C prior to use.

5.4.2 Transfection with JetPRIME®

If cells were used for transfections, they were counted in a Neuhauser chamber before seeding 100.000 cells/well on a coverslip for transfection on the next day. For transfection on the same day, 150.000-200.000 cells/well were seeded and given a minimum of 5 h to properly attach to the coverslip. The JetPRIME transfection was performed according to the manufacturer's instructions in a 12 well plate. First, 100 µl of JetPRIME® buffer were mixed with 1 µg of plasmid DNA, vortexed for 10 s and spun down. Next, 2 µl of JetPRIME® transfection reagent was added, the sample vortexed for 1 s and spun down, and left to incubate for 10 min in the dark. Then, the transfection mix was added to the cells and incubated ON. Cells were either fixed immediately or the medium exchanged. If two constructs were used, the amount of transfection reagent was doubled, while for three constructs, the amount of DNA and transfection reagent was halved per constructs.

5.4.3 Immunofluorescence

For immunofluorescent labeling, cells or immobilized synaptosomes were washed 2x with 1 ml PBS and fixed with ice-cold 4%PFA in 4% sucrose for 10 min at RT. After washing 3x with 1 ml PBS, the samples were either processed immediately or stored at 4°C in PBS. Unspecific binding sites were blocked and permeabilized with 20% normal goat serum and 0.1% Triton X-100 in PBS for 30 min at RT. Subsequently, primary antibodies were diluted in blocking buffer as given in For IF, primary and secondary antibodies were diluted in blocking buffer. For immunoblotting, primary antibodies were diluted in 1:1 *LI-COR Intercept® Blocking Buffer* and TBST while secondary antibodies were diluted in TBST.

Table 5 and incubated for 1 h at RT with the cells in a dark humidity chamber. The cells were washed 3x with PBS and then incubated with secondary antibodies or other fluorescent probes like phalloidin (diluted in blocking buffer as given in Table 6) for 1 h at RT in a dark humidity

chamber before washing again 3x with PBS. If cells were labelled with DAPI, the DAPI stock solution was diluted in PBS to a final concentration of 1 µg/ml and incubated for 10 min at RT with the cells. After a final wash in PBS, the sample was mounted on a microscopy slide with ImmuMount® and dried in the dark ON before imaging.

5.4.4 In-vitro cortical and hippocampal neuron culture

All of the procedures described here were performed under sterile conditions.

5.4.4.1 Poly-L-lysine coating

Prior to culture preparation, the well-plates, in which the neurons will be seeded, were coated with 0.1% Poly-L-lysine solution, and incubated at RT for 30 min. The solution was removed, and leftover liquid was left to dry before addition of the cell suspension.

5.4.4.2 Dissection of the Cortex and Hippocampus.

Newborn mice were sacrificed by decapitation, and the brain was dissected and transferred into a dish with cooled washing solution I. There, the meninges were removed, and the brain was separated in two halves along the hemispheres. Olfactory bulb, cerebellum, brainstem, and midbrain areas were removed to isolate the cortices and hippocampi, which were cut into smaller pieces. The tissue was transferred into a 15 ml tube and washed 2x in washing solution I followed by 2x washes in washing solution II lacking FBS, to wash out remaining FBS for improving the subsequent trypsin digest. Additionally, DNase was added to prevent DNA aggregation. Then, the tissue pieces were digested for ~15 min in a water bath at 37°C with gentle mixing in between. The digestion solution was removed, and the sample washed as before. The washing solution was removed as thoroughly as possible, and the tissue triturated by pipetting up and down less than 20x in 3 ml dissociation solution supplemented with 10 µl DNase. The volume was filled up to 8 ml with washing solution I, and the cells were pelleted at 800 rcf for 10 min at 4°C. The cell pellet was resuspended in plating medium, and the cells were counted with trypan blue, before seeding into the well plate. Cells were left in the incubator at 37°C with 5% CO_2 to settle for 30-90 min, before plating medium supplemented with 0.3 µM Tamoxifen was added. On day in vitro (DIV) 1 half of the plating medium was removed and refreshed by growth medium containing 2 µM Ara-C, 2% BL27 and 0.3 µM Tamoxifen. On DIV2, the same volume of growth medium as the previous day containing

4 µM Ara-C, 2% BL21 and 0.3 µM Tamoxifen was added. Cells were kept in culture until DIV14-16 to be used in experiments.

5.4.4.3 Cell lysate

To verify the inducibility of the ITSN 2KO, cell lysates were prepared, after control of proper neuron health. For this, the cells were placed on ice and washed once with DPBS. To lyse the cells, 10 µl Ripa-Lysis buffer were added. After a short incubation the cells were scratched off. The cell suspension was collected, and the protein concentration measured with a BCA assay. Laemmli Buffer was added to the sample and boiled at 95°C for 15 min. 50 µg protein were loaded onto an SDS-PAGE gel for downstream protein quantification.

5.4.4.4 Preparation of crude synaptosomes from primary cortico-hippocampal neurons

To investigate the prevalence of synaptic proteins of cultured primary cortico-hippocampal neurons, I adjusted the previously described protocol for a crude synaptosome fraction to cultured neurons. These adjustments were necessary, as the total amount of available material from a neuronal culture as compared to brain tissue is highly reduced. Prior to synaptosome preparation, neurons were observed under the microscope to ensure that the neurons were healthy and formed a dense network. The cells were put on ice, the medium was removed, and the cells were washed once with DBPS. About 100 µl of sucrose buffer supplemented with 1 µM PMSF and c0mplete® protease inhibitor were added prior to scratching the cells off the plate. The cell suspension was collected in a 1.5 ml reaction tube, and the volume was made up to 1 ml with supplemented sucrose buffer. Cells were homogenized with 12 strokes at 900 rpm while cooled down with ice cold water. The homogenized samples were centrifuged at 1000xg for 10 min at 4°C. The resulting pellet P1 was discarded and the supernatant S1 transferred into a fresh 1.5 ml reaction tube for another centrifugation at 15000 g for 15 min at 4°C. The resulting synaptosome pellet was resuspended in sucrose buffer and the protein concentration measured with a Bradford assay. Laemmli Buffer was added to the sample and boiled at 95°C for 15 min. 15 µg protein were loaded onto an SDS-PAGE gel for downstream protein quantification.

5.5 Enrichment analysis with DAVID

Two independent MS-IP datasets obtained by Marielle Eichhorn Grüning from AG Haucke at FMP-Berlin together with the group of Dr. Eberhard Krause were analyzed for protein

enrichment. They performed the MS-IPs with mouse hippocampal extract on an Orbital Elite mass spectrometer from Thermo Scientific after a liquid chromatography with Dionex Ultimate 3000 NCS-3500RS Nano. Peak lists were processed with the Mascot Distiller Version 2.5 and Mascot Search Engin Version 2.2. Hits of the two independent experiments were compared and proteins identified in both experiments. Only hits with a H/L ration ≥4 were taken as enriched by the IP. Those hits were analyzed for enrichment with the Database for Annotation, Visualization, and Integrated Discovery DAVID from the NIH (Table 12)with the DAVID *mus musculus* gene set as gene population background. The "Functional Annotation Clustering" function was performed with 136 identified proteins (out of 145 proteins and peptides) and a medium classification stringency based on the following gene ontology categories: GOTERM_BP_DIRECT, focusing on biological processes, GOTERM_CC_DIRECT focusing on cellular compartments, and GOTERM_MF_DIRECT, focusing on molecular function. This allows a condensed summary as it organized hierarchical as well as redundant or similar terms within groups (Huang et al., 2009).

5.6 Network visualization with STRING

To highlight and visualize the unexpectedly high number of FMRP interactors in the MS-IP datasets, FMRP interactors were identified in the MS713 dataset based interactors listed in Pasciuto & Bagni, 2014 and visualized in STRING (Table 12). The full STRING network is shown, where edges indicate functional and physical protein associations. The edges are shown based on confidence, so the line thickness represents the strength of data support. The minimum required interaction score was set to "low confidence (0.150)"

5.7 Statistical analysis

Statistical analyses were performed with GraphPad Prism (Table 12). If not stated otherwise, in case of normally distributed data, two groups were compared with an unpaired two-tailed student´s t-test. For comparisons between normalized values, a one sample t-test with the appropriate hypothetical value was used. For comparisons between more than two groups of relative values, if the one sample t-test reached significance, the Bonferroni correction for multiple testing was chosen as post hoc test. For the area distribution, mixed model effects were calculated with a Bonferroni correction for multiple testing. Each datapoint is representative of the mean value for a single experiment, and the standard error of the mean

(SEM) is indicated, if not stated differently. If given, intensity values represent the mean ± SEM. Exceptions were stated in the figure legends.

Bibliography

Allen, D. L., Harrison, B. C., Maass, A., Bell, M. L., Byrnes, W. C., & Leinwand, L. A. (2001). Cardiac and skeletal muscle adaptations to voluntary wheel running in the mouse. *Journal of Applied Physiology*, *90*(5), 1900–1908. https://doi.org/10.1152/jappl.2001.90.5.1900

Altrock, W. D., tom Dieck, S., Sokolov, M., Meyer, A. C., Sigler, A., Brakebusch, C., Fässler, R., Richter, K., Boeckers, T. M., Potschka, H., Brandt, C., Löscher, W., Grimberg, D., Dresbach, T., Hempelmann, A., Hassan, H., Balschun, D., Frey, J. U., Brandstätter, J. H., … Gundelfinger, E. D. (2003). Functional Inactivation of a Fraction of Excitatory Synapses in Mice Deficient for the Active Zone Protein Bassoon. *Neuron*, *37*(5), 787–800. https://doi.org/10.1016/S0896-6273(03)00088-6

Alvisi, G., Paolini, L., Contarini, A., Zambarda, C., Di Antonio, V., Colosini, A., Mercandelli, N., Timmoneri, M., Palù, G., Caimi, L., Ricotta, D., & Radeghieri, A. (2018). Intersectin goes nuclear: Secret life of an endocytic protein. *Biochemical Journal*, *475*(8), 1455–1472. https://doi.org/10.1042/BCJ20170897

Ashley, C. T., Wilkinson, K. D., Reines, D., & Warren, S. T. (1993). FMR1 Protein: Conserved RNP Family Domains and Selective RNA Binding. *Science*, *262*(5133), 563–566. https://doi.org/10.1126/science.7692601

Augustin, V. (2023). *The APP adaptor protein family Fe65 regulates neuronal outgrowth and spine plasticity by orchestrating actin dynamics*. Technische Universität Kaiserslautern.

Balice-Gordon, R., Breedlove, S., Bernstein, S., & Lichtmanl, J. (1990). Neuromuscular Junctions Shrink and Expand as Muscle Fiber Size Is Manipulated: In viva Observations in the Androgen-Sensitive Bulbocavernosus Muscle of Mice. *Journal of Neuroscience*, *10*(3), 2660–2671. https://doi.org/10.1523/JNEUROSCI.10-08-02660.1990

Balice-Gordon, R. J., & Lichtman, J. W. (1990). In vivo visualization of the growth of pre- and postsynaptic elements of neuromuscular junctions in the mouse. *Journal of Neuroscience*, *10*(3), 894–908. https://doi.org/10.1523/JNEUROSCI.10-03-00894.1990

Baptista, M. A. P., & Westerberg, L. S. (2017). Activation of compensatory pathways via Rac2 in the absence of the Cdc42 effector Wiskott-Aldrich syndrome protein in Dendritic cells. *Small GTPases*, *10*(2), 81–88. https://doi.org/10.1080/21541248.2016.1275363

Batista, A. F. R., Martínez, J. C., & Hengst, U. (2017). Intra-axonal Synthesis of SNAP25 Is Required for the Formation of Presynaptic Terminals. *Cell Reports*, *20*(13), 3085–3098. https://doi.org/10.1016/j.celrep.2017.08.097

Berg, J. M., Lee, C., Chen, L., Galvan, L., Cepeda, C., Chen, J. Y., Peñagarikano, O., Stein, J. L., Li, A., Oguro-Ando, A., Miller, J. A., Vashisht, A. A., Starks, M. E., Kite, E. P., Tam, E., Gdalyahu, A., Al-Sharif, N. B., Burkett, Z. D., White, S. A., … Geschwind, D. H. (2015). JAKMIP1, a Novel Regulator of Neuronal Translation, Modulates Synaptic Function and Autistic-like Behaviors in Mouse. *Neuron*, *88*(6), 1173–1191. https://doi.org/10.1016/j.neuron.2015.10.031

Bitsikas, V., Corrêa, I. R., Jr, & Nichols, B. J. (2014). Clathrin-independent pathways do not contribute significantly to endocytic flux. *eLife*, *3*, e03970. https://doi.org/10.7554/eLife.03970

Blundell, J., Blaiss, C. A., Etherton, M. R., Espinosa, F., Tabuchi, K., Walz, C., Bolliger, M. F., Südhof, T. C., & Powell, C. M. (2010). Neuroligin-1 Deletion Results in Impaired Spatial

Memory and Increased Repetitive Behavior. *Journal of Neuroscience*, *30*(6), 2115–2129. https://doi.org/10.1523/JNEUROSCI.4517-09.2010

Brew, H. M., Gittelman, J. X., Silverstein, R. S., Hanks, T. D., Demas, V. P., Robinson, L. C., Robbins, C. A., Mckee-johnson, J., Chiu, S. Y., Messing, A., & Tempel, B. L. (2007). Seizures and Reduced Life Span in Mice Lacking the Potassium Channel Subunit Kv1. 2 , but Hypoexcitability and Enlarged Kv1 Currents in Auditory Neurons. *Journal of Neurophysiology*, *93*(3), 1501–1525. https://doi.org/10.1152/jn.00640.2006.Genes

Briguet, A., Courdier-Fruh, I., Foster, M., Meier, T., & Magyar, J. P. (2004). Histological parameters for the quantitative assessment of muscular dystrophy in the *mdx*-mouse. *Neuromuscular Disorders*, *14*(10), 675–682. https://doi.org/10.1016/j.nmd.2004.06.008

Bruel, A. L., Vitobello, A., Thiffault, I., Manwaring, L., Willing, M., Agrawal, P. B., Bayat, A., Kitzler, T. M., Brownstein, C. A., Genetti, C. A., Gonzalez-Heydrich, J., Jayakar, P., Zyskind, J. W., Zhu, Z., Vachet, C., Wilson, G. R., Pruniski, B., Goyette, A. M., Duffourd, Y., … Faivre, L. (2022). ITSN1: A novel candidate gene involved in autosomal dominant neurodevelopmental disorder spectrum. *European Journal of Human Genetics*, *30*(1), 111–116. https://doi.org/10.1038/s41431-021-00985-9

Bulfield, G., Siller, W. G., Wight, P. A., & Moore, K. J. (1984). X chromosome-linked muscular dystrophy (mdx) in the mouse. *Proceedings of the National Academy of Sciences*, *81*(4), 1189–1192. https://doi.org/10.1073/pnas.81.4.1189

Burden, S. J., Depalma, R. L., & Gottesman, G. S. (1983). Crosslinking of proteins in acetylcholine receptor-rich membranes: Association between the β-subunit and the 43 kd subsynaptic protein. *Cell*, *35*(3, Part 2), 687–692. https://doi.org/10.1016/0092-8674(83)90101-0

Cajigas, I. J., Tushev, G., Will, T. J., tom Dieck, S., Fuerst, N., & Schuman, E. M. (2012). The Local Transcriptome in the Synaptic Neuropil Revealed by Deep Sequencing and High-Resolution Imaging. *Neuron*, *74*(3), 453–466. https://doi.org/10.1016/j.neuron.2012.02.036

Carr, J. C., Voskuil, C. C., Andrushko, J. W., MacLennan, R. J., DeFreitas, J. M., Stock, M. S., & Farthing, J. P. (2025). Cross-education attenuates muscle weakness and facilitates strength recovery after orthopedic immobilization in females: A pilot study. *Physiological Reports*, *13*(8), e70329. https://doi.org/10.14814/phy2.70329

Chen, S., Wang, J., Cicek, E., Roeder, K., Yu, H., & Devlin, B. (2020). De novo missense variants disrupting protein–protein interactions affect risk for autism through gene co-expression and protein networks in neuronal cell types. *Molecular Autism*, *11*(1), 76. https://doi.org/10.1186/s13229-020-00386-7

Chen, X., Fansler, M. M., Janjoš, U., Ule, J., & Mayr, C. (2024). The FXR1 network acts as a signaling scaffold for actomyosin remodeling. *Cell*, *187*(18), 5048-5063.e25. https://doi.org/10.1016/j.cell.2024.07.015

Chen, Y., Guo, L., Han, M., Zhang, S., Chen, Y., Zou, J., Bai, S., Cheng, G., & Zeng, Y. (2022). Cerebellum neuropathology and motor skill deficits in fragile X syndrome. *International Journal of Developmental Neuroscience*, *82*(7), 557–568. https://doi.org/10.1002/jdn.10217

Cheng, D., Hoogenraad, C. C., Rush, J., Ramm, E., Schlager, M. A., Duong, D. M., Xu, P., Wijayawardana, S. R., Hanfelt, J., Nakagawa, T., Sheng, M., & Peng, J. (2006). Relative and Absolute Quantification of Postsynaptic Density Proteome Isolated from Rat Forebrain and Cerebellum*S. *Molecular & Cellular Proteomics*, *5*(6), 1158–1170. https://doi.org/10.1074/mcp.D500009-MCP200

Cheng, L., Yung, A., Covarrubias, M., & Radice, G. L. (2011). Cortactin Is Required for N-cadherin Regulation of Kv1.5 Channel Function*. *Journal of Biological Chemistry*, *286*(23), 20478–20489. https://doi.org/10.1074/jbc.M111.218560

Cho, K.-O., Hunt, C. A., & Kennedy, M. B. (1992). The rat brain postsynaptic density fraction contains a homolog of the drosophila discs-large tumor suppressor protein. *Neuron*, *9*(5), 929–942. https://doi.org/10.1016/0896-6273(92)90245-9

Choi, Y.-J., & Lee, S.-G. (2012). The DEAD-box RNA helicase DDX3 interacts with DDX5, co-localizes with it in the cytoplasm during the G2/M phase of the cycle, and affects its shuttling during mRNP export. *Journal of Cellular Biochemistry*, *113*(3), 985–996. https://doi.org/10.1002/jcb.23428

Chyung, E., LeBlanc, H. F., Fallon, J. R., & Akins, M. R. (2018). Fragile X granules are a family of axonal ribonucleoprotein particles with circuit-dependent protein composition and mRNA cargos. *Journal of Comparative Neurology*, *526*(1), 96–108. https://doi.org/10.1002/cne.24321

Cingolani, L. A., & Goda, Y. (2008). Actin in action: The interplay between the actin cytoskeleton and synaptic efficacy. *Nature Reviews Neuroscience*, *9*(5), 344–356. https://doi.org/10.1038/nrn2373

Cioni, J.-M., Lin, J. Q., Holtermann, A. V., Koppers, M., Jakobs, M. A. H., Azizi, A., Turner-Bridger, B., Shigeoka, T., Franze, K., Harris, W. A., & Holt, C. E. (2019). Late Endosomes Act as mRNA Translation Platforms and Sustain Mitochondria in Axons. *Cell*, *176*(1), 56-72.e15. https://doi.org/10.1016/j.cell.2018.11.030

Coffman, K. A., Dum, R. P., & Strick, P. L. (2011). Cerebellar vermis is a target of projections from the motor areas in the cerebral cortex. *Proceedings of the National Academy of Sciences*, *108*(38), 16068–16073. https://doi.org/10.1073/pnas.1107904108

Cook, D., Nuro, E., Jones, E. V., Altimimi, H. F., Farmer, W. T., Gandin, V., Hanna, E., Zong, R., Barbon, A., Nelson, D. L., Topisirovic, I., Rochford, J., Stellwagen, D., Béïque, J.-C., & Murai, K. K. (2014). FXR1P Limits Long-Term Memory, Long-Lasting Synaptic Potentiation, and De Novo GluA2 Translation. *Cell Reports*, *9*(4), 1402–1416. https://doi.org/10.1016/j.celrep.2014.10.028

Corbalan-Garcia, S., & Gómez-Fernández, J. C. (2014). Signaling through C2 domains: More than one lipid target. *Biochimica et Biophysica Acta (BBA) - Biomembranes*, *1838*(6), 1536–1547. https://doi.org/10.1016/j.bbamem.2014.01.008

Cosen-Binker, L. I., & Kapus, A. (2006). Cortactin: The Gray Eminence of the Cytoskeleton. *Physiology*, *21*(5), 352–361. https://doi.org/10.1152/physiol.00012.2006

Cremona, O., Di Paolo, G., Wenk, M. R., Lüthi, A., Kim, W. T., Takei, K., Daniell, L., Nemoto, Y., Shears, S. B., Flavell, R. A., McCormick, D. A., & De Camilli, P. (1999). Essential Role of Phosphoinositide Metabolism in Synaptic Vesicle Recycling. *Cell*, *99*(2), 179–188. https://doi.org/10.1016/S0092-8674(00)81649-9

da Silva, S. H., Felippin, M. R., de Oliveira Medeiros, L., Hedin-Pereira, C., & Nogueira-Campos, A. A. (2025). A scoping review of the motor impairments in autism spectrum disorder. *Neuroscience & Biobehavioral Reviews*, *169*, 106002. https://doi.org/10.1016/j.neubiorev.2025.106002

D'Adamo, M. C., Liantonio, A., Conte, E., Pessia, M., & Imbrici, P. (2020). Ion Channels Involvement in Neurodevelopmental Disorders. *Neuroscience*, *440*, 337–359. https://doi.org/10.1016/j.neuroscience.2020.05.032

Dai, H., Shen, N., Araç, D., & Rizo, J. (2007). A Quaternary SNARE–Synaptotagmin–Ca2+–Phospholipid Complex in Neurotransmitter Release. *Journal of Molecular Biology*, *367*(3), 848–863. https://doi.org/10.1016/j.jmb.2007.01.040

Dardenne, E., Polay Espinoza, M., Fattet, L., Germann, S., Lambert, M.-P., Neil, H., Zonta, E., Mortada, H., Gratadou, L., Deygas, M., Chakrama, F. Z., Samaan, S., Desmet, F.-O., Tranchevent, L.-C., Dutertre, M., Rimokh, R., Bourgeois, C. F., & Auboeuf, D. (2014). RNA Helicases DDX5 and DDX17 Dynamically Orchestrate Transcription, miRNA, and Splicing Programs in Cell Differentiation. *Cell Reports*, *7*(6), 1900–1913. https://doi.org/10.1016/j.celrep.2014.05.010

Darnell, J. C., Van Driesche, S. J., Zhang, C., Hung, K. Y. S., Mele, A., Fraser, C. E., Stone, E. F., Chen, C., Fak, J. J., Chi, S. W., Licatalosi, D. D., Richter, J. D., & Darnell, R. B. (2011). FMRP stalls ribosomal translocation on mRNAs linked to synaptic function and autism. *Cell*, *146*(2), 247–261. https://doi.org/10.1016/j.cell.2011.06.013

Das, M., Scappini, E., Martin, N. P., Wong, K. A., Dunn, S., Chen, Y.-J., Miller, S. L. H., Domin, J., & O'Bryan, J. P. (2007). Regulation of Neuron Survival through an Intersectin-Phosphoinositide 3′-Kinase C2β-AKT Pathway. *Molecular and Cellular Biology*, *27*(22), 7906–7917. https://doi.org/10.1128/MCB.01369-07

Day, K. J., Kago, G., Wang, L., Richter, J. B., Hayden, C. C., Lafer, E. M., & Stachowiak, J. C. (2021). Liquid-like protein interactions catalyse assembly of endocytic vesicles. *Nature Cell Biology*, *23*(4), 366–376. https://doi.org/10.1038/s41556-021-00646-5

De Souza, R. W. A., Aguiar, A. F., Carani, F. R., Campos, G. E. R., Padovani, C. R., & Silva, M. D. P. (2011). High-Intensity Resistance Training with Insufficient Recovery Time Between Bouts Induce Atrophy and Alterations in Myosin Heavy Chain Content in Rat Skeletal Muscle. *The Anatomical Record*, *294*(8), 1393–1400. https://doi.org/10.1002/ar.21428

Delgado-Ramírez, M., & Rodríguez-Menchaca, A. A. (2019). Cytoskeleton disruption affects Kv2.1 channel function and its modulation by PIP2. *The Journal of Physiological Sciences*, *69*(3), 513–521. https://doi.org/10.1007/s12576-019-00671-y

Demirel, H. A., Powers, S. K., Naito, H., Hughes, M., & Coombes, J. S. (1999). Exercise-induced alterations in skeletal muscle myosin heavy chain phenotype: Dose-response relationship. *Journal of Applied Physiology*, *86*(3), 1002–1008. https://doi.org/10.1152/jappl.1999.86.3.1002

Deng, L., Kaeser, P. S., Xu, W., & Südhof, T. C. (2011). RIM Proteins Activate Vesicle Priming by Reversing Autoinhibitory Homodimerization of Munc13. *Neuron*, *69*(2), 317–331. https://doi.org/10.1016/j.neuron.2011.01.005

Desaki, J., & Uehara, Y. (1981). The overall morphology of neuromuscular junctions as revealed by scanning electron microscopy. *Journal of Neurocytology*, *10*(1), 101–110. https://doi.org/10.1007/BF01181747

Diebold, B. A., Fowler, B., Lu, J., Dinauer, M. C., & Bokoch, G. M. (2004). Antagonistic Cross-talk between Rac and Cdc42 GTPases Regulates Generation of Reactive Oxygen Species*. *Journal of Biological Chemistry*, *279*(27), 28136–28142. https://doi.org/10.1074/jbc.M313891200

Diering, G. H., & Huganir, R. L. (2018). The AMPA Receptor Code of Synaptic Plasticity. *Neuron*, *100*(2), 314–329. https://doi.org/10.1016/j.neuron.2018.10.018

Dodson, P. D., Billups, B., Rusznák, Z., Szucs, G., Barker, M. C., & Forsythe, I. D. (2003). Presynaptic Rat Kv1.2 Channels Suppress Synaptic Terminal Hyperexcitability

Following Action Potential Invasion. *The Journal of Physiology*, *550*(1), 27–33. https://doi.org/10.1113/jphysiol.2003.046250

D'Souza, M. N., Ramakrishna, S., Radhakrishna, B. K., Jhaveri, V., Ravindran, S., Yeramala, L., Nair, D., Palakodeti, D., & Muddashetty, R. S. (2022). Function of FMRP Domains in Regulating Distinct Roles of Neuronal Protein Synthesis. *Molecular Neurobiology*, *59*(12), 7370–7392. https://doi.org/10.1007/s12035-022-03049-1

Dubuisson, N., Versele, R., Planchon, C., Selvais, C. M., Noel, L., Abou-Samra, M., & Davis-López de Carrizosa, M. A. (2022). Histological Methods to Assess Skeletal Muscle Degeneration and Regeneration in Duchenne Muscular Dystrophy. *International Journal of Molecular Sciences*, *23*(24). https://doi.org/10.3390/ijms232416080

Dudman, J. T., & Krakauer, J. W. (2016). The basal ganglia: From motor commands to the control of vigor. *Current Opinion in Neurobiology*, *37*, 158–166. https://doi.org/10.1016/j.conb.2016.02.005

Duron, B., Jung-Caillol, M. C., & Marlot, D. (1978). Myelinated nerve fiber supply and muscle spindles in the respiratory muscles of cat: Quantitative study. *Anatomy and Embryology*, *152*(2), 171–192. https://doi.org/10.1007/BF00315923

Egorov, M., & Polishchuk, R. (2019). Identification of CDC42 Effectors Operating in FGD1-Dependent Trafficking at the Golgi. *Frontiers in Cell and Developmental Biology*, *7*. https://doi.org/10.3389/fcell.2019.00007

El Fatimy, R., Davidovic, L., Tremblay, S., Jaglin, X., Dury, A., Robert, C., De Koninck, P., & Khandjian, E. W. (2016). Tracking the Fragile X Mental Retardation Protein in a Highly Ordered Neuronal RiboNucleoParticles Population: A Link between Stalled Polyribosomes and RNA Granules. *PLoS Genetics*, *12*(7), 1–31. https://doi.org/10.1371/journal.pgen.1006192

Faruq, M., Srivastava, A. K., Suroliya, V., Kumar, D., Garg, A., Shukla, G., & Behari, M. (2014). Identification of FXTAS presenting with SCA 12 like phenotype in India. *Parkinsonism & Related Disorders*, *20*(10), 1089–1093. https://doi.org/10.1016/j.parkreldis.2014.07.001

Feng, W., & Zhang, M. (2009). Organization and dynamics of PDZ-domain-related supramodules in the postsynaptic density. *Nature Reviews Neuroscience*, *10*(2), 87–99. https://doi.org/10.1038/nrn2540

Feng, Y., Gutekunst, C.-A., Eberhart, D. E., Yi, H., Warren, S. T., & Hersch, S. M. (1997). Fragile X Mental Retardation Protein: Nucleocytoplasmic Shuttling and Association with Somatodendritic Ribosomes. *Journal of Neuroscience*, *17*(5), 1539–1547. https://doi.org/10.1523/JNEUROSCI.17-05-01539.1997

Fournier, K. A., Hass, C. J., Naik, S. K., Lodha, N., & Cauraugh, J. H. (2010). Motor Coordination in Autism Spectrum Disorders: A Synthesis and Meta-Analysis. *Journal of Autism and Developmental Disorders*, *40*(10), 1227–1240. https://doi.org/10.1007/s10803-010-0981-3

Friesland, A., Zhao, Y., Chen, Y.-H., Wang, L., Zhou, H., & Lu, Q. (2013). Small molecule targeting Cdc42–intersectin interaction disrupts Golgi organization and suppresses cell motility. *Proceedings of the National Academy of Sciences*, *110*(4), 1261–1266. https://doi.org/10.1073/pnas.1116051110

Galvez, R., & Greenough, W. T. (2005). Sequence of abnormal dendritic spine development in primary somatosensory cortex of a mouse model of the fragile X mental retardation syndrome. *American Journal of Medical Genetics Part A*, *135A*(2), 155–160. https://doi.org/10.1002/ajmg.a.30709

Gardiol, A., Racca, C., & Triller, A. (1999). Dendritic and Postsynaptic Protein Synthetic Machinery. *Journal of Neuroscience*, *19*(1), 168–179. https://doi.org/10.1523/JNEUROSCI.19-01-00168.1999

Gautam, M., Noakes, P. G., Moscoso, L., Rupp, F., Scheller, R. H., Merlie, J. P., & Sanes, J. R. (1996). Defective Neuromuscular Synaptogenesis in Agrin-Deficient Mutant Mice. *Cell*, *85*(4), 525–535. https://doi.org/10.1016/S0092-8674(00)81253-2

Geißler, V., Altmeyer, S., Stein, B., Uhlmann-Schiffler, H., & Stahl, H. (2013). The RNA helicase Ddx5/p68 binds to hUpf3 and enhances NMD of Ddx17/p72 and Smg5 mRNA. *Nucleic Acids Research*, *41*(16), 7875–7888. https://doi.org/10.1093/nar/gkt538

Gerth, F., Jäpel, M., Pechstein, A., Kochlamazashvili, G., Lehmann, M., Puchkov, D., Onofri, F., Benfenati, F., Nikonenko, A. G., Fredrich, K., Shupliakov, O., Maritzen, T., Freund, C., & Haucke, V. (2017). Intersectin associates with synapsin and regulates its nanoscale localization and function. *Proceedings of the National Academy of Sciences of the United States of America*, *114*(45), 12057–12062. https://doi.org/10.1073/pnas.1715341114

Gerth, F., Jäpel, M., Sticht, J., Kuropka, B., Schmitt, X. J., Driller, J. H., Loll, B., Wahl, M. C., Pagel, K., Haucke, V., & Freund, C. (2019). Exon Inclusion Modulates Conformational Plasticity and Autoinhibition of the Intersectin 1 SH3A Domain. *Structure*, *27*(6), 977-987.e5. https://doi.org/10.1016/j.str.2019.03.020

Glynn, D., Drew, C. J., Reim, K., Brose, N., & Morton, A. J. (2005). Profound ataxia in complexin I knockout mice masks a complex phenotype that includes exploratory and habituation deficits. *Human Molecular Genetics*, *14*(16), 2369–2385. https://doi.org/10.1093/hmg/ddi239

González-Rodríguez, P., Zampese, E., Stout, K. A., Guzman, J. N., Ilijic, E., Yang, B., Tkatch, T., Stavarache, M. A., Wokosin, D. L., Gao, L., Kaplitt, M. G., López-Barneo, J., Schumacker, P. T., & Surmeier, D. J. (2021). Disruption of mitochondrial complex I induces progressive parkinsonism. *Nature*, *599*(7886), 650–656. https://doi.org/10.1038/s41586-021-04059-0

Gonzalo, S., Greentree, W. K., & Linder, M. E. (1999). SNAP-25 Is Targeted to the Plasma Membrane through a Novel Membrane-binding Domain*. *Journal of Biological Chemistry*, *274*(30), 21313–21318. https://doi.org/10.1074/jbc.274.30.21313

Gray, E. G., & Whittaker, V. P. (1962). The isolation of nerve endings from brain. *Journal of Anatomy*, *96*(Pt 1), 79-88.8.

Graybiel, A. M. (1998). The Basal Ganglia and Chunking of Action Repertoires. *Neurobiology of Learning and Memory*, *70*(1), 119–136. https://doi.org/10.1006/nlme.1998.3843

Greco, C. M., Navarro, C. S., Hunsaker, M. R., Maezawa, I., Shuler, J. F., Tassone, F., Delany, M., Au, J. W., Berman, R. F., Jin, L.-W., Schumann, C., Hagerman, P. J., & Hagerman, R. J. (2011). Neuropathologic features in the hippocampus and cerebellum of three older men with fragile X syndrome. *Molecular Autism*, *2*(1), 2. https://doi.org/10.1186/2040-2392-2-2

Grillner, S., Robertson, B., & Stephenson-Jones, M. (2013). The evolutionary origin of the vertebrate basal ganglia and its role in action selection. *The Journal of Physiology*, *591*(22), 5425–5431. https://doi.org/10.1113/jphysiol.2012.246660

Gryaznova, T., Gubar, O., Burdyniuk, M., Kropyvko, S., & Rynditch, A. (2018). WIP/ITSN1 complex is involved in cellular vesicle trafficking and formation of filopodia-like protrusions. *Gene*, *674*, 49–56. https://doi.org/10.1016/j.gene.2018.06.078

Gryaznova, T., Kropyvko, S., Burdyniuk, M., Gubar, O., Kryklyva, V., Tsyba, L., & Rynditch, A. (2015). Intersectin adaptor proteins are associated with actin-regulating protein WIP

in invadopodia. *Cellular Signalling*, *27*(7), 1499–1508. https://doi.org/10.1016/j.cellsig.2015.03.006

Gubar, O., Morderer, D., Tsyba, L., Croisé, P., Houy, S., Ory, S., Gasman, S., & Rynditch, A. (2013). Intersectin: The crossroad between vesicle exocytosis and endocytosis. *Frontiers in Endocrinology*, *4*(AUG). https://doi.org/10.3389/fendo.2013.00109

Guerreiro, M. M., Camargo, E. E., Kato, M., Marques-De-Faria, A. P., Ciasca, S. M., Guerreiro, C. a. M., Menezes Netto, J. R., & Moura-Ribeiro, M. V. L. (1998). Fragile X syndrome: Clinical, electroencephalographic and neuroimaging characteristics. *Arquivos de Neuro-Psiquiatria*, *56*, 18–23. https://doi.org/10.1590/S0004-282X1998000100003

Guipponi, M., Scott, H. S., Chen, H., Schebesta, A., Rossier, C., & Antonarakis, S. E. (1998). Two Isoforms of a Human Intersectin (ITSN) Protein Are Produced by Brain-Specific Alternative Splicing in a Stop Codon. *Genomics*, *53*(3), 369–376. https://doi.org/10.1006/geno.1998.5521

Hafner, A.-S., Donlin-Asp, P. G., Leitch, B., Herzog, E., & Schuman, E. M. (2019). Local protein synthesis is a ubiquitous feature of neuronal pre- and postsynaptic compartments. *Science*, *364*(6441), eaau3644. https://doi.org/10.1126/science.aau3644

Hagerman, P. J., & Hagerman, R. J. (2015). Fragile X–associated tremor/ataxia syndrome. *Annals of the New York Academy of Sciences*, *1338*(1), 58–70. https://doi.org/10.1111/nyas.12693

Hagerman, R. J., Coffey, S. M., Maselli, R., Soontarapornchai, K., Brunberg, J. A., Leehey, M. A., Zhang, L., Gane, L. W., Fenton-Farrell, G., Tassone, F., & Hagerman, P. J. (2007). Neuropathy as a presenting feature in fragile X-associated tremor/ataxia syndrome. *American Journal of Medical Genetics Part A*, *143A*(19), 2256–2260. https://doi.org/10.1002/ajmg.a.31920

Hajdu, P., Martin, G. V., Chimote, A. A., Szilagyi, O., Takimoto, K., & Conforti, L. (2015). The C-terminus SH3-binding domain of Kv1.3 is required for the actin-mediated immobilization of the channel via cortactin. *Molecular Biology of the Cell*, *26*(9), 1640–1651. https://doi.org/10.1091/mbc.E14-07-1195

Hall, D. A., Birch, R. C., Anheim, M., Jønch, A. E., Pintado, E., O'Keefe, J., Trollor, J. N., Stebbins, G. T., Hagerman, R. J., Fahn, S., Berry-Kravis, E., & Leehey, M. A. (2014). Emerging topics in FXTAS. *Journal of Neurodevelopmental Disorders*, *6*(1), 31. https://doi.org/10.1186/1866-1955-6-31

Hallermann, S., Fejtova, A., Schmidt, H., Weyhersmüller, A., Silver, R. A., Gundelfinger, E. D., & Eilers, J. (2010). Bassoon Speeds Vesicle Reloading at a Central Excitatory Synapse. *Neuron*, *68*(4), 710–723. https://doi.org/10.1016/j.neuron.2010.10.026

Hammers, D. W., Hart, C. C., Matheny, M. K., Wright, L. A., Armellini, M., Barton, E. R., & Sweeney, H. L. (2020). The D2.mdx mouse as a preclinical model of the skeletal muscle pathology associated with Duchenne muscular dystrophy. *Scientific Reports*, *10*(1), 14070. https://doi.org/10.1038/s41598-020-70987-y

Hanus, C., Geptin, H., Tushev, G., Garg, S., Alvarez-Castelao, B., Sambandan, S., Kochen, L., Hafner, A.-S., Langer, J. D., & Schuman, E. M. (2016). Unconventional secretory processing diversifies neuronal ion channel properties. *eLife*, *5*, e20609. https://doi.org/10.7554/eLife.20609

Hara, T., Nakamura, K., Matsui, M., Yamamoto, A., Nakahara, Y., Suzuki-Migishima, R., Yokoyama, M., Mishima, K., Saito, I., Okano, H., & Mizushima, N. (2006). Suppression of basal autophagy in neural cells causes neurodegenerative disease in mice. *Nature*, *441*(7095), 885–889. https://doi.org/10.1038/nature04724

Harding, A. E. (1983). CLASSIFICATION OF THE HEREDITARY ATAXIAS AND PARAPLEGIAS. *The Lancet*, *321*(8334), 1151–1155. https://doi.org/10.1016/S0140-6736(83)92879-9

Harris, J. B., & Ribchester, R. R. (1979). The relationship between end-plate size and transmitter release in normal and dystrophic muscles of the mouse. *The Journal of Physiology*, *296*(1), 245–265. https://doi.org/10.1113/jphysiol.1979.sp013003

Harvey, A. L. (2001). Twenty years of dendrotoxins. *Toxicon*, *39*(1), 15–26. https://doi.org/10.1016/S0041-0101(00)00162-8

Hattan, D., Nesti, E., Cachero, T. G., & Morielli, A. D. (2002). Tyrosine Phosphorylation of Kv1. 2 Modulates Its Interaction with the Actin-binding Protein Cortactin *. *Journal of Biological Chemistry*, *277*(41), 38596–38606. https://doi.org/10.1074/jbc.M205005200

Henne, W. M., Boucrot, E., Meinecke, M., Evergren, E., Vallis, Y., Mittal, R., & McMahon, H. T. (2010). FCHo Proteins Are Nucleators of Clathrin-Mediated Endocytosis. *Science*, *328*(5983), 1281–1284. https://doi.org/10.1126/science.1188462

Herrmann, S., Ninkovic, M., Kohl, T., Lörinczi, É., & Pardo, L. A. (2012). Cortactin controls surface expression of the voltage-gated potassium channel KV10.1. *Journal of Biological Chemistry*, *287*(53), 44151–44163. https://doi.org/10.1074/jbc.M112.372540

Herson, P. S., Virk, M., Rustay, N. R., Bond, C. T., Crabbe, J. C., Adelman, J. P., & Maylie, J. (2003). A mouse model of episodic ataxia type-1. *Nature Neuroscience*, *6*(4), 378–383. https://doi.org/10.1038/nn1025

Hirokawa, N. (1989). The arrangement of actin filaments in the postsynaptic cytoplasm of the cerebellar cortex revealed by quick-freeze deep-etch electron microscopy. *Neuroscience Research*, *6*(3), 269–275. https://doi.org/10.1016/0168-0102(89)90066-7

Hotulainen, P., & Hoogenraad, C. C. (2010). Actin in dendritic spines: Connecting dynamics to function. *Journal of Cell Biology*, *189*(4), 619–629. https://doi.org/10.1083/jcb.201003008

Hou, P., Estrada, L., Kinley, A. W., Parsons, J. T., Vojtek, A. B., & Gorski, J. L. (2003). Fgd1, the Cdc42 GEF responsible for Faciogenital Dysplasia, directly interacts with cortactin and mAbp1 to modulate cell shape. *Human Molecular Genetics*, *12*(16), 1981–1993. https://doi.org/10.1093/hmg/ddg209

Huang, D. W., Sherman, B. T., & Lempicki, R. A. (2009). Systematic and integrative analysis of large gene lists using DAVID bioinformatics resources. *Nature Protocols*, *4*(1), 44–57. https://doi.org/10.1038/nprot.2008.211

Huber, K. M., Kayser, M. S., & Bear, M. F. (2000). Role for Rapid Dendritic Protein Synthesis in Hippocampal mGluR-Dependent Long-Term Depression. *Science*, *288*(5469), 1254–1256. https://doi.org/10.1126/science.288.5469.1254

Humphries, A. C., Donnelly, S. K., & Way, M. (2014). Cdc42 and the Rho GEF intersectin-1 collaborate with Nck to promote N-WASP-dependent actin polymerisation. *Journal of Cell Science*, *127*(3), 673–685. https://doi.org/10.1242/jcs.141366

Hunter, M. P., Nelson, M., Kurzer, M., Wang, X., Kryscio, R. J., Head, E., Pinna, G., & O'Bryan, J. P. (2011). Intersectin 1 contributes to phenotypes in vivo: Implications for Down's syndrome. *NeuroReport*, *22*(15), 767. https://doi.org/10.1097/WNR.0b013e32834ae348

Hussain, N. K., Jenna, S., Glogauer, M., Quinn, C. C., Wasiak, S., Guipponi, M., Antonarakis, S. E., Kay, B. K., Stossel, T. P., Lamarche-Vane, N., & McPherson, P. S. (2001). Endocytic protein intersectin-l regulates actin assembly via Cdc42 and N-WASP. *Nature Cell Biology*, *3*(10), 927–932. https://doi.org/10.1038/ncb1001-927

Hussain, N. K., Yamabhai, M., Ramjaun, A. R., Guy, A. M., Baranes, D., O'Bryan, J. P., Der, C. J., Kay, B. K., & McPherson, P. S. (1999). Splice variants of intersectin are components

of the endocytic machinery in neurons and nonneuronal cells. *Journal of Biological Chemistry*, *274*(22), 15671–15677. https://doi.org/10.1074/jbc.274.22.15671

Ivanov, A., Mikhailova, T., Eliseev, B., Yeramala, L., Sokolova, E., Susorov, D., Shuvalov, A., Schaffitzel, C., & Alkalaeva, E. (2016). PABP enhances release factor recruitment and stop codon recognition during translation termination. *Nucleic Acids Research*, *44*(16), 7766–7776. https://doi.org/10.1093/nar/gkw635

Jacquemont, S., Hagerman, R. J., Leehey, M., Grigsby, J., Zhang, L., Brunberg, J. A., Greco, C., Des Portes, V., Jardini, T., Levine, R., Berry-Kravis, E., Brown, W. T., Schaeffer, S., Kissel, J., Tassone, F., & Hagerman, P. J. (2003). Fragile X Premutation Tremor/Ataxia Syndrome: Molecular, Clinical, and Neuroimaging Correlates. *The American Journal of Human Genetics*, *72*(4), 869–878. https://doi.org/10.1086/374321

Jäpel, M., Gerth, F., Sakaba, T., Bacetic, J., Yao, L., Koo, S.-J., Maritzen, T., Freund, C., & Haucke, V. (2020). Intersectin-Mediated Clearance of SNARE Complexes Is Required for Fast Neurotransmission. *Cell Reports*, *30*(2), 409-420.e6. https://doi.org/10.1016/j.celrep.2019.12.035

Jeganathan, N., Predescu, D., Zhang, J., Sha, F., Bardita, C., Patel, M., Wood, S., Borgia, J. A., Balk, R. A., & Predescu, S. (2016). Rac1-mediated cytoskeleton rearrangements induced by intersectin-1s deficiency promotes lung cancer cell proliferation, migration and metastasis. *Molecular Cancer*, *15*(1), 59. https://doi.org/10.1186/s12943-016-0543-1

Jin, M., Iwamoto, Y., Shirazinejad, C., & Drubin, D. G. (2024). Intersectin1 promotes clathrin-mediated endocytosis by organizing and stabilizing endocytic protein interaction networks. *Cell Reports*, *43*(12), 114989. https://doi.org/10.1016/J.CELREP.2024.114989

Jones, R. A., Reich, C. D., Dissanayake, K. N., Kristmundsdottir, F., Findlater, G. S., Ribchester, R. R., Simmen, M. W., & Gillingwater, T. H. (2017). Correction to NMJ-morph reveals principal components of synaptic morphology influencing structure—Function relationships at the neuromuscular junction (Open Biology (2016) 6 (160240) DOI: 10.1098/rsob.160335). *Open Biology*, *7*(1). https://doi.org/10.1098/rsob.160240

Kaeser, P. S., Deng, L., Wang, Y., Dulubova, I., Liu, X., Rizo, J., & Südhof, T. C. (2011). RIM Proteins Tether Ca2+ Channels to Presynaptic Active Zones via a Direct PDZ-Domain Interaction. *Cell*, *144*(2), 282–295. https://doi.org/10.1016/j.cell.2010.12.029

Kanai, Y., Dohmae, N., & Hirokawa, N. (2004). Kinesin Transports RNA: Isolation and Characterization of an RNA-Transporting Granule. *Neuron*, *43*(4), 513–525. https://doi.org/10.1016/j.neuron.2004.07.022

Kandel, E. R., Barres, B. A., & Hudspeth, A. J. (2013). Nerve Cells, Neural Circuitry, and Behavior. In *Principles of neural science* (5th ed., pp. 21–38). McGraw-Hill Companies, Inc.

Kandel, E. R., & Siegelbaum, S. A. (2013). Signaling at the Nerve-Muscle Synapse: Directly Gated Transmission. In *Principles of neural science* (5th ed., pp. 189–209). McGraw-Hill Companies, Inc.

Kang, H., & Schuman, E. M. (1996). A Requirement for Local Protein Synthesis in Neurotrophin-Induced Hippocampal Synaptic Plasticity. *Science*, *273*(5280), 1402–1406. https://doi.org/10.1126/science.273.5280.1402

Kariya, S., Park, G.-H., Maeno-Hikichi, Y., Leykekhman, O., Lutz, C., Arkovitz, M. S., Landmesser, L. T., & Monani, U. R. (2008). Reduced SMN protein impairs maturation of the neuromuscular junctions in mouse models of spinal muscular atrophy. *Human Molecular Genetics*, *17*(16), 2552–2569. https://doi.org/10.1093/hmg/ddn156

Kerschensteiner, M., Reuter, M. S., Lichtman, J. W., & Misgeld, T. (2008). Ex vivo imaging of motor axon dynamics in murine triangularis sterni explants. *Nature Protocols*, *3*(10), 1645–1653. https://doi.org/10.1038/nprot.2008.160

Khayachi, A., Gwizdek, C., Poupon, G., Alcor, D., Chafai, M., Cassé, F., Maurin, T., Prieto, M., Folci, A., De Graeve, F., Castagnola, S., Gautier, R., Schorova, L., Loriol, C., Pronot, M., Besse, F., Brau, F., Deval, E., Bardoni, B., & Martin, S. (2018). Sumoylation regulates FMRP-mediated dendritic spine elimination and maturation. *Nature Communications*, *9*(1), 757. https://doi.org/10.1038/s41467-018-03222-y

Kinley, A. W., Weed, S. A., Weaver, A. M., Karginov, A. V., Bissonette, E., Cooper, J. A., & Parsons, J. T. (2003). Cortactin Interacts with WIP in Regulating Arp2/3 Activation and Membrane Protrusion. *Current Biology*, *13*(5), 384–393. https://doi.org/10.1016/S0960-9822(03)00107-6

Knowles, R. B., Sabry, J. H., Martone, M. E., Deerinck, T. J., Ellisman, M. H., Bassell, G. J., & Kosik, K. S. (1996). Translocation of RNA Granules in Living Neurons. *Journal of Neuroscience*, *16*(24), 7812–7820. https://doi.org/10.1523/JNEUROSCI.16-24-07812.1996

Koekkoek, S. K. E., Yamaguchi, K., Milojkovic, B. A., Dortland, B. R., Ruigrok, T. J. H., Maex, R., De Graaf, W., Smit, A. E., VanderWerf, F., Bakker, C. E., Willemsen, R., Ikeda, T., Kakizawa, S., Onodera, K., Nelson, D. L., Mientjes, E., Joosten, M., De Schutter, E., Oostra, B. A., … De Zeeuw, C. I. (2005). Deletion of *FMR1* in Purkinje Cells Enhances Parallel Fiber LTD, Enlarges Spines, and Attenuates Cerebellar Eyelid Conditioning in Fragile X Syndrome. *Neuron*, *47*(3), 339–352. https://doi.org/10.1016/j.neuron.2005.07.005

Koh, T.-W., Korolchuk, V. I., Wairkar, Y. P., Jiao, W., Evergren, E., Pan, H., Zhou, Y., Venken, K. J. T., Shupliakov, O., Robinson, I. M., O'Kane, C. J., & Bellen, H. J. (2007). Eps15 and Dap160 control synaptic vesicle membrane retrieval and synapse development. *Journal of Cell Biology*, *178*(2), 309–322. https://doi.org/10.1083/jcb.200701030

Koh, T.-W., Verstreken, P., & Bellen, H. J. (2004). Dap160/Intersectin Acts as a Stabilizing Scaffold Required for Synaptic Development and Vesicle Endocytosis. *Neuron*, *43*(2), 193–205. https://doi.org/10.1016/j.neuron.2004.06.029

Kohls, G., Yerys, B. E., & Schultz, R. T. (2014). Striatal Development in Autism: Repetitive Behaviors and the Reward Circuitry. *Biological Psychiatry*, *76*(5), 358–359. https://doi.org/10.1016/j.biopsych.2014.07.010

Koppers, M., Cagnetta, R., Shigeoka, T., Wunderlich, L. C., Vallejo-Ramirez, P., Lin, J. Q., Zhao, S., Jakobs, M. A. H., Dwivedy, A., Minett, M. S., Bellon, A., Kaminski, C., Harris, W. A., Flanagan, J. G., & Holt, C. E. (2019). Receptor-specific interactome as a hub for rapid cue-induced selective translation in axons. *eLife*, *8*. https://doi.org/10.7554/eLife.48718

Kovaleski, R. F., Callahan, J. W., Chazalon, M., Wokosin, D. L., Baufreton, J., & Bevan, M. D. (2020). Dysregulation of external globus pallidus-subthalamic nucleus network dynamics in parkinsonian mice during cortical slow-wave activity and activation. *The Journal of Physiology*, *598*(10), 1897–1927. https://doi.org/10.1113/JP279232

Kowalski, J. R., Egile, C., Gil, S., Snapper, S. B., Li, R., & Thomas, S. M. (2005). Cortactin regulates cell migration through activation of N-WASP. *Journal of Cell Science*, *118*(1), 79–87. https://doi.org/10.1242/jcs.01586

Kravitz, A. V., Freeze, B. S., Parker, P. R. L., Kay, K., Thwin, M. T., Deisseroth, K., & Kreitzer, A. C. (2010). Regulation of parkinsonian motor behaviours by optogenetic control of basal ganglia circuitry. *Nature*, *466*(7306), 622–626. https://doi.org/10.1038/nature09159

Kühn, U., & Pieler, T. (1996). XenopusPoly(A) Binding Protein: Functional Domains in RNA Binding and Protein – Protein Interaction. *Journal of Molecular Biology*, *256*(1), 20–30. https://doi.org/10.1006/jmbi.1996.0065

Kundu, K., Mann, M., Costa, F., & Backofen, R. (2014). MoDPepInt: An interactive web server for prediction of modular domain–peptide interactions. *Bioinformatics*, *30*(18), 2668–2669. https://doi.org/10.1093/bioinformatics/btu350

Kurochkina, N., & Guha, U. (2012). SH3 domains: Modules of protein–protein interactions. *Biophysical Reviews*, *5*(1), 29–39. https://doi.org/10.1007/s12551-012-0081-z

Lalonde, R., & Strazielle, C. (2007). Spontaneous and induced mouse mutations with cerebellar dysfunctions: Behavior and neurochemistry. *Brain Research*, *1140*, 51–74. https://doi.org/10.1016/j.brainres.2006.01.031

Lalonde, R., & Strazielle, C. (2011). Brain regions and genes affecting limb-clasping responses. *Brain Research Reviews*, *67*(1), 252–259. https://doi.org/10.1016/j.brainresrev.2011.02.005

Langen, M., Kas, M. J. H., Staal, W. G., van Engeland, H., & Durston, S. (2011). The neurobiology of repetitive behavior: Of mice…. *Neuroscience & Biobehavioral Reviews*, *35*(3), 345–355. https://doi.org/10.1016/j.neubiorev.2010.02.004

Lemmon, M. A. (2003). Phosphoinositide Recognition Domains. *Traffic*, *4*(4), 201–213. https://doi.org/10.1034/j.1600-0854.2004.00071.x

Liao, Y.-C., Fernandopulle, M. S., Wang, G., Choi, H., Hao, L., Drerup, C. M., Patel, R., Qamar, S., Nixon-Abell, J., Shen, Y., Meadows, W., Vendruscolo, M., Knowles, T. P. J., Nelson, M., Czekalska, M. A., Musteikyte, G., Gachechiladze, M. A., Stephens, C. A., Pasolli, H. A., … Ward, M. E. (2019). RNA Granules Hitchhike on Lysosomes for Long-Distance Transport, Using Annexin A11 as a Molecular Tether. *Cell*, *179*(1), 147-164.e20. https://doi.org/10.1016/j.cell.2019.08.050

Liaqat, K., Treat, K., Wilson, T. E., Conboy, E., & Vetrini, F. (2024). Further evidence of involvement of ITSN1 in autosomal dominant neurodevelopmental disorder. *Clinical Genetics*, *105*(4), 455–456. https://doi.org/10.1111/cge.14497

Ling, K. K. Y., Lin, M.-Y., Zingg, B., Feng, Z., & Ko, C.-P. (2010). Synaptic Defects in the Spinal and Neuromuscular Circuitry in a Mouse Model of Spinal Muscular Atrophy. *PLOS ONE*, *5*(11), e15457. https://doi.org/10.1371/journal.pone.0015457

Lua, B. L., & Low, B. C. (2005). Cortactin phosphorylation as a switch for actin cytoskeletal network and cell dynamics control. *FEBS Letters*, *579*(3), 577–585. https://doi.org/10.1016/j.febslet.2004.12.055

Lukas, F., Matthaeus, C., López-Hernández, T., Lahmann, I., Schultz, N., Lehmann, M., Puchkov, D., Pielage, J., Haucke, V., & Maritzen, T. (2024). Canonical and non-canonical integrin-based adhesions dynamically interconvert. *Nature Communications*, *15*(1), 2093. https://doi.org/10.1038/s41467-024-46381-x

Lukong, K. E., & Richard, S. (2008). Motor coordination defects in mice deficient for the Sam68 RNA-binding protein. *Behavioural Brain Research*, *189*(2), 357–363. https://doi.org/10.1016/j.bbr.2008.01.010

Majumder, M., Johnson, R. H., & Palanisamy, V. (2020). Fragile X-related protein family: A double-edged sword in neurodevelopmental disorders and cancer. *Critical Reviews in Biochemistry and Molecular Biology*, *55*(5), 409–424. https://doi.org/10.1080/10409238.2020.1810621

Malacombe, M., Ceridono, M., Calco, V., Chasserot-Golaz, S., McPherson, P. S., Bader, M., & Gasman, S. (2006). Intersectin-1L nucleotide exchange factor regulates secretory

granule exocytosis by activating Cdc42. *The EMBO Journal*, *25*(15), 3494–3503. https://doi.org/10.1038/sj.emboj.7601247

Mangus, D. A., Evans, M. C., & Jacobson, A. (2003). Poly(A)-binding proteins: Multifunctional scaffolds for the post-transcriptional control of gene expression. *Genome Biology*, *4*(7), 223. https://doi.org/10.1186/gb-2003-4-7-223

Marie, B., Sweeney, S. T., Poskanzer, K. E., Roos, J., Kelly, R. B., & Davis, G. W. (2004). Dap160/Intersectin Scaffolds the Periactive Zone to Achieve High-Fidelity Endocytosis and Normal Synaptic Growth. *Neuron*, *43*(2), 207–219. https://doi.org/10.1016/j.neuron.2004.07.001

Mariotti, C., Fancellu, R., & Di Donato, S. (2005). An overview of the patient with ataxia. *Journal of Neurology*, *252*(1814), 511–518. https://doi.org/10.1007/s00415-005-0814-z

Markowitz, J. E., Gillis, W. F., Beron, C. C., Neufeld, S. Q., Robertson, K., Bhagat, N. D., Peterson, R. E., Peterson, E., Hyun, M., Linderman, S. W., Sabatini, B. L., & Datta, S. R. (2018). The Striatum Organizes 3D Behavior via Moment-to-Moment Action Selection. *Cell*, *174*(1), 44-58.e17. https://doi.org/10.1016/j.cell.2018.04.019

Martina, J. A., Bonangelino, C. J., Aguilar, R. C., & Bonifacino, J. S. (2001). Stonin 2: An Adaptor-like Protein That Interacts with Components of the Endocytic Machinery. *Journal of Cell Biology*, *153*(5), 1111–1120. https://doi.org/10.1083/jcb.153.5.1111

Maruoka, N. D., Steele, D. F., Au, B. P.-Y., Dan, P., Zhang, X., Moore, E. D. W., & Fedida, D. (2000). α-Actinin-2 couples to cardiac Kv1.5 channels, regulating current density and channel localization in HEK cells. *FEBS Letters*, *473*(2), 188–194. https://doi.org/10.1016/S0014-5793(00)01521-0

Masnada, S., Hedrich, U. B. S., Gardella, E., Schubert, J., Kaiwar, C., Klee, E. W., Lanpher, B. C., Gavrilova, R. H., Synofzik, M., Bast, T., Gorman, K., King, M. D., Allen, N. M., Conroy, J., Ben Zeev, B., Tzadok, M., Korff, C., Dubois, F., Ramsey, K., … Rubboli, G. (2017). Clinical spectrum and genotype–phenotype associations of KCNA2-related encephalopathies. *Brain*, *140*(9), 2337–2354. https://doi.org/10.1093/brain/awx184

Mattina, S. R., Ng, S. Y., Mikhail, A. I., Stouth, D. W., Jornacion, C. E., Rebalka, I. A., Hawke, T. J., & Ljubicic, V. (2025). Volitional exercise elicits physiological and molecular improvements in the severe D2.mdx mouse model of Duchenne muscular dystrophy. *The Journal of Physiology*. https://doi.org/10.1113/JP286768

Matus, A. (1999). Postsynaptic actin and neuronal plasticity. *Current Opinion in Neurobiology*, *9*(5), 561–565. https://doi.org/10.1016/S0959-4388(99)00018-5

McArdle, J. J., Angaut-Petit, D., Mallart, A., Bournaud, R., Faille, L., & Brigant, J. L. (1981). Advantages of the triangularis sterni muscle of the mouse for investigations of synaptic phenomena. *Journal of Neuroscience Methods*, *4*(2), 109–115. https://doi.org/10.1016/0165-0270(81)90044-3

Méndez-Albelo, N. M., Sandoval, S. O., Xu, Z., & Zhao, X. (2024). An in-depth review of the function of RNA-binding protein FXR1 in neurodevelopment. *Cell and Tissue Research*, *398*(2), 63–77. https://doi.org/10.1007/s00441-024-03912-8

Merianda, T. T., Lin, A. C., Lam, J. S. Y., Vuppalanchi, D., Willis, D. E., Karin, N., Holt, C. E., & Twiss, J. L. (2009). A functional equivalent of endoplasmic reticulum and Golgi in axons for secretion of locally synthesized proteins. *Molecular and Cellular Neuroscience*, *40*(2), 128–142. https://doi.org/10.1016/j.mcn.2008.09.008

Mientjes, Edwin. J., Willemsen, R., Kirkpatrik, L. L., Nieuwenhuizen, I. M., Hoogeveen-Westerveld, M., Verweij, M., Reis, S., Bardone, B., Hoogeveen, A. T., Oostra, B. A., & Nelson, D. L. (2004). Fxr1 knockout mice show a striated muscle phenotype:

Implications for Fxr1p function in vivo. *Human Molecular Genetics*, *13*(13), 1291–1302. https://doi.org/10.1093/hmg/ddh150

Mikhaylova, M., Bera, S., Kobler, O., Frischknecht, R., & Kreutz, M. R. (2016). A Dendritic Golgi Satellite between ERGIC and Retromer. *Cell Reports*, *14*(2), 189–199. https://doi.org/10.1016/j.celrep.2015.12.024

Moon, I. S., Apperson, M. L., & Kennedy, M. B. (1994). The major tyrosine-phosphorylated protein in the postsynaptic density fraction is N-methyl-D-aspartate receptor subunit 2B. *Proceedings of the National Academy of Sciences*, *91*(9), 3954–3958. https://doi.org/10.1073/pnas.91.9.3954

Mostofsky, S. H., Mazzocco, M. M. M., Aakalu, G., Warsofsky, I. S., Denckla, M. B., & Reiss, A. L. (1998). Decreased cerebellar posterior vermis size in fragile X syndrome. *Neurology*, *50*(1), 121–130. https://doi.org/10.1212/WNL.50.1.121

Murdoch, J. D., Rostosky, C. M., Gowrisankaran, S., Arora, A. S., Soukup, S.-F., Vidal, R., Capece, V., Freytag, S., Fischer, A., Verstreken, P., Bonn, S., Raimundo, N., & Milosevic, I. (2016). Endophilin-A Deficiency Induces the Foxo3a-Fbxo32 Network in the Brain and Causes Dysregulation of Autophagy and the Ubiquitin-Proteasome System. *Cell Reports*, *17*(4), 1071–1086. https://doi.org/10.1016/j.celrep.2016.09.058

Nagaya, N., & Papazian, D. M. (1997). Potassium Channel ä and β Subunits Assemble in the Endoplasmic Reticulum*. *Journal of Biological Chemistry*, *272*(5), 3022–3027. https://doi.org/10.1074/jbc.272.5.3022

Napoli, I., Mercaldo, V., Boyl, P. P., Eleuteri, B., Zalfa, F., De Rubeis, S., Di Marino, D., Mohr, E., Massimi, M., Falconi, M., Witke, W., Costa-Mattioli, M., Sonenberg, N., Achsel, T., & Bagni, C. (2008). The Fragile X Syndrome Protein Represses Activity-Dependent Translation through CYFIP1, a New 4E-BP. *Cell*, *134*(6), 1042–1054. https://doi.org/10.1016/j.cell.2008.07.031

Narayanan, U., Nalavadi, V., Nakamoto, M., Pallas, D. C., Ceman, S., Bassell, G. J., & Warren, S. T. (2007). FMRP Phosphorylation Reveals an Immediate-Early Signaling Pathway Triggered by Group I mGluR and Mediated by PP2A. *Journal of Neuroscience*, *27*(52), 14349–14357. https://doi.org/10.1523/JNEUROSCI.2969-07.2007

Nesti, E., Everill, B., & Morielli, A. D. (2004). Endocytosis as a Mechanism for Tyrosine Kinase-dependent Suppression of a Voltage-gated Potassium Channel. *Molecular Biology of the Cell*, *15*(9), 4073–4088. https://doi.org/10.1091/mbc.e03-11-0788

Nishimura, T., Yamaguchi, T., Tokunaga, A., Hara, A., Hamaguchi, T., Kato, K., Iwamatsu, A., Okano, H., & Kaibuchi, K. (2006). Role of Numb in Dendritic Spine Development with a Cdc42 GEF Intersectin and EphB2. *Molecular Biology of the Cell*, *17*(3), 1273–1285. https://doi.org/10.1091/mbc.E05-07-0700

Nizhynska, V., Neumueller, R., & Herbst, R. (2007). Phosphoinositide 3-kinase acts through RAC and Cdc42 during agrin-induced acetylcholine receptor clustering. *Developmental Neurobiology*, *67*(8), 1047–1058. https://doi.org/10.1002/dneu.20371

Novokhatska, O., Dergai, M., Houssin, N., Tsyba, L., Moreau, J., & Rynditch, A. (2011). Intersectin 2 nucleotide exchange factor regulates Cdc42 activity during *Xenopus* early development. *Biochemical and Biophysical Research Communications*, *408*(4), 663–668. https://doi.org/10.1016/j.bbrc.2011.04.081

Novokhatska, O., Dergai, M., Tsyba, L., Skrypkina, I., Filonenko, V., Moreau, J., & Rynditch, A. (2013). Adaptor Proteins Intersectin 1 and 2 Bind Similar Proline-Rich Ligands but Are Differentially Recognized by SH2 Domain-Containing Proteins. *PLOS ONE*, *8*(7), e70546. https://doi.org/10.1371/journal.pone.0070546

Ochi, E., Nosaka, K., Tsutaki, A., Kouzaki, K., & Nakazato, K. (2015). Repeated bouts of fast velocity eccentric contractions induce atrophy of gastrocnemius muscle in rats. *Journal of Muscle Research and Cell Motility*, *36*(4), 317–327. https://doi.org/10.1007/s10974-015-9426-0

Ohno, K., Brengman, J., Tsujino, A., & Engel, A. G. (1998). Human endplate acetylcholinesterase deficiency caused by mutations in the collagen-like tail subunit (ColQ) of the asymmetric enzyme. *Proceedings of the National Academy of Sciences*, *95*(16), 9654–9659. https://doi.org/10.1073/pnas.95.16.9654

Okamoto, K.-I., Nagai, T., Miyawaki, A., & Hayashi, Y. (2004). Rapid and persistent modulation of actin dynamics regulates postsynaptic reorganization underlying bidirectional plasticity. *Nature Neuroscience*, *7*(10), 1104–1112. https://doi.org/10.1038/nn1311

Okamoto, M., Schoch, S., & Südhof, T. C. (1999). EHSH1/Intersectin, a Protein That Contains EH and SH3 Domains and Binds to Dynamin and SNAP-25: A PROTEIN CONNECTION BETWEEN EXOCYTOSIS AND ENDOCYTOSIS?*. *Journal of Biological Chemistry*, *274*(26), 18446–18454. https://doi.org/10.1074/jbc.274.26.18446

Okrut, J., Prakash, S., Wu, Q., Kelly, M. J. S., & Taunton, J. (2015). Allosteric N-WASP activation by an inter-SH3 domain linker in Nck. *Proceedings of the National Academy of Sciences*, *112*(47), E6436–E6445. https://doi.org/10.1073/pnas.1510876112

Orengo, J. P., Nitschke, L., Heijden, M. E. van der, Ciaburri, N. A., Orr, H. T., & Zoghbi, H. Y. (2022). Reduction of mutant ATXN1 rescues premature death in a conditional SCA1 mouse model. *JCI Insight*, *7*(8). https://doi.org/10.1172/jci.insight.154442

Paget-Blanc, V., Pfeffer, M. E., Pronot, M., Lapios, P., Angelo, M. F., Walle, R., Cordelières, F. P., Levet, F., Claverol, S., Lacomme, S., Petrel, M., Martin, C., Pitard, V., De Smedt Peyrusse, V., Biederer, T., Perrais, D., Trifilieff, P., & Herzog, E. (2022). A synaptomic analysis reveals dopamine hub synapses in the mouse striatum. *Nature Communications*, *13*(1), 1–19. https://doi.org/10.1038/s41467-022-30776-9

Palmen, S. J. M. C., van Engeland, H., Hof, P. R., & Schmitz, C. (2004). Neuropathological findings in autism. *Brain*, *127*(12), 2572–2583. https://doi.org/10.1093/brain/awh287

Pankivskyi, S., Pastré, D., Steiner, E., Joshi, V., Rynditch, A., & Hamon, L. (2021). ITSN1 regulates SAM68 solubility through SH3 domain interactions with SAM68 proline-rich motifs. *Cellular and Molecular Life Sciences*, *78*(4), 1745–1763. https://doi.org/10.1007/s00018-020-03610-y

Pasciuto, E., & Bagni, C. (2014). SnapShot: FMRP interacting proteins. *Cell*, *159*(1), 218-218.e1. https://doi.org/10.1016/j.cell.2014.08.036

Passmore, L. A., & Coller, J. (2023). Roles of mRNA poly(A) tails in regulation of eukaryotic gene expression. *Nature Reviews Molecular Cell Biology*, *23*, 93–106.

Peça, J., Feliciano, C., Ting, J. T., Wang, W., Wells, M. F., Venkatraman, T. N., Lascola, C. D., Fu, Z., & Feng, G. (2011). Shank3 mutant mice display autistic-like behaviours and striatal dysfunction. *Nature*, *472*(7344), 437–442. https://doi.org/10.1038/nature09965

Pechstein, A., Bacetic, J., Vahedi-Faridi, A., Gromova, K., Sundborger, A., Tomlin, N., Krainer, G., Vorontsova, O., Schäfer, J. G., Owe, S. G., Cousin, M. A., Saenger, W., Shupliakov, O., & Haucke, V. (2010). Regulation of synaptic vesicle recycling by complex formation between intersectin 1 and the clathrin adaptor complex AP2. *Proceedings of the National Academy of Sciences of the United States of America*, *107*(9), 4206–4211. https://doi.org/10.1073/pnas.0911073107

Pechstein, A., Gerth, F., Milosevic, I., Jäpel, M., Eichhorn-Grünig, M., Vorontsova, O., Bacetic, J., Maritzen, T., Shupliakov, O., Freund, C., & Haucke, V. (2015). Vesicle uncoating regulated by SH3-SH3 domain-mediated complex formation between endophilin and intersectin at synapses. *EMBO Reports*, *16*(2), 232–239. https://doi.org/10.15252/embr.201439260

Peterson, F. C., Deng, Q., Zettl, M., Prehoda, K. E., Lim, W. A., Way, M., & Volkman, B. F. (2007). Multiple WASP-interacting Protein Recognition Motifs Are Required for a Functional Interaction with N-WASP*. *Journal of Biological Chemistry*, *282*(11), 8446–8453. https://doi.org/10.1074/jbc.M609902200

Pietropaolo, S., Guilleminot, A., Martin, B., D'Amato, F. R., & Crusio, W. E. (2011). Genetic-Background Modulation of Core and Variable Autistic-Like Symptoms in Fmr1 Knock-Out Mice. *PLOS ONE*, *6*(2), e17073. https://doi.org/10.1371/journal.pone.0017073

Pilpel, Y., Kolleker, A., Berberich, S., Ginger, M., Frick, A., Mientjes, E., Oostra, B. A., & Seeburg, P. H. (2009). Synaptic ionotropic glutamate receptors and plasticity are developmentally altered in the CA1 field of Fmr1 knockout mice. *The Journal of Physiology*, *587*(4), 787–804. https://doi.org/10.1113/jphysiol.2008.160929

Pinon-Lataillade, G., Masson, C., Bernardino-Sgherri, J., Henriot, V., Mauffrey, P., Frobert, Y., Araneda, S., & Angulo, J. F. (2004). KIN17 encodes an RNA-binding protein and is expressed during mouse spermatogenesis. *Journal of Cell Science*, *117*(16), 3691–3702. https://doi.org/10.1242/jcs.01226

Piochon, C., Kloth, A. D., Grasselli, G., Titley, H. K., Nakayama, H., Hashimoto, K., Wan, V., Simmons, D. H., Eissa, T., Nakatani, J., Cherskov, A., Miyazaki, T., Watanabe, M., Takumi, T., Kano, M., Wang, S. S.-H., & Hansel, C. (2014). Cerebellar plasticity and motor learning deficits in a copy-number variation mouse model of autism. *Nature Communications*, *5*(1), 5586. https://doi.org/10.1038/ncomms6586

Pollard, T. D., & Cooper, J. A. (2009). Actin, a Central Player in Cell Shape and Movement. *Science*, *326*(5957), 1208–1212. https://doi.org/10.1126/science.1175862

Pratt, S. J. P., Shah, S. B., Ward, C. W., Inacio, M. P., Stains, J. P., & Lovering, R. M. (2013). Effects of in vivo injury on the neuromuscular junction in healthy and dystrophic muscles. *The Journal of Physiology*, *591*(2), 559–570. https://doi.org/10.1113/jphysiol.2012.241679

Pratt, S. J. P., Valencia, A. P., Le, G. K., Shah, S. B., & Lovering, R. M. (2015). Pre- and postsynaptic changes in the neuromuscular junction in dystrophic mice. *Frontiers in Physiology*, *6*. https://doi.org/10.3389/fphys.2015.00252

Predescu, S. A., Predescu, D. N., Timblin, B. K., Stan, R. V., & Malik, A. B. (2003). Intersectin Regulates Fission and Internalization of Caveolae in Endothelial Cells. *Molecular Biology of the Cell*, *14*(12), 4997–5010. https://doi.org/10.1091/mbc.e03-01-0041

Prigogine, C., Ruiz, J. M., Cebolla, A. M., Deconinck, N., Servais, L., Gailly, P., Dan, B., & Cheron, G. (2024). Cerebellar dysfunction in the mdx mouse model of Duchenne muscular dystrophy: An electrophysiological and behavioural study. *European Journal of Neuroscience*, *60*(10), 6470–6489. https://doi.org/10.1111/ejn.16566

Pucharcos, C., Casas, C., Nadal, M., Estivill, X., & de la Luna, S. (2001). The human intersectin genes and their spliced variants are differentially expressed. *Biochimica et Biophysica Acta (BBA) - Gene Structure and Expression*, *1521*(1), 1–11. https://doi.org/10.1016/S0167-4781(01)00276-7

Pucharcos, C., Estivill, X., & de la Luna, S. (2000). Intersectin 2, a new multimodular protein involved in clathrin-mediated endocytosis1. *FEBS Letters*, *478*(1), 43–51. https://doi.org/10.1016/S0014-5793(00)01793-2

Pucharcós, C., Fuentes, J.-J., Casas, C., de la Luna, S., Alcántara, S., Arbonés, M. L., Soriano, E., Estivill, X., & Pritchard, M. (1999). Alu-splice cloning of human Intersectin (ITSN), a putative multivalent binding protein expressed in proliferating and differentiating neurons and overexpressed in Down syndrome. *European Journal of Human Genetics*, *7*(6), 704–712. https://doi.org/10.1038/sj.ejhg.5200356

Rai, D. K., Lawrence, P., Kloc, A., Schafer, E., & Rieder, E. (2015). Analysis of the interaction between host factor Sam68 and viral elements during foot-and-mouth disease virus infections | Virology Journal | Full Text. *Virology Journal*, *12*(224). https://doi.org/10.1186/s12985-015-0452-8

Redgrave, P., Prescott, T. J., & Gurney, K. (1999). The basal ganglia: A vertebrate solution to the selection problem? *Neuroscience*, *89*(4), 1009–1023. https://doi.org/10.1016/S0306-4522(98)00319-4

Rodal, A. A., Motola-Barnes, R. N., & Littleton, J. T. (2008). Nervous Wreck and Cdc42 Cooperate to Regulate Endocytic Actin Assembly during Synaptic Growth. *Journal of Neuroscience*, *28*(33), 8316–8325. https://doi.org/10.1523/JNEUROSCI.2304-08.2008

Rodríguez Cruz, P. M., Cossins, J., Beeson, D., & Vincent, A. (2020). The Neuromuscular Junction in Health and Disease: Molecular Mechanisms Governing Synaptic Formation and Homeostasis. *Frontiers in Molecular Neuroscience*, *13*(December), 1–22. https://doi.org/10.3389/fnmol.2020.610964

Rodríguez Cruz, P. M., Palace, J., & Beeson, D. (2018). The Neuromuscular Junction and Wide Heterogeneity of Congenital Myasthenic Syndromes. *International Journal of Molecular Sciences*, *19*(6), Article 6. https://doi.org/10.3390/ijms19061677

Roos, J., & Kelly, R. B. (1998). Dap160, a Neural-specific Eps15 Homology and Multiple SH3 Domain-containing Protein That Interacts with *Drosophila*Dynamin*. *Journal of Biological Chemistry*, *273*(30), 19108–19119. https://doi.org/10.1074/jbc.273.30.19108

Rose, S., Malabarba, M. G., Krag, C., Schultz, A., Tsushima, H., Di Fiore, P. P., & Salcini, A. E. (2007). Caenorhabditis elegans Intersectin: A Synaptic Protein Regulating Neurotransmission. *Molecular Biology of the Cell*, *18*(12), 5091–5099. https://doi.org/10.1091/mbc.e07-05-0460

Rosendale, M., Van, T. N. N., Grillo-Bosch, D., Sposini, S., Claverie, L., Gauthereau, I., Claverol, S., Choquet, D., Sainlos, M., & Perrais, D. (2019). Functional recruitment of dynamin requires multimeric interactions for efficient endocytosis. *Nature Communications*, *10*(1), 4462. https://doi.org/10.1038/s41467-019-12434-9

Sakaba, T., Kononenko, N. L., Bacetic, J., Pechstein, A., Schmoranzer, J., Yao, L., Barth, H., Shupliakov, O., Kobler, O., Aktories, K., & Haucke, V. (2013). Fast neurotransmitter release regulated by the endocytic scaffold intersectin. *Proceedings of the National Academy of Sciences*, *110*(20), 8266–8271. https://doi.org/10.1073/pnas.1219234110

Samsó, P., Koch, P. A., Posor, Y., Lo, W.-T., Belabed, H., Nazare, M., Laporte, J., & Haucke, V. (2022). Antagonistic control of active surface integrins by myotubularin and phosphatidylinositol 3-kinase C2β in a myotubular myopathy model. *Proceedings of the National Academy of Sciences*, *119*(40), e2202236119. https://doi.org/10.1073/pnas.2202236119

Sanes, J. R. (2003). The Basement Membrane/Basal Lamina of Skeletal Muscle*. *Journal of Biological Chemistry*, *278*(15), 12601–12604. https://doi.org/10.1074/jbc.R200027200

Sankaranarayanan, S., Atluri, P. P., & Ryan, T. A. (2003). Actin has a molecular scaffolding, not propulsive, role in presynaptic function. *Nature Neuroscience*, *6*(2), 127–135. https://doi.org/10.1038/nn1002

Santolini, E., Salcini, A. E., Kay, B. K., Yamabhai, M., & Di Fiore, P. P. (1999). The EH Network. *Experimental Cell Research*, *253*(1), 186–209. https://doi.org/10.1006/excr.1999.4694

Sasaki, Y. (2020). Local Translation in Growth Cones and Presynapses, Two Axonal Compartments for Local Neuronal Functions. *Biomolecules*, *10*(5), Article 5. https://doi.org/10.3390/biom10050668

Sellier, C., Freyermuth, F., Tabet, R., Tran, T., He, F., Ruffenach, F., Alunni, V., Moine, H., Thibault, C., Page, A., Tassone, F., Willemsen, R., Disney, M. D., Hagerman, P. J., Todd, P. K., & Charlet-Berguerand, N. (2013). Sequestration of DROSHA and DGCR8 by Expanded CGG RNA Repeats Alters MicroRNA Processing in Fragile X-Associated Tremor/Ataxia Syndrome. *Cell Reports*, *3*(3), 869–880. https://doi.org/10.1016/j.celrep.2013.02.004

Sellier, C., Rau, F., Liu, Y., Tassone, F., Hukema, R. K., Gattoni, R., Schneider, A., Richard, S., Willemsen, R., Elliott, D. J., Hagerman, P. J., & Charlet-Berguerand, N. (2010). Sam68 sequestration and partial loss of function are associated with splicing alterations in FXTAS patients. *The EMBO Journal*, *29*(7), 1248–1261. https://doi.org/10.1038/emboj.2010.21

Seltzer, S., Giannopoulos, P. N., Bismar, T. A., Trifiro, M., & Paliouras, M. (2023). Investigation of androgen receptor-dependent alternative splicing has identified a unique subtype of lethal prostate cancer. *Asian Journal of Andrology*, *25*(3), 296. https://doi.org/10.4103/aja202263

Sengar, A. S., Wang, W., Bishay, J., Cohen, S., & Egan, S. E. (1999). The EH and SH3 domain Ese proteins regulate endocytosis by linking to dynamin and Eps15. *The EMBO Journal*, *18*(5), 1159–1171. https://doi.org/10.1093/emboj/18.5.1159

Shen, M., Guo, Y., Dong, Q., Gao, Y., Stockton, M. E., Li, M., Kannan, S., Korabelnikov, T., Schoeller, K. A., Sirois, C. L., Zhou, C., Le, J., Wang, D., Chang, Q., Sun, Q.-Q., & Zhao, X. (2021). FXR1 regulation of parvalbumin interneurons in the prefrontal cortex is critical for schizophrenia-like behaviors. *Molecular Psychiatry*, *26*(11), 6845–6867. https://doi.org/10.1038/s41380-021-01096-z

Shen, W., Hernandez-lopez, S., Tkatch, T., Held, J. E., Surmeier, D. J., Hernandez-lopez, S., Tkatch, T., Held, J. E., Surmeier, D. J., & Kv, K. (2003). Kv1.2-Containing K+ Channels Regulate Subthreshold Excitability of Striatal Medium Spiny Neurons. *Journal of Neurophysiology*, *91*(3), 1337–1349. https://doi.org/10.1152/jn.00414.2003

Sherman, B. T., Hao, M., Qiu, J., Jiao, X., Baseler, M. W., Lane, H. C., Imamichi, T., & Chang, W. (2022). DAVID: A web server for functional enrichment analysis and functional annotation of gene lists (2021 update). *Nucleic Acids Research*, *50*(W1), W216–W221. https://doi.org/10.1093/nar/gkac194

Shi, Y., Wang, J., Yuan, Q., Chen, Y., Zhao, M., Li, X., Wang, Z., Zhou, H., Zhu, F., Wei, B., Jiang, Y., Zhao, J., Qjao, Y., Dong, Z., & Lip, K. (2024). DDX5 promotes esophageal squamous cell carcinoma growth through sustaining VAV3 mRNA stability. *Oncogene*, *43*, 3240–3254. https://doi.org/10.1038/s41388-024-03162-6

Shirai, T., Uemichi, K., Takemasa, T., & Kitaoka, Y. (2025). Unilateral electrical stimulation of mice induces transcriptional response in stimulated leg with limited effect on non-stimulated contralateral leg. *Experimental Physiology*, *n/a*(n/a). https://doi.org/10.1113/EP092394

Shumilina, E. V., Negulyaev, Y. A., Morachevskaya, E. A., Hinssen, H., & Khaitlina, S. Y. (2003). Regulation of Sodium Channel Activity by Capping of Actin Filaments. *Molecular Biology of the Cell*, *14*(4), 1709–1716. https://doi.org/10.1091/mbc.e02-09-0622

Siegelbaum, S. A., Kandel, E. R., & Südhof, T. C. (2013). Transmitter Release. In *Principles of neural science* (5th ed., pp. 260–288). McGraw-Hill Companies, Inc.

Skuladottir, A. T., Tragante, V., Sveinbjornsson, G., Helgason, H., Sturluson, A., Bjornsdottir, A., Jonsson, P., Palmadottir, V., Sveinsson, O. A., Jensson, B. O., Gudjonsson, S. A., Ivarsdottir, E. V., Gisladottir, R. S., Gunnarsson, A. F., Walters, G. B., Jonsdottir, G. A., Thorgeirsson, T. E., Bjornsdottir, G., Holm, H., … Stefansson, K. (2024). Loss-of-function variants in ITSN1 confer high risk of Parkinson's disease. *Npj Parkinson's Disease*, *10*(1), 1–4. https://doi.org/10.1038/s41531-024-00752-9

So, J., Pasculescu, A., Dai, A. Y., Williton, K., James, A., Nguyen, V., Creixell, P., Schoof, E. M., Sinclair, J., Barrios-Rodiles, M., Gu, J., Krizus, A., Williams, R., Olhovsky, M., Dennis, J. W., Wrana, J. L., Linding, R., Jorgensen, C., Pawson, T., & Colwill, K. (2015). Integrative analysis of kinase networks in TRAIL-induced apoptosis provides a source of potential targets for combination therapy. *Science Signaling*, *8*(371), rs3–rs3. https://doi.org/10.1126/scisignal.2005700

Spencer, C. M., Alekseyenko, O., Serysheva, E., Yuva-Paylor, L. A., & Paylor, R. (2005). Altered anxiety-related and social behaviors in the Fmr1 knockout mouse model of fragile X syndrome. *Genes, Brain and Behavior*, *4*(7), 420–430. https://doi.org/10.1111/j.1601-183X.2005.00123.x

St. Paul, A., Corbett, C., Peluzzo, A., Kelemen, S., Okune, R., Haines, D. S., Preston, K., Eguchi, S., & Autieri, M. V. (2023). FXR1 regulates vascular smooth muscle cell cytoskeleton, VSMC contractility, and blood pressure by multiple mechanisms. *Cell Reports*, *42*(4), 112381. https://doi.org/10.1016/j.celrep.2023.112381

Steward, O., & Levy, W. B. (1982). Preferential localization of polyribosomes under the base of dendritic spines in granule cells of the dentate gyrus. *Journal of Neuroscience*, *2*(3), 284–291. https://doi.org/10.1523/JNEUROSCI.02-03-00284.1982

Stringer, C., Wang, T., Michaelos, M., & Pachitariu, M. (2021). Cellpose: A generalist algorithm for cellular segmentation. *Nature Methods*, *18*(1), 100–106. https://doi.org/10.1038/s41592-020-01018-x

Suetsugu, S., Hattori, M., Miki, H., Tezuka, T., Yamamoto, T., Mikoshiba, K., & Takenawa, T. (2002). Sustained Activation of N-WASP through Phosphorylation Is Essential for Neurite Extension. *Developmental Cell*, *3*(5), 645–658. https://doi.org/10.1016/S1534-5807(02)00324-6

Sung, Y. J., Conti, J., Currie, J. R., Brown, W. T., & Denman, R. B. (2000). RNAs That Interact with the Fragile X Syndrome RNA Binding Protein FMRP. *Biochemical and Biophysical Research Communications*, *275*(3), 973–980. https://doi.org/10.1006/bbrc.2000.3405

Suzuki, H. I., Yamagata, K., Sugimoto, K., Iwamoto, T., Kato, S., & Miyazono, K. (2009). Modulation of microRNA processing by p53. *Nature*, *460*(7254), 529–533. https://doi.org/10.1038/nature08199

Tarun, S. Z., Wells, S. E., Deardorff, J. A., & Sachs, A. B. (1997). Translation initiation factor eIF4G mediates in vitro poly(A) tail-dependent translation. *Proceedings of the National Academy of Sciences*, *94*(17), 9046–9051. https://doi.org/10.1073/pnas.94.17.9046

Tauer, J., Canevazzi, G. H. R., Schiettekatte-Maltais, J., Rauch, F., Bergeron, R., & Veilleux, L. (2021). Muscle-bone properties after prolonged voluntary wheel running in a mouse model of dominant severe osteogenesis imperfecta. *Journal of Musculoskeletal &*

Neuronal Interactions. https://www.semanticscholar.org/paper/44f2692d05cd2ed113e1eceb790e772fcf5933ea

Terry, R. L., & Wells, D. J. (2016). Histopathological Evaluation of Skeletal Muscle with Specific Reference to Mouse Models of Muscular Dystrophy. *Current Protocols in Mouse Biology*, *6*(4), 343–363. https://doi.org/10.1002/cpmo.19

Thomas, S., Ritter, B., Verbich, D., Sanson, C., Bourbonnière, L., McKinney, R. A., & McPherson, P. S. (2009). Intersectin Regulates Dendritic Spine Development and Somatodendritic Endocytosis but Not Synaptic Vesicle Recycling in Hippocampal Neurons*. *Journal of Biological Chemistry*, *284*(18), 12410–12419. https://doi.org/10.1074/jbc.M809746200

Tsai, P. T., Hull, C., Chu, Y., Greene-Colozzi, E., Sadowski, A. R., Leech, J. M., Steinberg, J., Crawley, J. N., Regehr, W. G., & Sahin, M. (2012). Autistic-like behaviour and cerebellar dysfunction in Purkinje cell Tsc1 mutant mice. *Nature*, *488*(7413), 647–651. https://doi.org/10.1038/nature11310

Tsyba, L., Nikolaienko, O., Dergai, O., Dergai, M., Novokhatska, O., Skrypkina, I., & Rynditch, A. (2011). Intersectin multidomain adaptor proteins: Regulation of functional diversity. *Gene*, *473*(2), 67–75. https://doi.org/10.1016/j.gene.2010.11.016

Tubridy, N., Fontaine, B., & Eymard, B. (2001). Congenital myopathies and congenital muscular dystrophies. *Current Opinion in Neurology*, *14*(5), 575.

Valsecchi, V., Boido, M., Amicis, E. D., Piras, A., & Vercelli, A. (2015). Expression of Muscle-Specific MiRNA 206 in the Progression of Disease in a Murine SMA Model. *PLOS ONE*, *10*(6), e0128560. https://doi.org/10.1371/journal.pone.0128560

Veeraragavan, S., Graham, D., Bui, N., Yuva-Paylor, L. A., Wess, J., & Paylor, R. (2012). Genetic reduction of muscarinic M4 receptor modulates analgesic response and acoustic startle response in a mouse model of fragile X syndrome (FXS). *Behavioural Brain Research*, *228*(1), 1–8. https://doi.org/10.1016/j.bbr.2011.11.018

Vickers, C. A., Dickson, K. S., & Wyllie, D. J. A. (2005). Induction and maintenance of late-phase long-term potentiation in isolated dendrites of rat hippocampal CA1 pyramidal neurones. *The Journal of Physiology*, *568*(3), 803–813. https://doi.org/10.1113/jphysiol.2005.092924

Villacé, P., Marión, R. M., & Ortín, J. (2004). The composition of Staufen-containing RNA granules from human cells indicates their role in the regulated transport and translation of messenger RNAs. *Nucleic Acids Research*, *32*(8), 2411–2420. https://doi.org/10.1093/nar/gkh552

Vollweiter, D. (2021). *Intersectins regulate cortico-striatal neurotransmission and autism-related behaviors*. Freie Universität Berlin.

Vollweiter, D., Shergill, J. K., Hilse, A., Kochlamazashvili, G., Koch, S. P., Mueller, S., Boehm-Sturm, P., Haucke, V., & Maritzen, T. (2023). Intersectin deficiency impairs cortico-striatal neurotransmission and causes obsessive–compulsive behaviors in mice. *Proceedings of the National Academy of Sciences*, *120*(35), e2304323120. https://doi.org/10.1073/pnas.2304323120

Walker, J. H., Boustead, C. M., & Witzemann, V. (1984). The 43-K protein, v1, associated with acetylcholine receptor containing membrane fragments is an actin-binding protein. *The EMBO Journal*, *3*(10), 2287–2290. https://doi.org/10.1002/j.1460-2075.1984.tb02127.x

Wang, H., Dictenberg, J. B., Ku, L., Li, W., Bassell, G. J., & Feng, Y. (2008). Dynamic Association of the Fragile X Mental Retardation Protein as a Messenger Ribonucleoprotein between

Microtubules and Polyribosomes. *Molecular Biology of the Cell*, *19*(1), 105–114. https://doi.org/10.1091/mbc.e07-06-0583

Wang, J.-B., Wu, W. J., & Cerione, R. A. (2005). Cdc42 and Ras Cooperate to Mediate Cellular Transformation by Intersectin-L*. *Journal of Biological Chemistry*, *280*(24), 22883–22891. https://doi.org/10.1074/jbc.M414375200

Wen, P. J., Osborne, S. L., Zanin, M., Low, P. C., Wang, H.-T. A., Schoenwaelder, S. M., Jackson, S. P., Wedlich-Söldner, R., Vanhaesebroeck, B., Keating, D. J., & Meunier, F. A. (2011). Phosphatidylinositol(4,5)bisphosphate coordinates actin-mediated mobilization and translocation of secretory vesicles to the plasma membrane of chromaffin cells. *Nature Communications*, *2*(1), 491. https://doi.org/10.1038/ncomms1500

Weyer, S. W., Klevanski, M., Delekate, A., Voikar, V., Aydin, D., Hick, M., Filippov, M., Drost, N., Schaller, K. L., Saar, M., Vogt, M. A., Gass, P., Samanta, A., Jäsignschke, A., Korte, M., Wolfer, D. P., Caldwell, J. H., & Müller, U. C. (2011). APP and APLP2 are essential at PNS and CNS synapses for transmission, spatial learning and LTP. *EMBO Journal*, *30*(11), 2266–2280. https://doi.org/10.1038/emboj.2011.119

Williams, M. R., Markey, J. C., Doczi, M. A., & Morielli, A. D. (2007). An essential role for cortactin in the modulation of the potassium channel Kv1. 2. *Proceedings of the National Academy of Sciences of the United States of America*, *104*(44), 17412–17417. https://doi.org/10.1073/pnas.0703865104

Wilson, L. B., Tregellas, J. R., Hagerman, R. J., Rogers, S. J., & Rojas, D. C. (2009). A voxel-based morphometry comparison of regional gray matter between fragile X syndrome and autism. *Psychiatry Research: Neuroimaging*, *174*(2), 138–145. https://doi.org/10.1016/j.pscychresns.2009.04.013

Winther, Å. M. E., Vorontsova, O., Rees, K. A., Näreoja, T., Sopova, E., Jiao, W., & Shupliakov, O. (2015). An Endocytic Scaffolding Protein together with Synapsin Regulates Synaptic Vesicle Clustering in the Drosophila Neuromuscular Junction. *Journal of Neuroscience*, *35*(44), 14756–14770. https://doi.org/10.1523/JNEUROSCI.1675-15.2015

Witkowska, A., & Haucke, V. (2021). Liquid-like protein assemblies initiate endocytosis. *Nature Cell Biology*, *23*(4), 301–302. https://doi.org/10.1038/s41556-021-00665-2

Won, H., Lee, H.-R., Gee, H. Y., Mah, W., Kim, J.-I., Lee, J., Ha, S., Chung, C., Jung, E. S., Cho, Y. S., Park, S.-G., Lee, J.-S., Lee, K., Kim, D., Bae, Y. C., Kaang, B.-K., Lee, M. G., & Kim, E. (2012). Autistic-like social behaviour in Shank2-mutant mice improved by restoring NMDA receptor function. *Nature*, *486*(7402), 261–265. https://doi.org/10.1038/nature11208

Wong, K. A., Wilson, J., Russo, A., Wang, L., Okur, M. N., Wang, X., Martin, N. P., Scappini, E., Carnegie, G. K., & O'Bryan, J. P. (2012). Intersectin (ITSN) Family of Scaffolds Function as Molecular Hubs in Protein Interaction Networks. *PLOS ONE*, *7*(4), e36023. https://doi.org/10.1371/journal.pone.0036023

Xie, C., Xiong, W., Li, J., Wang, X., Xu, C., & Yang, L. (2019). Intersectin 1 (ITSN1) identified by comprehensive bioinformatic analysis and experimental validation as a key candidate biological target in breast cancer . *OncoTargets and Therapy*, *12*, 7079–7093. https://doi.org/10.2147/OTT.S216286

Xie, G., Harrison, J., Clapcote, S. J., Huang, Y., Zhang, J.-Y., Wang, L.-Y., & Roder, J. C. (2010). A New Kv1.2 Channelopathy Underlying Cerebellar Ataxia*. *Journal of Biological Chemistry*, *285*(42), 32160–32173. https://doi.org/10.1074/jbc.M110.153676

Xing, Z., Ma, W., Kit, & Tran, E., J. (2019). The DDX5/Dbp2 subfamily of DEAD-box RNA helicases. *Wiley Interdisciplinary Reviews. RNA*, *10*(2), e1519. https://doi.org/10.1002/wrna.1519

Yamabhai, M., Hoffman, N. G., Hardison, N. L., McPherson, P. S., Castagnoli, L., Cesareni, G., & Kay, B. K. (1998). Intersectin, a Novel Adaptor Protein with Two Eps15 Homology and Five Src Homology 3 Domains*. *Journal of Biological Chemistry*, *273*(47), 31401–31407. https://doi.org/10.1074/jbc.273.47.31401

Yang, Y.-M., Arsenault, J., Bah, A., Krzeminski, M., Fekete, A., Chao, O. Y., Pacey, L. K., Wang, A., Forman-Kay, J., Hampson, D. R., & Wang, L.-Y. (2018). Identification of a molecular locus for normalizing dysregulated GABA release from interneurons in the Fragile X brain. *Molecular Psychiatry*, *25*(9), 2017–2035. https://doi.org/10.1038/s41380-018-0240-0

Yee, J. X., Rastani, A., & Soden, M. E. (2022). The potassium channel auxiliary subunit Kvβ2 (Kcnab2) regulates Kv1 channels and dopamine neuron firing. *Journal of Neurophysiology*, *128*(1), 62–72. https://doi.org/10.1152/jn.00194.2022

Yu, Y., Chu, P.-Y., Bowser, D. N., Keating, D. J., Dubach, D., Harper, I., Tkalcevic, J., Finkelstein, D. I., & Pritchard, M. A. (2008). Mice deficient for the chromosome 21 ortholog Itsn1 exhibit vesicle-trafficking abnormalities. *Human Molecular Genetics*, *17*(21), 3281–3290. https://doi.org/10.1093/hmg/ddn224

Zeke, A., Lukács, M., Lim, W. A., & Reményi, A. (2009). Scaffolds: Interaction platforms for cellular signalling circuits. *Trends in Cell Biology*, *19*(8), 364–374. https://doi.org/10.1016/j.tcb.2009.05.007

Zhang, H., Guo, Z., Liu, X., Zhao, Y., Chen, Y., Zhang, M., Fu, L., Gu, F., & Ma, Y. (2021). Endocytic protein intersectin1-S shuttles into nucleus to suppress the DNA replication in breast cancer. *Cell Death & Disease*, *12*(10), 1–17. https://doi.org/10.1038/s41419-021-04218-1

Zhang, H., Song, L., Cong, H., & Tien, P. (2015). Nuclear Protein Sam68 Interacts with the Enterovirus 71 Internal Ribosome Entry Site and Positively Regulates Viral Protein Translation. *Journal of Virology*, *89*(19), 10031–10043. https://doi.org/10.1128/jvi.01677-15

Zhang, J., Ryder, K. D., Bethel, J. A., Ramirez, R., & Duncan, R. L. (2006). PTH-Induced Actin Depolymerization Increases Mechanosensitive Channel Activity to Enhance Mechanically Stimulated 2+ Signaling in Osteoblasts*1*. *Journal of Bone and Mineral Research*, *21*(11), 1729–1737. https://doi.org/10.1359/jbmr.060722

Zhang, W., Shen, Y., Xiong, G., Guo, Y., Deng, L., Li, B., Yang, J., & Qi, C. (2013). Crystal structure of human Intersectin-2L C2 domain. *Biochemical and Biophysical Research Communications*, *431*(1), 76–80. https://doi.org/10.1016/j.bbrc.2012.12.087

Zhang, Y., O'Connor, J. P., Siomi, M. C., Srinivasan, S., Dutra, A., Nussbaum, R. L., & Dreyfuss, G. (1995). The fragile X mental retardation syndrome protein interacts with novel homologs FXR1 and FXR2. *The EMBO Journal*, *14*(21), 5358–5366. https://doi.org/10.1002/j.1460-2075.1995.tb00220.x

Zhang, Y., Zhang, X.-F., Fleming, M. R., Amiri, A., El-Hassar, L., Surguchev, A. A., Hyland, C., Jenkins, D. P., Desai, R., Brown, M. R., Gazula, V.-R., Waters, M. F., Large, C. H., Horvath, T. L., Navaratnam, D., Vaccarino, F. M., Forscher, P., & Kaczmarek, L. K. (2016). Kv3.3 Channels Bind Hax-1 and Arp2/3 to Assemble a Stable Local Actin Network that Regulates Channel Gating. *Cell*, *165*(2), 434–448. https://doi.org/10.1016/j.cell.2016.02.009

Zhao, L.-L., Zhao ,Li-Li, Wu ,Aiping, Bi ,Li-Jun, Liu ,Pei, Zhang ,Xian-En, Jiang ,Taijiao, Jin ,Gang, & and Qi, Z. (2009). Length-dependent regulation of the Kv1.2 channel activation by its C-terminus. *Molecular Membrane Biology*, *26*(3), 186–193. https://doi.org/10.1080/09687680802714741

Zhou, X., Feliciano, P., Shu, C., Wang, T., Astrovskaya, I., Hall, J. B., Obiajulu, J. U., Wright, J. R., Murali, S. C., Xu, S. X., Brueggeman, L., Thomas, T. R., Marchenko, O., Fleisch, C., Barns, S. D., Snyder, L. G., Han, B., Chang, T. S., Turner, T. N., … Chung, W. K. (2022). Integrating de novo and inherited variants in 42,607 autism cases identifies mutations in new moderate-risk genes. *Nature Genetics*, *54*(9), 1305–1319. https://doi.org/10.1038/s41588-022-01148-2

Appendix

Supplementary figures and tables

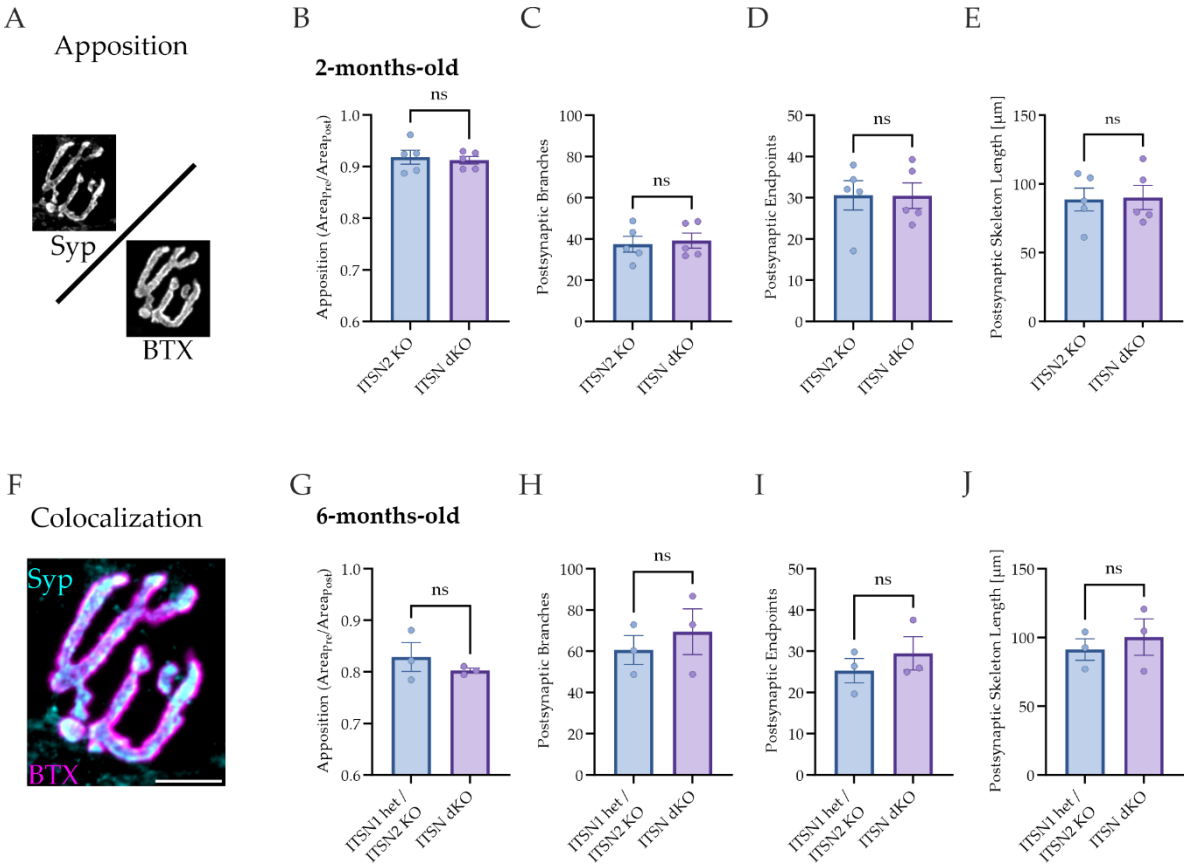

Figure S 1: Analyses of additional morphological characteristics of the NMJ confirm homogeneity between NMJs of 2- and 6-months-old ITSN2 KO and ITSNdKO mice.

A) The apposition is an alternative measure to the colocalization often used to describe juxtaposition of NMJs (Augustin, 2023; Weyer et al., 2011). It is defined as the ratio between the presynaptic and postsynaptic area. As this ratio is solely based on a comparison between the areas, it lacks information about the actual overlap, as included in the Manders Coefficient for colocalization. Exemplary image to highlight the difference to F). B)-E) Apposition, number of postsynaptic branches and endpoints and total length of the postsynaptic skeleton do not differ between 2-months old ITSN2 KO and ITSN dKO mice. Similarly, for 6-months-old mice, the apposition (G), postsynaptic branches and endpoints (H-I) and total length of the postsynaptic skeleton (J) do not differ. Statistical analysis performed with a two-tailed, unpaired t-test. ns < 0.05. N(2-months)=5, N(6-months)=3.

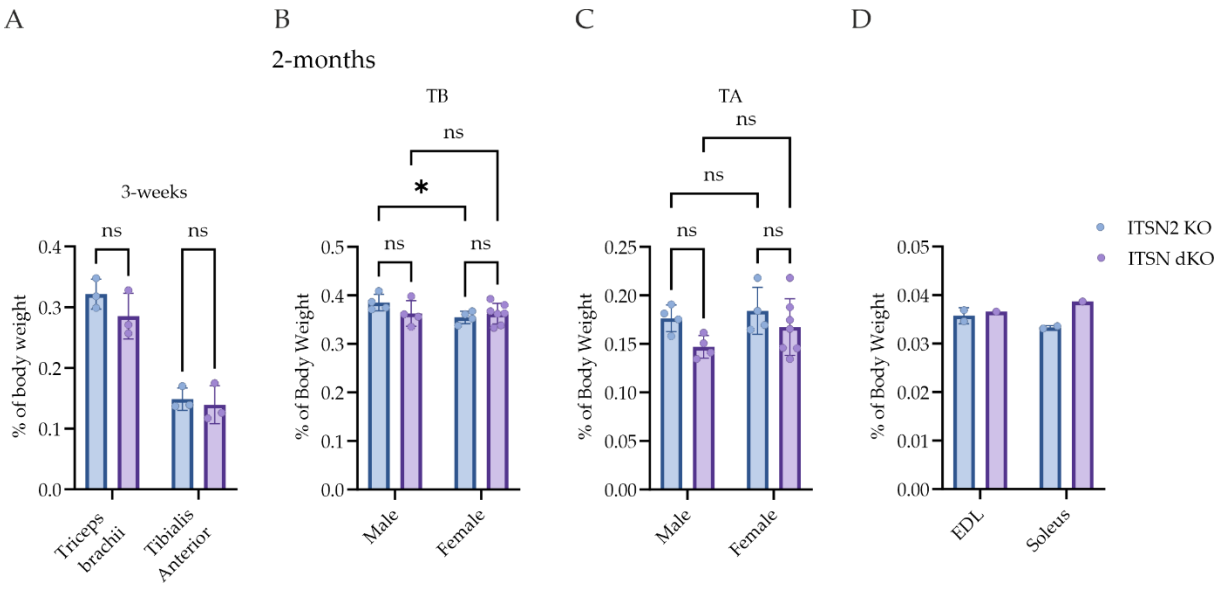

Figure S 2: Muscle weights of 2-months-old ITSN2 KO and ITSN dKO mice differentiated by sex confirms similarity in muscle weight.

A) *Relative TB and TA weight of 3-weeks-old ITSN ITSN2 KO and ITSN dKO mice does not show significant developmental delay. B) Relative TB weight differentiated by sex. Female muscles weight a bit less than male ones, even reaching significance for the ITSN2 KO mice. C) Relative TA weight differentiated by sex. For both male and female mice, ITSN dKO muscles are slightly reduced in weight, but do not reach significance. D) Preliminary soleus weight for 2-months-old ITSN2 KO and ITSN dKO mice. For the 3-weeks-timpoint several two-sided t-tests were performed, while for the 2-month-old sex differentiation a two-way ANOVA with an uncorrected Fishers's LSD test was performed. ns p≥0.05, *p < 0.05. N(3-weeks-old)=3, N(ITSN2 KO)=4, N(ITSN dKO, male)= 4, N(ITSN dKO, female)=7, N(ITSN2 KO, EDL and soleus)=2, N(ITSN dKO, EDL and soleus)=1.*

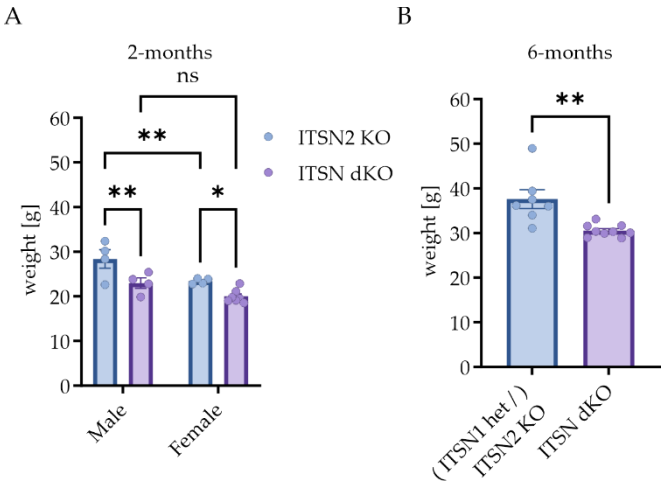

Figure S 3: ITSN dKO weight is reduced in 2- and 6-months old mice.

A) *Total body weight of ITSN2 KO and ITSN dKO of about 2-months age, differentiated by sex. As expected, male mice are a bit heavier than females for both genotypes, though for the dKO this difference does not reach statistical significance. Nevertheless, comparing ITSN dKO mice to ITSN2 KO mice of the same sex, the dKO mice are significantly lighter in weight. A two-way ANOVA with an uncorrected Fishers's LSD test was performed. ns p≥0.05, *p < 0.05, **p < 0.01. B) For male 6-month old mice the ITSN dKO mice exhibit a significant reduction in body weight. The control condition included ITSN1 het / ITSN2 KO and ITSN2 KO mice. Statistical analysis performed with a two-tailed, unpaired t-test. **p < 0.01. N(2-months, ITSN2 KO)= 4, N(2-months, ITSN dKO, male)= 4, N(2-months, ITSN dKO, female)= 7, N(6-months, ITSN2 KO)=7, N(6-months, ITSN dKO)= 9.*

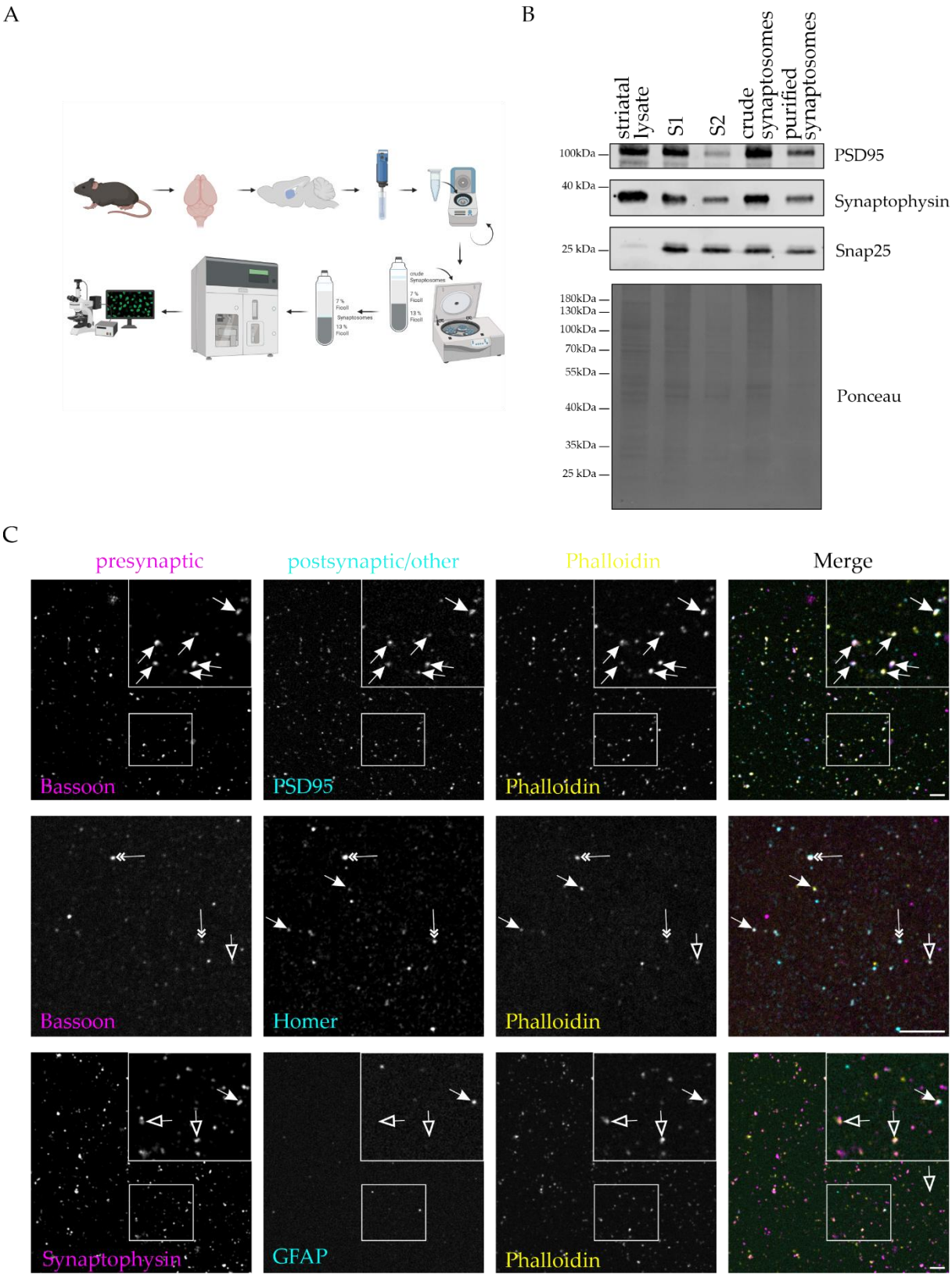

Figure S 4: Confirmation of synaptosome purification and immobilization.

A) Workflow for synaptosome purification and immobilization. Briefly, mice are sacrificed, and the striatum is dissected. Several striata are homogenized and crude synaptosomes prepared by two subsequent centrifugations. Crude synaptosomes are layered on a sucrose gradient and purified by high-speed centrifugation. Purified synaptosomes are sorted by FACS into singlet and aggregated synaptosomes based on size and membrane content. Subsequently, singlets are immobilized by centrifugation onto cover slip, fixed and stained, before confocal images are acquired.

Workflow created with Biorender.com. B) Representative image of immunoblotted samples taken during synaptosome purification. An equal amount of sample was taken at each step and equal volumes loaded onto the gel. The final sample before sorting contains pre- and postsynaptic markers, like PSD95, synaptophysin and SNAP25 C) Immunofluorescence staining of immobilized synaptosomes confirms synaptic purification. Top lane is stained for the presynaptic protein bassoon and postsynaptic protein PSD95 and shows co-occurrence of both markers at many locations (white arrows). This suggests purification and immobilization of intact synaptosomes. The middle lane is probed for presynaptic bassoon and the postsynaptic scaffold homer. Again, some objects are positive for both pre- and postsynaptic markers (marked with a double tipped arrow head), but single postsynaptic (filled white arrow) and presynaptic (empty arrow head) objects are observed. Both objects contain the actin cytoskeletal marker phalloidin as well. The bottom lane was stained with another presynaptic marker, synaptophysin, the astrocytic protein GFAP as a negative control, and phalloidin. GFAP sparsely overlaps with synaptophysin or phalloidin (filled white arrow) or only phalloidin, while synaptophysin and phalloidin (empty arrow head) overlap frequently. Therefore, measured actin is more likely to be synaptic than astrocytic actin.

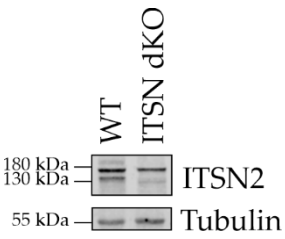

Figure S 5: ITSN2 antibody gives unspecific band at ~180 kDa.

To confirm the specificity of the ITSN2 antibody, brain lysate of a WT and a constitutive ITSN dKO brain lysate were probed with it. Again, the lane at ~180 kDa is present even in the dKO, suggesting it is unspecific antibody binding.

Table S 1: Top GO-terms for biological processes (BP) based on p-value.

Category	Term	PValue	Fold Enrichment	Bonferroni	Benjamini	FDR
BP	GO:0008104~protein localization	1.28E-11	1.48E+01	1.23E-08	1.23E-08	1.17E-08
BP	GO:0001732~formation of cytoplasmic translation initiation complex	4.83E-09	8.87E+01	4.63E-06	2.31E-06	2.21E-06
BP	GO:0051086~chaperone mediated protein folding independent of cofactor	2.65E-08	1.39E+02	2.54E-05	8.46E-06	8.07E-06
BP	GO:0000398~mRNA splicing, via spliceosome	7.12E-08	1.32E+01	6.82E-05	1.51E-05	1.44E-05
BP	GO:1904851~positive regulation of establishment of protein localization to telomere	7.89E-08	1.11E+02	7.57E-05	1.51E-05	1.44E-05
BP	GO:0048488~synaptic vesicle endocytosis	1.23E-07	2.98E+01	1.18E-04	1.97E-05	1.88E-05
BP	GO:0061640~cytoskeleton-dependent cytokinesis	5.04E-07	7.39E+01	4.83E-04	6.90E-05	6.58E-05
BP	GO:0050821~protein stabilization	8.42E-07	9.85E+00	8.07E-04	8.35E-05	7.96E-05
BP	GO:0061077~chaperone-mediated protein folding	8.49E-07	3.41E+01	8.14E-04	8.35E-05	7.96E-05
BP	GO:0075525~viral translational termination-reinitiation	8.71E-07	1.77E+02	8.35E-04	8.35E-05	7.96E-05
BP	GO:0006457~protein folding	1.95E-06	1.38E+01	1.87E-03	1.70E-04	1.62E-04

Category	Term	PValue	Fold Enrichment	Bonferroni	Benjamini	FDR
BP	GO:0007339~binding of sperm to zona pellucida	3.00E-06	2.66E+01	2.88E-03	2.40E-04	2.29E-04
BP	GO:0006413~translational initiation	8.11E-06	2.18E+01	7.74E-03	5.97E-04	5.70E-04
BP	GO:0032212~positive regulation of telomere maintenance via telomerase	3.09E-05	2.77E+01	2.92E-02	2.12E-03	2.02E-03
BP	GO:0006338~chromatin remodeling	5.09E-05	4.30E+00	4.77E-02	3.25E-03	3.10E-03
BP	GO:0032880~regulation of protein localization	1.46E-04	1.20E+01	1.31E-01	8.75E-03	8.34E-03
BP	GO:0007409~axonogenesis	2.27E-04	1.09E+01	1.96E-01	1.26E-02	1.20E-02
BP	GO:0006884~cell volume homeostasis	2.37E-04	3.28E+01	2.03E-01	1.26E-02	1.20E-02
BP	GO:1903241~U2-type prespliceosome assembly	2.95E-04	1.11E+02	2.46E-01	1.49E-02	1.42E-02
BP	GO:1903076~regulation of protein localization to plasma membrane	3.60E-04	2.86E+01	2.92E-01	1.72E-02	1.64E-02

Table S 2: Top GO-terms for cellular components (CC) based on p-value.

Category	Term	PValue	Fold Enrichment	Bonferroni	Benjamini	FDR
CC	GO:0005737~cytoplasm	2.36E-19	2.66E+00	8.12E-17	8.12E-17	6.21E-17
CC	GO:0098978~glutamatergic synapse	2.68E-18	7.80E+00	9.21E-16	4.60E-16	3.52E-16
CC	GO:0045202~synapse	2.43E-17	8.45E+00	8.38E-15	2.79E-15	2.13E-15
CC	GO:0014069~postsynaptic density	1.33E-15	1.30E+01	4.58E-13	1.14E-13	8.73E-14
CC	GO:0043209~myelin sheath	1.09E-14	1.84E+01	3.74E-12	7.51E-13	5.74E-13
CC	GO:0098794~postsynapse	3.78E-14	1.08E+01	1.30E-11	2.16E-12	1.65E-12
CC	GO:0005829~cytosol	6.01E-13	2.75E+00	2.07E-10	2.95E-11	2.26E-11
CC	GO:0005686~U2 snRNP	3.76E-12	8.33E+01	1.29E-09	1.62E-10	1.24E-10
CC	GO:0098793~presynapse	4.65E-12	1.08E+01	1.60E-09	1.78E-10	1.36E-10
CC	GO:0030425~dendrite	1.36E-11	7.15E+00	4.69E-09	4.69E-10	3.58E-10
CC	GO:0008021~synaptic vesicle	3.82E-11	1.59E+01	1.31E-08	1.19E-09	9.13E-10
CC	GO:0005684~U2-type spliceosomal complex	6.36E-11	5.83E+01	2.19E-08	1.82E-09	1.39E-09
CC	GO:0043025~neuronal cell body	2.15E-10	6.54E+00	7.38E-08	5.68E-09	4.34E-09
CC	GO:0030424~axon	1.87E-09	7.20E+00	6.44E-07	4.60E-08	3.51E-08
CC	GO:0002199~zona pellucida receptor complex	2.24E-09	1.01E+02	7.72E-07	5.14E-08	3.93E-08
CC	GO:0005856~cytoskeleton	4.87E-09	6.73E+00	1.68E-06	1.05E-07	8.01E-08
CC	GO:0005874~microtubule	6.35E-09	8.92E+00	2.18E-06	1.28E-07	9.82E-08

Category	Term	PValue	Fold Enrichment	Bonferroni	Benjamini	FDR
CC	GO:0005852~eukaryotic translation initiation factor 3 complex	7.53E-09	8.20E+01	2.59E-06	1.44E-07	1.10E-07
CC	GO:0071005~U2-type precatalytic spliceosome	1.08E-08	2.91E+01	3.71E-06	1.95E-07	1.49E-07
CC	GO:0033290~eukaryotic 48S preinitiation complex	1.47E-08	7.28E+01	5.04E-06	2.52E-07	1.93E-07

Table S 3: Top GO-term for molecular function (MF) based on p-value.

Category	Term	PValue	Fold Enrichment	Bonferroni	Benjamini	FDR
MF	GO:0005515~protein binding	2.52E-26	3.19E+00	8.61E-24	8.61E-24	7.29E-24
MF	GO:0042802~identical protein binding	4.75E-11	3.63E+00	1.62E-08	7.44E-09	6.31E-09
MF	GO:0140662~ATP-dependent protein folding chaperone	6.55E-11	5.80E+01	2.23E-08	7.44E-09	6.31E-09
MF	GO:0005524~ATP binding	2.94E-10	4.09E+00	1.00E-07	2.50E-08	2.12E-08
MF	GO:0044183~protein folding chaperone	7.68E-09	3.05E+01	2.62E-06	5.24E-07	4.44E-07
MF	GO:0051082~unfolded protein binding	1.02E-08	2.13E+01	3.49E-06	5.82E-07	4.94E-07
MF	GO:0003723~RNA binding	2.00E-07	4.80E+00	6.82E-05	9.75E-06	8.26E-06
MF	GO:0003743~translation initiation factor activity	6.99E-07	2.24E+01	2.38E-04	2.98E-05	2.53E-05
MF	GO:0003779~actin binding	9.60E-07	7.17E+00	3.27E-04	3.64E-05	3.08E-05
MF	GO:0051015~actin filament binding	9.84E-06	8.66E+00	3.35E-03	3.36E-04	2.84E-04
MF	GO:0005543~phospholipid binding	2.42E-05	1.22E+01	8.23E-03	7.51E-04	6.37E-04
MF	GO:0003729~mRNA binding	4.56E-05	6.99E+00	1.54E-02	1.30E-03	1.10E-03
MF	GO:0005516~calmodulin binding	4.96E-05	8.36E+00	1.68E-02	1.30E-03	1.10E-03
MF	GO:0042803~protein homodimerization activity	1.19E-04	3.65E+00	3.99E-02	2.91E-03	2.46E-03
MF	GO:0031625~ubiquitin protein ligase binding	1.40E-04	5.95E+00	4.65E-02	3.12E-03	2.64E-03
MF	GO:0016887~ATP hydrolysis activity	1.46E-04	5.14E+00	4.87E-02	3.12E-03	2.64E-03
MF	GO:0019899~enzyme binding	2.90E-04	4.69E+00	9.42E-02	5.82E-03	4.93E-03
MF	GO:0031072~heat shock protein binding	3.72E-04	1.47E+01	1.19E-01	6.50E-03	5.51E-03
MF	GO:0046982~protein heterodimerization activity	3.96E-04	5.10E+00	1.26E-01	6.50E-03	5.51E-03
MF	GO:0005200~structural constituent of cytoskeleton	4.12E-04	1.43E+01	1.31E-01	6.50E-03	5.51E-03

List of Abbreviations

Abbreviation	Full length terminology
ACh	Acetylcholine
AChRs	Acetylcholine receptors
AMPAR	α-amino-3-hydroxy-5-methyl-4-isoxazole propionic acid receptors
APS	Ammonium peroxidisulphate
Ara-C	1-β-D-Arabinofuranosyl-cytosine-hydrochloride
ASD	Autism spectrum disorder
ATP	Adenosine-5'-triphosphate disodium salt hydrate
BP	Biological process
BSA	Bovine Serum Albumin
CC	Coiled coil
CC	Cellular component
CME	Clathrin-mediated endocytosis
CTTN	Cortactin
DDX	DEAD-box protein
DH	Dbl homology domain
DHA	Docosahexaenoic acid
DIV	Day in vitro
dKO	Double knock-out
DMD	Duchenne muscular dystrophy
DMEM	Dulbecco's modified Eagle's medium
DNAse	Desoxyribonuclease
DPBS	Dulbecco's Phosphate Buffered Saline
DTT	1,4-Dithiothreitol
EDL	Extensor digitorum longus
EDTA	Ethylenediamine tetraacetic acid-Na2-salt-2H2O
EGTA	Ethylene glycol bis-(2-aminoethyl ether) tetraacetic acid
EH	Eps15 homology domains
eIF	Eukaryotic translation initiation factor
ER	Endoplasmic reticulum
FBS	Fetal bovine serum
FCHo	F-BAR domain-containing Fer/Cip4 homology domain-only proteins
FMRP	Fragile X mental retardation protein
FXRs	Fragile X-related RNA-binding proteins
FXS	Fragile X syndrome
FXTAS	Fragile X-associated tremor/ataxia syndrome
GEF	Guanine nucleotide exchange factor
GO	Gene ontology
HBSS	Hanks' Balanced Salt Solution
HCl	Hydrochloric acid
HE	Hematoxylin and eosin
Hepes	4-(2-Hydroxyethyl)-piperazine-1-ethansulfic acid
IPTG	Isopropyl-β D-thiogalactopyranoside

Abbreviation	Full length terminology
ITSN	Intersectin
ITSN-L	ITSN long isoform
ITSN-S	ITSN short isoform
KO	Knock-out
Kv	Voltage-gated potassium
MEM	Minimum Essential Medium
MF	Molecular function
$MgSO_4$	Magnesium sulfate heptahydrate
NaCl	Sodium chloride
NaF	Sodium fluorid
NaF	Sodiumfluorid
NDHII	Nuclear DNA helicase II
NLS	Nuclear localization signal
NMDAR	N-methyl-D-aspartate receptors
NMJ	Neuromuscular junction
N-WASP	Neuronal Wiskott-Aldrich syndrome protein
ON	Overnight
PABP	Poly(A)-binding protein
PB	Sodium phosphate-buffer
PBS	Phosphate-buffered Saline
PCR	Polymerase chain reaction
Pen/Strep	Penicillin-Streptomycin
PFA	Paraformaldehyde
PH	Pleckstrin homology domain
PIC	Protease inhibitor complex
PIPES	1,4-Piperazine diethanesulfonic acid
PMSF	Phenylmethylsulfonylfluorid
PSD	Postsynaptic density
RIM	Rab3-interacting molecules
RNP	Ribonucleoprotein
RT	Room temperature
SDS	Sodium dodecyl sulfate
SDS-PAGE	Sodium dodecyl sulfate polyacrylamide gel electrophoresis
SH3	Src homology 3 domains
SNc	Substantia nigra pars compacta
TA	Tibialis anterior
TB	Triceps brachii
TEMED	N,N,N,N-Tetramethylethylendiamin
Tris-HCl	Tris-hydrochlorid
WIP	WASP interacting protein
WT	Wildtype
Co-IP	Co-immunoprecipitation
MS	Mass spectrometry

Abbreviation	Full length terminology
RRM	RNA recognition motif
mRNP	Messenger RNP
LB	Luria broth
TBS	Tris-buffered saline

List of figures

List of supplementary figures

List of tables

List of supplementary tables

Macros

Z-projections

```
// get files
input = getDirectory("Choose a Directory");
list = getFileList(input);
output = input + "Z Projections" + File.separator;

//batch mode
setBatchMode(true);
if (File.exists(output))
   exit("Destination directory already exists; remove it and then run this macro
again");

File.makeDirectory(output);

// sum each image
for (i=0; i<list.length; i++) {
        if(endsWith(list[i], ".nd2")) {
                    run("Bio-Formats Importer", "open=["+ input + list[i] + "]
autoscale color_mode=Colorized rois_import=[ROI manager] view=Hyperstack
stack_order=XYCZT");
                run("Z Project...", "projection=[Sum Slices]");
                saveAs("tiff", output + getTitle);
                close();
                close();
        }
}
```

Split channels

```
input = getDirectory("Choose a Directory");
list = getFileList(input);
outp input = getDirectory("Choose a Directory");
list = getFileList(input);
output = input + "Single Channels" + File.separator;
setBatchMode(true);
if (File.exists(output))
   exit("Destination directory already exists; remove it and then run this macro
again");
File.makeDirectory(output);
for (i=0; i<list.length; i++) {
        if(startsWith(list[i], "SUM")) {
                    run("Bio-Formats Importer", "open=["+ input + list[i] +"]
autoscale color_mode=Colorized rois_import=[ROI manager] view=Hyperstack
stack_order=XYCZT");
                run("Split Channels");
                saveAs("tiff", output + getTitle);
                close();
                close();
        }
}ut = input + "Single Channels" + File.separator;
setBatchMode(true);
if (File.exists(output))
   exit("Destination directory already exists; remove it and then run this macro
again");
File.makeDirectory(output);
for (i=0; i<list.length; i++) {
        if(startsWith(list[i], "SUM")) {
                    run("Bio-Formats Importer", "open=["+ input + list[i] +"]
autoscale color_mode=Colorized rois_import=[ROI manager] view=Hyperstack
stack_order=XYCZT");
                run("Split Channels");
                saveAs("tiff", output + getTitle);
                close();
```

```
                close();
        }
}
```

CellProfiler Pipeline for NMJ Analysis

```
CellProfiler Pipeline: http://www.cellprofiler.org
Version:5
DateRevision:426
GitHash:
ModuleCount:28
HasImagePlaneDetails:False

Images:[module_num:1|svn_version:'Unknown'|variable_revision_number:2|show_window:F
alse|notes:['To begin creating your project, use the Images module to compile a
list of files and/or folders that you want to analyze. You can also specify a set
of rules to include only the desired files in your selected
folders.']|batch_state:array([], dtype=uint8)|enabled:True|wants_pause:False]
    :
    Filter images?:Images only
    Select the rule criteria:and (extension does isimage) (directory doesnot
containregexp "[\\\\/]\\.")

Metadata:[module_num:2|svn_version:'Unknown'|variable_revision_number:6|show_window
:False|notes:['The Metadata module optionally allows you to extract information
describing your images (i.e, metadata) which will be stored along with your
measurements. This information can be contained in the file name and/or location,
or in an external file.']|batch_state:array([],
dtype=uint8)|enabled:True|wants_pause:False]
    Extract metadata?:No
    Metadata data type:Text
    Metadata types:{}
    Extraction method count:1
    Metadata extraction method:Extract from file/folder names
    Metadata source:File name
    Regular expression to extract from file name:^(?P<Plate>.*)_(?P<Well>[A-P][0-
9]{2})_s(?P<Site>[0-9])_w(?P<ChannelNumber>[0-9])
    Regular expression to extract from folder name:(?P<Date>[0-9]{4}_[0-9]{2}_[0-
9]{2})$
    Extract metadata from:All images
    Select the filtering criteria:and (file does contain "")
    Metadata file location:Elsewhere...|
    Match file and image metadata:[]
    Use case insensitive matching?:No
    Metadata file name:None
    Does cached metadata exist?:No

NamesAndTypes:[module_num:3|svn_version:'Unknown'|variable_revision_number:8|show_w
indow:False|notes:['The NamesAndTypes module allows you to assign a meaningful name
to each image by which other modules will refer to it.']|batch_state:array([],
dtype=uint8)|enabled:True|wants_pause:False]
    Assign a name to:Images matching rules
    Select the image type:Grayscale image
    Name to assign these images:DNA
    Match metadata:[]
    Image set matching method:Order
    Set intensity range from:Image metadata
    Assignments count:2
    Single images count:0
    Maximum intensity:255.0
    Process as 3D?:No
    Relative pixel spacing in X:1.0
    Relative pixel spacing in Y:1.0
    Relative pixel spacing in Z:1.0
    Select the rule criteria:and (file does contain "C1")
    Name to assign these images:BTX
    Name to assign these objects:Cell
```

```
    Select the image type:Grayscale image
    Set intensity range from:Image metadata
    Maximum intensity:255.0
    Select the rule criteria:and (file does contain "C2")
    Name to assign these images:Syp
    Name to assign these objects:Nucleus
    Select the image type:Grayscale image
    Set intensity range from:Image metadata
    Maximum intensity:255.0

Groups:[module_num:4|svn_version:'Unknown'|variable_revision_number:2|show_window:F
alse|notes:['The Groups module optionally allows you to split your list of images
into image subsets (groups) which will be processed independently of each other.
Examples of groupings include screening batches, microtiter plates, time-lapse
movies, etc.']|batch_state:array([], dtype=uint8)|enabled:True|wants_pause:False]
    Do you want to group your images?:No
    grouping metadata count:1
    Metadata category:None

CorrectIlluminationCalculate:[module_num:5|svn_version:'Unknown'|variable_revision_
number:2|show_window:False|notes:[]|batch_state:array([],
dtype=uint8)|enabled:True|wants_pause:False]
    Select the input image:Syp
    Name the output image:IllumSyp
    Select how the illumination function is calculated:Regular
    Dilate objects in the final averaged image?:No
    Dilation radius:1
    Block size:60
    Rescale the illumination function?:Yes
    Calculate function for each image individually, or based on all images?:Each
    Smoothing method:Fit Polynomial
    Method to calculate smoothing filter size:Automatic
    Approximate object diameter:10
    Smoothing filter size:10
    Retain the averaged image?:No
    Name the averaged image:IllumBlueAvg
    Retain the dilated image?:No
    Name the dilated image:IllumBlueDilated
    Automatically calculate spline parameters?:Yes
    Background mode:auto
    Number of spline points:5
    Background threshold:2.0
    Image resampling factor:2.0
    Maximum number of iterations:40
    Residual value for convergence:0.001

CorrectIlluminationCalculate:[module_num:6|svn_version:'Unknown'|variable_revision_
number:2|show_window:False|notes:[]|batch_state:array([],
dtype=uint8)|enabled:True|wants_pause:False]
    Select the input image:BTX
    Name the output image:IllumBTX
    Select how the illumination function is calculated:Regular
    Dilate objects in the final averaged image?:No
    Dilation radius:1
    Block size:60
    Rescale the illumination function?:Yes
    Calculate function for each image individually, or based on all images?:Each
    Smoothing method:Fit Polynomial
    Method to calculate smoothing filter size:Automatic
    Approximate object diameter:10
    Smoothing filter size:10
    Retain the averaged image?:No
    Name the averaged image:IllumBlueAvg
    Retain the dilated image?:No
    Name the dilated image:IllumBlueDilated
    Automatically calculate spline parameters?:Yes
    Background mode:auto
    Number of spline points:5
```

```
    Background threshold:2.0
    Image resampling factor:2.0
    Maximum number of iterations:40
    Residual value for convergence:0.001

CorrectIlluminationApply:[module_num:7|svn_version:'Unknown'|variable_revision_numb
er:5|show_window:False|notes:[]|batch_state:array([],
dtype=uint8)|enabled:True|wants_pause:False]
    Select the input image:BTX
    Name the output image:CorrBTX
    Select the illumination function:IllumBTX
    Select how the illumination function is applied:Divide
    Select the input image:Syp
    Name the output image:CorrSyp
    Select the illumination function:IllumSyp
    Select how the illumination function is applied:Divide
    Set output image values less than 0 equal to 0?:Yes
    Set output image values greater than 1 equal to 1?:Yes

Align:[module_num:8|svn_version:'Unknown'|variable_revision_number:3|show_window:Fa
lse|notes:[]|batch_state:array([], dtype=uint8)|enabled:True|wants_pause:False]
    Select the alignment method:Mutual Information
    Crop mode:Keep size
    Select the first input image:CorrSyp
    Name the first output image:AlignedSyp
    Select the second input image:CorrBTX
    Name the second output image:AlignedBTX

MeasureColocalization:[module_num:9|svn_version:'Unknown'|variable_revision_number:
5|show_window:False|notes:[]|batch_state:array([],
dtype=uint8)|enabled:True|wants_pause:False]
    Select images to measure:AlignedBTX, AlignedSyp
    Set threshold as percentage of maximum intensity for the images:15.0
    Select where to measure correlation:Across entire image
    Select objects to measure:
    Run all metrics?:Yes
    Calculate correlation and slope metrics?:Yes
    Calculate the Manders coefficients?:Yes
    Calculate the Rank Weighted Colocalization coefficients?:Yes
    Calculate the Overlap coefficients?:Yes
    Calculate the Manders coefficients using Costes auto threshold?:Yes
    Method for Costes thresholding:Accurate

RescaleIntensity:[module_num:10|svn_version:'Unknown'|variable_revision_number:3|sh
ow_window:False|notes:[]|batch_state:array([],
dtype=uint8)|enabled:True|wants_pause:False]
    Select the input image:Syp
    Name the output image:RescaledSyp
    Rescaling method:Stretch each image to use the full intensity range
    Method to calculate the minimum intensity:Custom
    Method to calculate the maximum intensity:Custom
    Lower intensity limit for the input image:0.0
    Upper intensity limit for the input image:1.0
    Intensity range for the input image:0.0,1.0
    Intensity range for the output image:0.0,1.0
    Select image to match in maximum intensity:None
    Divisor value:1.0
    Divisor measurement:None

RescaleIntensity:[module_num:11|svn_version:'Unknown'|variable_revision_number:3|sh
ow_window:False|notes:[]|batch_state:array([],
dtype=uint8)|enabled:True|wants_pause:False]
    Select the input image:BTX
    Name the output image:RescaledBTX
    Rescaling method:Stretch each image to use the full intensity range
    Method to calculate the minimum intensity:Custom
    Method to calculate the maximum intensity:Custom
    Lower intensity limit for the input image:0.0
```

```
    Upper intensity limit for the input image:1.0
    Intensity range for the input image:0.0,1.0
    Intensity range for the output image:0.0,1.0
    Select image to match in maximum intensity:None
    Divisor value:1.0
    Divisor measurement:None

MeasureImageIntensity:[module_num:12|svn_version:'Unknown'|variable_revision_number
:4|show_window:False|notes:[]|batch_state:array([],
dtype=uint8)|enabled:True|wants_pause:False]
    Select images to measure:RescaledBTX, RescaledSyp
    Measure the intensity only from areas enclosed by objects?:No
    Select input object sets:
    Calculate custom percentiles:No
    Specify percentiles to measure:10,90

ImageMath:[module_num:13|svn_version:'Unknown'|variable_revision_number:5|show_wind
ow:False|notes:[]|batch_state:array([],
dtype=uint8)|enabled:True|wants_pause:False]
    Operation:Subtract
    Raise the power of the result by:1.0
    Multiply the result by:1.0
    Add to result:0.0
    Set values less than 0 equal to 0?:Yes
    Set values greater than 1 equal to 1?:Yes
    Replace invalid values with 0?:Yes
    Ignore the image masks?:No
    Name the output image:SubBackgroundSyp
    Image or measurement?:Image
    Select the first image:RescaledSyp
    Multiply the first image by:1.0
    Measurement:
    Image or measurement?:Measurement
    Select the second image:None
    Multiply the second image by:1.0
    Measurement:Intensity_LowerQuartileIntensity_RescaledSyp

ImageMath:[module_num:14|svn_version:'Unknown'|variable_revision_number:5|show_wind
ow:False|notes:[]|batch_state:array([],
dtype=uint8)|enabled:True|wants_pause:False]
    Operation:Subtract
    Raise the power of the result by:1.0
    Multiply the result by:1.0
    Add to result:0.0
    Set values less than 0 equal to 0?:Yes
    Set values greater than 1 equal to 1?:Yes
    Replace invalid values with 0?:Yes
    Ignore the image masks?:No
    Name the output image:SubBackgroundBTX
    Image or measurement?:Image
    Select the first image:RescaledBTX
    Multiply the first image by:1.0
    Measurement:
    Image or measurement?:Measurement
    Select the second image:None
    Multiply the second image by:1.0
    Measurement:Intensity_LowerQuartileIntensity_RescaledBTX

EnhanceOrSuppressFeatures:[module_num:15|svn_version:'Unknown'|variable_revision_nu
mber:7|show_window:False|notes:[]|batch_state:array([],
dtype=uint8)|enabled:True|wants_pause:False]
    Select the input image:SubBackgroundSyp
    Name the output image:EnhancedSyp
    Select the operation:Enhance
    Feature size:10
    Feature type:Neurites
    Range of hole sizes:1,10
    Smoothing scale:11.5
```

```
    Shear angle:0.0
    Decay:0.95
    Enhancement method:Tubeness
    Speed and accuracy:Fast
    Rescale result image:No

EnhanceOrSuppressFeatures:[module_num:16|svn_version:'Unknown'|variable_revision_nu
mber:7|show_window:False|notes:[]|batch_state:array([],
dtype=uint8)|enabled:False|wants_pause:False]
    Select the input image:SubBackgroundBTX
    Name the output image:EnhancedBTX
    Select the operation:Enhance
    Feature size:10
    Feature type:Neurites
    Range of hole sizes:1,10
    Smoothing scale:7.5
    Shear angle:0.0
    Decay:0.95
    Enhancement method:Tubeness
    Speed and accuracy:Fast
    Rescale result image:No

IdentifyPrimaryObjects:[module_num:17|svn_version:'Unknown'|variable_revision_numbe
r:15|show_window:False|notes:[]|batch_state:array([],
dtype=uint8)|enabled:True|wants_pause:False]
    Select the input image:EnhancedSyp
    Name the primary objects to be identified:IdentifyPre
    Typical diameter of objects, in pixel units (Min,Max):15,300
    Discard objects outside the diameter range?:Yes
    Discard objects touching the border of the image?:Yes
    Method to distinguish clumped objects:Intensity
    Method to draw dividing lines between clumped objects:Shape
    Size of smoothing filter:5
    Suppress local maxima that are closer than this minimum allowed distance:50
    Speed up by using lower-resolution image to find local maxima?:No
    Fill holes in identified objects?:Never
    Automatically calculate size of smoothing filter for declumping?:No
    Automatically calculate minimum allowed distance between local maxima?:No
    Handling of objects if excessive number of objects identified:Continue
    Maximum number of objects:500
    Use advanced settings?:Yes
    Threshold setting version:12
    Threshold strategy:Global
    Thresholding method:Otsu
    Threshold smoothing scale:1.3488
    Threshold correction factor:1.15
    Lower and upper bounds on threshold:0.0,1.0
    Manual threshold:0.0
    Select the measurement to threshold with:None
    Two-class or three-class thresholding?:Three classes
    Log transform before thresholding?:No
    Assign pixels in the middle intensity class to the foreground or the
background?:Foreground
    Size of adaptive window:50
    Lower outlier fraction:0.05
    Upper outlier fraction:0.05
    Averaging method:Mean
    Variance method:Standard deviation
    # of deviations:2.0
    Thresholding method:Minimum Cross-Entropy

IdentifyPrimaryObjects:[module_num:18|svn_version:'Unknown'|variable_revision_numbe
r:15|show_window:False|notes:[]|batch_state:array([],
dtype=uint8)|enabled:True|wants_pause:False]
    Select the input image:SubBackgroundBTX
    Name the primary objects to be identified:IdentifyedPost
    Typical diameter of objects, in pixel units (Min,Max):15,300
    Discard objects outside the diameter range?:Yes
```

```
    Discard objects touching the border of the image?:Yes
    Method to distinguish clumped objects:Intensity
    Method to draw dividing lines between clumped objects:Shape
    Size of smoothing filter:5
    Suppress local maxima that are closer than this minimum allowed distance:50
    Speed up by using lower-resolution image to find local maxima?:No
    Fill holes in identified objects?:Never
    Automatically calculate size of smoothing filter for declumping?:No
    Automatically calculate minimum allowed distance between local maxima?:No
    Handling of objects if excessive number of objects identified:Continue
    Maximum number of objects:500
    Use advanced settings?:Yes
    Threshold setting version:12
    Threshold strategy:Global
    Thresholding method:Otsu
    Threshold smoothing scale:1.3488
    Threshold correction factor:1.15
    Lower and upper bounds on threshold:0.0,1
    Manual threshold:0.0
    Select the measurement to threshold with:None
    Two-class or three-class thresholding?:Three classes
    Log transform before thresholding?:No
    Assign pixels in the middle intensity class to the foreground or the
background?:Foreground
    Size of adaptive window:50
    Lower outlier fraction:0.05
    Upper outlier fraction:0.05
    Averaging method:Mode
    Variance method:Standard deviation
    # of deviations:2.0
    Thresholding method:Otsu

ConvertObjectsToImage:[module_num:19|svn_version:'Unknown'|variable_revision_number
:1|show_window:False|notes:[]|batch_state:array([],
dtype=uint8)|enabled:True|wants_pause:True]
    Select the input objects:IdentifyPre
    Name the output image:SypMask
    Select the color format:Binary (black & white)
    Select the colormap:tab20c

ConvertObjectsToImage:[module_num:20|svn_version:'Unknown'|variable_revision_number
:1|show_window:False|notes:[]|batch_state:array([],
dtype=uint8)|enabled:True|wants_pause:False]
    Select the input objects:IdentifyedPost
    Name the output image:BTXMask
    Select the color format:Binary (black & white)
    Select the colormap:tab20b

SaveImages:[module_num:21|svn_version:'Unknown'|variable_revision_number:16|show_wi
ndow:False|notes:[]|batch_state:array([],
dtype=uint8)|enabled:True|wants_pause:False]
    Select the type of image to save:Image
    Select the image to save:SypMask
    Select method for constructing file names:From image filename
    Select image name for file prefix:Syp
    Enter single file name:OrigBlue
    Number of digits:4
    Append a suffix to the image file name?:Yes
    Text to append to the image name:SypMask
    Saved file format:tiff
    Output file location:Elsewhere…
    Image bit depth:8-bit integer
    Overwrite existing files without warning?:Yes
    When to save:Every cycle
    Record the file and path information to the saved image?:No
    Create subfolders in the output folder?:No
    Base image folder:Elsewhere...|
    How to save the series:T (Time)
```

```
    Save with lossless compression?:No

SaveImages:[module_num:22|svn_version:'Unknown'|variable_revision_number:16|show_wi
ndow:False|notes:[]|batch_state:array([],
dtype=uint8)|enabled:True|wants_pause:False]
    Select the type of image to save:Image
    Select the image to save:BTXMask
    Select method for constructing file names:From image filename
    Select image name for file prefix:BTX
    Enter single file name:OrigBlue
    Number of digits:4
    Append a suffix to the image file name?:Yes
    Text to append to the image name:BTXMask
    Saved file format:tiff
    Output file location:Elsewhere...
    Image bit depth:8-bit integer
    Overwrite existing files without warning?:Yes
    When to save:Every cycle
    Record the file and path information to the saved image?:No
    Create subfolders in the output folder?:No
    Base image folder:Elsewhere...|
    How to save the series:T (Time)
    Save with lossless compression?:No

MorphologicalSkeleton:[module_num:23|svn_version:'Unknown'|variable_revision_number
:1|show_window:False|notes:[]|batch_state:array([],
dtype=uint8)|enabled:True|wants_pause:False]
    Select the input image:BTXMask
    Name the output image:BTXSkeleton

MeasureImageSkeleton:[module_num:24|svn_version:'Unknown'|variable_revision_number:
1|show_window:False|notes:['measures branches and endpoints for complexity
calculation ']|batch_state:array([], dtype=uint8)|enabled:True|wants_pause:False]
    Select an image to measure:BTXSkeleton

MeasureImageAreaOccupied:[module_num:25|svn_version:'Unknown'|variable_revision_num
ber:5|show_window:False|notes:[]|batch_state:array([],
dtype=uint8)|enabled:True|wants_pause:False]
    Measure the area occupied by:Binary Image
    Select binary images to measure:BTXSkeleton
    Select object sets to measure:

Morph:[module_num:26|svn_version:'Unknown'|variable_revision_number:5|show_window:F
alse|notes:[]|batch_state:array([], dtype=uint8)|enabled:True|wants_pause:False]
    Select the input image:BTXMask
    Name the output image:BTXhull
    Select the operation to perform:convex hull
    Number of times to repeat operation:Once
    Repetition number:2
    Rescale values from 0 to 1?:Yes

MeasureImageAreaOccupied:[module_num:27|svn_version:'Unknown'|variable_revision_num
ber:5|show_window:False|notes:['for BTX skeleton gives total length of branches as
skeleton is just 1 pixel ']|batch_state:array([],
dtype=uint8)|enabled:True|wants_pause:False]
    Measure the area occupied by:Binary Image
    Select binary images to measure:BTXMask, BTXSkeleton, BTXhull, SypMask
    Select object sets to measure:

ExportToSpreadsheet:[module_num:28|svn_version:'Unknown'|variable_revision_number:1
3|show_window:False|notes:[]|batch_state:array([],
dtype=uint8)|enabled:True|wants_pause:False]
    Select the column delimiter:Comma (",")
    Add image metadata columns to your object data file?:No
    Add image file and folder names to your object data file?:Yes
    Select the measurements to export:Yes
    Calculate the per-image mean values for object measurements?:No
    Calculate the per-image median values for object measurements?:No
```

```
    Calculate the per-image standard deviation values for object measurements?:No
    Output file location:Elsewhere…
    Create a GenePattern GCT file?:No
    Select source of sample row name:Metadata
    Select the image to use as the identifier:None
    Select the metadata to use as the identifier:None
    Export all measurement types?:Yes
    Press button to select
measurements:Image|Correlation_RWC_AlignedSyp_AlignedBTX,Image|Correlation_RWC_Alig
nedBTX_AlignedSyp,Image|Correlation_Manders_AlignedSyp_AlignedBTX,Image|Correlation
_Manders_AlignedBTX_AlignedSyp,Image|Correlation_K_AlignedSyp_AlignedBTX,Image|Corr
elation_K_AlignedBTX_AlignedSyp,Image|Correlation_Costes_AlignedSyp_AlignedBTX,Imag
e|Correlation_Costes_AlignedBTX_AlignedSyp,Image|Correlation_Slope_AlignedBTX_Align
edSyp,Image|Correlation_Correlation_AlignedBTX_AlignedSyp,Image|Correlation_Overlap
_AlignedBTX_AlignedSyp,Image|AreaOccupied_AreaOccupied_SypMask,Image|AreaOccupied_A
reaOccupied_BTXhull,Image|AreaOccupied_AreaOccupied_BTXMask,Image|AreaOccupied_Area
Occupied_BTXSkeleton,Image|Skeleton_Endpoints_BTXSkeleton,Image|Skeleton_Branches_B
TXSkeleton,Image|Count_IdentifyPre,Image|Count_IdentifyedPost,Image|FileName_BTX,Im
age|FileName_Syp
    Representation of Nan/Inf:NaN
    Add a prefix to file names?:Yes
    Filename prefix:NMJ Analysis
    Overwrite existing files without warning?:Yes
    Data to export:Do not use
    Combine these object measurements with those of the previous object?:No
    File name:DATA.csv
    Use the object name for the file name?:Yes
```

Cellpose analysis

```
// needs serveral Plugins: Cellpose and PBIOP, Bio-Formats
// set measure settings beforehand, need Area, Circulartiy, Feret diameter, maybe
perimeter
// test settings for cellpose before running for analysis

// get images and create folder within directory for results
input = getDirectory("Choose a Directory");
list = getFileList(input);
output = input + "Myofiber results" + File.separator;
if (File.exists(output))
   exit("Destination directory already exists; remove it and then run this macro
again");
File.makeDirectory(output);

//activate batch mode
//setBatchMode(true); deactivated, made problems

// command to do so for every image in directory
for (i=0; i<list.length; i++) {
             if(endsWith(list[i], ".nd2")) {
                           run("Bio-Formats Importer", "open=["+ input + list[i] +
"] autoscale color_mode=Colorized rois_import=[ROI manager] view=Hyperstack
stack_order=XYCZT");
                           orgName =getTitle();
                run("Cellpose Advanced", "diameter=30 cellproba_threshold=0.0
flow_threshold=0.4 anisotropy=1.0 diam_threshold=12.0 model=cyto2 nuclei_channel=0
cyto_channel=1 dimensionmode=2D stitch_threshold=-1.0 omni=false cluster=false
additional_flags=");
                saveAs("tiff", output + orgName + "cellpose");
                run("Label image to ROIs", "rm=[RoiManager[size=581,
visible=true]]");
                // Saving ROIs to a .zip file
                roiManager("save", output + orgName + ".zip")
                // Measure Area, Ferret diameter, Circ
                roiManager("measure");
                selectWindow("Results");
```

```
                saveAs("Results", output + orgName + ".csv" );
                roiManager("delete");
                close();
                close();
        }
}
```

Acknowledgements

First, I would like to thank my supervisor Prof. Dr. Tanja Maritzen for giving me the opportunity to work on this interesting project and supporting and guiding me throughout this journey. I am deeply grateful for your open ear at any time and scientific advice, even mid experiment.

I would like to thank Prof. Dr. Jan Pielage and Prof. Dr. Volker Haucke, for their supportive feedback and for bringing in new ideas and directions during our TAC meetings.

Also, I would like to thank Prof. Dr. Stefan Kins and Prof. Dr. Jan Pielage for readily accepting to be part of my thesis committee.

Also, a big thank you goes to Gabriele Amoroso, for a wonderful coordination of the grad school classes and activities. You were always there to help us, listening to our feedback and supporting us wherever possible. I am especially grateful for your help organizing the trip to Bordeaux, to learn the synaptosome purification by FACS. Here, special thanks to Vincent Paget-Blanc, Etienne Herzog and David Perrais for giving me the opportunity to learn this special technique in their lab. Thank you, Dario Lasser, for sticking through several failed attempts to get the STED microscopy to work.

Also, I would like to thank the entire AG Maritzen, including current members and previous students. Thank you for being wonderful colleagues, for countless game nights and self-made pizza, for a lot of cakes and for always ending presentations with a meme. You made moving to a new city and finding friends here way easier than I imagined. I owe special thanks to Jasmeet Kaur Shergill, for teaching me neuronal cell culture and the tryptic digest, as well as to always keep going. You were always there, for every stupid question and for little chats during incubation times. Thank you to Fiorella Mazzone and Marlen Duchmann for always reminding me it's okay to say no and to step up for what I want. Also outside of our lab, I am very grateful that I met you Büsra and will miss our Coffee breaks.

Special thanks to my friends outside of the lab, for always supporting me. I am especially grateful for Sophie Wölbert and Anna Stölting, for proofreading this thesis. A heartfelt thank you to Anna and Lina, I am fortunate that you stayed by my side for most of my academic

journey, always there when times got tough and encouraging me to go on but also celebrating the god times together.

I am deeply grateful for my parents and family for giving me the possibility to study and supporting me financially, especially during the Bachelor and Master, and mentally.

And finally, thank you Max! You had to live with me and all the stress and emotions that came along with this PhD thesis and weathered it all with unending patience. Hopefully, I can soon answer your question “Are you doctor yet?” with a “yes!”.

Curriculum vitae

Alexandra Hilse

Education

Since 02/2022	Rheinland-Pfälzische Technische Universität Kaiserslautern-Landau, Germany PhD studies *Title: Dissecting the molecular mechanisms by which intersectins shape neurotransmission*
10/2019-12/2021	Albert-Ludwigs-Universität Freiburg, Germany Master of Science in Biology, specializing in Neurobiology *Thesis: Alteration in neurons in the human epileptic cortex*
10/2016-10/2019	Albert-Ludwigs-Universität Freiburg, Germany Bachelor of Science in Biology *Thesis: Characterization of mitral cells in the mouse olfactory bulb*
08/2007-03/2016	Lina-Hilger-Gymnasium Bad Kreuznach, Germany General matriculation standard

Other activities

Since 2022	Rheinland-Pfälzische Technische Universität Kaiserslautern-Landau, Germany Supervison of bachelor and master students
07/2023-03/2025	RTG 2737 Stressistance, Kaiserslautern, Germany Vice-spokesperson of the student body

Publications

- Ziegler-Waldkirch, S., Friesen, M., Loreth, D., Sauer, J. F., Kemna, S., **Hilse, A.**, Erny, D., Helm, C., D Errico, P., Prinz, M., Bartos, M., & Meyer-Luehmann, M. (2022). Seed-induced Aβ deposition alters neuronal function and impairs olfaction in a mouse model of Alzheimer's disease. *Molecular psychiatry*, *27*(10), 4274–4284. https://doi.org/10.1038/s41380-022-01686-5

- Vollweiter, D., Shergill, J. K., **Hilse, A.**, Kochlamazashvili, G., Koch, S. P., Mueller, S., Boehm-Sturm, P., Haucke, V., & Maritzen, T. (2023). Intersectin deficiency impairs cortico-striatal neurotransmission and causes obsessive-compulsive behaviors in mice. *Proceedings of the National Academy of Sciences of the United States of America*, *120*(35), e2304323120. https://doi.org/10.1073/pnas.2304323120